Universidade de Aveiro Departamento de Química
2017

Luís Pedro Correia Pinto Ferreira

Desenvolvimento de Modelos Tumorais 3D Multicelulares como Plataformas para Testes de Novas Terapias Anticancerígenas

Development of Multicellular 3D Cancer Testing Platforms for Evaluation of New anti-Cancer Therapies

Universidade de Aveiro Departamento de Química
2017

Luís Pedro Correia Pinto Ferreira

Desenvolvimento de Modelos Tumorais 3D Multicelulares como Plataformas para Testes de Novas Terapias Anticancerígenas

Development of Multicellular 3D Cancer Testing Platforms for Evaluation of New anti-Cancer Therapies

Dissertação apresentada à Universidade de Aveiro para cumprimento dos requisitos necessários à obtenção do grau de Mestre em Bioquímica Clínica, realizada sob a orientação científica do Doutor Vítor Gaspar e do Professor Doutor João Mano, Professor Catedrático do Departamento de Química da Universidade de Aveiro

o júri

presidente

Professor Doutor Pedro Miguel Dimas Neves Domingues
Professor Auxiliar do Departamento de Química da Universidade de Aveiro

Professor Doutor João Filipe Colardelle da Luz Mano
Professor Catedrático da Universidade de Aveiro

Professora Doutora Ana Paula Gomes Moreira Pêgo
Professora Associada no Instituto de Ciências Biomédicas Abel Salazar da Universidade do Porto

Acknowledgments

First and foremost, I would like to express my gratitude to Professor Doctor João Mano for having bestowed upon me the opportunity to work amidst such an exceptional group of researchers. More so, for the heartful welcome I received from all members. Compass, shall indeed orient further research in the field of tissue engineering. Secondly, I thank my Super-supervisor Dr. Vitor Gaspar for inviting me into the world of tumor modeling with open arms, friendship and above all else calm amidst my doubts and mistakes. I feel that in this year, thanks to his guidance, I learn more regarding hard-work and scientific research than in the entirety of my academic journey. “Far way in a well there lived a spheroid”.

Thirdly I would like to thank all those that both on the lab and at home supported me during the most stressful and gentle moments. To my girlfriend Teresa, who help me each and every day to better both my research and my spirit. To my family for supporting me on all accounts and always helping. To my friends, Guilherme, Pedro Maia, and Pedro Ruivo who eased my mind on the lesser days. Through friendship and laughter. And finally, but most importantly to my comrade Pedro Lavrador without you this would not have been the same. Thank you brother for all the help

palavras-chave Cultura Celular 3D, Células Estaminais Mesenquimais Associadas ao Tumor, Cancro, Validação Pré-Clínica, Drug-Screening, Cocultura, Microambiente Tumoral

resumo

O cancro do pulmão (CP) é um dos cancros mais diagnosticados a nível mundial e também um dos mais mortíferos. Atualmente, as terapias administradas a nível clínico para o tratamento do CP são ainda extremamente ineficazes e limitadas no que diz respeito ao aumento da taxa de sobrevivência dos pacientes oncológicos. Esta realidade demonstra a necessidade de investigar ativamente novas terapias para o tratamento desta neoplasia.

No entanto a validação pré-clínica de terapias inovadoras para o CP tem-se revelado extremamente difícil devido à inexistência de plataformas que sejam adequadas para testes a nível laboratorial, uma vez que as culturas celulares in vitro bidimensionais (2D), recomendadas pelas agências regulatórias são incapazes de mimetizar as caraterísticas principais dos tumores humanos. Estas limitações têm originado uma fraca correlação entre a performance das terapias nos estudos in vitro e a obtida em ensaios clínicos controlados.

Neste contexto, os modelos de tumores tridimensionais (3D) in vitro têm vindo a ser reconhecidos como uma solução para este problema, pois podem recapitular várias componentes do microambiente tumoral. Das várias plataformas 3D in vitro de CP investigadas atualmente muito poucas avaliaram o papel da inclusão de células estaminais mesenquimais (MSCs). Para colmatar esta lacuna, o trabalho de investigação desenvolvido no âmbito desta dissertação descreve a produção e otimização de novos modelos hétero-celulares 3D in vitro. Estas plataformas são compostas por células tumorais do CP (A549) e do seu estroma, nomeadamente fibroblastos da pele e células estaminais mesenquimais derivadas da medula óssea (BM-MSCs). Estes três tipos de células foram co-cultivadas em micropartículas poliméricas de policaprolactona revestidas por ácido hialurónico, com o objetivo de incluir este componente da matriz extracelular que se encontra presente no microambiente do CP. Esta abordagem permitiu formar a nível laboratorial microtecidos multicelulares 3D híbridos que melhor mimetizam a heterogeneidade celular das neoplasias pulmonares. Os resultados obtidos demonstraram que os microtumores formados através da técnica de sobreposição-líquida são reprodutíveis em termos de morfologia e tamanho, apresentaram núcleos necróticos, organização celular 3D e produziram proteínas do microambiente tumoral. Além destas caraterísticas, os dados obtidos através de microscopia de fluorescência revelaram que as BM-MSCs migram para o interior dos microtumores ao longo do tempo. A avaliação da citotoxicidade da Doxorubicina, um fármaco anti-tumoral rotineiramente utilizado a nível clínico, demonstrou que a inclusão de micropartículas aumenta a resistência das células tumorais em modelos homotípicos. Nos modelos tri-cultura heterotípicos a citotoxicidade foi comparável à obtida em microtumores sem micropartículas. Estes resultados evidenciam assim o papel importante dos fibroblastos e das BM-MSCs na resposta dos microtumores. Numa visão global, os modelos 3D formados recapitulam com mais exatidão o microambiente do cancro do pulmão e poderão servir no futuro como plataformas de teste para descobrir ou aperfeiçoar novas terapias, ou combinações de terapêuticas, para este tipo de neoplasia.

keywords 3D cell culture, Tumor Associated Mesenchymal stem cells, Cancer, Preclinical Validation Models, Drug-Screening, Coculture, Tumor Microenvironment

abstract Lung cancer (LC) is one the most commonly diagnosed cancers worldwide, being also one of the deadliest. Currently, clinically administered therapies for treatment of LC are still extremely ineffective and limited in increasing oncologic patients survival rates. This reality evidences the necessity of actively investigating novel therapies for the treatment of LC. However, preclinical validation of novel therapies as revealed itself as an extremely arduous process, due to the lack of suitable laboratory testing platforms since the recommend in vitro bi-dimensional (2D) cell cultures are unable to fully mimic the main hallmarks of human tumors.

In this context, in vitro tridimensional (3D) tumor models are being increasingly recognized as a solution due to their ability to correctly recapitulate several characteristics of the tumor microenvironment (TME). Amongst currently developed 3D in vitro platforms for the study of LC, few have included or studied the role of mesenchymal stem cells (MSCs). To provide further insights into this hypothesis, the research work developed in this thesis describes the production and optimization of novel heterotypic in vitro 3D models, comprised by non-small-cell lung cancer cells (A549) and stromal cells, namely skin fibroblasts (HFs), and bone-marrow derived mesenchymal stem cells (BM-MSCs). These three diverse cell populations were co-cultured in hyaluronic acid coated polymeric polycaprolactone microparticles (LbL-MPs) as to include this key extracellular matrix component of LC TME. This approach allowed the formation of 3D multicellular heterotypic microtissues (3D-MCTS) that better recapitulate the cellular heterogeneity of LC TME in the laboratory. The obtained findings demonstrate that these models formed via the liquid-overlay technique were reproducible in terms of morphology and size, presented necrotic core formation, 3D cellular organization, and deposited matrix proteins in a similar manner as in the TME. Besides this, fluorescence microscopy data revealed that BM-MSCs migrated overtime into the microtumors core . Performed doxorubicin in vitro cytotoxicity assays revealed that the inclusion of LbL-MPs lead to an increased resistance of homotypic A549 monoculture models against this anti-cancer drug commonly used in clinical treatments. Alongside, the cytotoxicity obtained in triculture heterotypic models was comparable to that of microtumors without LbL-MPs inclusion, showcasing the role of HFs and BM-MSCs in microtumors response to therapy. Globally, the herein bioengineered 3D models were able to recapitulate with an increased precision the TME of LC, making them suitable test platforms for development or improvement of standalone or combinatorial therapies for this type of neoplasia.

Contents

List of Figures

List of Tables

List of Abbreviations and Acronyms

AT-MSC's	Adipose tissue stem cells
bFGF	Basic fibroblast growth factor
2D	Bi-dimensional
BM-MSC	Bone-marrow derived mesenchymal stem cell
CAF	Cancer associated fibroblasts
CSC's	Cancer stem cells
CD	Cluster of Differentiation
Dox	Doxorubicin
EC	Endothelial cells
EGF	Epidermal growth factor
EGFR	Epidermal growth factor receptor
EMT	Epithelial to Mesenchymal Transition
ECM	Extracellular matrix
ECM	Extra-cellular matrix
FGF	Fibroblast growth factor
FHIT	Fragile histidine triad protein
GFP	Green fluorescent protein
HGF	Hepatocyte growth factor
HF	Human dermal fibroblasts
LbL-MPs	Hyaluronic acid coated polymeric polycaprolactone microparticles
HA	Hydroxyapatite
IGF	Insulin growth factor
IGFBP	Insulin growth factor binding proteins
IL	Interleukin
LbL	Layer-by-Layer
LC	Lung cancer
A549	Lung cancer cells used
L-CSCs	Lung cancer stem cells
MHC-II	Major histocompatibility complex ii
MMP	Matrix metalloproteinase
MSC	Mesenchymal stem cell
MSC-CC	Mesenchymal Stem Cell to Cancer Cells
MSC's	Mesenchymal stem cells
ME	Microencapsulation
MPs	Microparticles
MAPK	Mitogen-activated Protein Kinases
MCP	Monocyte chemoattractant protein
MM	Multiple myeloma
NSCLC	Non-small Cell Lung Cancer
NT-MPs	Non-treated Microparticles
PDGF	Platelet-derived growth factor

PLG	Poly(d,l-lactide-co-glycolide)
PLGA	Poly(lactic-co-glycolic acid)
PLL	Poly-L-Lysine
Poly-HEMA	Poly-2-hydroxyethyl methacrylate
PCL	Polycaprolactone
PEG	Polyethyleneglycol
PGA	Polyglycoslide or poly(glycolic acid)
PLA	Polylactic acid
PCVM	Preclinical validation model
RFP	Red fluorescent protein
RGD	Tripeptide Arg-Gly-Asp
SEM	Scanning electron microscopy
SCLC	Small cell lung cancer
SDF	Stromal cell-derived factor
3D	Three-dimensional
TREAT-ME1	Treatment of Advanced Gastrointestinal Tumors with Genetically Modified Autologous Mesenchymal Stromal Cells
TGF	Tumor growth factor
TME	Tumor microenvironment
TNF	Tumor necrosis factor
TA-MSC's	Tumor-associated mesenchymal stem cells
UV	Ultra-violet light
VEGF	Vascular endothelial growth factor
WJ-MSC's	Wharton jelly mesenchymal stem cells
3D-MCTS	3D multicellular Spheroids

List of Publications

I Review article: "*Mesenchymal Stem Cells Relevance in Multicellular Bioengineered 3D In vitro Tumor Models".* Manuscript Published doi: 10.1002/biot.201700079. Page **14**.

II Review article: *"Globe-like Scaffolds for Assembly of 3D Tumor Spheroids - Advances and Prospects"*. Manuscript in preparation. Page **47**.

III Article: *"Bioinstructive Microparticles for Self-Assembly of Mesenchymal Stem Cell 3D Tumor Spheroid Hybrids"*. Manuscript in preparation. Page **92**.

1. Introduction

1.1. The Reality of Lung Cancer Incidence and Current Therapies

Malignant Neoplasia derived conditions represent the second leading cause of dead in developed countries, being only surpassed by heart disease related mortality[2]. Cancer mortality accounts for 13% of global deaths [3], with lung cancer representing the leading cause of cancer related mortality worldwide [2,4,5]. Lung cancer related disorders present themselves in two major forms: (i) non-small-cell lung cancer (NSCLC), the most prevalent, and (ii) small-cell lung cancer (SCLC), extremely rare in non-smokers [6]. NSCLC represents more than 80% of lung cancer cases, having a predicted 5-years survival rate of 15.9%, that has seen minimal improvements over the last decades [7].

Lung cancer and NSCLC compose a heterogenous group of conditions which are still poorly understood from both a molecular and cellular point of view [8], with most cases of NSCLC being diagnosed in advanced stages. Even if caught up early, a poor long-term prognosis can be expected [2] due to a lack of effective targeted therapies for each presentation, resulting from differences both at an: **(i)** histological level (e.g. adenocarcinoma, squamous cell carcinoma, and large-cell lung cancer), **(ii)** genetic level (e.g. squamous-cell carcinoma and adenocarcinoma exhibit diverse frequencies in EGFR amplification, KRAS mutation, BRAF mutation), **(iii)** epigenetic level (e.g. methylation of p16 and FHIT genes in premalignant squamous-cell carcinoma, which rarely occurs in adenocarcinoma), and at the **(iv)** tumor microenvironment level (e.g. presence of supporting stroma cells and ECM) [8–10].

Discovery and approval of new therapeutics for lung and other cancers is a challenging task with research costs surpassing the 1 billion dollar mark per drug [11,12], and taking approximately 10-12 years per compound for approval to be reached by regulatory agencies (e.g., FDA and EMA). A part from this, during pre-clinical drug validation stages patients are also exposed to treatments for which effectiveness and severity of side effects are yet to be determined [3,13]. Targeted therapies for lung cancer, such as monoclonal antibodies, evidence the highest success rate for achieving approval from the regulatory agencies with 14 % of candidate therapies attaining marketing approval and clinical use [14].Furthermore, novel therapy combination targeting both cancer cells and TME signaling provides new improved treatment option. Examples of such therapies include

the combination of MET inhibitors (e.g. tivantinib) with tyrosine kinase inhibitors (e.g. erlotinib a EGFR receptor inhibitor), or with anti-angiogenesis compounds (e.g. ramucirumab a VEGF receptor inhibitors) [15]. Although presenting a chance for improved therapy, these combinations also come with increased potential risk of adverse side-effects. Increasing the chances of therapy rejection and limiting therapy success

The efficiency and safety of chemotherapeutics for lung cancer treatment is undermined mainly by the appearance of multidrug-resistant cancer populations, by the establishment of distant metastasis, or by the onset of severe therapy associated side effects, which ultimately lead to a halt in treatment [16]. Resistance to therapy can only be solved through combinatorial chemotherapy or radiotherapy regiments, which although more effective in cancer ablation, present an increased risk to patients general health status [17]. The acquisition of cancer resistance can occur through mutations in single cancer cells [16], or in as a by-product of complex micro-evolutive process and communications established between cancer cells and the unique tumor microenvironment [18]. In the following section the general components of the tumor microenvironment and their influence in disease progression will be discussed in the context of general

1.2. Tumor Microenvironment – Hallmarks and Heterogenic Components

The transformation of a normal human cell to that bearing a malignant phenotype is generally beset by several hallmarks that cells acquire through accumulation of consecutive genetic alterations, alongside with an active crosstalk with the microenvironment, during a micro-evolutionary process known as Tumorigenesis [19]. These hallmarks are mainly the: (i) capability of providing sustained proliferative signaling cues; (ii) evading growth suppression; (iii) resistance to apoptosis and cell cycle arrest, for example via p53 silencing through MDM2 and MDMX action [20], or loss of function due to mutation [21]; (iv) enabling replicative immortality, for example through overexpression of telomerase; (v) induction of angiogenesis; and eventually (vi) acquisition of invasive and metastatic potential through the process of epithelial to mesenchymal transition (EMT) [19] and have been extensively discussed in the literature in the last years [22]. Tumor hallmarks acquisition can be both hampered or aided through interactions between cancer cells and the adjacent tumor microenvironment, constituted by the extracellular matrix (ECM), and the

cellular stromal components (e.g., tissue resident cells, recruited cells from the blood) [23,24].

The different tumors identified to date can be grouped in two major categories, namely solid and hematological tumors [25]. Approximately, 90% of all human cancers arise from mutations of epithelial cells, resulting in a tumor mass that is denser than the surrounding tissue and are classified as solid cancers [25,26]. The evolution of these solid cancers is considered to be the end-result of genetic dysregulation in combination with the establishment of a complex set of interactions that take place between heterogeneous cancer cell populations (i.e., cancer cells and cancer stem cells [27]) and the surrounding stromal cellular components of the tumor microenvironment as well as their unique ECM [18,28]. The latter plays a crucial role in disease progression and metastatic processes and a deeper knowledge of its constituents is crucial for the development of more effective cancer treatments.

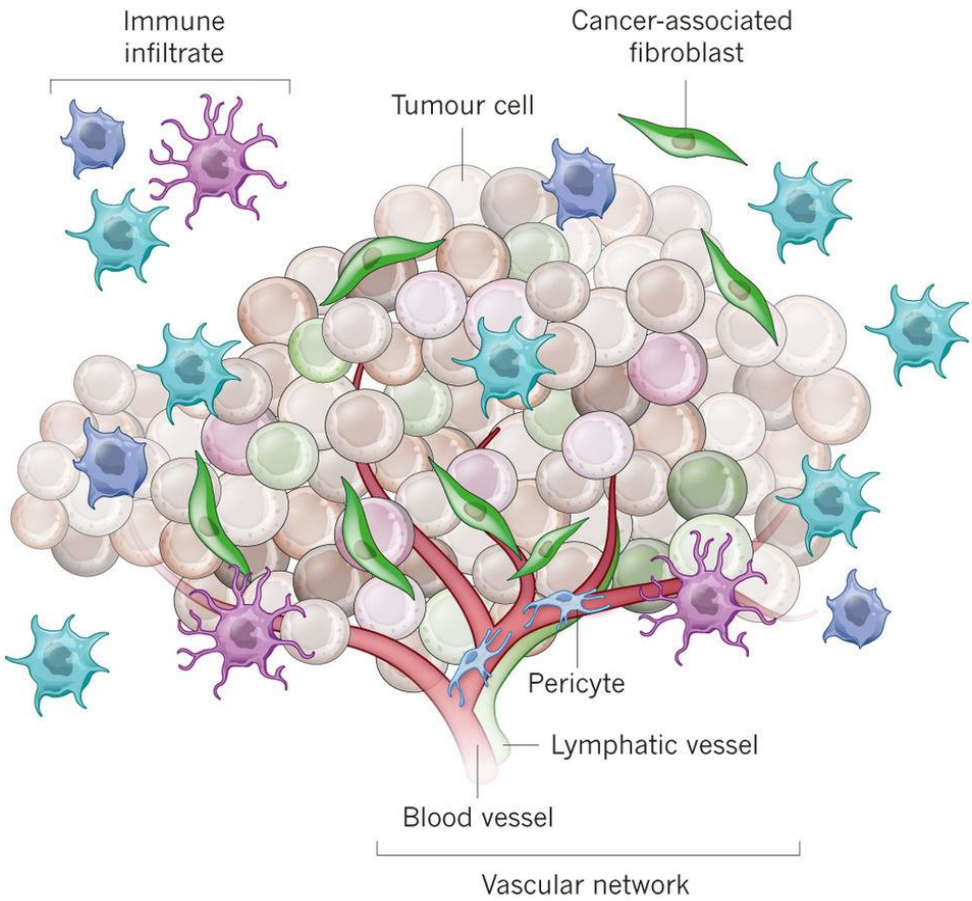

Figure 1. Example of the TME transition from healthy tissue to TME, demonstrating diverse populations present in the process of cancer evolution.

In normal tissues, the extracellular matrix (ECM) is mainly comprised by fibronectin, collagens (e.g., fibrillar and non-fibrilar collagens with types I-V being the most common), elastins, fibrilins, fibulins, vitronectin, laminins and other glycoproteins [29]. The ECM is a spatially well defined 3D mesh of structural and signaling macromolecules that interact with cells via specific matrix imbedded signaling ligands such integrin-binding RGD motifs and heparin-binding domains [30,31]. These ligands regulate critical cellular functions such as growth, migration and differentiation [31]. However, this communication is bidirectional, with cells often modifying physical and biomechanical properties of the ECM through matrix deposition or degradation through the enzymatic action of matrix metalloproteinases (MMPs) [32]. In cancer these and other matrix remodeling enzymes, such as lysyl oxydases [33] responsible for collagen cross-linking or hyaluronidases [34] responsible for the degradation of hyaluronic acid, are often found to be upregulated and are produced both by cancer and cancer-associated stromal cells [32]. Examples of these effectors are MMP-9, MMP-2 and a wide range of integrins (e.g. α6β4 and αvβ3 [35,36]) for which overexpression is considered as an hallmark of increased cancer motility [36]. ECM degradation can originate the release of latent bound growth factors and cytokines, such as epidermal growth factor (EGF), vascular endothelial growth factor (VEGF) and tumor necrosis factor alpha (TNF-α), all of which influence cancer cells proliferation and survival within the tumor microenvironment *via* either paracrine, or juxtracrine signaling [37]. It is important to underline that such biomolecules also induce persistent inflammation, an important aspect since inflammation supports cancer progression for example in the regards of angiogenesis [38]. In fact, due to underlying tissue inflammation, cancer associated fibroblasts (CAF) and stromal associated fibroblasts (SAF) produce copious amounts of collagen type I, III and IV in ovarian cancer, as well as different growth factors that promote tumor growth (e.g. TGF-β, PDGF). Alongside, in the TME there is a clear overexpression of lysyl oxidase (LOX) , an enzyme that induces collagen crosslinking thus contributing for an increase in ECM stiffness [39].

Besides its integral role in cancer progression, the ECM also plays a crucial part in modulating cancer cells response to commonly administered cancer chemotherapeutics (e.g., paclitaxel, doxorubicin, cisplatin), acting firstly as a physical barrier hindering drugs diffusion into the tumor, and secondly as a promoter of multidrug resistance phenotypes in cancer cells [18]. This is evident when cancer cells come in contact with hyaluran rich ECM

regions, for which the main receptors are CD44 and RAMM both overexpress in cancer cells, promoting immune system evasion through CD44 upregulation in cancer cells accompanied resulting metabolic changes [40].

Another major hallmark of the TME is its diversity in cellular components and cellular crosstalk. These surrounding populations play a significant role in tumor progression and metastasis including: (i) vascular endothelial cells, (ii) pericytes, (iii) adipocytes, (iv) fibroblasts, (v) immune cells, (vi) cancer associated fibroblasts (CAF), and (vii) mesenchymal stem cells (MSCs), also known as tumor associated mesenchymal stem cells (TA-MSCs). All these cells play significant roles in sustaining cancer cells proliferation and resistance to treatment. The exact interactions of each stromal cell type with cancer cells, their crosstalk via soluble and insoluble mediators has been recently reviewed elsewhere [39,41–44] . Yet, it is important to emphasize that despite the general knowledge of the TME, each tumor type is comprised by its unique microenvironment according to tissue specific characteristics.

1.3. Non-small Cell Lung Cancer Tumor Microenvironment Cellular Landscape

Lung cancer tumor microenvironment exact constitution is not yet fully characterized. Akin to other cancers, the lung TME is characterized at a cellular level by the presence of: (i) immune cells such as tumor associated macrophages (TAMs), natural killer cells (NK), cytotoxic and regulatory T lymphocytes, tumor associated neutrophils, myeloid-derived suppressor cells (MDSC) [45,46,1]; (ii) stromal associated cells such as fibroblast and cancer associated fibroblasts (CAFs) which are some of the main contributors to ECM dynamic modification via protein deposition and degradation [47–49]; (iii) stem like cells such as bone-marrow derived mesenchymal stem cells (BM-MSCs) [50], or adipose tissue derived stem cells (AD-MSCs) [51], which play a paramount role in cancer progression, invasion, metastasis and resistance acquisition [50]; and (iv) vascular cells such as endothelial cells, and pericytes, both of them paramount in the process of angiogenesis [52]. All together these diverse cellular populations establish, as previously discussed an intricate network of interactions, such as depicted in figure X, that can either bolster or hinder cancer progression.

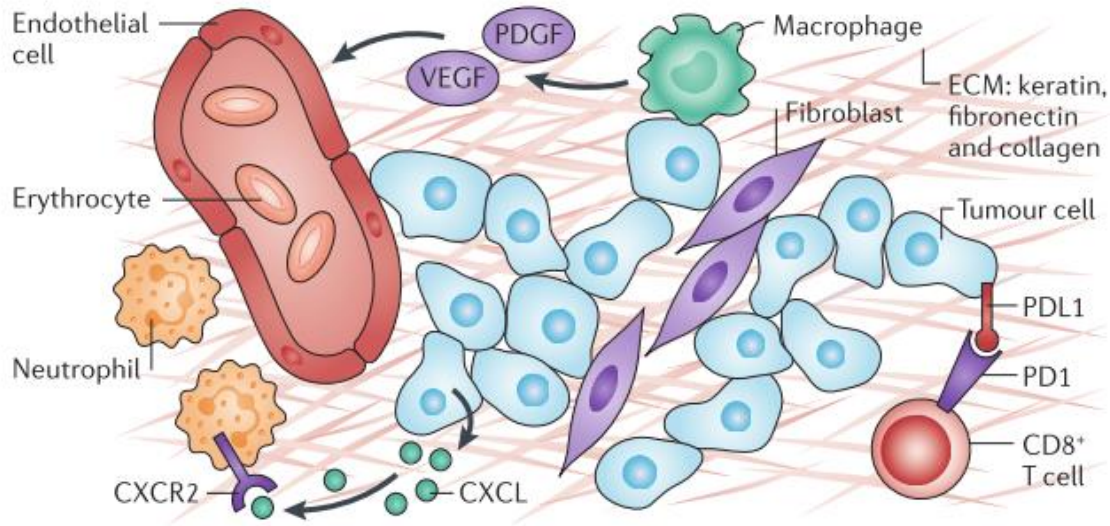

Figure 2. Schematic representation of lung tumor microenvironment. The onset of tumor progression can lead to the recruitment of several diverse cellular populations such as MSCs or cells of the immune system for example through the action of CXCL chemokines, recognized by CXCR2 receptors on the surface of both cell types [53,54]. Upon establishing themselves in the TME the various cells initiate a process of communication, forming a complex weave of interactions that can lead for example to immune suppression either directly through interaction of T cells with PDL1 overexpressed ligands on tumor cells surface, or indirectly through the release of PDGF and VEGF by either Macrophages or associated MSCs and CAFs. In all, diverse populations can either act favoring specific processes of cancer progression such as CAFs and Macrophages interactions with endothelial and other vasculature related cells, or hinder them [55,56]. depending on the type of cells and respective interactions that are established [57]. Image adapted from Chen and coworkers 2015 [9].

1.3.1. The role of immune system cells in Lung Tumor Microenvironment

At initial stages of tumor development the TME recruits several immune cells, through the release of several factors namely chemokines, cytokines, pro-inflammatory factors, (figure 2) recruiting for example neutrophils through the release of compounds of the CXCL family, particularly CXCR2, during the process of angiogenesis [9]. The tumor immune microenvironment initially acts as an anti-tumoral force, cells of the immune system acting to detect and destroy tumors, namely through the actions of effector T cells, mature dendritic cells or natural killer cells [1], leading to processes of inflammation and delaying cancer proliferation. However, due to the nature of the communications established between immune cells, cancer cells and other cells of the TME, this role can ultimately be thwarted [1].

The ability to manipulate surrounding cells provides to tumors one of their greatest advantages, allowing the disease to adapt to treatment and evade host endogenous immune system defenses [18,58]. While currently non-small cell lung cancer therapies mainly focus

on the central driver mutations suffered by cancer cells, such as BRAF [59], KRAS [60], EGFR [61], HER2 [62] and MET [62] mutations, novel therapies targeting the lung TME are emerging. Among these therapies, those based on the administration of anti-angiogenic compounds such as Bevacizumab® [63], a monoclonal antibody that targets VEGF, or therapies based in cellular targeting to the TME. Regarding this methodology, MSCs due to their natural tropism for the TME, hold great promise, being transduced for example with interleukin-24 (IL-24) [64] or genetically modified with oncolytic adenoviruses [65], which respectively have been shown to exert anti-angiogenic, and inhibitory effects on the growth of lung tumors both *in vitro* and *in vivo*. The combination of TME targeting therapies with conventional anti-tumoral compounds is already started to be implemented [15], providing treatment regiments that might benefit the majority of populations suffering from NSCLC, for which the survivability rate is currently 15 % at 5 years [66,67]. Contributions by the TME towards the progression or inhibition of cancer tumorigenesis and metastasis processes are thus a theme of increasing debate and recognition, with recent findings promising to uncover novel therapeutic targets [9,1].

Depending on cancer development stage, the type of cancer, the origin of cancer cells (e.g., breast, prostate, colon, pancreas, lung), the immune populations found on the TME will vary, with for example tumor associated macrophages (TAM) exhibiting two functional phenotypes, a pro-tumorigenic M2 (TAM-M2), and another normally considered anti-tumorigenic M1 (TAM-M1) (Figure 3) This heterogeneity in tumor infiltrated immune cells is crucial for disease progression/metastasis and for the final treatment outcome. A recent study by Almatroodi and coworkers has further characterized TAMs M1 and M2 populations in patients with NSCLC of diverse histological classifications, adenocarcinoma (ADC), squamous cell carcinoma (SCC), and large cell carcinoma (LCC). The findings indicate an increase in M2 populations in all NSCLC classes, however the expression of inducible isoform of nitric oxide synthase iNOS (a biomarker for M1 TAMs), was heterogenous and dependent on the type of cancer, being decreased in patients with ADC or SCC, but not in patients with LCC NSCLC [68]. From the available studies it is clear that tumors with distinct genetic mutations present diversity in immune infiltrates, with regard to cell type and phenotype [9]. Apart from immune cells other cellular stromal components play a significant role in disease progression and treatment resistance.

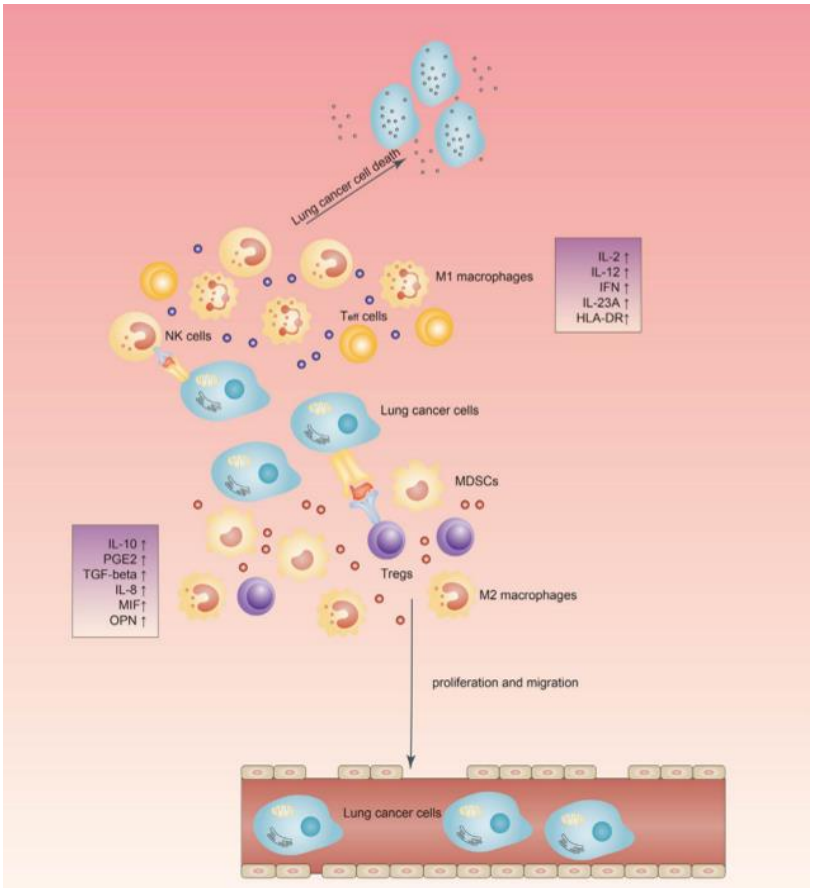

Figure 3. Diversity of responses obtained from the immune microenvironment of Lung cancer can lead to enhancement of drug efficiency in NSCLC through the actions of specific cells such as NK cells, T effective cells and M1 macrophages releasing proinflammatory cytokines such as IL-2, IL12, IL-23A and others. Conversely the immune microenvironment can also hinder treatment leading to promoting of lung cancer progression and invasion, has happens through the interactions of Treg-cells, M2 macrophages and associated anti-inflammatory cytokines and signaling factors such as IL-10 and TGF-β. Image adapted from Wang, and coworkers, 2017 [1]

1.3.2. The role of Cancer Associated Fibroblasts (CAFs)

Cancer associated fibroblasts (CAFs) are one the main cellular components of NSCLC stroma. The mechanism involved in their establishment is still to be fully uncovered however they are known to arise from normal two main precursors: (i) fibroblasts or (ii) MSCs either from bone or adipose tissue [42,69]. The latter migrate from the bone-marrow differentiating firstly to myofibroblasts and afterwards to CAFs within the tumor environment. TA-MSCs establish an intricate communication with malignant cells and their pivotal will be further discussed in the following chapters [70–72]. Adding to this, various reports demonstrate that normal fibroblasts alter their phenotype during NSCLC disease progression to become CAFs. [70]

CAFs assume a central role in malignant disease as they are known to promote tumor growth, fuel invasion and support metastasis, being actively involved in ECM deposition and degradation by secreting high levels of proteases (e.g., MMP-2 and MMP-9), that degrade the matrix and release entrapped soluble mediators [9]. They are also known to secret an elevated number of pro-metastatic factors such as TGF-β, HGF, SDF-1 amongst others. In the lung TME CAFs are at the forefront of cancer-stromal cell interactions, often altering protein expression patterns in lung cancer cells increasing the expression of several integrins, and anti-apoptotic proteins (e.g., Bcl-2) by means of TGF-β secretion [72]. Another end-result from such intricate crosstalk is the establishment of a collagen and keratin enriched ECM, a major hallmark of lung squamous cell carcinomas, and of fibronectin fibers deposition in desmoplastic lung adenocarcinomas [9]. From a biological perspective CAFs are characterized by the overexpression of alpha smooth-muscle actin (α-SMA) and fibroblast activation protein (FAP) [73], and the down-regulation of cell cycle arrest and tumor suppressor genes such as p53, the so termed guardian of the genome [70,74], making them readily identifiable and aiding in disease prognosis.

1.3.3. The role of Vascular Cells

The pulmonary tissues in which non-small cell lung cancers develop are generally well irrigated by an intricate and all-encompassing vascular network. As such, not all cases of NSCLC demonstrate pro-angiogenic features, with tumors taking advantage of the pre-existing vasculature and presenting a more invasive phenotype [75]. However, as previously referred, as a consequence of uncontrolled cancer cells proliferation, conditions for hypoxia are soon established at the tumor core [76]. Hypoxia in conjunction with the actions by other cells, such as degradation of ECM and release of pro-angiogenic factors by immune cells [77], promote the formation of new vasculature, for which two of the main structural contributors in the TME are endothelial cells and pericytes [52]. The presence of these cells has been correlated with angiogenesis and metastasis [52]. In various animal studies, it has been demonstrated that lung cancer TME's uncappable of recruiting pericytes to aid in angiogenesis on the latter stages of hypoxic core development, develop unbalanced pericyte-endothelial communication that resulted in deficient perivascular ECM deposition patterns and leakier vasculature formation, enhancing hypoxic conditions and promoting an increase in lung metastasis [78,79]. However, pericyte depletion in non-hypoxic tumors was found to suppress angiogenesis diminishing tumor growth and preventing metastasis [78]. In NSCLC

the level of angiogenesis is considered as an unfavorable prognostic [80]. This pathological angiogenesis results from the enrichment of the TME with growth and transcription factors such as Hypoxia-inducible factor 1-alpha (HIF-1α), released in low oxygen conditions, and known to up-regulate angiogenesis process's and of glycolysis in involving cells [76]. These factors are released by several cells of the TME besides cancer cells, such as myeloid cells known for secreting VEGF, bFGF, and PDGF which contribute for vasculature remodeling [77]. This recruitment of endothelial cells and pericytes leads to the formation of novel vasculature that supports tumor growth and metastasis [77].

In addition to the above mentioned stromal elements, MSCs are receiving an increased attention due to their diverse influence in the TME. In fact, as it will be discussed MSCs are involved and responsible for numerous aspects of malignant disease spanning from: (i) TME-associated immune system cells regulation; (ii) ECM modification; (iii) establishment of CAFs and (iv) sustainment of epithelial to mesenchymal transition in cancer cells. Such diverse effects in cancer add on to the motivation of further exploring the role of MSCs in cancer. In the following chapter the role of MSCs in cancer will be discussed in light of recent reports regarding MSCs interactions with cancer and stromal cells in the TME.

1.4. Mesenchymal Stem Cells Relevance in Multicellular Bioengineered 3D *In vitro* Tumor Models

Subchapter 1.4.

This subchapter is based on the review article entitled

"*Mesenchymal Stem Cells Relevance in Multicellular Bioengineered 3D In vitro Tumor Models*"

(Manuscript Published doi: 10.1002/biot.201700079)

Mesenchymal Stem Cells Relevance in Multicellular Bioengineered 3D In vitro Tumor Models

Luís P. Ferreira[1] , Vítor M. Gaspar[1], Rui Henrique[2,3,4], Carmen Jerónimo[2], João F. Mano[1]

[1]Department of Chemistry, CICECO, University of Aveiro, Campus Universitário de Santiago, 3810-193, Aveiro, Portugal

[2]Cancer Biology and Epigenetics Group, IPO Porto Research Center (CI-IPOP), Portuguese Oncology Institute of Porto (IPO Porto)

[3]Department of Pathology, Portuguese Oncology Institute of Porto (IPO Porto)

[4]Department of Pathology and Molecular Immunology, Institute of Biomedical Sciences Abel Salazar (ICBAS), University of Porto

[#]Corresponding author:
Professor João F. Mano
Department of Chemistry, CICECO – Aveiro Institute of Materials
University of Aveiro, Campus Universitário de Santiago
3810-193, Aveiro, Portugal
E-mail: jmano@ua.pt
Telephone: +351 234370733

Abstract

In vitro 3D tumor microenvironment mimicking models are gathering momentum as alternatives to traditional 2D flat monolayer cultures due to their potential for recapitulating major cancer hallmarks. To fulfill such potential, it is crucial that 3D tumor testing platforms completely emulate *in vitro* the complex *in vivo* tumor niche and its cellular constituents. Mesenchymal stem cells (MSCs) are recognized to play a pivotal multi-modulatory role in cancer, generating interest as biological targets and as key tumor suppressing, or tumor promoting effectors. This review discusses the biological influence of different types of MSCs in the tumor microenvironment and showcases recent studies that engineer 3D MSCs-cancer cells co-cultures as advanced *in vitro* therapy testing platforms. A special focus is given to MSCs-Cancer 3D co-culture set-up parameters, challenges, and future opportunities. Understanding cancer-MSCs crosstalk and their underlying effects is envisioned to support the development of advanced 3D *in vitro* disease models for discovery of forefront cancer treatments

Keywords: 3D Models, Co-culture, Drug Testing, *In vitro* Tumors, Mesenchymal Stem cells

1 Introduction

In vitro pre-clinical cancer models are mainly based on the use of 2D cancer cell monolayers and laboratory animal models [1,2]. Historically, both methodologies have been recommended by regulatory agencies to aid in the discovery and validation of anti-cancer therapies that are to be administered in human clinical trials [1,3]. However, while these platforms have contributed immensely to explore cancer development and biomarkers discovery, they are still inadequate approximations of human tumors [4,5].

Particularly, in 2D *in vitro* flat and monotypic cell culture models, cancer cells experience highly artificial environments often comprised of plastic or glass cell-adhesive surfaces, forcing cells to grow in an environment which lacks major extracellular matrix (ECM) and stromal cell components [6]. As a consequence, cultured cancer cells are exposed to an unnatural 2D spatial organization and non-physiological conditions, presenting a higher area of exchange with cell culture media in comparison to what naturally occurs in 3D tissues *in vivo* [6]. Such results in an abnormal morphology, loss of structural organization and cell polarization, with lower cell adhesion occurring for example due to loss of integrin-ECM interactions [7]. Therefore, cells phenotype and their response to different treatments is not representative of complex human tumors, thus creating a gap between *in vitro/in vivo* data correlation.

On the other hand, despite animal models constitute a more laborious and economically demanding alternative, they are more representative of the *in vivo* scenario than conventional 2D *in vitro* cell cultures [8]. A significant number of early stage preclinical *in vivo* drug screening studies are performed in small animal murine models. However, these often lack a correct representation of the tumor stroma and present expression variances in the structural homology of molecular targets, which can result in highly variable therapeutic responses [8–11]. Such variability is somewhat detrimental for the validation of candidate anti-cancer therapeutics and particularly limiting in the case of combinatorial cancer therapies high-throughput screening. Such treatment modality demands a higher level of reproducibility and predictability of safety/efficacy parameters as the cocktails of bioactive molecules could trigger a wide range of biological responses (e.g., additive toxicity, antagonism). The use of *in vivo* models in the context of combinatorial anti-cancer therapies entails significant ethical concerns due to the large number of test groups, not easily allowing high-throughput screening of different combinations. In addition, the correlation between *in*

vivo animal studies and human clinical trials is very limited, thus evidencing the necessity of developing more realistic testing platforms that can provide robust preclinical data [8,9,12].

Hence, the development of *in vivo*-mimicking, and reproducible preclinical *in vitro* validation models to efficiently predict the biological performance of anti-cancer therapies may contribute to increase the translation speed of novel therapies from the bench-to-bedside. The bioengineering of such models must be based on similarities to human biology and disease specific features, so as to ensure higher predictability of preclinical research and exclude non-adequate anti-cancer therapeutic candidates prior to human clinical trials [3,13].

The demand for understanding cancer development and develop more advanced treatments has resulted on a growing number of studies exploring the potential of advanced three-dimensional (3D) tumor models as more viable testing platforms. 3D multicellular tumor models are generally self-assembled compact cellular agglomerates that may be cultured *in vitro* during relatively short or prolonged periods of time using different techniques that include hanging drop, bioreactors or organ-on-a-chip platforms [14,15]. Such platforms try to incorporate the spatial complexity, cellular heterogeneity, nutrient/pH characteristic of the *in vivo* tumor microenvironment [14]. In this context various types of malignant cells were shown to possess gene expression patterns and phenotypes similar to those encountered *in vivo* when cultured in 3D [16]. Such evidence is an added-value to these models, since on one hand they provide the desired spatial distribution and on the other they ensure several biological functions found in human cancers [17].

This review summarizes the recent advances made in the field of 3D *in vitro* multicellular tumor models that more closely recapitulate the tumor microenvironment and its diverse components by including co-cultured cancer-stromal cells, including mesenchymal stem cells (MSCs). MSCs are now well-recognized to take multi-modal roles in oncological disease progression and metastasis, for which depending on MSCs tissue of origin and the type of tumor, they either play a beneficial or detrimental role [18]. This interesting duality is discussed considering the most recent literature reports and a critical perspective is given towards the development of MSCs-Cancer 3D *in vitro* co-culture tumor models.

2 The Dual Role of Mesenchymal Stem Cells in the Heterogeneous 3D Tumor Microenvironment

Mesenchymal stem cells (MSC) otherwise also known as multipotent mesenchymal stromal cells, were first described as fibroblast-like cells, about 50 years ago [19]. They are a subset of multipotent precursor stromal cells, with fibroblast-like morphology. MSCs represent a cell sub-population that can be found residing in the mesenchyme of a wide variety of tissues, including: (i) umbilical cord Wharton jelly, (ii) placenta, (iii) peripheral and fetal blood, (iv) adipose tissues (generally defined as adipose-derived stem cells (AT-MSCs)), (v) skeletal muscle, (vi) heart, (vii) liver, (viii) lung tissues and(iv) bone marrow [20]. Constituting a heterogeneous cellular population, MSCs have diverse morphologies, and are commonly identified through specific cell surface markers. Under the guidelines issued by the International Society of Cellular Therapy, MSCs in *in vitro* cultures must be able to adhere to plastic treated surfaces in standard tissue culture conditions; with more than 95% of the population expressing CD105, CD90, CD73, and with less than 2% presenting positive CD45, CD14, CD34 or CD11b, CD79a or CD19 and major histocompatibility complex II (MHC-II) markers. Besides this, *in vitro* cultured MSCs must also show multilineage differentiation capacity. MSCs traditionally differentiate into chondrocytes, adipocytes and osteoblastic lineages under controlled *in vitro* differentiating conditions [21]. A small sub-population of bone-marrow derived MSCs may still be negative for CD44, CD45, MHC I, MHC II and c-kit, displaying the capacity to differentiate as well into nerve, pancreas and lung cells under certain culture conditions [22].

MSCs are reported to exhibit immunosuppressive and immunomodulatory properties [23], as well as being able to migrate and induce modifications in damaged or inflamed tissues [24].These abilities are normally explored under the context of cell-based therapies for tissue repair and regeneration, either via direct cell-cell contact or by means of paracrine signaling [24]. MSCs are also described to have high tumor tropism, a process that is generally mediated by chemokines and growth factors [25]. Upon migrating into the tumor microenvironment (TME) and establishing contact with this complex, MSCs can be hijacked by cancer cells, either through cell-cell or paracrine interactions, leading to either beneficial or detrimental roles in the evolution of cancer [26]. For instance, MSCs recruited to the TME of breast cancers have shown to possess increased secretion of neovascularization and epithelial-mesenchymal transition (EMT) promoting factors, such as Notch1 and TGF-β1,

thus promoting tumor growth and metastasis [27–29]. Positive interactions between cancer cells and MSCs are not restricted to a specific phenotype of MSCs. For example, umbilical cord derived MSCs have shown to greatly increase cholangiocarcinoma proliferation, migration and resistance (Figure 1) [30]. MSCs can also indirectly aid the evolution of cancer by regulating the activity of other TME cells [25]. For example, breast cancer-associated bone-marrow MSCs (BM-MSCs) are known to increase the frequency of regulatory T cells, and decreasing the lysis activity of natural killer cells and cytotoxic T lymphocytes by the secretion of TGF-β1, resulting in a poorer prognosis due to unchecked tumor progression [30,31].

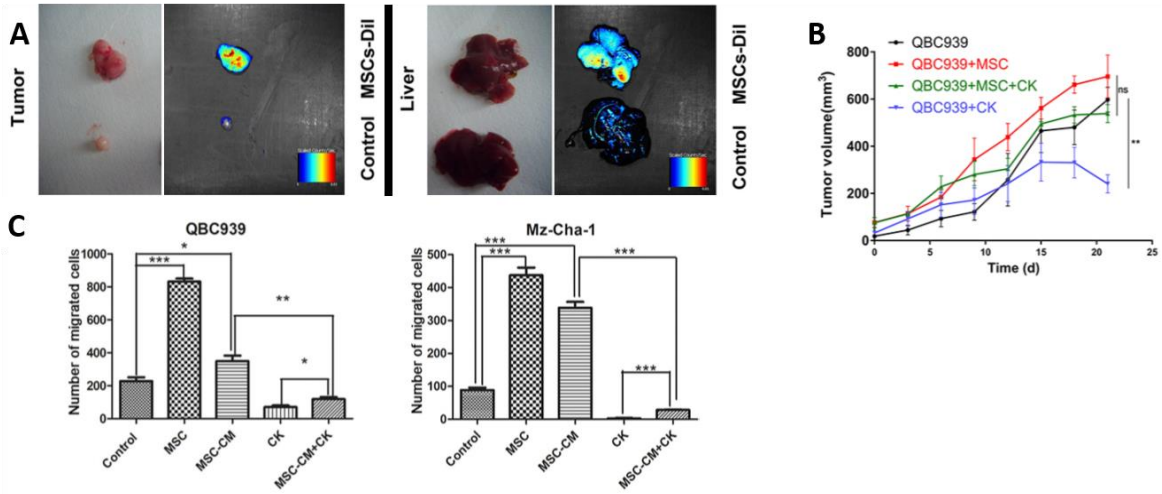

Figure 1.. Human umbilical cord-derived mesenchymal stem cells interactions with human cholangiocarcinoma cell lines using a xenograft model and invasion assays. (A) MSCs capacity to migrate to the tumor site *in vivo*; (B) Increased growth of QBC939 cell line derived tumors; (C-E) increased resistance both *in vitro* and *in vivo* to the effects of the anti-cancer drug compound K, translated into higher rates of cell migration and cancer cell survival. Adapted from [119], with permission from Oncotarget under creative commons 3.0 license.

Contrariwise, MSCs have also been reported to exert anti-tumor effects [32], with several studies having demonstrated the role of MSCs in increasing the growth and metastasis of tumors [18,33]. In an elegant a study performed by Quiao and co-workers, 2008, MSCs derived from fetal dermal tissue where shown to inhibit the proliferation of two human hepatocarcinoma cell lines (H7402, HepG2), when co-cultured [34]. Such resulted in an increased apoptosis for H7402 cells via the down regulation of the Wnt/β-catenin pathway as proposed by these researchers [34].

Interestingly, it is important to emphasize that this effect is closely correlated with MSCs tissue of origin (Figure 2). As reported by Attar-Schneider *et al*, 2015, BM-MSCs can

reduce both cellular proliferation, viability and migration of non-small lung cancer cells as a result of the down regulation of translation initiation factors and mitogen-activated protein kinases (MAPK) signaling [35]. However, the same is not true for Wharton jelly-derived MSCs which show antagonistic effects to those portrayed by BM-MSCs in lung cancer stem cells (L-CSCs), acting in a pro-tumorigenic manner [32]. Conversely, conditioned media derived from human fetal MSCs showed high levels of insulin growth factor binding proteins (IGFBP), which when used in hepatocellular carcinoma cell culture, ends up sequestering free IGF, inhibiting cancer cell proliferation [36]. Due to this anti-proliferative potential, MSCs have been proposed to be used as Trojan-horse like vehicles for anti-cancer therapy by taking advantage of their tropism towards cancer cells [37]. By exploiting this feature, TREAT-ME1, the first worldwide clinical trial exploring the use of Herpes simplex virus genetically engineered MSCs for treatment of gastrointestinal tumors via RANTES/CCL5-ganciclovir prodrug therapy combination [25]. However, the lack of knowledge on how MSCs behave within the TME means that patients undergoing these treatments must be carefully monitored. Thus, understanding how MSCs from different tissue origins affect, and are affected, by tumors is of paramount importance for future therapeutic applications (Figure 2).

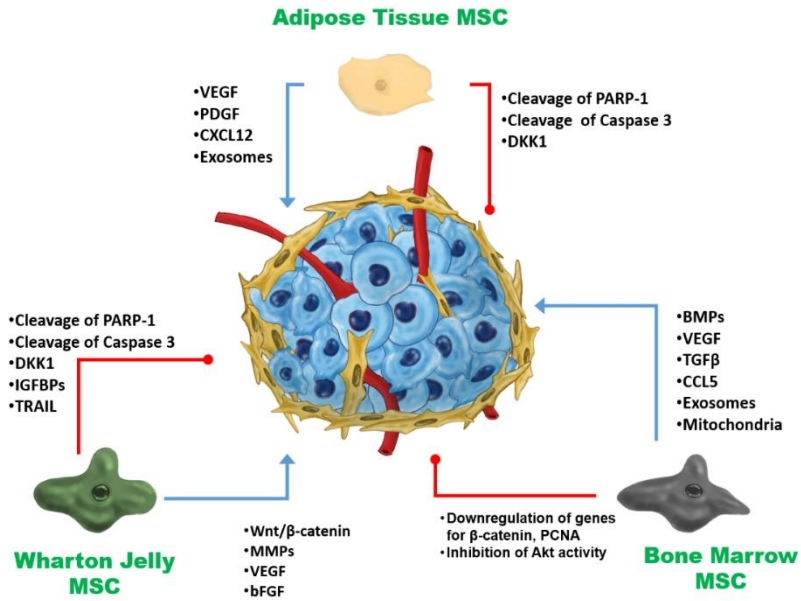

Figure 2. MSCs-cancer cell interaction is dependent on tissue of origin. MSCs can release several factors which can hinder or promote tumor progression at several levels. (red dots – tumor inhibition; blue arrows – tumor progression).

2.1. MSCs Tropism towards the Tumor Microenvironment

Mesenchymal stromal cells interactions with cancer cells and the tumor microenvironment result in part from the similarities existent between the TME and those of a regenerating wound [18]. Generally, the TME continuously produces and releases various cytokines and other signaling mediators, that act as chemoattractants for several immune cells such as monocytes, T lymphocytes and mast cells. This establishes the grounds for a perpetual state of inflammation in the surrounding tissues [38,39]. Such signals derived from the tumor microenvironment, include: VEGF, TGF-β1, EGF, HGF, bFGF, PDGF, IL-8, neurotrophin-3, IL-1β, TNF-α, monocyte chemoattractant protein-1 (MCP-1 or CCL2), and C-X-C motif chemokine ligand 12 (CXCL12) also known as stromal cell-derived factor 1 (SDF-1) which act as homing beacons on various cells including MSCs which exhibit the capacity to accurately migrate via chemotaxis [33]. This tumor tropism towards primary and metastatic tumor sites by MSCs has been extensively observed both *in vivo* and *in vitro* in numerous cancers, such as those of breast, brain, colon, pancreas, skin, ovarian, and lung, and is characterized by MSCs infiltration [26,33]. The extent of MSCs migration appears to be directly influenced by the extent of chemoattractant signals released by the TME. Recent reports emphasize that factors such as increased inflammation, hypoxia and cell dead (related or not to tumor treatment), increase MSCs migration to tumor tissues [30]. Such event is for example observed in radiotherapy treated breast cancer, which results in an increased release of release of TGF-β1 and platelet-derived growth factor BB (PDGF-BB) by tumor cells [40]. The underlying mechanism responsible for the tumor-directed migratory capacity of MSCs remains however to be fully uncovered. This is a crucial piece of information that must be explored in the future, before MSCs-based treatments can be translated into clinical practice. [26].

2.2. MSCs conversion to Tumor-associated MSCs – Role in Progression and Metastasis

Upon infiltrating on the TME, MSCs are converted into tumor-associated mesenchymal stem cells (TA-MSCs) (Figure 3). Depending on their original tissue, and on the type of cancer, TA-MSCs are known to acquire gene-expression profiles that exhibit increased secretion of tumor promoting factors [41]. TA-MSCs populations have been reported to increase the population of cancer stem cells (CSCs), and induce malignant cells to enter EMT, thereby promoting enhanced motility, invasiveness and survival [41]. In turn, this can induce a refractory profile in the tumor, a factor that can lead to the establishment

of metastasis [42]. TA-MSCs have been found to engage in multiple interactions with cancer cells [41]; besides paracrine signaling, communication has also been achieved through the exchange of exosome cell-derived vesicles [43], mitochondria [44] and also cell membrane components [45]. Interestingly, these interactions have been reported to occur in a bidirectional mode. It is important to emphasize that the effects of the exchanged molecules vary with the type of cancer and MSCs population [25]. As previously stated, EMT requires the formation of a reactive stroma, capable of secreting specific EMT-inducing factors and rearranging the surrounding tumor-specific ECM. Various factors that promote the appearance of this reactive stroma such as fibroblast growth factor (FGF), hepatocyte growth factor (HGF), epidermal growth factor (EGF) are produced by MSCs upon impregnation into the tumor niche [33,46]. Some studies point out that this conversion from regular MSCs to TA-MSCs can also be performed *in vitro* through 2D co-culture of TA-MSCs with MSCs, indicating that naive MSC conversion can be augmented once in vicinity of the TME [41].

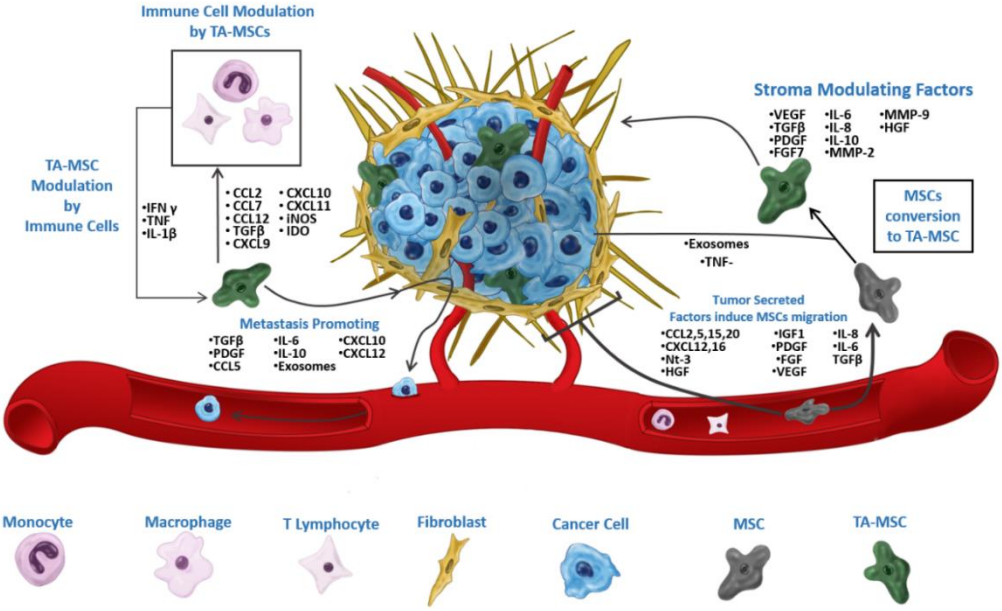

Figure 3. MSC migrate towards the tumor, with different mechanism playing major roles in diverse cancers (Glioblastoma -CCL2 and CCL25) (Hepatocarcinoma - CCL15 and CCL20). Migrated MSCs suffer a conversion process, releasing a myriad of factors that aid the tumor by rearranging the surrounding ECM, promoting tumor angiogenesis, proliferation, immune suppression and ultimately EMT and metastasis. 101,102,109,117,123.

Besides directly increasing cancer cells EMT, MSCs also increase vasculogenesis or increase the secretion of growth factors, creating a suitable environment to support disease progression [47,33]. Moreover, as aforementioned, MSCs are capable of modulating the metabolism of cancer cells through the excretion of exosomes generally loaded with

proteins, DNA, and non-coding RNA (ncRNA) [43]. This effect can be particularly seen in the interactions that occur when cancer cells metastasize into the bone-marrow, a process in which MSCs secrete chemoattractant factors recognized by cancer cells [41]. In this fatal alliance between metastatic cancer cells and MSCs, factors such as MCP-1 (CCL2) and SDF-1 (CXCL12) appear to play a key role [26,33]. Once metastasis are established in the marrow, MSCs are hijacked into helping in the creation of a niche that protects the tumor against chemotherapeutic agents [18,25,48].

In summary, several factors affect MSCs-cancer cells interactions and MSCs TME interactions, including: (i) the type and source of MSCs including their different cytokines expression (ii) the interactions with other elements of the TME; and (iv) the *in vitro* and *in vivo* conditions in which MSCs are cultured [49,50]. The nature of these interactions and how they take place, either by direct or indirect interference with cancer cells and surrounding stroma, requires further exploration in the future. With such knowledge holding great promise in the context of new therapies discovery, both at the development level by facilitating the discovery of key therapeutic targets, and at the drug-screening stage by allowing the development of more realistic *in vitro* 3D tumors.

3. *In vitro* 3D Tumor models to test candidate anti-cancer therapies

3D cell cultures of cancer cells take aim to recapitulate *in vitro* the complexity of human cancer allowing for better preclinical analysis of new pharmaceuticals, with the goals of permitting the evaluation of possible side effects, and the collection of meaningful compound behavior data before proceeding to human clinical trials [51]. When successfully engineered, 3D *in vitro* tumor models provide a more robust correlation with the *in vivo* biological performance of candidate compounds [52]. In order to fully mimic human tumors, the ideal *in vitro* 3D cancer culture model should reproduce *in vitro* all the interactions and selective pressures that occur in the human body. Unfortunately, the complexity of this task is tremendous and as such, a balance must be found between the model's capacity to faithfully recreate the TME, while assuring ease of analysis and lowering production costs to efficiently allow high-throughput screening methodologies.

3D models production methodologies extend over a gamut of techniques which can be grouped into: (i) scaffold-free, (ii) scaffold-based and (iii) combinatorial methodologies. Regardless of the production methodology, all these platforms have as a unifying element:

the establishment of 3D multicellular structures, or microtissues, comprised of one or more cell types, either derived from immortalized cancer cells cultures or from patient's primary cells [4,52–54]. 3D cell culture methods, range from monotypic cell line cellular spheroids (single cell type), for instance cultured in non-adherent substrates or through hanging-drop techniques [55], up to complex co-culture systems comprising heterotypic cell lines (e.g., tumor stroma cells including fibroblasts) in a complex tumor ECM-like supporting matrix, or even associated with microfluidic systems for dynamic nutrient perfusion [56].

3D Multicellular tumor spheroids (3D-MCTS) are seen as gold standard bioengineered microtissues for drug screening [57]. 3D-MCTS are generally comprised by an actively proliferating outer cell layer and a necrotic core [58,59]. Moreover, upon aggregation into spherical structures3D-MCTSacquire nutrient, pH, and oxygen gradients ranging from spheroids periphery to their core [59]. These characteristics are in accordance with those of solid tumors with more than 400-600 μm [60] [61]. In these models, the lack of vasculature, similar to that of avascular solid tumors, and the establishment of a compact cell aggregate, hinders the mass transport of nutrients, metabolites and oxygen [59]. Additionally, their 3D nature confers them the ability to portray cell-cell biochemical interactions, tumor gene expression patterns, and even growth kinetics similar to those observed *in vivo* [59]. It has also been reported that 3D-MCTS models promote cancer cells genetic/epigenetic modifications towards a more aggressive, tumorigenic and multi-drug resistant phenotype [62,63]. Apart from these parameters, heterotypic 3D-MCTS (resulting from co-culture of cancer-stromal cells), are able to mimic the deposition of ECM-components similar to those found in solid tumors [57,59,64]. An important parameter, since the ECM-based barrier that hinders O_2 and nutrients mass transfer also restricts the penetration of therapeutic agents in the tumor. The existence of ECM creates a suitable *in vitro* environment for testing and studying new pharmacological therapies and mimics *in vivo* conditions [65]. This correlation, resulting from the incorporation of diverse cell lines, is also observed in scaffold-based models that provide an ECM-mimicking environment without requiring previous cell mediated ECM deposition [64]. The advantages and disadvantages of various 3D models production methodologies have been extensively discussed in several reviews [51,54,56,59,66–71]. These different formulation technologies are addressed herein mainly in the context of heterotypic cancer-MSCs 3D *in vitro* models establishment.

4 Cancer-MSCs Co-culture Relevance in 3D *In vitro* tumor models

Irrespectively of 3D disease models production methodology, heterotypic cell co-cultures comprising cancer-stromal cells provide a better reproduction of the complex tumor microenvironment when compared to monotypic 3D models (comprised by cancer cells alone) [72]. Different bi- or tri- co-culture systems combining cancer cells and stromal cells have thus far been employed for the study of cancer-TME specific interactions and drug screenings [51,54,59].

Recent findings regarding 3D co-culture of cancer-adipose cells, cancer-immune cells, cancer-fibroblasts, cancer-endothelial cells and their physiologically relevant interactions have been reviewed in detail [54]. Stemming from this dual and multiple- cell culture concept, MSCs addition in *in vitro* 3D cancer disease models is still far from being fully explored, particularly when considering their important role in both cancer proliferation and metastasis [73]. In fact, having been found to play such an important role in cancer progression and therapy resistance, MSCs must be considered as key elements in the tumor milieu [41]. As such, their inclusion in *in vitro* 3D tumor models is a necessary step to achieve a more predictive model that closely mimics native *in vivo* conditions. So far, few articles have been published concerning MSCs interactions with cancer cells in *in vitro* 3D co-culture tumor models (Table 1), and their main findings will be addressed in the following sections.

Table 1. Literature reports of co-culture human mesenchymal stem cells with cancer cells in a 3D co-culture environment.

Type of MSC	Cancer Cell Line used	*In vitro* Model		Tested Therapeutics	Ref.
BM-MSC	Human Pancreatic Cancer - MIA-Pa-Ca2	Spheroids (Formed by MIA-PaCa-2 cells, primary fibroblasts, and HUVEC)	Forced Floating 96 multiwell plates with nonadherent round bottom	None	[243]
BM-MSC	Human Breast cancer MCF7 - MDA-MB-231	Spheroids	Forced Floating Wells Coated with 2% GTG agarose without matrix proteins	None	[244]
BM-MSC	Human Breast Cancer - MDA-ICB-3 - MCF-7 - SUM149	Spheroids	Forced Floating Ultra-low attachment Plates	None	[245]
BM-MSC	Human Breast Cancer - MCF-7 - MDA-MB-231	Spheroids	Forced Floating Wells Coated with 2% GTG agarose without matrix proteins	Kinase inhibitors (TKI258, RAD001 and RAF265)	[83]
AM-MSC	Human Ovarian Cancer - OVCAR 3 - SKOV 3	Spheroids / Scaffold	Forced Floating Ultralow attachment 48 well plate and posteriorly cultured in Amniochorionic Membrane containing MSC	None	[246]
BM-MSC	Human Colon Cancer - HT29 - HCT-116	Scaffold	Cell Culture 3D Scaffold from 3D Biotek LLC	None	[247]
AT-MSC	Human Head and Neck Squamous Cell Cancer (HNSCC) - HLaC78	Spheroids	Forced Floating 96-multiwell plates coated with 0.1% agar	None	[118]
BM-MSC	Human Ovarian Cancer - SKOV3 (HTB-77) - OVCAR3 (HTB-161) | Human Breast Cancer MDA-MB231 - MCF7	Spheroids	Forced floating Ultralow attachment 24 well plate	Doxorubicin	[248]
BM-MSC	Human Breast Cancer - MDA-MB-231	Spheroids	Forced floating Wells coated with 2% SeaKem® GTG agarose without MP	None	[249]
BM-MSC	Human Prostate Cancer - LNCaP - C4-2 - PC3	Agitation Based	Rotating Wall Vessel (RWV)	None	[250]
BM-MSC	Human Breast Cancer - MDA-MB-231 | Human Osteosarcoma - MG-63	Scaffold	Silk protein fibroin scaffold	Paclitaxel	[192]
BM-MSC	Human Leukaemia - HL-60 - Kasumi-1 - MV411	Scaffold	PGA/PLLA 90/10 copolymer discs	Doxorubicin or Cytarabine	[251]
PG-MSC	Human Prostate Cancer -LNCaP	Spheroids	Formed either in direct contact or on laminin-coated coverslips	None	[252]

BM-MSC	Human Prostate Cancer - Du145	Spheroids	Forced Floating 96 well plate coated with PHOM	None	[253]
BM-MSC	Human Breast Cancer - MDA-MB-231 - MCF7	Scaffold	Polystyrene particles added to collagen I to form a Gel	None	[103]
BM-MSC	Human Breast Cancer - MDA-MB-231 - MCF7	Scaffold	Porous Scaffold composed nanocrystalline Hydroxyapatite (nHA) and Chitosan	None	[254]
WJ-MSC	Human Hepatic Cancer - HCCLM3	Contained Spheroids	Alginate Beads	Cisplatin	[255]
BM-MSC	Human Colorectal Cancer - HCT8 - DLD1 - Colo320DM - HT29 - HCT116 - T84	Spheroids	Forced Floating 96-well-plates coated with 0.7% SeaKem® GTG Agarose	None	[256]
WJ-MSC	Human Lung Cancer - AC-LCSC-229 and 223 - SCC-LCSC-136 and 36	Spheroids	Forced Floating Unspecified non-treated flasks to reduce cell adherence	None	[107]
BM-MSC	Human Lung Cancer - A549	Spheroids	Hanging drop 25000 per well in a tri culture method (ratios of 5:3:2 - A549 - Endothelial Lung Cells - Mesenchymal stem cells)	Paclitaxel and Gemcitabine	[257]
MM Marrow Derived MSCs	Human Multiple Myeloma (MM) Aspirates	Scaffold	Hydrogel composed by 0.5% PuraMatrix	IMiDs, Bortezomib, Carfilzomib, Doxorubicin, Dexamethasone, Melphalan	[258]
BM-MSC	Human Glioma - U-87 - U373	Spheroids embedded into a Scaffold	Spheroids embedded in Collagen I, Laminin or Matrigel	None	[259]

4.1. MSCs Influence in Cancer - Dual Co-Culture 3D Models

Regarding the available studies, in most circumstances MSCs exert a positive influence in cancer progression, either by increasing malignant cells proliferation, migration, invasion, drug resistance and/or cancer stem cell proliferation. Alternatively, only few studies report MSCs as having negative effects in cancer cells [74–77]. The report by Dittmer and co-workers, [74] demonstrated that BM-MSCs can invade MCF-7 and MDA-MB-231 breast cancer 3D aggregates, originating disorganized structures by disrupting cell-cell adhesion, mainly through E-cadherin cleavage and nuclear translocation, without however increasing EMT and ERK1/2 activity. These researchers used a lower ratio of MSCs to cancer cells (1:500, and 1:1000) when compared to other studies performed by Mcandrews

and colleagues (MSCs:Cancer cells, 1:1 ratio [27]), or Zhu and co-workers (MSCs:Cancer cells, 1:2 and 1:5 ratio [78]), in which different ratios were employed to establish the co-culture of MSCs and breast cancer cells in hydrogel-based scaffolds. The data collected by Dittmer, suggests that low numbers of MSCs are capable of increasing breast cancer cell migration [74]. On another report, Klopp and colleagues, 2010, obtained a more organized and spherical 3D model upon inclusion of BM-MSCs when using the same cell lines as models [79]. The authors attributed these differences to the incorporation of MSCs prior to the formation of the aggregates and to the lack of serum-containing media. In a different approach Dittmer also evaluated if the presence of MSCs in MCF-7 and MDA-MB-231 spheroids affected their susceptibility to 4 tyrosine kinase inhibitors. The interesting results that were obtained indicate that in both spheroids (MCF-7:MSCs and MDA-MB-231:MSCs), the effect of the administered therapeutic anti-cancer drugs was augmented, pinpointing the decreased resistance to alterations in ERK1/2 phosphorylation and PKCα [75].

Several subsequent studies [27,78,80,81], using scaffold-based technologies for 3D models assembly provide evidence that BM-MSCs exert a positive effect in cancer cell survival and migratory capacity. In fact, cells co-cultured in tissue mimetic scaffolds including those based on: (i) collagen hydrogels [27]; (ii) silk-fibroin scaffolds [81], or (iii) porous chitosan scaffolds containing hydroxyapatite organotypic as bone mimetics [78] laden with undifferentiated or differentiated MSCs, evidence their capability to up-regulate the expression of EMT-related genes in cancer cells, to induce higher migratory capacity (Figure 4), and to enhance proliferation through different signaling factors. For example through the release of cyclic AMP [78], and TGF-β phosphorylation [27].

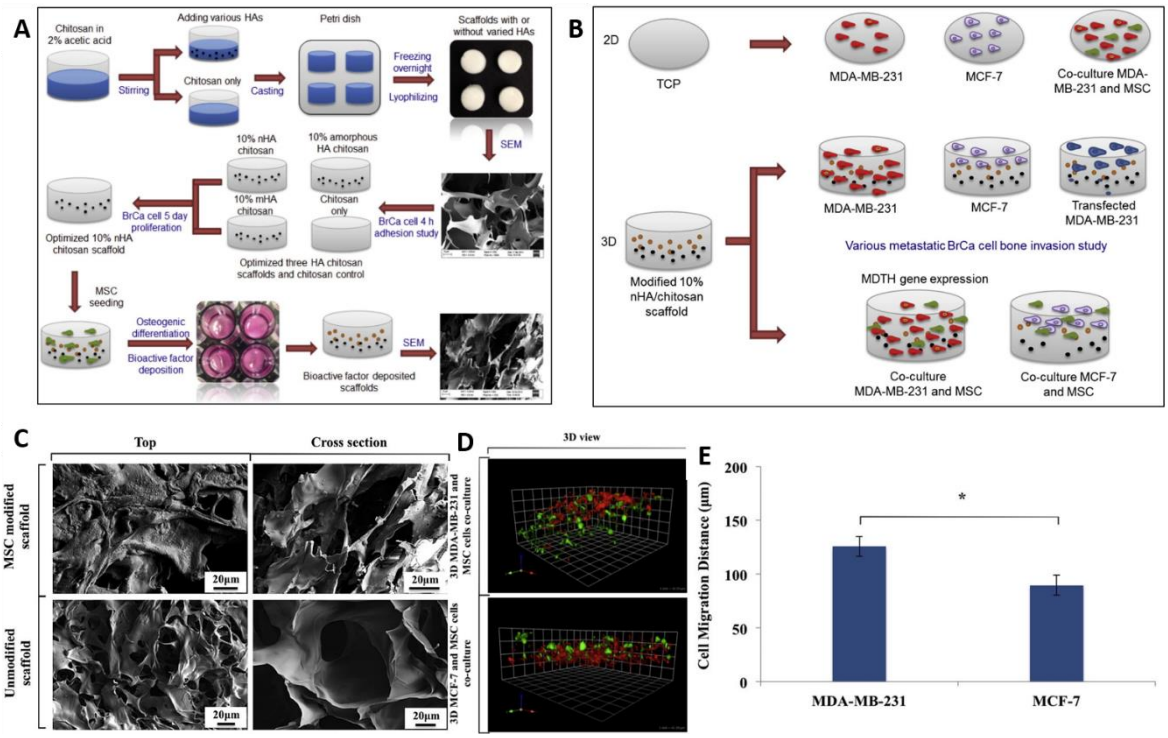

Figure 4. Scaffold-based bone metastasis model. (A, B) Schematics of 3D *in vitro* platforms development and analysis; (C) SEM images of bone-mimetic scaffolds of chitosan and hydroxyapatite with or without previous MSCs culture derived modifications (D) MSCs co-culture with breast cancer cells (MCF-7 and MDA-MB-231) in bone-mimetic scaffold; (E) breast cancer cells evidenced a higher migratory capacity, with MDA-MB-231 evidencing the highest migration distance when co-cultured. This enhanced migratory capacity correlated with a higher expression of MTDH gene, which accompanied almost linearly increased co-culture ratios of MSCs and breast cancer cells. Adapted from [254], with permission from Elsevier®.

Moreover, MSCs are also able to increase cancer stem cell populations [80] and cancer cells resistance to therapeutics. In a study by Jakubikova and colleagues, the interactions between BM-MSCs and multiple myeloma (MM) where analyzed using a co-culture model derived from cellular populations extracted from patients in different stages of MM [82]. The results obtained by the authors demonstrated that in comparison to MM cells alone, the co-cultured cells exhibited resistance to an extensive panel of pharmacological agents, both novel and conventional, replicating clinical observations (Figure 5).

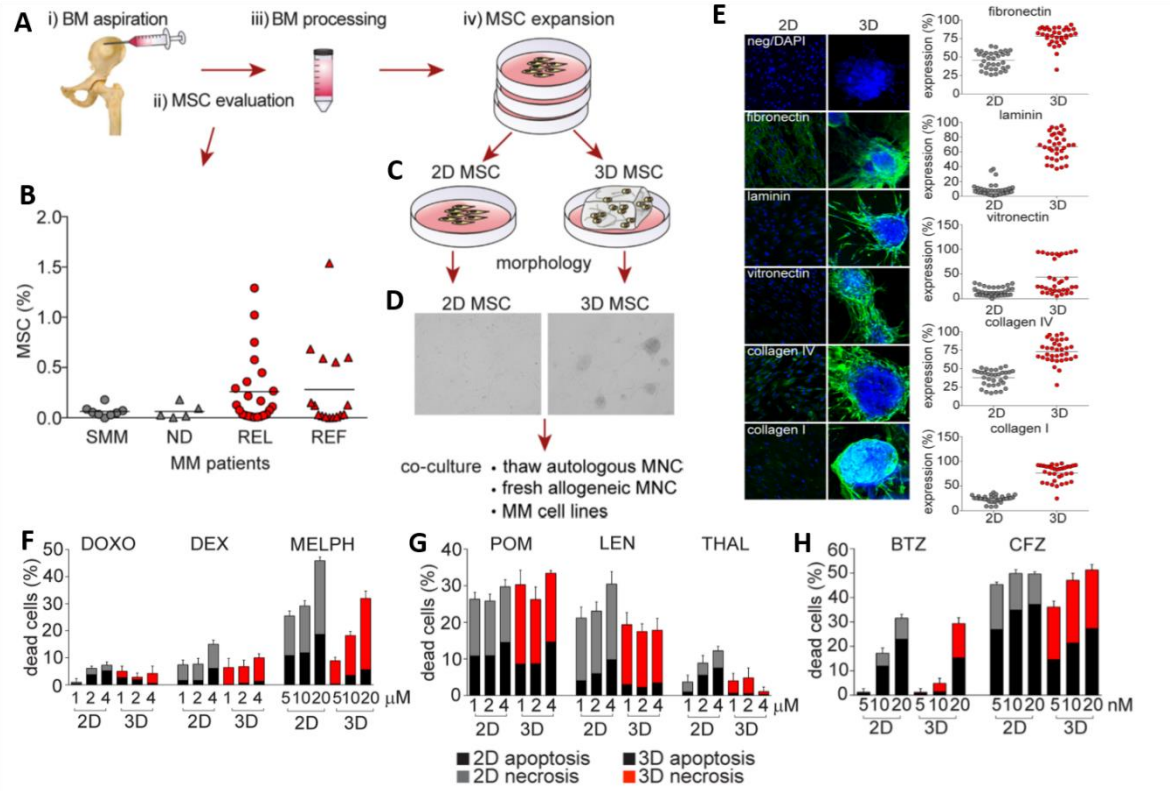

Figure 5. Establishment of a hydrogel-based 3D multiple myeloma (MM) model. (A) Collection of aspirates from multiple myeloma (MM) patients in several disease stage; (B) MSCs populations characterization by flow-cytometry and classified as smoldering MM (SMM), newly diagnosed MM (ND), relapsed MM (REL) and relapsed/refractory MM (REF) patients; (C and D) After extensive characterization of retrieved MSCs and MM cells, co-cultures where established both in 2D and 3D; (E) 3D to 2D comparison of co-cultured models showed significantly distinct cellular profiles, with 3D model presenting amongst other findings increased matrix deposition; Increased resistance of MM 2D and 3D models to (F) standard treatments, (G) immunomodulatory drugs and (H) proteasome inhibitors. Adapted from [258], with permission from Oncotarget under creative commons 3.0 license.

More recently, the development of an interesting MSCs-cancer cells scaffold-based 3D *in vitro* model for drug screening was also described by Han and co-workers. In this model MSCs and human non-small cell lung carcinoma cells A549 cells where co-cultured in wells coated with a multi-layer film of chitosan and hyaluronan (Figure 6) [83]. In this layer-by-layer structured biomaterial, cancer cells and MSCs efficiently self-organized into spheroids, presenting a core–shell structure wherein A549 cells exhibited enriched 2-fold upregulation of EMT-related genes, in comparison with 2D cultures. This remarkable enrichment was also observed in conditioned medium experiments with 2D cultures exhibiting lower EMT and tumorigenicity associated factors than those of direct co-culture [83]. Interestingly, *in vivo* assays demonstrated that co-culture derived implants presented

higher malignancy, therefore highlighting the importance of MSCs cancer cell direct contact in tumor progression.

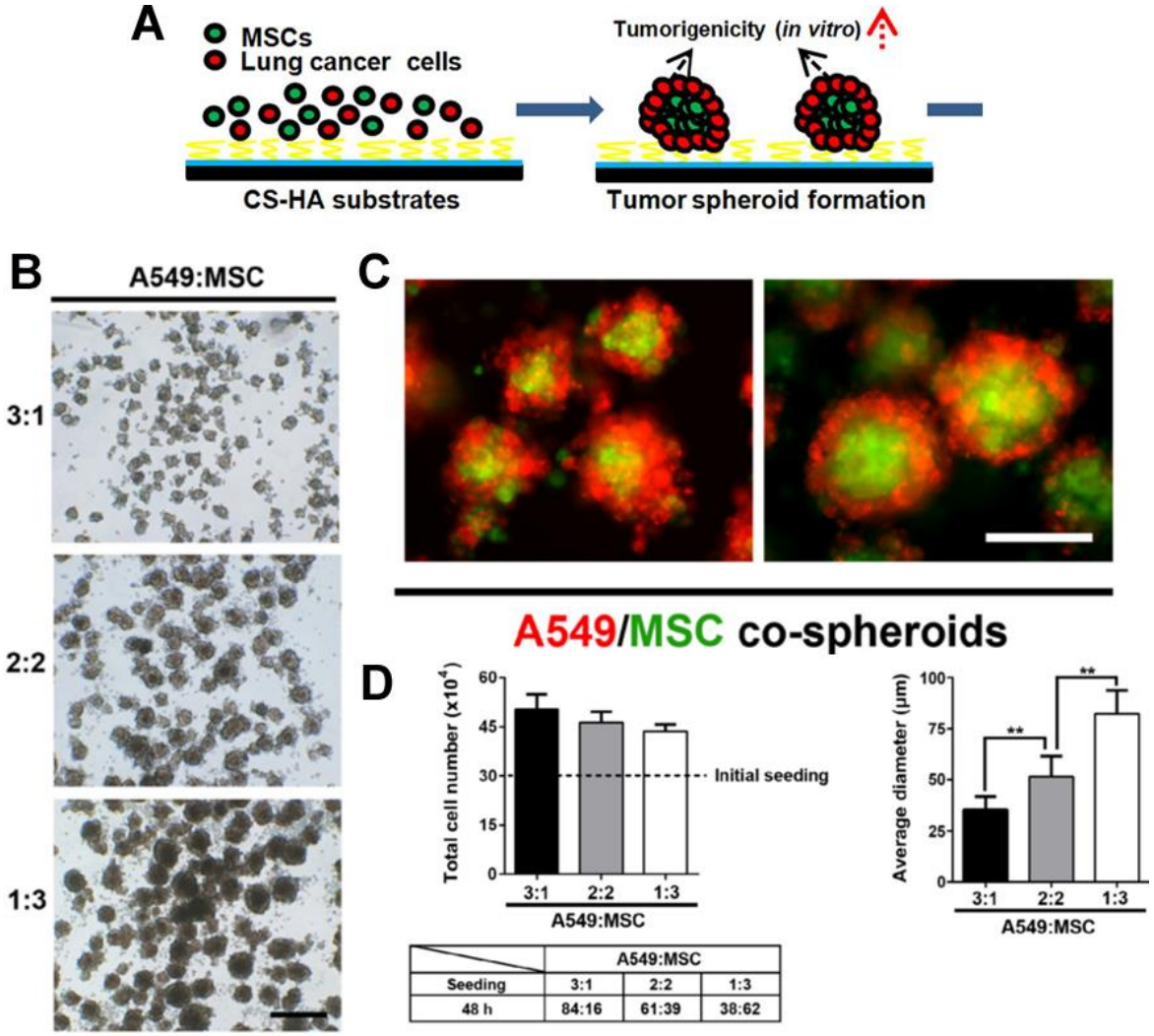

Figure 6. A549 and BM-MSCs 3D models co-culture performed in chitosan-hyaluronic acid coated wells. (A) Schematics of the biomaterial-based scaffold and workflow for assembly of 3D models; (B) Morphology of spheroids with diverse seeding ratios; (C) Fluorescence based analyzes of spheroid structure, 200 µm scale bar in panel; (D) Average diameter, total cell number of tumor spheroids, and cell ratio at 48h of co-culture. Adapted from [260] with permission from Elsevier®.

On the other hand, the establishment of negative interactions between BM-MSCs and cancer cells has been reported in human colon cancer cell lines HT29 and HCT-116, which presented decreased proliferation when co-cultured *in vitro* in a three-dimensional scaffold (of unmentioned composition) with BM-MSCs [76]. In this study BM-MSCs where found to secret PAI-1, a factor closely associated with aggressive colon cancer [84], and showed to have a direct effect in cancer cell proliferation. In the case of HCT-116 cancer cells BM-MSCs excreted PAI-1 was shown to yielded a negative influence in cellular proliferation,

while with HT29 this interaction lead to a positive outcome, in which high concentrations of PAI-1 increased cell proliferation [76]. However, when taking into account all factors secreted by MSCs, these exerted a negative effect resulting in a decrease in cancer cell proliferation in the order of 50% [84]. This fact becomes extremely relevant when one considers that MSCs of different origins are known to express different levels of cytokines and signaling factors in the same context [85,86], emphasizing once again the necessity of further studying the influence of MSCs from diverse sources. Still regarding human colon cancer Widder and co-workers, 2016, have demonstrated that BM-MSCs were able to increase HCT8 E-cadherin deficient cell line capacity to assemble into 3D spheroids, whilst increasing HCT8 cell proliferation [87]. This elegant study showcased a close relation between HCT8 and MSCs-specific secretoma, in comparison to that of fibroblasts (CCD18Co). Furthermore, differential MSCs and fibroblasts spatial distribution was observed amongst 3D spheroids, with external deposition in colorectal cancer cell line DLD1 spheroids and with homogeneous internal deposition in colorectal cancer cell line HCT8 spheroids [87]. The remarkable increase in spheroid adhesion provided by MSCs co-culture for HCT8 is proposed by the authors to be correlated with a b1-integrin dependent mechanism, and aided through ECM deposition specifically via the production of collagen I, which also highlights the importance of 3D *in vitro* disease models in the context of cancer cell-stromal cell interaction studies.

4.2. MSCs role in Complex Heterotypic Co-cultures and Organotypic Bone-Metastasis Models

Regarding the development of more complex heterotypic co-culture models, the study by Beckermen and colleagues, established a triculture spheroid system comprised by MIA-PaCa-2 cells, primary fibroblasts, and HUVEC cells [88]. These spheroids were then immersed in a methylcellulose/collagen solution and transferred to a fibronectin-coated plate previously cultivated with BM-MSCs in order to simulate and analyze MSCs migration towards tumor-associated blood vessels. The authors observed a positive effect on MSCs migration towards the triculture spheroids, in which VEGF appeared to be the prevalent factor with PDGF and EGF also displaying significant chemoattractant properties [88]. *In vivo* studies in mice demonstrated the capacity of ectopically injected BM-MSCs of migrating towards xenografts of human pancreatic cancer, in which BM-MSCs lead to an

increase in the number of CD31+ early vascular structures, an event that directly correlates with the density of tumor vascularization, as was observed, with tumors with twice the vascularization of those in obtained in controls [88]. Another triculture was performed by Lamichane and co-workers, 2016, in which A549 cells were co-cultured with human pulmonary microvascular endothelial cells and BM-MSC [89]. The tracking of the different cellular populations was accomplished through transfection with lentiviral particles encoding red fluorescent (RFP) and green fluorescent (GFP) transgene reporters, and followed for 15 days. The results showed a decline in the endothelial population, and an accentuated increase both in MSCs, which primarily formed the core of the spheroid, and cancer cells. From the endothelial cells co-cultured in these spheroids only a small population remained viable, being hypothesized by the authors to have survived by close association with MSCs within the hypoxic regions of the necrotic core. The spheroids exhibited increased multidrug resistance markers expression (ABC-B1 mRNA and ROS). However, no increased drug resistance in the 3D models was obtained when compared to standard 2D co-cultures. In fact, only some concentrations showed a prevailing difference between models, with the 3D model presenting always an increased cellular viability in comparison to the 2D model [89].

The importance of the 3D organization in cancer cell-mesenchymal communication was sophisticatedly addressed in a study performed by Pasquier and co-workers [90]. This report employed both ovarian and breast cancer cell lines and the authors demonstrated the existence of a ubiquitous mechanism of cytoplasmic material transference through the usage of tunneling nanotubules in spatially adjacent cells, using 3D spheroid triculture systems [90]. The results indicated that mitochondrial transference between cancer cells and stromal cells took place, preferably, between endothelial cells (EC) and cancer cells, also occurring in the same mode between explant tissue and co-cultured EC cells. This exchange endowed cancer cells with a proliferative advantage by rescuing them from erratic aerobic respiration dysfunctions and endowed them with a significant resistance to chemotherapeutic agents [90]. This report further demonstrates the necessity for analyzing cancer cells-MSCs interactions in a tumor stroma context.

In addition to being used for the establishment of 3D drug testing platforms or in the study of the complex interactions with cancer MSCs have also been employed for establishment of organotypic 3D *in vitro* bone metastasis models. Such approach takes

advantage of the multilineage differentiation potential of BM-MSCs, namely their capacity to differentiate into osteoblasts. In this context, Jeon and colleagues, have developed a collagen I hydrogel laden with BM-MSCs differentiated into osteoblasts co-cultured with vascular endothelial cells (HUVECs) and enclosed it in a microfluidic device (Figure 7) [91].

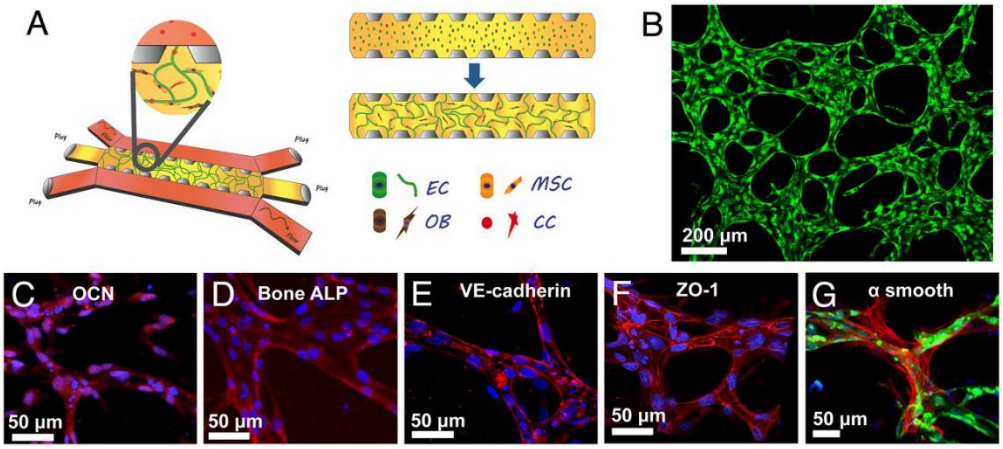

Figure 7. Breast-to-bone metastasis microfluidic chip-based model. (A) Schematics of the vascular heterotypic model with two channels for culture medium addition and injection of breast cancer cells and biochemical signals exchange with the collagen I hydrogel in the center channel EC – Endothelial cells (HUVECs), MSCs, OB – Obsteoblast differentiated cells (from MSCs lineage), CC- Cancer cells. All these cells were seeded in the hydrogel; (B) Microvascular network formed in the hydrogel (HUVECs-green); (C to G) Evaluation of the established organotypic bone microenvironment, with Osteocalcin (red), Alkaline phosphatase (red), VE-Cadherin (red), ZO-1 (red) and α-smooth (red) biomarkers evaluation. Adapted from [264] with permission from Proceedings of the the National Academy of Sciences of the United States of America (PNAS).

The co-culture of osteo-differentiated MSCs and HUVECs promoted the formation of endothelium around the microfluidic channels and the deposition of bone-marrow specific biomolecules and matrix. This highly organotypic model was then used to evaluate the behavior of breast cancer cells that were injected in the channels of the hydrogel-containing chip. The obtained results demonstrate that cancer cells in the triculture microfluidic model have a higher pro-metastatic potential, with higher rates of extravasation, migration and invasion. Such increased aggressiveness was evidenced by the breast cancer micro-metastatic pockets containing 4-60 cells that formed at 5 days of co-culture [91]. However, it is important to point out that due to the lack of MSCs population tracking during differentiation into osteoblasts it impossible to establish a direct connection between cells invasiveness and their interactions with possibly present non-osteogenic differentiated MSCs. This evidences the requirement for long-term cell tracking in these *in vitro* models, a parameter that will be further discussed.

4.3. Importance of MSCs Tissue of Origin and Cancer Heterogeneity

It is relevant to highlight that the origin of MSCs may also play an important role in cancer and consequently on the development of more advanced 3D *in vitro* disease models. In fact, a comparison between the effects of co-culturing Wharton Jelly-derived MSCs (WJ-MSCs) or BM-MSCs with lung cancer stem cells, either in 3D using multicellular spheroids or in 2D demonstrated contrasting effects between WJ-MSCs and BM-MSCs towards lung cancer stem cells (LCSC), with different subtypes of LCSC presenting different responses to WJ-MSC, especially when co-cultured in 3D [32]. Tumor heterogeneity may also play a role in cancer-MSCs interactions and hence influence the conclusions extrapolated from *in vitro* models. A recent study by Breznik and co-workers, 2017, demonstrated how phenotypically different cell lines used as models for glyoblastoma can lead to different MSC-cancer cells interactions and outcomes, with U87 cells showing decreased invasive potential, and U373 cells displaying the opposite, both *in vivo* and *in vitro* [92]. The researchers attributed this difference to alternatively favored metabolic pathways resulting from TGF-β release by MSCs. Thus underlining the importance of accounting for the heterogeneity and phenotypic variations present in actively proliferating tumors [92]. These results emphasize the necessity of considering the use of MSCs from several tissue origins, as well as different types of malignant cells to account for intrinsic *in vivo* tumor cellular heterogeneity.

5 Key Technical Parameters for Establishment of Cancer Cells-MSCs 3D *In vitro* Co-Culture Models

The number of variables that can affect the interaction and co-culture of such diverse cell populations makes achieving a valid co-culture model containing MSCs extremely difficult. In this context, it is important to emphasize that the relative lack of knowledge about the exact composition of both non-cellular and cellular components of the TME drastically reduces the ability to implement *in vivo* similar co-culture ratios. In addition, different cancer types are expected to possess diversified cell populations and thus, different ratios, such as those characteristic of brain and NSLC [93,94]. Moreover, variability may derive from different stages of the same cancer as verified in MM by [82]. The creation of *in vivo* mimicking *in vitro* 3D models for the study of cancer cells-MSC interactions have thus far relied in the usage of basic approaches. In a study by Zhu and colleagues, 3 diverse

ratios (1:1, 1:2 and 1:5) where used for the co-culture of BM-MSC with breast cancer cells, the authors evaluated MTDH, an oncogene that promotes proliferation and enhances chemoresistance [95], to be up-regulated in co-cultures containing higher ratios of MSC to cancer cells, when compared to lower MSC ratios [78]. In a study by Oerlecke and colleagues, 2013, as few as 1 MSC per 300 breast cancer cell was enough to obtain a significant increase in both Smad3 and CREB phosphorylation in BCC [80]. These findings showcase the necessity of correctly representing the diverse cellular populations of the TME in 3D laboratory models that aim to recapitulate the reality found *in vivo,* since different concentration of MSCs release dissimilar factors and cytokines that can lead to antagonistic responses [25].

In terms of cell culture specifications, MSCs are known to present diverse media requirements, as well as growth, proliferation, matrix deposition and differentiation capabilities [22] when compared with other cellular components of the TME. With all these processes being affected by the previously referred factors, and by others such as the pre-existing scaffolds morphology and composition, which depending on the cell type might induce diversified phenotypes for example amongst cancer cells [96,97]. This complicates the establishment of a heterotypic co-culture model that suits all the necessities of the various cellular populations [98]; especially when modified mediums for the co-culture of cells are still rather underdeveloped [99]. Another problem that arises from these models is how co-culture populations can proliferate/change over extended periods of time, altering the initial experimental parameters as the trial progresses [72]. Such cell modifications can occur, for example, simply through the deposition of extracellular matrix, alteration/degradation of pre-existing scaffolds for 3D culture [54], or in a more complex facet, through the differentiation of the multipotent cells into diverse cellular populations otherwise not accounted for in the model [100]. When accounting for model alterations concerning the co-culture of MSCs and cancer cells, another variance that must be considered is how cancer cell cannibalism towards MSCs may affect the model progression [101]. This phenomenon, was recently addressed by using hanging drop-assembled 3D tumor spheroids which successfully replicated the relatively unstudied process of cellular cannibalism by MDA-MB-231 breast cancer cells (MDA-BCC) directed at MSCs surrounding populations in which cancer cells internalized and consequently degraded MSCs (Figure 8). Such resulted in the acquisition of unique molecular signature profiles by cannibal MDA-BCC cells,

presenting an enriched molecular profile for pro-survival factors and tumor suppressor agents, as well as inflammatory mediators which marked these cells as detaining a senescence-associated secretory phenotype [101]. The authors were, thus, able to replicate *in vitro* a process of paramount importance in cancer cell metastasis and therapy survival, where MSCs once again are shown to have a vital role.

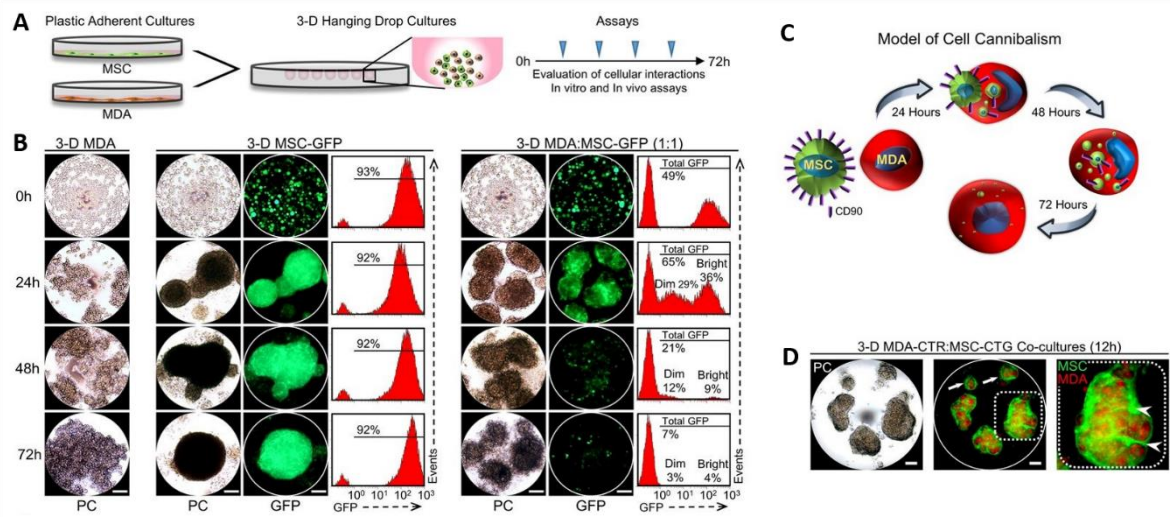

Figure 8.- Evaluation of cancer cell cannibalism towards MSCs. Upon cannibalism MDA-MB cells acquired an enriched molecular profile for pro-survival factors and tumor suppressor agents, as well as inflammatory mediators before entering a state of dormancy. (A) Scheme of co-culture method; (B) MSCs population decline visible in phase-contrast microscopy and flow cytometry; (C) MSCs cannibalism by MDA breast cancer cells; (D) MDA-MSCs in small aggregates as visualized through immunofluorescence imaging, prior to MSCs decline. Adapted from [272] with permission from Proceedings of the the National Academy of Sciences of the United States of America (PNAS).

Apart from this, the various alterations that cellular populations ratios can suffer during culture must be carefully monitored, creating a necessity of tracking and analyzing each diversified cellular population in direct contact on 3D co-culture models. To this end, immunostaining techniques can be of use to a certain point, for example when identifying non-stem cell populations or analyzing matrix deposition [102]. Unfortunately, for the differentiation of both cancer stem cells and MSC populations, difficulties might arise due to expression of overlapping receptors or other markers [21,103,104]. The use of cell tracking techniques, such as transfection with non-integrative GFP transgenes via viral or non-viral vectors has been employed as an alternative. However, these methodologies are highly expensive and still present some technical constraints such as transient expression or influence in cells behavior [73,88,105]. Overall, the difficulty of tracking cellular populations hinders the ability to use more complex models for the analysis of specific cellular interactions. Such is the case with explant derived organoids, in which events such

as the differentiation of MSCs lineages into osteo-differentiated MSCs must be prevented or dully tagged [106,107].

In summary, the establishment of a 3D MSC-cancer co-culture testing platform encompasses several challenges, namely: (i) different initial seeding ratios can lead to distinct results; (ii) the spatiotemporal manner in which cells are introduced to the model can lead to diverse morphological organizations [79]; with (iii) diverse cells presenting diverse proliferative rates [108]; (iv) *in vitro* cellular division limits (Hayflick limit); (v) and requirement of different types of medium; with all this diversity resulting in the need of (vi) differentially tracking each cell population over time and space.

6. Conclusions

Upon analysis of different literature reports with 3D cultured MSCs, so far, they mainly focus on the use of co-cultured MSCs-tumor cells 3D spheroids. Only few articles take advantage of scaffold-based approaches and microfluidic chips, but mainly in the study of breast cancer metastasis into bone [78,81,109,110]. Developments in complex scaffold design for tissue engineering could be valuable in producing structures that could provide mechanical/biochemical cues and 3D spatial organization of MSCs and cancer cells [111]. Although the use of simple MSCs-cancer cells 3D co-cultures provides *in vitro* models compatible with high-throughput screening, (one of the main requirements for developing models for pharmaceutics testing and discovery), several important TME associated factors are disregarded, including tumor-specific ECM, and other stromal cells-cancer cells bidirectional interactions, spatiotemporal mechanical and biochemical cues. Clearly, this lack of ECM and stromal cells representation must be overcome if a representative model is to be achieved, possibly through the usage of complex functionalized scaffolds [112]. These scaffolds can be arranged in various forms in combination with microfluidic chips capable of providing a transport system in which mechanical cues obtained at different perfusion rates, combined with controllable biochemical signals, resembling those of an *in vivo* organism, allowing to increase the complexity of the designed 3D models [98]. It is also important to highlight that the widespread use of BM-MSCs populations in MSCs-cancer cell interactions can result in a bias towards the influence of this particular subset of cells [25,85,86].

In conclusion, further improvements to the currently available 3D *in vitro* tumor models will allow to develop valid platforms that permit the inclusion of MSCs in a way that

more closely mimics *in vivo* conditions. While the analysis of individual interactions between these and other cells of the TME can provide a glimpse into the complex weave of communication and mutual regulation that takes place across the intricate setting present in malignant pathologies, ultimately the goal shall be to achieve a model that can be composed of both cancer cells, MSCs and other related stromal cells and immune system cells, in tissue specific ECM-like scaffolds [113]. This will require a combinatorial approach of current technologies, both in the fields of biomaterials and bioengineering [99], in an effort to provide laboratory models that can be used for widespread screening of anti-cancer therapeutics in a number of different cancer types.

6 References

[1] Ruggeri BA, Camp F, Miknyoczki S. Animal models of disease: Pre-clinical animal models of cancer and their applications and utility in drug discovery. Biochem Pharmacol 2014;87. 150–61.

[2] Shoemaker RH. The NCI60 human tumour cell line anticancer drug screen. Nat Rev Cancer 2006;6. 813–23.

[3] Begley CG, Ellis LM. Drug development: Raise standards for preclinical cancer research. Nature 2012;483. 531–3.

[4] Nyga A, Cheema U, Loizidou M. 3D tumour models: Novel *in vitro* approaches to cancer studies. J Cell Commun Signal 2011;5. 239–48.

[5] Breslin S, O'Driscoll L. Three-dimensional cell culture: The missing link in drug discovery. Drug Discov Today 2013;18. 240–9.

[6] Pampaloni F, Reynaud EG, Stelzer EHK. The third dimension bridges the gap between cell culture and live tissue. Nat Rev Mol Cell Biol 2007;8. 839–45.

[7] Smalley KSM, Lioni M, Herlyn M. Life isn't flat: taking cancer biology to the next dimension. In Vitro Cell Dev Biol Anim 2006;42. 242–7.

[8] McGonigle P, Ruggeri B. Animal models of human disease: Challenges in enabling translation. Biochem Pharmacol 2014;87. 162–71.

[9] Mak IW, Evaniew N, Ghert M. Lost in translation: animal models and clinical trials in cancer treatment. Am J Transl Res 2014;6. 114–8.

[10] Denayer T, Stöhrn T, Van Roy M. Animal models in translational medicine: Validation and prediction. New Horizons Transl Med 2014;2. 5–11.

[11] Aparicio S, Hidalgo M, Kung AL. Examining the utility of patient-derived xenograft mouse models. Nat Rev Cancer 2015;15. 311–6.

[12] Toniatti C, Jones P, Graham H, Pagliara B, Draetta G. Oncology drug discovery: Planning a turnaround. Cancer Discov 2014;4. 397–404.

[13] Horvath P, Aulner N, Bickle M, Davies AM, Nery E Del, Ebner D, et al. Screening out irrelevant cell-based models of disease. Nat Rev Drug Discov 2016. doi:10.1038/nrd.2016.175.

[14] Costa EC, Gaspar VM, Coutinho P, Correia IJ. Optimization of liquid overlay technique to formulate heterogenic 3D co-cultures models. Biotechnol Bioeng 2014;111. 1672–85.

[15] Neto AI, Correia CR, Oliveira MB, Rial-Hermida MI, Alvarez-Lorenzo C, Reis RL, et al. A novel hanging spherical drop system for the generation of cellular spheroids and high throughput combinatorial drug screening. Biomater Sci 2015;3. 581–5.

[16] Kenny PA, Bissell MJ. Tumor reversion: Correction of malignant behavior by microenvironmental cues. Int J Cancer 2003;107. 688–95.

[17] Mehta G, Hsiao AY, Ingram M, Luker GD, Takayama S. Opportunities and challenges for use of tumor spheroids as models to test drug delivery and efficacy. J Control Release 2012;164. 192–204.

[18] Bergfeld SA, DeClerck YA. Bone marrow-derived mesenchymal stem cells and the tumor microenvironment. Cancer Metastasis Rev 2010;29. 249–61.

[19] A.J. Friedenstein, R.K. Chailakhjan KSL. The development of fibroblast colonies in monolayer cultures of guinea-pig bone marrow and spleen cells. Cell Tissue Kinet 1970. 393–403.

[20] Phinney DG, Prockop DJ. Concise review: mesenchymal stem/multipotent stromal cells: the state of transdifferentiation and modes of tissue repair--current views. Stem Cells 2007;25. 2896–902.

[21] Dominici M, Le Blanc K, Mueller I, Slaper-Cortenbach I, Marini F, Krause D, et al. Minimal criteria for defining multipotent mesenchymal stromal cells. The International Society for Cellular Therapy position statement. Cytotherapy 2006;8. 315–7.

[22] Serakinci N, Fahrioglu U, Christensen R. Mesenchymal stem cells, cancer challenges and new directions. Eur J Cancer 2014;50. 1522–30.

[23] Sun Z, Wang S, Zhao RC. The roles of mesenchymal stem cells in tumor inflammatory microenvironment. J Hematol Oncol 2014;7. 14.

[24] Heissig B, Dhahri D, Eiamboonsert S, Salama Y, Shimazu H, Munakata S, et al. Role of mesenchymal stem cell-derived fibrinolytic factor in tissue regeneration and cancer progression. Cell Mol Life Sci 2015;72. 4759–70.

[25] Gwendal L, Paula Y L, Lazennec G, Lam PY. Recent discoveries concerning the tumor - mesenchymal stem cell interactions. Biochim Biophys Acta - Rev Cancer 2016;1866. 290–9.

[26] Hong I-S, Lee H-Y, Kang K-S. Mesenchymal stem cells and cancer: Friends or enemies? Mutat Res 2014;768. 1–9.

[27] McAndrews KM, McGrail DJ, Ravikumar N, Dawson MR. Mesenchymal Stem Cells Induce Directional Migration of Invasive Breast Cancer Cells through TGF-β. Sci Rep 2015;5. 16941.

[28] Eid JE, Garcia CB. Reprogramming of mesenchymal stem cells by oncogenes. Semin Cancer Biol 2015;32. 18–31.

[29] Yang Y, Otte A, Hass R. Human Mesenchymal Stroma/Stem Cells Exchange Membrane Proteins and Alter Functionality During Interaction with Different Tumor Cell Lines. Stem Cells Dev 2014;0. 1–18.

[30] Patel SA, Meyer JR, Greco SJ, Corcoran KE, Bryan M, Rameshwar P. Mesenchymal stem cells protect breast cancer cells through regulatory T cells: role of mesenchymal stem cell-derived TGF-beta. J Immunol 2010;184. 5885–94.

[31] Kuhn NZ, Tuan RS. Regulation of stemness and stem cell niche of mesenchymal stem cells: Implications in tumorigenesis and metastasis. J Cell Physiol 2010;222. 268–77.

[32] Vulcano F, Milazzo L, Ciccarelli C, Eramo A, Sette G, Mauro A, et al. Wharton's jelly mesenchymal stromal cells have contrasting effects on proliferation and phenotype of cancer stem cells from different subtypes of lung cancer. Exp Cell Res 2016;345. 190–8.

[33] Norozi F, Ahmadzadeh A, Shahrabi S, Vosoughi T, Saki N. Mesenchymal stem cells as a double-edged sword in suppression or progression of solid tumor cells. Tumor Biol 2016. 1–11.

[34] Qiao L, Xu Z, Zhao T, Zhao Z, Shi M, Zhao RC, et al. Suppression of tumorigenesis by human mesenchymal stem cells in a hepatoma model. Cell Res 2008;18. 500–7.

[35] Attar-Schneider O, Zismanov V, Drucker L, Gottfried M. Secretome of human bone marrow mesenchymal stem cells: an emerging player in lung cancer progression and mechanisms of translation initiation. Tumour Biol 2015. 4755–65.

[36] Yulyana Y, Ho IA, Sia KC, Newman JP, Toh XY, Endaya BB, et al. Paracrine factors of human fetal

MSCs inhibit liver cancer growth through reduced activation of IGF-1R/PI3K/Akt signaling. Mol Ther 2015;23. 746–56.

[37] Ramdasi S, Sarang S, Viswanathan C. Potential of mesenchymal stem cell based application in cancer. Int J Hematol Stem Cell Res 2015;9. 41–9.

[38] Sorokin L. The impact of the extracellular matrix on inflammation. Nat Rev Immunol 2010;10. 712–23.

[39] Elinav E, Nowarski R, Thaiss CA, Hu B, Jin C, Flavell RA. Inflammation-induced cancer: crosstalk between tumours, immune cells and microorganisms. Nat Rev Cancer 2013;13. 759–71.

[40] Klopp AH, Spaeth EL, Dembinski JL, Woodward WA, Munshi A, Meyn RE, et al. Tumor irradiation increases the recruitment of circulating mesenchymal stem cells into the tumor microenvironment. Cancer Res 2007;67. 11687–95.

[41] Shi Y, Du L, Lin L, Wang Y. Tumour-associated mesenchymal stem/stromal cells: emerging therapeutic targets. Nat Rev Drug Discov 2016. doi:10.1038/nrd.2016.193.

[42] Scherzed a., Hackenberg S, Radeloff A, Froelich K, Rak K, Hagen R, et al. Human Mesenchymal Stem Cells Promote Cancer Motility and Cytokine Secretion *in vitro*. Cells Tissues Organs 2013. 327–37.

[43] Lopatina T, Gai C, Deregibus MC, Kholia S, Camussi G. Cross Talk between Cancer and Mesenchymal Stem Cells through Extracellular Vesicles Carrying Nucleic Acids. Front Oncol 2016;6. 125.

[44] Caicedo A, Fritz V, Brondello J-M, Ayala M, Dennemont I, Abdellaoui N, et al. MitoCeption as a new tool to assess the effects of mesenchymal stem/stromal cell mitochondria on cancer cell metabolism and function. Sci Rep 2015;5. 9073.

[45] Carnet O, Lecomte J, Masset A, Primac I, Durré T, Maertens L, et al. Mesenchymal Stem Cells Shed Amphiregulin at the Surface of Lung Carcinoma Cells in a Juxtacrine Manner. Neoplasia (United States) 2015;17. 552–63.

[46] Yang X, Hao J, Mao Y, Jin Z-Q, Cao R, Zhu C-H, et al. bFGF promotes migration and induces cancer-associated fibroblasts differentiation of mouse bone mesenchymal stem cells to promote tumor growth. Stem Cells Dev 2016;25. scd.2016.0217.

[47] Chong M, Lim J, Goh J, Sia MW, Chan JKY, Teoh SH. Co-culture of Mesenchymal Stem Cells and Endothelial Cells as an Organotypic Model of Prostate Cancer Metastasis. Mol Pharm 2014. doi:10.1021/mp500141b.

[48] Cammarota F, Laukkanen MO. Mesenchymal Stem / Stromal Cells in Stromal Evolution and Cancer Progression 2015;2016. doi:10.1155/2016/4824573.

[49] Cesarz Z, Tamama K. Spheroid Culture of Mesenchymal Stem Cells. Stem Cells Int 2016;2016. doi:10.1155/2016/9176357.

[50] Waterman RS, Henkle SL, Betancourt AM. Mesenchymal Stem Cell 1 (MSC1)-Based Therapy Attenuates Tumor Growth Whereas MSC2-Treatment Promotes Tumor Growth and Metastasis. PLoS One 2012;7. doi:10.1371/journal.pone.0045590.

[51] Ravi M, Paramesh V, Kaviya SR, Anuradha E, Paul Solomon FD. 3D cell culture systems: Advantages and applications. J Cell Physiol 2015;230. 16–26.

[52] Cox MC, Reese LM, Bickford LR, Verbridge SS. Toward the Broad Adoption of 3D Tumor Models in the Cancer Drug Pipeline. ACS Biomater Sci Eng 2015;1. 877–94.

[53] Thoma CR, Zimmermann M, Agarkova I, Kelm JM, Krek W. 3D cell culture systems modeling tumor growth determinants in cancer target discovery. Adv Drug Deliv Rev 2014;69–70. 29–41.

[54] Fong EL, Harrington DA, Farach-Carson MC, Yu H, Els F. Heralding a New Paradigm in 3D Tumor Modeling. Biomaterials 2016;108. 197–213.

[55] Oliveira MB, Neto AI, Correia CR, Rial-Hermida MI, Alvarez-Lorenzo C, Mano JF. Superhydrophobic Chips for Cell Spheroids High-Throughput Generation and Drug Screening. ACS Appl Mater Interfaces 2014;6. 9488–95.

[56] van Duinen V, Trietsch SJ, Joore J, Vulto P, Hankemeier T. Microfluidic 3D cell culture: From tools to tissue models. Curr Opin Biotechnol 2015;35. 118–26.

[57] Labarbera D V, Reid BG, Yoo BH. The multicellular tumor spheroid model for high-throughput cancer drug discovery 2012. 819–30.

[58] Fennema E, Rivron N, Rouwkema J, van Blitterswijk C, De Boer J. Spheroid culture as a tool for creating 3D complex tissues. Trends Biotechnol 2013;31. 108–15.

[59] Weiswald LB, Bellet D, Dangles-Marie V. Spherical cancer models in tumor biology. Neoplasia 2015;17. 1–15.

[60] Kunz-Schughart LA, Kreutz M, Knuechel R. Multicellular spheroids: A three-dimensional *in vitro* culture system to study tumour biology. Int J Exp Pathol 1998;79. 1–23.

[61] MUELLER-KLIESER W. Three-dimensional cell cultures: from molecular mechanisms to clinical applications. Am J Physiol - Cell Physiol 1997;273. C1109–23.

[62] Chen L, Xiao Z, Meng Y, Zhao Y, Han J, Su G, et al. The enhancement of cancer stem cell properties of MCF-7 cells in 3D collagen scaffolds for modeling of cancer and anti-cancer drugs. Biomaterials 2012;33. 1437–44.

[63] Ponti D, Costa A, Zaffaroni N, Pratesi G, Petrangolini G, Coradini D, et al. Isolation and In vitro Propagation of Tumorigenic Breast Cancer Cells with Stem/Progenitor Cell Properties. Cancer Res 2005;65. 5506–11.

[64] Timmins NE, Nielsen LK. Generation of multicellular tumor spheroids by the hanging-drop method. Methods Mol Med 2007;140. 141–51.

[65] Zanoni M, Piccinini F, Arienti C, Zamagni A, Santi S, Polico R, et al. 3D tumor spheroid models for *in vitro* therapeutic screening: a systematic approach to enhance the biological relevance of data obtained. Sci Rep 2016;6. 19103.

[66] Kapałczyńska M, Kolenda T, Przybyła W, Zajączkowska M, Teresiak A. 2D and 3D cell cultures – a comparison of different types of cancer cell cultures 2D and 3D cell cultures – a comparison of different 2016. doi:10.5114/aoms.2016.63743.

[67] Wong KHK, Chan JM, Kamm RD, Tien J. Microfluidic Models of Vascular Functions. Annu Rev Biomed Eng 2012;14. 205–30.

[68] Benien P, Swami A. 3D tumor models: history, advances and future perspectives. Futur Oncol 2014;10. 1311–27.

[69] Alemany-Ribes M, Semino CE. Bioengineering 3D environments for cancer models. Adv Drug Deliv Rev 2014;79. 40–9.

[70] Holzapfel BM, Wagner F, Thibaudeau L, Levesque JP, Hutmacher DW. Concise review: Humanized models of tumor immunology in the 21st century: Convergence of cancer research and tissue engineering. Stem Cells 2015;33. 1696–704.

[71] Katt ME, Placone AL, Wong AD, Xu ZS, Searson PC. In Vitro Tumor Models: Advantages, Disadvantages, Variables, and Selecting the Right Platform. Front Bioeng Biotechnol 2016;4. 12.

[72] Astashkina A, Grainger DW. Critical analysis of 3-D organoid *in vitro* cell culture models for high-throughput drug candidate toxicity assessments. Adv Drug Deliv Rev 2014;69–70. 1–18.

[73] Mandel K, Yang Y, Schambach A, Glage S, Otte A, Hass R. Mesenchymal stem cells directly interact with breast cancer cells and promote tumor cell growth *in vitro* and *in vivo*. Stem Cells Dev 2013;22. 3114–27.

[74] Dittmer A, Hohlfeld K, Lützkendorf J, Müller LP, Dittmer J. Human mesenchymal stem cells induce E-cadherin degradation in breast carcinoma spheroids by activating ADAM10. Cell Mol Life Sci 2009;66. 3053–65.

[75] Dittmer A, Fuchs A, Oerlecke I, Leyh B, Kaiser S, Martens JWM, et al. Mesenchymal stem cells and carcinoma-associated fibroblasts sensitize breast cancer cells in 3D cultures to kinase inhibitors. Int J Oncol 2011;39. 689–96.

[76] Hogan NM, Joyce MR, Murphy JM, Barry FP, O'Brien T, Kerin MJ, et al. Impact of Mesenchymal Stem Cell secreted PAI-1 on colon cancer cell migration and proliferation. Biochem Biophys Res Commun 2013;435. 574–9.

[77] Kim W, Barron DA, San Martin R, Chan KS, Tran LL, Yang F, et al. RUNX1 is essential for mesenchymal stem cell proliferation and myofibroblast differentiation. Proc Natl Acad Sci U S A 2014;111. 16389–94.

[78] Zhu W, Wang M, Fu Y, Castro NJ, Fu SW, Zhang LG. Engineering a biomimetic three-dimensional nanostructured bone model for breast cancer bone metastasis study. Acta Biomater 2015;14. 164–74.

[79] Klopp AH, Lacerda L, Gupta A, Debeb BG, Solley T, Li L, et al. Mesenchymal stem cells promote mammosphere formation and decrease E-Cadherin in normal and malignant breast cells. PLoS One 2010;5. 1–9.

[80] Oerlecke I, Bauer E, Dittmer A, Leyh B, Dittmer J. Cyclic AMP Enhances TGFβ Responses of Breast Cancer Cells by Upregulating TGFβ Receptor I Expression. PLoS One 2013;8. doi:10.1371/journal.pone.0054261.

[81] Talukdar S, Kundu SC. Engineered 3D silk-based metastasis models: Interactions between human breast adenocarcinoma, mesenchymal stem cells and osteoblast-like cells. Adv Funct Mater 2013;23. 5249–60.

[82] Jakubikova J, Cholujova D, Hideshima T, Gronesova P, Soltysova A, Harada T, et al. A novel 3D mesenchymal stem cell model of the multiple myeloma bone marrow niche: biologic and clinical applications. Oncotarget 2016;7. 77326–41.

[83] Han H-WW, Hsu S hui. Chitosan-hyaluronan based 3D co-culture platform for studying the crosstalk of lung cancer cells and mesenchymal stem cells. Acta Biomater 2016;42. 157–67.

[84] Märkl B, Renk I, Oruzio D V., Jähnig H, Schenkirsch G, Schöler C, et al. Tumour budding, uPA and PAI-1 are associated with aggressive behaviour in colon cancer. J Surg Oncol 2010;102. 235–41.

[85] Park CW, Kim K-S, Bae S, Son HK, Myung P-K, Hong HJ, et al. Cytokine secretion profiling of human mesenchymal stem cells by antibody array. Int J Stem Cells 2009;2. 59–68.

[86] Hwang JH, Shim SS, Seok OS, Lee HY, Woo SK, Kim BH, et al. Comparison of cytokine expression in mesenchymal stem cells from human placenta, cord blood, and bone marrow. J Korean Med Sci 2009;24. 547–54.

[87] Widder M, Lützkendorf J, Caysa H, Unverzagt S, Wickenhauser C, Benndorf RA, et al. Multipotent mesenchymal stromal cells promote tumor growth in distinct colorectal cancer cells by a beta1-integrin-dependent mechanism. Int J Cancer 2016;138. 964–75.

[88] Beckermann BM, Kallifatidis G, Groth A, Frommhold D, Apel A, Mattern J, et al. VEGF expression by mesenchymal stem cells contributes to angiogenesis in pancreatic carcinoma. Br J Cancer 2008;99. 622–31.

[89] Lamichhane SP, Arya N, Kohler E, Xiang S, Christensen J, Shastri VP. Recapitulating epithelial tumor microenvironment *in vitro* using three dimensional triculture of human epithelial, endothelial, and mesenchymal cells. BMC Cancer 2016;16. 581.

[90] Pasquier J, Guerrouahen BS, Al Thawadi H, Ghiabi P, Maleki M, Abu-Kaoud N, et al. Preferential transfer of mitochondria from endothelial to cancer cells through tunneling nanotubes modulates chemoresistance. J Transl Med 2013;11. doi:10.1186/1479-5876-11-94.

[91] Bersini S, Jeon JS, Dubini G, Arrigoni C, Chung S, Charest JL, et al. A microfluidic 3D invitro model for specificity of breast cancer metastasis to bone. Biomaterials 2014;35. 2454–61.

[92] Breznik B, Motaln H, Vittori M, Rotter A, Lah T. Mesenchymal stem cells differentially affect the invasion of distinct glioblastoma cell lines. Oncotarget 2017;8. 25482–99.

[93] Charles NA, Holland EC, Gilbertson R, Glass R, Kettenmann H. The brain tumor microenvironment. Glia 2011;59. 1169–80.

[94] Badalà F, Nouri-mahdavi K, Raoof DA. The Tumor Microenvironment in Non-Small Cell Lung

Cancer. Computer (Long Beach Calif) 2008;144. 724–32.

[95] Hu G, Chong RA, Yang Q, Wei Y, Blanco MA, Li F, et al. MTDH Activation by 8q22 Genomic Gain Promotes Chemoresistance and Metastasis of Poor-Prognosis Breast Cancer. Cancer Cell 2009;15. 9–20.

[96] Berg EL, Hsu YC, Lee JA. Consideration of the cellular microenvironment: Physiologically relevant co-culture systems in drug discovery. Adv Drug Deliv Rev 2014;69–70. 190–204.

[97] Roth A, Singer T. The application of 3D cell models to support drug safety assessment: Opportunities & challenges. Adv Drug Deliv Rev 2014;69–70. 179–89.

[98] Skardal A, Devarasetty M, Forsythe S, Atala A, Soker S. A reductionist metastasis-on-a-chip platform for *in vitro* tumor progression modeling and drug screening. Biotechnol Bioeng 2016;113. 2020–32.

[99] Kashaninejad N, Nikmaneshi MR, Moghadas H, Oskouei AK, Rismanian M, Barisam M, et al. Organ-tumor-on-a-chip for chemosensitivity assay: A critical review. Micromachines 2016;7. doi:10.3390/mi7080130.

[100] Zhang J, Sun D, Fu Q, Cao Q, Zhang H. Bone mesenchymal stem cells differentiate into myofibroblasts in the tumor microenvironment. Oncol 201650–644. 2016 .

[101] Bartosh TJ, Ullah M, Zeitouni S, Beaver J, Prockop DJ. Cancer cells enter dormancy after cannibalizing mesenchymal stem/stromal cells (MSCs). Proc Natl Acad Sci U S A 2016. 201612290.

[102] Mitra M, Mohanty C, Harilal A, Maheswari UK, Sahoo SK, Krishnakumar S. A novel *in vitro* three-dimensional retinoblastoma model for evaluating chemotherapeutic drugs. Mol Vis 2012;18. 1361–78.

[103] Park SC, Nguyen NT, Eun JR, Zhang Y, Jung YJ, Tschudy-Seney B, et al. Identification of cancer stem cell subpopulations of CD34+ PLC/PRF/5 that result in three types of human liver carcinomas. Stem Cells Dev 2015;24. 1008–21.

[104] Leon G, MacDonagh L, Finn SP, Cuffe S, Barr MP. Cancer stem cells in drug resistant lung cancer: Targeting cell surface markers and signaling pathways. Pharmacol Ther 2016;158. 71–90.

[105] Karlsson H, Fryknäs M, Larsson R, Nygren P. Loss of cancer drug activity in colon cancer HCT-116 cells during spheroid formation in a new 3-D spheroid cell culture system. Exp Cell Res 2012;318. 1577–85.

[106] Alasmari A, Lin SC, Dibart S, Salih E. Bone microenvironment-mediated resistance of cancer cells to bisphosphonates and impact on bone osteocytes/stem cells. Clin Exp Metastasis 2016;33. 563–88.

[107] Lynch ME, Chiou AE, Lee MJ, Marcott SC, Polamraju P V., Lee Y, et al. Three-Dimensional Mechanical Loading Modulates the Osteogenic Response of Mesenchymal Stem Cells to Tumor-Derived Soluble Signals. Tissue Eng Part A 2016;22. 1006–15.

[108] Baksh D, Yao R, Tuan RS. Comparison of Proliferative and Multilineage Differentiation Potential of Human Mesenchymal Stem Cells Derived from Umbilical Cord and Bone Marrow. Stem Cells 2007;25. 1384–92.

[109] Zhu W, Holmes B, Glazer RI, Zhang LG. 3D printed nanocomposite matrix for the study of breast cancer bone metastasis. Nanomedicine Nanotechnology, Biol Med 2016;12. 69–79.

[110] Zhou X, Zhu W, Nowicki M, Miao S, Cui H, Holmes B, et al. 3D Bioprinting a Cell-Laden Bone Matrix for Breast Cancer Metastasis Study. ACS Appl Mater Interfaces 2016. acsami.6b10673.

[111] Oliveira SM, Reis RL, Mano JF. Towards the design of 3D multiscale instructive tissue engineering constructs: Current approaches and trends. Biotechnol Adv 2015;33. 842–55.

[112] Weiss MS, Bernabé BP, Shikanov A, Bluver DA, Mui MD, Shin S, et al. The impact of adhesion peptides within hydrogels on the phenotype and signaling of normal and cancerous mammary epithelial cells. Biomaterials 2012;33. 3548–59.

[113] Oliveira MB, Mano JF. High-throughput screening for integrative biomaterials design: Exploring

advances and new trends. Trends Biotechnol 2014;32. 627–36.

[114] Touboul C, Lis R, Al Farsi H, Raynaud CM, Warfa M, Althawadi H, et al. Mesenchymal stem cells enhance ovarian cancer cell infiltration through IL6 secretion in an amniochorionic membrane based 3D model. J Transl Med 2013;11. 28.

[115] Sung S-Y, Liao C-H, Wu H-P, Hsiao W-C, Wu I-H, Jinpu, et al. Loss of let-7 microRNA upregulates IL-6 in bone marrow-derived mesenchymal stem cells triggering a reactive stromal response to prostate cancer. PLoS One 2013;8. e71637.

[116] Aljitawi OS, Li D, Xiao Y, Zhang D, Ramachandran K, Stehno-Bittel L, et al. A novel three-dimensional stromal-based model for *in vitro* chemotherapy sensitivity testing of leukemia cells. Leuk Lymphoma 2014;55. 378–91.

[117] Chowdhury R, Webber JP, Gurney M, Mason MD, Tabi Z, Clayton A. Cancer exosomes trigger mesenchymal stem cell differentiation into pro-angiogenic and pro-invasive myofibroblasts. Oncotarget 2015;6. 715–31.

[118] Liu C, Liu Y, Xu X, Guo X, Sun G, Ma X. Mesenchymal stem cells enhance the metastasis of 3D-cultured hepatocellular carcinoma cells. BMC Cancer 2016;16. 566.

[119] Wang W, Zhong W, Yuan J, Yan C, Hu S, Tong Y, et al. Involvement of Wnt/β-catenin signaling in the mesenchymal stem cells promote metastatic growth and chemoresistance of cholangiocarcinoma. Oncotarget 2015;6. 42276–89.

[120] Reagan MR, Kaplan DL. Concise review: Mesenchymal stem cell tumor-homing: detection methods in disease model systems. Stem Cells 2011;29. 920–7.

[121] Bersini S, Jeon JS, Dubini G, Arrigoni C, Chung S, Charest JL, et al. Biomaterials A micro fl uidic 3D *in vitro* model for speci fi city of breast cancer metastasis to bone. Biomaterials 2014;35. 2454–61.

1.5. Globe-like Scaffolds for Assembly of 3D Tumor Spheroids - Advances and Prospects

Subchapter 1.5.

This subchapter is based on the review article entitled

"***Globe-like Scaffolds for Assembly of 3D Tumor Spheroids - Advances and Prospects***"

Manuscript in preparation

Globe-like Scaffolds for Assembly of 3D Tumor Spheroids - Advances and Prospects

Ferreira, L.P., Gaspar, V.M., Mano, J.F.

[1]Department of Chemistry, CICECO – Aveiro Institute of Materials, University of Aveiro, Campus Universitário de Santiago, 3810-193, Aveiro, Portugal

[#]Corresponding author:
Professor João F. Mano
Department of Chemistry, CICECO – Aveiro Institute of Materials
University of Aveiro, Campus Universitário de Santiago
3810-193, Aveiro, Portugal
E-mail: jmano@ua.pt
Telephone: +351 234370733

Abstract

Three-dimensional Multicellular tumor models (3D-MCTS) are receiving an ever-growing focus as drug testing platforms due to their potential to recapitulate major physiological features of human tumors in controlled *in vitro* conditions. In line with this momentum, the techniques for assembly of 3D *in vitro* models are rapidly evolving towards an all-round inclusion of tumor microenvironment (TME) components in such microtissues. However, few methodologies have been able to provide such elements. Customized globe-like platforms such as microparticles and microcapsules provide a reproducible and cost-effective technology to imprint unique microenvironment hallmarks into 3D spheroids. Herein, a comprehensive overview of novel advances on the integration of tumor-ECM components and biomechanical cues into *in vitro* 3D-MCTS assembled in microparticle or microcapsule-based platforms is provided. Future improvements regarding spatiotemporal adaptability during microtumors *in vitro* culture are also critically discussed in light of the realistic potential of these platforms to mimic the dynamic TME. From a critical perspective it is clear that a cost-effective production of such 3D TME-MCTS globe-like models will unlock their potential to be used in high-throughput screening of therapeutic compounds. It is also envisioned that their ease of handling will contribute for their combination with other advanced technologies that can mimic the fluidics of human tumors.

Keywords: 3D Models, Spheroids, Drug Testing, *In vitro* Tumors, Microparticles, Microencapsulation

1. Introduction

Although conventionally recommended by regulatory agencies as pre-clinical validation models, 2D cell cultures fail in providing *in vivo* similar conditions for cell growth [1–3]. These models lack the ability to correctly mimic tumor heterogeneity, extracellular matrix (ECM) components and architecture, as well as multidrug-resistance (MDR) mechanisms observed *in vivo* [3]. Addressing the shortcomings of conventional 2D cultures through engineering of more predictable models, capable of simulating *in vivo* solid tumors, could improve anti-cancer drug discovery and drug performance analysis [1]. Such will contribute to reduce the number of false positive results obtained during preclinical validation of novel compounds.

Three-dimensional *in vitro* models have been gaining increased momentum in the field of drug-screening and cancer research do to their ability for better capturing the complexity of the tumor microenvironment (TME) [4,5]. 3D culture models are capable of recapitulating tumors cellular heterogeneity, ECM interactions and tridimensional architecture. In fact, the reproduction of such characteristics in 3D promotes the establishment of nutrient, oxygen and signaling factors gradients, as well as the establishment of unique gene expression patterns, that are similar to those observed *in vivo* [6].

From the currently available *in vitro* tumor models, 3D-MCTS remain one of the most commonly explored [7,8]. Their relative ease of assembly, general reproducibility and the ability to capture cellular heterogeneity renders them suitable tumor surrogates for preclinical validation of novel therapeutic compounds [9]. Up to date various 3D MCTS models have been used to modulate the cellular components of the TME of different tumors including those of breast [10], colon [11], pancreas [12], lung [13]. However, the majority of these models still lack the correct representation of tumor-specific ECM. A critical component that is known to extensively influence cancer evolution through critical biochemical and biomechanical cues [14].

To overcome this limitation, various studies have attempted the inclusion of ECM mimetic matrices in the form of globle-like scaffolds, namely, microparticles (MPs) or microcapsules. Both technologies, are extensively used in the field of tissue engineering and stem cell research [15,16] and offer further opportunities to mimic the TME. These composite models allow the study of singular biochemical and mechanical characteristics of

the TME ECM through inclusion of modular matrix mimetic scaffolds [17]. Such unlocks the opportunity to model cell-ECM interactions and to evaluate the inclusion of ECM components in the response to anti-cancer therapeutics.

This review showcases recent advances in the field of complex 3D MCTS assembly through inclusion of globe-like scaffolds. We begin by summarizing current scaffold-free and scaffold-based 3D microtumor production technologies and present up-to-date examples in the use of microparticles and microspheres to assembly advanced 3D MCTS. These interesting 3D platforms are discussed in light of the recent literature reports. A critical perspective regarding future developments of new models that fully recapitulate the cellular and acellular components of the TME *in vitro* is also provided.

2. 3D Models Production Methods

Ideally 3D tumor models must be able to recapitulate the diverse cellular crosstalk established during cancer cells contact with surrounding stromal cells and tumor-specific ECM. This crosstalk is well recognized to contribute to disease progression [18] depending on the type of cells and ECM configurations involved, for example with increased stiffening of the matrix or increased deposition of some of its components having been linked with tumor invasion promotion or arrest [19–21]. At a cellular level, such dichotomy is well portrayed by the communications established between immune cells and mesenchymal stem cells present in the TME, which can lead to promotion of angiogenesis through the release of pro-inflammatory cytokines [22,23]. To assure *in vivo* similarity, 3D models must be capable of mimicking the mechanical proprieties, spatial arrangement and biochemical composition of the tumor-ECM. In fact, the development of novel 3D tumor models should always try to recapitulate specific conditions and stages of specific tumors under highly reproducible conditions, so as to assure a direct correlation between *in vitro* and *in vivo* performance [14].

The production methodologies for 3D multicellular tumor models can be divided mainly in three categories: (i) scaffold-based models which take advantage of diverse natural or synthetic scaffolds for the culture of cells in a 3D surrogate of *in vivo* tumor-ECM [5,17,24], (ii) scaffold-free based models, which take advantage of cells suspension or hanging-drop based techniques for the formation of 3D MCTS [25–27], and (iii) combinatorial hybrid approaches. The following sections will discuss the differences and

advantages/disadvantages of these specific manufacturing technologies so as to provide a broad overview of the 3D MCTS production field.

2.2.1. Scaffold-free 3D Models Production

Scaffold-free methods are based on implementation of non-adherent conditions for cell culture, taking advantage for instance microgravity settings to force cultured cells to interact and adhere to one another [28]. The main aim is to promote the formation of spherical (spheroids) or more loosely aggregated microtissues (cellular aggregates) [29,30]. Scaffold-free assembled models can be divided into three categories: (i) multicellular tumor spheroid models (3D MCTS), initially implement in 1970s by Sutherland and coworkers [31], these spheroids are created through culture of cancer cell lines or isolated primary cells under non-adherent conditions that force cell adhesion leading to compact cellular aggregates formation; (ii) tissue-derived tumor spheres and (iv) organotypic multicellular spheroids, both obtained by disruption of tumor tissues through mechanical and enzymatical dissociation, with posterior culture of obtained fragments in non-adherent conditions [30]. The most commonly studied and used are the 3D-MCTS, being easier to assemble and maintain than tissue-derived tumor spheres or organotypic multicellular spheroids, these spheroids have been extensively used in the field of 3D tumor modelling.

Static-based scaffold-free methods such as Forced-floating or Hanging-drop techniques allow the assembly of highly reproducible 3D MCTS in terms of size and morphology [29]. These techniques make use for example of poly-2-hydroxyethyl methacrylate (poly-HEMA) [32], agarose coated multiwell plates [25], or of super-hydrophobic surfaces [33], in order to prevent adhesion between cultured cells and culture-plate surfaces, promoting instead cell-cell interactions and consequently cell-cell adhesion and aggregation [34]. These 3D MCTS can be formed either by monotypic or heterotypic co-cultures [29,35]. Overtime, most of the newly formed 3D MCTS start to secret their own ECM. Such increases their solidity and diminishes their size as a bystander effect of contraction, further approaching these models to the *in vivo* reality [29].

Stirring-based techniques can be grouped into two classes: (i) spinner-flask bioreactors in which the culture media is internally impelled by spinning blades, and (ii) rotational bioreactors [36]. Such methods take advantage of mechanical forces that maintain cells in continuous suspension during culture [29]. By comparison to stirred tank bioreactors, rotational bioreactors have the advantage that the internal flow is generated by rotation of

the container and not through blade mechanisms, this imparting a lower shear-stress to the cultivated cells [29].

In comparison to stationary methods, stirring based methodologies are able to effectively produce high amounts of 3D MCTS, having the advantage of allowing easy medium exchange and modifications to cell culture conditions *in situ* [37]. However, regarding reproducibility of formed spheroids, stirring based techniques lack the level of control over the morphology and size of spheroids present in stationary methodologies [38]. Consequently, 3D spheroids and cellular aggregates obtained in bioreactors frequently exhibit variable shapes, density and other morphological parameters, leading to inconsistent responses to chemotherapeutic agents [14,39]. Since cellular concentration is dictated for the entire batch, different internal dynamic flows can also result in diversified cellular adhesion patterns or effective initial concentrations [36].

The combination of both stirring and forced adhesion methods could overcome such limitations, for example by firstly using hanging-drop or liquid-overlay techniques to obtain highly uniform spheroids and then translocating them into bioreactors for modulating the influence of fluid dynamics in chemotherapeutics penetration into compact 3D models [40]. Overall, the main advantages of scaffold-free stirring-based methods are (i) the ease of manufacturing multiple microtissue spheroids per batch, (ii) the ability to maintain prolonged culture times, (iii) the ability to modify the culture media and growth conditions to better simulate the changes occurring *in vivo*, and (iv) the ability examine the evolution of the cultures through time either by direct analysis *in situ* [41], or with for example 384 hanging-drop arrays as described by Hisao and Tung [42].

2.2. Scaffold-Based 3D Models Production

Tumor evolution *in vivo* is intimately correlated with the interactions between cells of TME and their supporting ECM which serves both structural and signaling functions [43]. Being composed mainly of fibronectin, collagen (types I-V), elastin, entactin, fibrilin, fibulin, vitronectin, laminin and other glycoproteins such as hyaluronic acid [44]. During the process of tumorigenesis alterations in ECM composition and structure can occur due to cancer cells and stromal associated degradation and deposition of ECM leading to events such as collagen stiffening in breast cancer [45], increased hyaluronic acid deposition and degradation in several cancers [46–48], or increased matrix degradation through metalloproteinase enzymatic digestion (e.g., MMP9, MMP2) [49] in breast [50] and lung

cancer [51], cumulatively leading to increased invasion and epithelial-to-mesenchymal-transition (EMT), and consequently metastasis.

It is the nature of these interactions that scaffold-based tumor models aim to recapitulate, leading to the activation of for example cell-matrix signaling mechanisms through the inclusion of small signaling molecules, tethered protein signaling domains, or through variation of mechanical properties of the scaffold such as matrix stiffening through fibrillar alignment of collagen [52,53]. This promotes different metabolic profiles that more closely resemble *in vivo* tumor dynamics [54]. Such models have to be engineered taking into account ECM tissue and patient specificity, with diverse compositions and arrangements seen for the same tumor class resulting in diverse response rates to therapy [14]. Scaffold based 3D culture methods take advantage of natural, synthetic or hybrid biomaterials to culture cells in three-dimensions [17,29], with each class presenting its own advantages or disadvantages for portraying *in vivo* tissues (Table 1). ´

Table 2. advantages and disadvantages of the various scaffold materials used in scaffold based approaches.

Class	Origin	Examples	Advantages	Disadvantages	ref
Natural	**Mammalian**	Collagen	• Contain *in vivo* similar domains (e.g laminin, elastin, fibronectin) • Cellular adhesive proprieties • Recapitulate interactions present *in vivo* • Enzymatically degradable	• Exact Composition is unknown • Batch-to-batch variability • For some materials limited level of control over matrix stiffness	[55]
		Matrigel			[56]
		Hyaluronic Acid			[57]
		Decellularized Matrix			[58]
	Non-mammalian	Alginate	• Present decreased immunogenicity • Elevated biocompatibility More affordable	• May require further alteration to simulate *in vivo* tissues • Fabrication methods can be cytotoxic	[59]
		Chitosan			[60]
		Silk-fibroin			[61]
Synthetic		Polyethylene glycol (PEG)	• Structurally complex and well defined • Highly tunable mechanical proprieties	• Lack ECM similar domains • Require further modification for increased bioadhesion and biocompatibility • Degradation can result in cytotoxic byproducts	[62]
		Polylactic acid (PLA)			[63]
		Polycaprolactone (PCL)			[64]
		Poly(lactic-co-glycolic acid) PLGA			[63]

Hybrid	Alginate-RGD PEG-RGD PEG-fibrinogen	• Combine the ease of modification of synthetic and in vivo similar domains of natural materials	• Fabrication methods can be cytotoxic • Proprieties of natural materials could be affected	[65] [66] [67]

These ECM mimetic scaffolds can be manufactured into diverse structures such as: (i) fibrillar porous meshes, (ii) porous and non-porous microstructures (microparticles or microcapsules), and (iii) micro-patterned surfaces, via 3D bioprinting technologies [24,29,68,69]. Materials and production methodologies of scaffold-based methodologies have been extensively reviewed elsewhere [17,70–72]. The different materials are selected by their specific characteristics, such as rate of biodegradation, biocompatibility, elasticity, ease of manipulation and resemblance to tumor-specific ECM. In the following sections the most commonly used materials for these models is given, starting with natural-derived scaffolds and moving to synthetic and innovative semi-synthetic approaches.

2.2.1. Natural-materials based Scaffolds

From natural material-based scaffolds the most commonly used hydrogel scaffold for *in vitro* production of 3D MCTS [24] is Matrigel®, an hydrogel matrix comprised by basement membrane proteins derived from Engelbreth–Holm–Swarm mouse tumor cells [73]. These hydrogels can be formed prior to cell culture or assembled under standard culture conditions [74,75]. Often such hydrogels require laborious preparation involving ice thawing to prevent premature polymerization, since the material is liquid at 4º C and quickly gells into an hydrogel at physiological temperature (37 ºC) [75]. When gelled, Matrigel® forms a randomly weaved mesh of fibers that withholds a large amount of excess fluid, which can hinder the control of matrix stiffness [76]. Due to their natural origin these scaffolds introduce ECM specific signaling molecules and binding domains, such as laminin, collagen, elastin, entactin, fibronectin, fibrinogen, different growth factors (e.g., EGF, bFGF, PDGF), amongst others [77]. Such bioactive components provide for example integrin and MMP binding sites, both of them imperative in tissue organization and cancer metastasis [44]. As a result of their origin, natural-based scaffolds exhibit similar structural interactions to those found in humans providing a suitable *in vivo*-like matrix where different cell lines can proliferate and differentiate for example into cancer stem cells [77,78]. However, due to

Matrigel animal origin, these models also exhibit significant "batch-to-batch" variations [77], which results in low reproducibility and inaccurate analysis of candidate therapeutics [14]. Furthermore, the complex protein domains present and the mechanic properties of the natural-based scaffolds are not easily tuned, which results in some difficulty in providing reproducible tissue specific ECM like environments [14]. For example, Matrigel does not contain proper ratios of collagen type I or hyaluronic acid as those found in the matrix of *in vivo* tumors [52].

Other examples of natural based scaffolds commonly used for the assembly of 3D tumor models are collagen, hyaluronic acid, alginate, chitosan and silk fibroin hydrogels, as well as decellularized extracellular matrices. Most of them present low immunogenicity, tunable mechanical proprieties, high biocompatibility and cell adhesive proprieties [79]. The advantages and disadvantages of these alternative materials for assembly of 3D tumor models are summarized in (Table 1). These materials have recently received increased focus as scaffolds for assembly of 3D tumor models in several reviews available elsewhere [70–72,79–82].

2.2.2. Synthetic materials-based scaffolds

Alternatives to nature derived scaffolds include the synthetic polymer-based scaffolds, which although lacking correct representation of several biomolecular aspects of the TME (i.e., the presence of specific growth factors, or protein domains responsible for cellular adhesion), strive to effectively mimic ECM mechanical and structural proprieties [71]. To this end several biocompatible, biodegradable polymers have been synthesized and reported in the literature in the recent decades, with some of the most commonly used being polyethyleneglycol (PEG), polylactic acid (PLA), polyglycoslide or poly(glycolic acid) (PGA), and their derivatives poly(lactic-co-glycolic acid) (PLGA) and poly(d,l-lactide-co-glycolide) (PLG), and polycaprolactone (PCL) [5,83]. Such hybrid materials will be discussed in the following chapters. Overall, although the variability of "batch to batch" formulations and the lack of a precise control over scaffolds mechanical characteristics is eliminated with synthetic polymers [84], these lack the before mentioned protein-specific cell adhesion domains, impregnated growth factors or cytokines that are important for tumors cellular organization. Moreover, the cells cultured in thee platforms are devoid of tumor-like gene expression patterns, unable to metastasize or to display multi-drug resistance phenotypes [24,85]. Expectedly, such issues affect the production of robust tumor-

mimicking 3D *in vitro* MCTS models. To overcome such drawbacks synthetic materials are often combined with other polymers such as polyvinyl alcohol (PVA), or with natural derived biopolymers such as chitosan, hyaluronic acid or polydopamine, in order to attain more *in vivo*-like growth conditions [63,86,87].

2.2.3. Hybrid Scaffold Based Models

The development of hybrid-based scaffolds for assembly of 3D MCTS allows the incorporation of natural bioactive sites, and bioadhesive properties into the highly tunable matrix of synthetic scaffolds [79,83]. These act as a white-canvas to be conjugated with natural polymers such as fibrin [88] hyaluronic acid [57], or specific bioactive molecules (e.g., BMP-2, RGD peptides). PEG and its derivatives (PEG-diacrylate) is the foremost common example in terms of conjugation with bioactive molecules or scaffolds, U.V. light polymerization, or through chemical coupling. In fact, as demonstrated by Weiss and co-workers, PEG hydrogels were successfully functionalized through crosslinking with peptide containing RGD domains [89], increasing its cellular adhesive proprieties. In addition, MMP or plasmin-sensitive sequences have also been chemically imprinted into PEG-hydrogels [81,84]. Inclusion of these bioactive moieties increased cellular interactions (e.g., cell-ECM and cell-cell), and mimicked tumor-ECM specific degradability [90]. Providing both highly characterized and controllable scaffolds, that at the same time can mimic tumor-ECM, through inclusion of necessary matrix domains for correct cellular 3D organization and proliferation [29,76,77].

Compared to conventional scaffold-base and scaffold-free approaches, advanced hybrid scaffold base models provide novel and interesting platforms in which to modulate, with relative ease, several aspects of tumor progression. Hybrid scaffolds could allow the modular study of the role of specific matrixial components in events such as metastasis [91] or angiogenesis [92]. However, one of the main drawback all scaffold models suffer when compared to scaffold-free systems is relative low-through-put and laborious analysis procedures required [14]. Advanced hybrid scaffolds provide novel and interesting platforms in which to modulate with relative ease several aspects of tumor progression, such as metastasis or angiogenesis, while permitting the evaluation of specific ECM components influence. Combinations of both scaffold-based and scaffold-free methods have been reported in the literature [93,94]. A recent work by Hirt and coworkers in 2015, demonstrated the combination of bioreactor-based methodologies to developed a drug-screening model of

colon cancer with HT-29 cells cultured in porous scaffolds under perfusion flow [95]. The model showed a high correlation with tumor xenografts regarding the testing of a cytotoxic compound (5-Fluorouracil), and a clinically effective compound (BCL-2 inhibitor ABT-199), with 2D cultures evidencing antagonistic responses [95]. Other promising models have combined bioreactors with microfluidic platforms [96]. Microfluidic systems entail the use of micrometer sized channels that open the possibility to produce 3D MCTS under flow perfusion conditions [97]. Ultimately, scaffold-microfluidic combinations allow for a more precise control over cancer cells growth by dynamically controlling cell culture media composition and manipulating drugs mass transfer via modification of liquid flow rate [98]. These characteristics make microfluidic systems ideal to perform angiogenesis, migration, or flow perfusion studies in the context of tumor perfusion and tumor invasion, EMT, cells dissemination and metastasis [24,99,100]. Several recent studies using microfluidic systems in combination with scaffold and even spheroid technologies, have tried to establish an ideal organ-on-a-chip model that allows the study therapeutic compounds interactions with lung, intestine, liver and other tissues of the body, whilst also studying its effects on diseased cells. Such developments have been recently reviewed elsewhere [94,101–105], and derive out of the scope of this review.

Considering the specificities of the drug-screening process, namely the necessity of high-throughput, ease of analysis, reliability and predictability of the PCVMs, an ideal approach could require [106,107] the combination scaffold-based models and their ability to represent ECM biochemical and mechanical complexity, with the ease of analysis obtained from simple scaffold-free based models. Following the example of stem cells research in tissue e*ngineering [16], such a combination could be achieve using for example the inclusion of MPs containing specific ECM mimetic components. Such a combination would allow inclusion of both cellular and matrixial components of the TME into a spherical\globular scaffold, leading to the formation of composite spheroids compatible with current analysis methodologies. An alternative methodology, more explored in literature, would be the encapsulation of cancer cells inside hydrogel microcapsules [15]. Microencapsulation techniques have shown the capacity of confining and standardizing spheroid growth while providing a matrixial component otherwise lacking [15]. Several spherical *in vitro* tumor mimicking cancer models have been achieved, providing innovative platforms for the study of tumor biology and drug-screening assays. Herein,

microencapsulation and microparticle scaffold will be reviewed under the light of recent reports.

3. Composite Heterogenic Spheroids - Novel Complex Globular Alternatives

As previously stated, 3D-MCTS are currently the *in* vitro golden standard for performing drug-screening assays [28], due to their ability to correctly recapitulate several features of the tumor microenvironment, such as: (i) cell-cell interactions; (ii) matrix deposition; (iii) cell-ECM interactions; (iv) internal structure organization, resulting in hypoxic and consequently necrotic core establishment; (v) drug-resistance stemming both from drug resistant population phenotype stimulation, and penetration limitations [26]. This approach provides a platform that can be easily assembled and facilitates HTP studies [108] in comparison with more complex scaffold or microfluidic based models. However, as previously discussed, spheroid-based methodologies are not without disadvantages [14].

By comparison to scaffold based models, 3D-MCTS main limitation is the lack of previously existing ECM support structure. As a result, contrarily to what happens *in vivo*¸ the ECM will not be able to guide or influence the model evolution from the onset, ultimately failing to provide the necessary initial cues for certain cancer phenotypes to arise [14]. Consequently, the acquisition of phenotypes less capable of resembling those found *in vivo* can be observed in certain culture settings. For instance, Brancato and coworkers, 2017 [109], reported that for spheroids of either CAF or normal fibroblasts, different cell metabolism, cell growth, matrix deposition rates and mechanical properties were observed when culturing cells with or without support of porous gelatin MPs [109]. Through the utilization of such MPs the authors were able to better replicate the functional and metabolical differences found *in vivo* between healthy and neoplasic tissues containing CAF's [109]. This work serves to exemplify how introduction of MPs into spheroids-based tumor model allows to surpass such limitations.

3.1. Microparticles for 3D models Assembly

MPs have been previously and more extensively applied in the field of tissue engineering mainly in four areas of application: (i) delivery of incorporated or surface-attached molecular cues or tethered protein into tissues or cell aggregates; (ii) reporting changes in culture conditions; (iii) serving as scaffolds for cell attachment and providing

necessary cues for cell differentiation or phenotype stimulation, and (iv) introduction or preservation of local targeted heterogeneity or homogeneity [16]. Regarding their role in tumor model development most studies have made use of MPs mainly has a structural and molecular cue providing tools, with few works exploring MPs potential so far. Studies involving MPs-based scaffolds for the production of *in vitro* tumor models are still few [63,67,110–114], with most studies found to date employing either non-modified synthetic polymers, or combined natural-synthetic scaffolds such as the previously discussed PEG-Fibrinogen model, later developed by Pradhan and coworkers into the format of MPs [67].

Emerging works have described the utilization of MPs scaffolds as a means of introducing previously lacking ECM components into 3D-MCTS, promoting stem-like or multidrug resistance profiles [109,110] [112]. Production methodologies mainly involved the application of modified double emulsion protocols and sieving, with the combination of both techniques allowing a high yield of MPs in the desired size ranges [67,109–111,113]. Sahoo and co-workers, 2005, [63] produced porous MPs based scaffolds which allowed cells to interact with a semi-rigid or rigid ECM-like structure. The obtained PLGA/PLA MPs presented elevated diameters (~100-260 μm) and consequently grand surface areas. After a period of 5 days MPs found themselves completely covered in cell layers, attaining a spherical aggregate morphology overtime, and thus being able to retain the ability to promote compact cell-cell adhesion characteristics found in 3D scaffold-free techniques. This approach allows the formation of 3D-MCTS when coupled with forced-floating, hanging drop or stirring-based methodologies [63].

In the context of particle porosity, the work of Bae and coworkers [113] established a cryopreservable tumor model of MCF-7 using PLGA microspheres with an average particle diameter of 393±5 μm, an exterior pore size ranging from 10-70μm with innterwinded porosity (Figure 1). The particles were used for cancer cell culture in stirred suspension bioreactors, achieving an elevated growth rate (2.8-fold cell expansion over seven days), increased resistance to doxorubicin when compared to 2D counterparts, as well as maintaining viability and metabolic profiles after the process of cryopreservation. Moreover, the model exhibited increased effectiveness in establishing tumors on athymic female mice, with MCF-7 cells cultured on microspheres presenting a 4-fold increase in tumor formation [113].

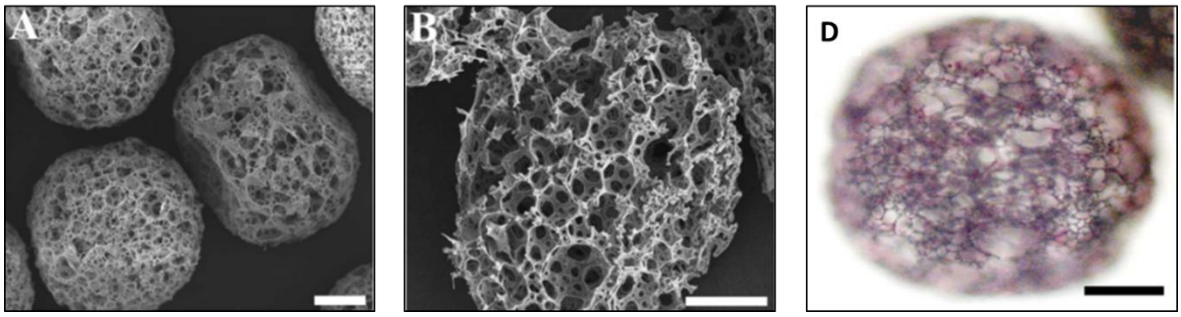

Figure 3. PLGA microspheres produced by Bae and coworkers as a cryopreservable model, as seen in SEM, presenting pores of extreme sizes capable of permitting interiorization of cells (A,B). Hematoxylin-Eosin staining of MCF-7 cells cultured on the microspheres in spinner flasks at the 5th day of culture. White and Black bars represent 100µm. Image adapted from the work of Bae and coworkers [113].

So far, the majority of studies produced polymeric MPs as supporting scaffolds for assembling breast cancer cell spheroids, but mostly restricted to the MCF-7 lineage [67,109–111,113,115]. Several studies made use of MPs scaffolds as a mean of culturing breast cancer cells for measuring cytotoxic effect of diverse pharmacological compounds such as doxorubicin, paclitaxel and tamoxifen [110,111,113]. In this context, Horning and coworkers, 2008, used a combination of PLA and CH to create MPs with diameters of 160-182 µm for culturing MCF-7 cells and evaluating its cytotoxicity profile against doxorubicin, paclitaxel and tamoxifen [111]. The authors performed a comparison analysis between 2D and 3D models, and observed that drug internalization was significantly delayed in the 3D model. (Figure 2). I fact, while in the 3D models containing MPs doxorubicin only reached the spheroid core region after 8 h of incubation, in 2D models such observations were visible within the first hour.

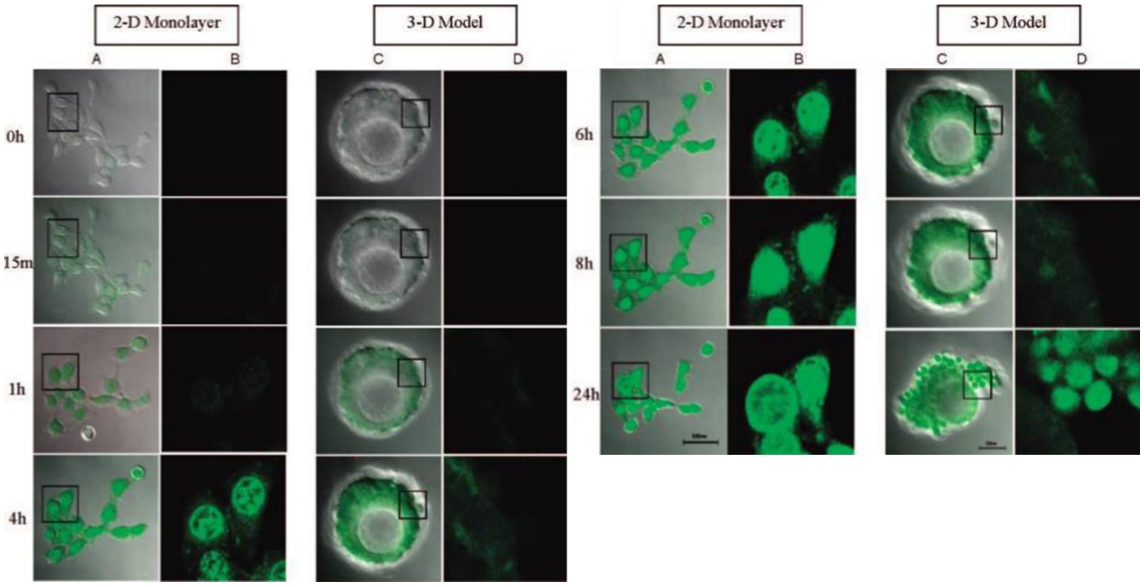

Figure 4. Doxorubicin penetration over time in both 2-D monolayer cultures and 3-D of MCF-7 cells, following incubation with 2.500 ng/ml of therapeutic compound. B and D columns are enlarged sections of the images in the right, demonstrating the slower penetration of doxorubicin in spheroids over periods of 24h. Image adapted from Horning and coworkers [111].

The ability to recapitulate *in vivo* arrangements and expression patterns may pave the future for screening novel therapeutics targeting specific TME hallmarks. Another study by Brancato and coworkers, improved on the previous porous gelatin microparticle based model of stroma through the addition of MCF-7 cancer cells. This breast cancer coculture model containing porous gelatin MPs, was used to test a targeted nanoparticle drug delivery system [110]. Comparative analysis confirmed elevated expression of MMP-2 and other metalloproteinases in the 3D model versus 2D cultures, hence better mimicking *in vivo* overexpression by breast cancer cells in the TME. Strikingly, this enzymatic overexpression was effectively exploited via an enzyme-responsive targeted delivery system, comprised by PLGA-PEG nanoparticles and a tumor targeting pro-drug activated by MMP2 degradation. Results evidenced increased specificity of targeting system in MPs based models, with the efficacy of the nanoparticles being confirmed through increased cytotoxicity in the 3D model [110].

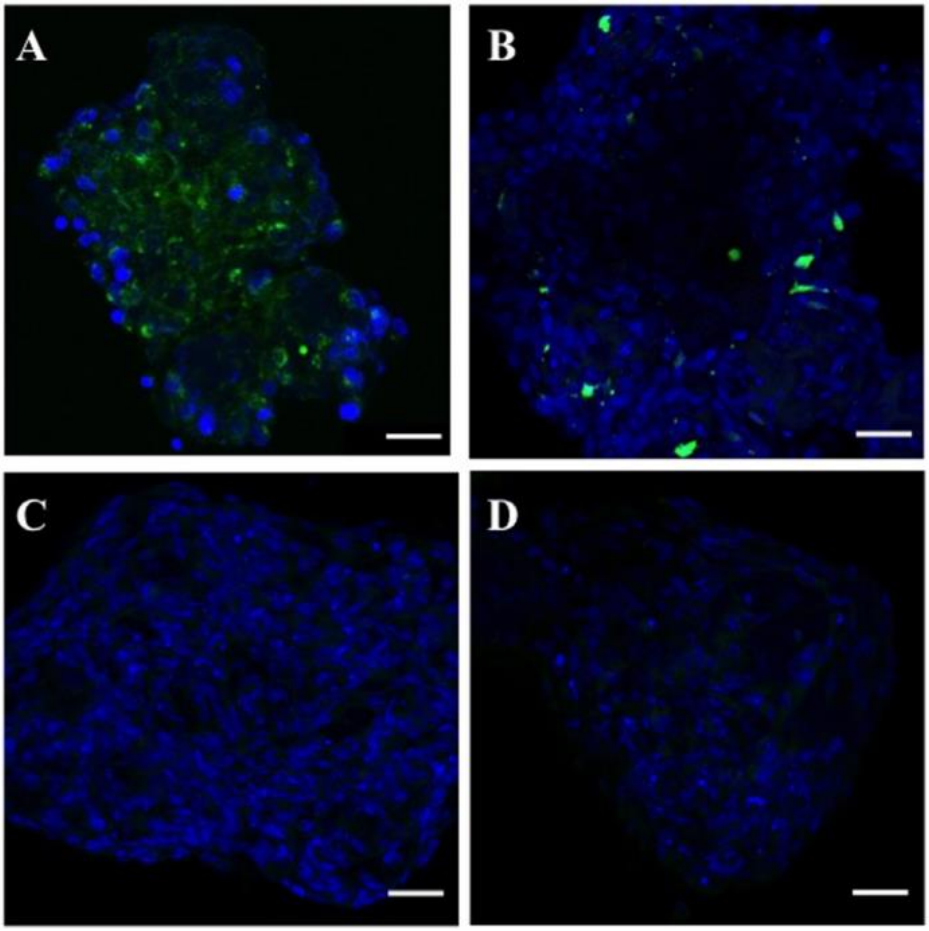

Figure 5. Fluorescence microscopy analysis of Doxorubicin distribution (green). Spheroids containing both CAF, MCF-7 cells and gelatin MPs (A,B) exhibited higher retention of Doxorubicin than spheroids treated with PLGA-PEG dox carrying non-targeting nanoparticles. Furthermore in spheroids formed by normal fibroblasts and gelatin microparticles alone, almost no release of doxorubicin seems to have taken place. Demonstrating the models potential for mimicking in vivo overexpression of metalloproteinases, and the delivery systems capacity for targeting the TME. Image adapted from Brancato and coworkers, 2017b [110].

Despite extensive implementation of microparticle-based scaffolds in tissue engineering applications, there is still a tremendous untapped potential for exploring these assemblies in the field of *in vitro* tumor modelling. In fact, most models containing MPs merely focus their utilization cell culture vehicles and facile retrieval from bioreactors. Production of finely tuned microparticle structures using advanced 3D printing and micropatterning technologies [116], or through the utilization of flow-focusing microfluidic devices [117], could allow to study the role of specific signaling cues. These novel approaches may shed light upon their specific roles and enhance our capacity to modulate the TME.

3.2. Microencapsulated 3D Tumor models

Microencapsulation (ME) of cancer cells or spheroids is a promising strategy for tumor modelling that has received considerable attention in recent years [5]. ME can serve as a mean of representing spatially defined ECM-like scaffolds. This strategy allows cancer and stromal cells, in mono or cocultures, to grow and establish both cell-cell and cell-ECM interactions in a limited, yet, not fully isolated environment. Furthermore, the encapsulation of cancer cells, particularly in spherical-shaped, size-controlled microcapsules with semi-permeable membranes, allows bidirectional diffusion of nutrients, oxygen, therapeutic compounds and low to medium molecular weight signaling molecules (e.g., growth factors and cytokines). In addition, ME can serve as a mean of preventing the penetration of high molecular weight objects such as antibodies and immune cells [118], having been originally employed as a tool for cell transplantation and immune isolation. In the field of tumor modelling, ME has been employed in a diverse set of ways that will be discussed in the following examples [15].

The ability to restrain direct cellular contact makes microencapsulated 3D-MCTS an ideal model to study the diverse paracrine interactions occurring in the TME between the different cellular populations. This capacity was exploited by Yeung and coworkers in 2015 [119], for the study of non-direct communication between neuroblastoma and bone-marrow derived mesenchymal stem cells. By using a collagen microsphere system, the authors demonstrated mesenchymal stem cells ability to promote neuroblastoma growth [119]. A study by Cui and coworkers [120], demonstrated the feasibility of easy cell recovery through thermal-dissociation of microcapsules incorporating HeLa cells which were readily recovered as aggregates under specific temperature conditions. Another study, by Huang and coworkers [121], reported a microcapsule model formed by gelation of a newly discovered peptide for encapsulation of MCF-7 cells. The methodology employed for microcapsule formation allowed cells to be encapsulated at physiological pH and temperature, in minimum essential medium (MEM), decreasing cytotoxic effects sometimes associated with microencapsulation processes [15,122]. Through shear stress, caused by pipetting, the gel was easily converted back to its liquid form allowing recovery of breast cancer cells [121]. Furthermore, cytotoxicity assays with cisplatin revealed that the models were suitable for drug-screening assays, by allowing free penetration of the drug. Such ability to isolate

specific cells further increases the capacity of studying genetic and phenotypic alterations in specific sub-sets of the cultured cells.

Similarly to MPs, microcapsules can also serve as a technology for inclusion of tumor ECM components. Several studies demonstrated that for neuroblastoma [119], lung [123] and breast [118,119,124,125] cancer microencapsulated spheroids establish cell-cell signaling interactions similar to those observed *in vivo.* Moreover internal ECM matrix components deposition occurs inside the microcapsules, leading to increased resistance when compared to conventional 2D models. Such makes these 3D microencapsulated models possibly suitable for drug-screening assays and research in tumor drug resistance. Interestingly ME 3D-MCTS models can mimic for example both solid tumor density [125], cell-matrix interactions, and the mechanical and physical pressures resultant from uncontrolled expansion of tumor masses, which can promote cancer metastasis and lead to profile alterations in cancer cells [122]. In fact, as demonstrated by Guzman and coworkers [126], depending on the elasticity of the chosen microcapsule, these can allow the study of the invasive processes carried out for example by invasive breast cancer [126] and other epithelial tumors [127], recreating the breaching of the involving basement membrane layer that surrounds the primary tumor site. Furthermore, as elegantly demonstrated by Alessandri and coworkers, 2013 [122], microcapsules can be used to study the buildup of intra-tumoral pressure, decurrent from the increasing of tumor mass generating increasing pressure on adjacent tissues and conversely compressing the tumor [128].

Microcapsule-encompassed spheroids are assembled through several methodologies, the most common of which being generation of liquid-core structures through utilization of microfluidic devices and hydrogel reticulation methods [118,122,125,129–131]. Frequently assembled microcapsules present diameters in the order of a few 100 μm to 500 μm, an exception being the study produced by Pradhan and coworkers, 2014 [115]. The authors assembled Poly(ethylene glycol) diacrylate (PEGDA) milibeads through the usage of a single droplet emulsion technique in which the PEGDA droplets were crosslinked in oil solutions through a dual-photoinitiator system. The authors consistently created monodisperse milibeads with geometric diameters that ranged from 1671.24 ± 34.91 μm to 3089.07 ± 55.58 μm (Figure 3) for encapsulating MCF-7 cells [115]. Moreover, the developed modelachieved good cell-cell and cell-matrix adhesion, proliferation and

establishment of extensive necrotic chore regions at day 5 of culture, accompanied by proliferative outer rims, akin to those characteristic of *in vivo* tumors (figure 4) [115].

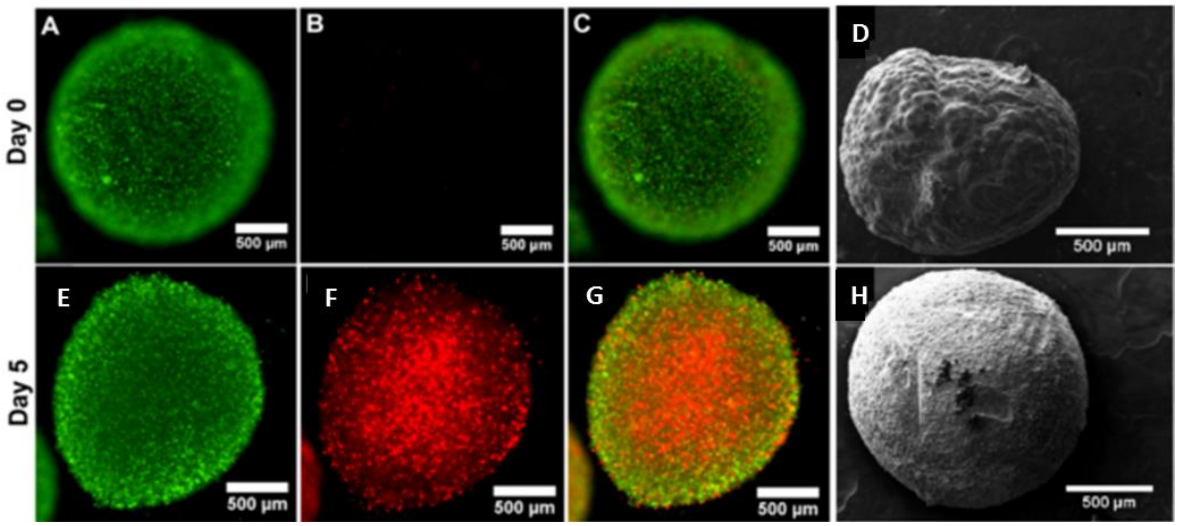

Figure 6. Tumor mili-sized particles capable of recapitulating tumor conditions lead to the establishment of necrotic cores around the 5 day of culture. Live cells are stained with a green fluorescent marker, while dead ones appear in red. Difference between day 0 (A,B,C) and day 5 of culture (E,F,G). Ultrastructure of tumor mili-sized beads without (H) and with (D) encapsulated tumor cells, as observed through SEM. Image adapted from Pradhan and coworkers [115].

Microfluidic-based approaches use flow-focusing, T-junction chips or more complex channel designs [15,28] to generate droplets of cell suspensions mixed with pre-selected biocompatible polymers or hydrogels. In these strategies, spherification into globe-like structures is achieved by exposure to a crosslinking agent, such as calcium bath solutions or UV light, which triggers gelation and produces microcapsules containing the desired cells. Encapsulated cells assemble overtime to form matrix-encapsulated spheroids capable of establishing both cell-cell and cell-matrix interactions [132]. An excellent example of such application is the former mentioned study by Alessandri and coworkers, 2013 [122]. In this study, a model of colon carcinoma based on murine CT26 colon cancer cell line was assembled through a simple and highly reproducible method, based in a microfluidic co-extrusion chip assembled by co-centering three glass capillaries extruding sequentially cell solution, calcium free solution and alginate solution into a calcium bath [122]. The authors were able to assemble highly elastic spherical microcapsules that acted as quantitative mechanical sensors to measure the internal pressure resultant from the expanding tumor cells. Moreover, the researchers found that peripheral cells inserted in the encapsulated model readily escaped the spheroid environment, while the spheroid invasive profile was not present in non-confinement 3D models (figure 5) [122].

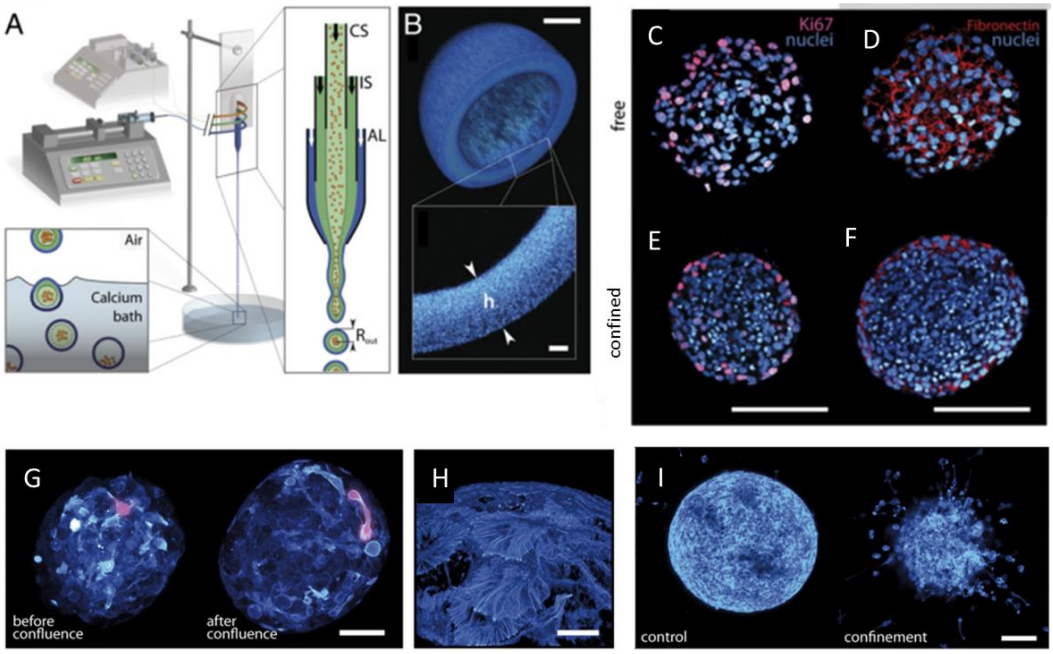

Figure 7. Schematic of the microfluidic chip for production of globe-like microcapsules. (A,B) Schematic of the process used to produce alginate microcapsules, and confocal micrographs after staining with dextran (B). CT26 cultured in alginate matrix (E,F) and in free-spheroid form (C,D) 3D models were cryosectioned and analyzed through immunolabeling DAPI (blue), KI67 (magenta), and fibronectin (red). Magnification confocal microscopy image of the surface of a fixed spheroid after staining with phalloidin-Alexa 488 (Hot LUT, cyan) (H). After reaching confluence both confined and control spheroids (G) were inserted into a collagen based scaffold to access invasion capacity, after 48 h cultured cells in confined models started to invade collagen matrix while freely formed spheroids retained their spherical shape (I). Scale bars: B=50 μm; C, D, E, and F=100 μm; G=50 μm; H=10 μm; I=100 μm. Adapted from Alessandri and coworkers [122] with permission from Proceedings of the the National Academy of Sciences of the United States of America (PNAS).

Additional approaches to microcapsule production consist in the utilization of coaxial electrospraying based encapsulation, or alternatively aerosol based microencapsulation [131]. Leong and coworkers [131], demonstrated the feasibility of microencapsulating keratocytes (HaCaT) and cancer cells of oral squamous cell carcinoma (ORL-48) inside alginate microcapsules polymerized in a calcium bath. Produced microtissues were capable of self-arranging into spheroids inside the alginate microcapsules, remaining viable until after 16 days of culture. Other commonly employed techniques for microcapsule production involve simple procedures such as emulsion technique-based microencapsulation, or syringe pump extrusion and micromolding [15]. The work developed by Lee and coworkers, 2011 [130], is an excellent example of the latter technique. In this study, the authors used diffusion-mediated encapsulation, performed in PDMS-micromolds where hepatocarcinoma spheroids were previously assembled. Such spheroids were subjected to posterior deposition

of encapsulating alginate hydrogel through nano-porous membranes that allowed control over deposition rates of crosslinking agents [130]. Lastly, 3D bio-printing has also been used by Xu and coworkers, 2011 [133], to produce HTP automated encapsulation of ovarian cancer cells and fibroblast coculture droplets in Matrigel™. This approach allows the study of coculture interactions in diverse settings due to high control over initial cell density and spatial arrangement of patterned structure of the model.

Identically MPs, microcapsules can be used as a means of incorporating specific ECM mimetic components allowing the establishment of *in vivo* like interactions between internalized cells and exterior membrane as was shown by Xu and coworkers, 2010 [123]. In this study, the authors encapsulated A549 cells in a gelatin and glycosaminoglycans matrix modified with the addition VEGF, bFGF and a laminin peptide to improve cell adhesion, in an attempt to substitute commonly used Matrigel™ and establishing an improved xenograft model using enriched 3D encapsulated lung cancer cells *in vivo*. Results showed that the obtained model was comparable to Matrigel based 3D-MCTS xerographs while allowing complete control over initial matrix composition [123].

4. Conclusions

The need for expediting drug research both at the preclinical validation level and discovery of novel targets is crucial for the management of currently incurable diseases such as cancer. Research regarding development of novel 3D *in vitro* models is increasingly contributing to this goal by providing innovative platforms capable of efficiently, predictively, and robustly mimicking the complex *in vivo* reality of the TME in what regards its cellular and ECM components. Among the vast array of 3D cell culture methodologies that have been developed to date for *in vitro* tumor modeling, 3D spheroid based models are the most promising regarding production of high throughput-affordable tumor mimetics. Microencapsulation and microparticle-based production technologies are capable of recreating complex cell-cell, mechanical and physiological characteristics that characterize *in vivo* solid tumors. Such are highly valuable characteristics since standard 3D spheroid models lack correct ECM representation and confinement of soluble mediators (e.g., growth factors, cytokines) in controlled environments such as those found in human tumors niche.

Overall, there is a tremendous potential for improving 3D spheroid-based drug screening platforms by combining the knowledge acquired in scaffold-based methodologies with microencapsulation or microparticle inclusion techniques to form globe-like

microtumor constructs [15,16]. Such cell-in-globe approaches have the potential to mimic a plethora of features such as mechanical cues upon cancer cells proliferation into microcapsules walls, as well as specific ECM configurations. Moreover, microencapsulation provides the means of studying in detail both direct and indirect cell-cell and cell-matrix interactions found in the TME. A deeper knowledge about such crosstalk and events will open the opportunity to develop more advanced therapies that inhibit the process of tissue invasion and metastasis. From a therapeutic perspective metastasis inhibition will open a new window of opportunity to increase patients survival rates past 5 years.

In a future perspective, the nature of 3D spheroid models and the unique features provided by microencapsulation and microparticle technologies could also be combined with dynamic bioreactor-based culturing technologies so as to provide an added layer of *in vivo*-like conditions. Moreover, further improvements to cell-in-globe like 3D models are expected with their combination with advanced organ-on-a-chip platforms.

5. References

[1] Cox MC, Reese LM, Bickford LR, Verbridge SS. Toward the Broad Adoption of 3D Tumor Models in the Cancer Drug Pipeline. ACS Biomater Sci Eng 2015;1. 877–94.

[2] Begley CG, Ellis LM. Drug development: Raise standards for preclinical cancer research. Nature 2012;483. 531–3.

[3] Stock K, Estrada MF, Vidic S, Gjerde K, Rudisch A, Santo VE, et al. Capturing tumor complexity *in vitro*: Comparative analysis of 2D and 3D tumor models for drug discovery. Sci Rep 2016;6. 28951.

[4] Chwalek K, Bray LJ, Werner C. Tissue-engineered 3D tumor angiogenesis models: Potential technologies for anti-cancer drug discovery. Adv Drug Deliv Rev 2014;79. 30–9.

[5] Fong ELS, Harrington DA, Farach-Carson MC, Yu H. Heralding a new paradigm in 3D tumor modeling. Biomaterials 2016;108. 197–213.

[6] Friedrich J, Seidel C, Ebner R, Kunz-Schughart LA. Spheroid-based drug screen: considerations and practical approach. Nat Protoc 2009;4. 309–24.

[7] Hickman JA, Graeser R, de Hoogt R, Vidic S, Brito C, Gutekunst M, et al. Three-dimensional models of cancer for pharmacology and cancer cell biology: Capturing tumor complexity *in vitro*/ex vivo. Biotechnol J 2014;9. 1115–28.

[8] Katt ME, Placone AL, Wong AD, Xu ZS, Searson PC. In Vitro Tumor Models: Advantages, Disadvantages, Variables, and Selecting the Right Platform. Front Bioeng Biotechnol 2016;4. 12.

[9] Chatzinikolaidou M. Cell spheroids: the new frontiers in *in vitro* models for cancer drug validation. Drug Discov Today 2016;21. 1553–60.

[10] Dittmer A, Hohlfeld K, Lützkendorf J, Müller LP, Dittmer J. Human mesenchymal stem cells induce E-cadherin degradation in breast carcinoma spheroids by activating ADAM10. Cell Mol Life Sci 2009;66. 3053–65.

[11] Karlsson H, Fryknäs M, Larsson R, Nygren P. Loss of cancer drug activity in colon cancer HCT-116 cells during spheroid formation in a new 3-D spheroid cell culture system. Exp Cell Res 2012;318. 1577–85.

[12] Beckermann BM, Kallifatidis G, Groth A, Frommhold D, Apel A, Mattern J, et al. VEGF expression by mesenchymal stem cells contributes to angiogenesis in pancreatic carcinoma. Br J Cancer 2008;99. 622–31.

[13] Han HW, Hsu S hui. Chitosan-hyaluronan based 3D co-culture platform for studying the crosstalk of lung cancer cells and mesenchymal stem cells. Acta Biomater 2016;42. 157–67.

[14] Astashkina A, Grainger DW. Critical analysis of 3-D organoid *in vitro* cell culture models for high-throughput drug candidate toxicity assessments. Adv Drug Deliv Rev 2014;69–70. 1–18.

[15] Kang AR, Park JS, Ju J, Jeong GS, Lee SH. Cell encapsulation via microtechnologies. Biomaterials 2014;35. 2651–63.

[16] Ahrens CC, Dong Z, Li W. Engineering Cell Aggregates through Incorporated Polymeric Microparticles. Acta Biomater 2017. doi:10.1016/j.actbio.2017.08.003.

[17] Thiele J, Ma Y, Bruekers SMC, Ma S, Huck WTS. 25th anniversary article: Designer hydrogels for cell cultures: A materials selection guide. Adv Mater 2014;26. 125–48.

[18] Asghar W, El Assal R, Shafiee H, Pitteri S, Paulmurugan R, Demirci U. Engineering cancer microenvironments for *in vitro* 3-D tumor models. Mater Today 2015;18. 539–53.

[19] Wu J, Sheng S, Liang X, Tang Y. The role of tumor microenvironment in collective tumor cell invasion. Futur Oncol 2017;13. 991–1002.

[20] Balkwill FR, Capasso M, Hagemann T. The tumor microenvironment at a glance. J Cell Sci 2012;125. 5591–6.

[21] Kenny PA, Bissell MJ. Tumor reversion: Correction of malignant behavior by microenvironmental cues. Int J Cancer 2003;107. 688–95.

[22] Murdoch C, Muthana M, Coffelt SB, Lewis CE. The role of myeloid cells in the promotion of tumour angiogenesis. Nat Rev Cancer 2008;8. 618–31.

[23] Chaturvedi P, Gilkes DM, Takano N, Semenza GL. Hypoxia-inducible factor-dependent signaling between triple-negative breast cancer cells and mesenchymal stem cells promotes macrophage recruitment. Proc Natl Acad Sci 2014;111. E2120–9.

[24] Alemany-Ribes M, Semino CE. Bioengineering 3D environments for cancer models. Adv Drug Deliv Rev 2014;79. 40–9.

[25] Ivascu A, Kubbies M. Rapid Generation of Single-Tumor Spheroids for High-Throughput Cell Function and Toxicity Analysis. J Biomol Screen 2006;11. 922–32.

[26] Costa EC, Moreira AF, de Melo-Diogo D, Gaspar VM, Carvalho MP, Correia IJ. 3D tumor spheroids: an overview on the tools and techniques used for their analysis. Biotechnol Adv 2016;34. 1427–41.

[27] Thoma CR, Zimmermann M, Agarkova I, Kelm JM, Krek W. 3D cell culture systems modeling tumor growth determinants in cancer target discovery. Adv Drug Deliv Rev 2014;69–70. 29–41.

[28] Nath S, Devi GR. Three-dimensional culture systems in cancer research: Focus on tumor spheroid model. Pharmacol Ther 2016;163. 94–108.

[29] Breslin S, O'Driscoll L. Three-dimensional cell culture: The missing link in drug discovery. Drug Discov Today 2013;18. 240–9.

[30] Weiswald LB, Bellet D, Dangles-Marie V. Spherical cancer models in tumor biology. Neoplasia 2015;17. 1–15.

[31] Sutherland RM, Mccredie JA. Growth of Multicell Spheroids in Tissue Culture as a Model of Nodular Carcinomas<xref ref-type="fn" rid="FN2">2</xref> JNCI J Natl Cancer Inst 1971. 113–20.

[32] Rodday B, Hirschhaeuser F, Walenta S, Mueller-Klieser W. Semiautomatic Growth Analysis of Multicellular Tumor Spheroids. J Biomol Screen 2011;16. 1119–24.

[33] Oliveira MB, Salgado CL, Song W, Mano JF. Combinatorial on-chip study of miniaturized 3D porous scaffolds using a patterned superhydrophobic platform. Small 2013;9. 768–78.

[34] Foty R. A Simple Hanging Drop Cell Culture Protocol for Generation of 3D Spheroids. J Vis Exp 2011;20. 4–7.

[35] Timmins NE, Nielsen LK. Generation of multicellular tumor spheroids by the hanging-drop method. Methods Mol Med 2007;140. 141–51.

[36] Barzegari A, Saei AA. An update to space biomedical research: Tissue engineering in microgravity bioreactors. BioImpacts 2012;2. 23–32.

[37] Kimlin LC, Casagrande G, Virador VM. In vitro three-dimensional (3D) models in cancer research: An update. Mol Carcinog 2013;52. 167–82.

[38] Villasante A, Vunjak-Novakovic G. Tissue-engineered models of human tumors for cancer research. Expert Opin Drug Discov 2015;10. 257–68.

[39] Gencoglu MF, Barney LE, Hall CL, Brooks EA, Schwartz AD, Corbett DC, et al. Comparative Study of Multicellular Tumor Spheroid Formation Methods and Implications for Drug Screening. ACS Biomater Sci Eng 2017. acsbiomaterials.7b00069.

[40] Hirschhaeuser F, Leidig T, Rodday B, Lindemann C, Mueller-Klieser W. Test system for trifunctional antibodies in 3D-MCTS culture. J Biomol Screen Off J Soc Biomol Screen 2009;14. 980–90.

[41] Ferrarini M, Steimberg N, Ponzoni M, Belloni D, Berenzi A, Girlanda S, et al. Ex-Vivo Dynamic 3-D Culture of Human Tissues in the RCCS™ Bioreactor Allows the Study of Multiple Myeloma Biology and Response to Therapy. PLoS One 2013;8. 1–10.

[42] Hsiao AY, Tung YC, Qu X, Patel LR, Pienta KJ, Takayama S. 384 hanging drop arrays give excellent Z-factors and allow versatile formation of co-culture spheroids. Biotechnol Bioeng 2012;109. 1293–304.

[43] Correia AL, Bissell MJ. The tumor microenvironment is a dominant force in multidrug resistance. Drug Resist Updat 2012;15. 39–49.

[44] Rozario T, DeSimone DW. The extracellular matrix in development and morphogenesis: A dynamic view. Dev Biol 2010;341. 126–40.

[45] Barcus CE, O'Leary KA, Brockman JL, Rugowski DE, Liu Y, Garcia N, et al. Elevated collagen-I augments tumor progressive signals, intravasation and metastasis of prolactin-induced estrogen receptor alpha positive mammary tumor cells. Breast Cancer Res 2017;19. 9.

[46] Stern R. Hyaluronidases in Cancer Biology. Hyaluronan Cancer Biol 2009;18. 207–20.

[47] Wu M, Cao M, He Y, Liu Y, Yang C, Du Y, et al. A novel role of low molecular weight hyaluronan in breast cancer metastasis. FASEB J 2014;1. 1–9.

[48] Misra S, Hascall VC, Markwald RR, Ghatak S. Interactions between hyaluronan and its receptors (CD44, RHAMM) regulate the activities of inflammation and cancer. Front Immunol 2015;6. doi:10.3389/fimmu.2015.00201.

[49] Egeblad M, Werb Z. New functions for the matrix metalloproteinases in cancer progression. Nat Rev Cancer 2002;2. 161–74.

[50] Chen L, Xiao Z, Meng Y, Zhao Y, Han J, Su G, et al. The enhancement of cancer stem cell properties of MCF-7 cells in 3D collagen scaffolds for modeling of cancer and anti-cancer drugs. Biomaterials 2012;33. 1437–44.

[51] Mishra DK, Sakamoto JH, Thrall MJ, Baird BN, Blackmon SH, Ferrari M, et al. Human Lung Cancer Cells Grown in an Ex Vivo 3D Lung Model Produce Matrix Metalloproteinases Not Produced in 2D Culture. PLoS One 2012;7. 3–12.

[52] Conklin MW, Eickhoff JC, Riching KM, Pehlke CA, Eliceiri KW, Provenzano PP, et al. Aligned collagen is a prognostic signature for survival in human breast carcinoma. Am J Pathol 2011;178. 1221–32.

[53] Kumar S. Cellular mechanotransduction: Stiffness does matter. Nat Mater 2014;13. 918–20.

[54] Takai A, Fako V, Dang H, Forgues M, Yu Z, Budhu A, et al. Three-dimensional Organotypic Culture Models of Human Hepatocellular Carcinoma. Sci Rep 2016;6. 21174.

[55] Riching KM, Cox BL, Salick MR, Pehlke C, Riching AS, Ponik SM, et al. 3D collagen alignment limits protrusions to enhance breast cancer cell persistence. Biophys J 2015;107. 2546–58.

[56] Lü WD, Zhang L, Wu CL, Liu ZG, Lei GY, Liu J, et al. Development of an acellular tumor extracellular matrix as a three-dimensional scaffold for tumor engineering. PLoS One 2014;9. doi:10.1371/journal.pone.0103672.

[57] Croll TI, O'Connor AJ, Stevens GW, Cooper-White JJ. A blank slate? Layer-by-layer deposition of hyaluronic acid and chitosan onto various surfaces. Biomacromolecules 2006;7. 1610–22.

[58] Xiong G, Flynn TJ, Chen J, Trinkle C, Xu R. Development of an ex vivo breast cancer lung colonization model utilizing a decellularized lung matrix. Integr Biol 2015;7. 1518–25.

[59] Chen MCW, Gupta M, Cheung KC. Alginate-based microfluidic system for tumor spheroid formation and anticancer agent screening. Biomed Microdevices 2010;12. 647–54.

[60] Tsao CT, Kievit FM, Wang K, Erickson AE, Ellenbogen RG, Zhang M. Chitosan-based thermoreversible hydrogel as an in Vitro tumor microenvironment for testing breast cancer therapies. Mol Pharm 2014;11. 2134–42.

[61] Talukdar S, Kundu SC. A non-mulberry silk fibroin protein based 3D *in vitro* tumor model for evaluation of anticancer drug activity. Adv Funct Mater 2012;22. 4778–88.

[62] Soman P, Kelber JA, Lee JW, Wright TN, Vecchio KS, Klemke RL, et al. Cancer cell migration within 3D layer-by-layer microfabricated photocrosslinked PEG scaffolds with tunable stiffness. Biomaterials 2012;33. 7064–70.

[63] Sahoo SK, Panda AK, Labhasetwar V. Characterization of porous PLGA/PLA microparticles as a scaffold for three dimensional growth of breast cancer cells. Biomacromolecules 2005;6. 1132–9.

[64] Calimeri T, Battista E, Conforti F, Neri P, Di Martino MT, Rossi M, et al. A unique three-dimensional SCID-polymeric scaffold (SCID-synth-hu) model for *in vivo* expansion of human primary multiple myeloma cells. Leukemia 2011;25. 707–11.

[65] Fischbach C, Kong HJ, Hsiong SX, Evangelista MB, Yuen W, Mooney DJ. Cancer cell angiogenic capability is regulated by 3D culture and integrin engagement. Proc Natl Acad Sci U S A 2009;106. 399–404.

[66] Orgovan N, Peter B, Bosze S, Ramsden JJ, Szabó B, Horvath R. Dependence of cancer cell adhesion kinetics on integrin ligand surface density measured by a high-throughput label-free resonant waveguide grating biosensor. Sci Rep 2014;4. doi:10.1038/srep04034.

[67] Pradhan S, Clary JM, Seliktar D, Lipke EA. A three-dimensional spheroidal cancer model based on PEG-fibrinogen hydrogel microspheres. Biomaterials 2017;115. 141–54.

[68] Chimene D, Lennox KK, Kaunas RR, Gaharwar AK. Advanced Bioinks for 3D Printing: A Materials Science Perspective. Ann Biomed Eng 2016;44. 2090–102.

[69] Do A, Khorsand B, Geary SM, Salem AK. 3D Printing of Scaffolds for Tissue Regeneration Applications. Adv Heal Mater 2015;4. 1742–62.

[70] Caliari SR, Burdick JA. A practical guide to hydrogels for cell culture. Nat Methods 2016;13. 405–14.

[71] Zhang YS, Khademhosseini A. Advances in engineering hydrogels. Science (80-) 2017;356. eaaf3627.

[72] Webber MJ, Khan OF, Sydlik SA, Tang BC, Langer R. A Perspective on the Clinical Translation of Scaffolds for Tissue Engineering. Ann Biomed Eng 2015;43. 641–56.

[73] Benton G, Kleinman HK, George J, Arnaoutova I. Multiple uses of basement membrane-like matrix (BME/Matrigel) *in vitro* and *in vivo* with cancer cells. Int J Cancer 2011;128. 1751–7.

[74] Annabi B, Naud E, Lee YT, Eliopoulos N, Galipeau J. Vascular progenitors derived from murine bone marrow stromal cells are regulated by fibroblast growth factor and are avidly recruited by vascularizing tumors. J Cell Biochem 2004;91. 1146–58.

[75] Kleinman HK, Martin GR. Matrigel: Basement membrane matrix with biological activity. Semin Cancer Biol 2005;15. 378–86.

[76] Nyga A, Cheema U, Loizidou M. 3D tumour models: Novel *in vitro* approaches to cancer studies. J Cell Commun Signal 2011;5. 239–48.

[77] Badylak SF, Freytes DO, Gilbert TW. Reprint of: Extracellular matrix as a biological scaffold material: Structure and function. Acta Biomater 2015;23. S17–26.

[78] Pampaloni F, Reynaud EG, Stelzer EHK. The third dimension bridges the gap between cell culture and live tissue. Nat Rev Mol Cell Biol 2007;8. 839–45.

[79] Liu Z, Vunjak-Novakovic G. Modeling tumor microenvironments using custom-designed biomaterial scaffolds. Curr Opin Chem Eng 2016;11. 94–105.

[80] Worthington P, Pochan DJ, Langhans SA. Peptide Hydrogels – Versatile Matrices for 3D Cell Culture in Cancer Medicine. Front Oncol 2015;5. 92.

[81] Wang F, Li Y, Shen Y, Wang A, Wang S, Xie T. The functions and applications of RGD in tumor therapy and tissue engineering. Int J Mol Sci 2013;14. 13447–62.

[82] Lu T, Li Y, Chen T. Techniques for fabrication and construction of three-dimensional scaffolds for tissue engineering. Int J Nanomedicine 2013;8. 337–50.

[83] Forsayeth J, Bankiewicz KS. Page 1 of 52. 1855. doi:10.2136/sssaj2013.08.0372.

[84] Gill BJ, Gibbons DL, Roudsari LC, Saik JE, Rizvi ZH, Roybal JD, et al. A synthetic matrix with independently tunable biochemistry and mechanical properties to study epithelial morphogenesis and EMT in a lung adenocarcinoma model. Cancer Res 2012;72. 6013–23.

[85] Ravi M, Paramesh V, Kaviya SR, Anuradha E, Paul Solomon FD. 3D cell culture systems: Advantages and applications. J Cell Physiol 2015;230. 16–26.

[86] Eap S, Ferrand A, Machi V, Ball V, Huck O, Benkirane-Jessel N. Polydopamine Particles Effect on Melanoma Cells Proliferation and Melanin Secretion. Adv Chem Eng Sci 2013;3. 1–10.

[87] Parajó Y, d'Angelo I, Welle A, Garcia-Fuentes M, Alonso MJ. Hyaluronic acid/Chitosan nanoparticles as delivery vehicles for VEGF and PDGF-BB. Drug Deliv 2010;17. 596–604.

[88] Del Bufalo F, Manzo T, Hoyos V, Yagyu S, Caruana I, Jacot J, et al. 3D modeling of human cancer: A PEG-fibrin hydrogel system to study the role of tumor microenvironment and recapitulate the *in vivo* effect of oncolytic adenovirus. Biomaterials 2016;84. 76–85.

[89] Weiss MS, Bernabé BP, Shikanov A, Bluver DA, Mui MD, Shin S, et al. The impact of adhesion peptides within hydrogels on the phenotype and signaling of normal and cancerous mammary epithelial cells. Biomaterials 2012;33. 3548–59.

[90] Zhu J. Bioactive Modification of Poly(ethylenglykol) Hydrogels for Tissue Engineering. Biomaterials 2010;31. 4639–56.

[91] Zhu W, Wang M, Fu Y, Castro NJ, Fu SW, Zhang LG. Engineering a biomimetic three-dimensional nanostructured bone model for breast cancer bone metastasis study. Acta Biomater 2015;14. 164–74.

[92] Saik JE, Gould DJ, Watkins EM, Dickinson ME, West JL. Covalently immobilized platelet-derived growth factor-BB promotes angiogenesis in biomimetic poly(ethylene glycol) hydrogels. Acta Biomater 2011;7. 133–43.

[93] Coppeta JR, Mescher MJ, Isenberg BC, Spencer AJ, Kim ES, Lever AR, et al. A portable and reconfigurable multi-organ platform for drug development with onboard microfluidic flow control. Lab Chip 2017;17. 134–44.

[94] Lei Y, Li J, Wang N, Yang X, Hamada Y, Li Q, et al. An on-chip model for investigating the interaction between neurons and cancer cells. Integr Biol 2016;8. 359–67.

[95] Hirt C, Papadimitropoulos A, Muraro MG, Mele V, Panopoulos E, Cremonesi E, et al. Bioreactor-engineered cancer tissue-like structures mimic phenotypes, gene expression profiles and drug resistance patterns observed "*in vivo*." Biomaterials 2015;62. 138–46.

[96] Shamloo A, Amirifar L. A microfluidic device for 2D to 3D and 3D to 3D cell navigation. J Micromechanics Microengineering 2016;26. 15003.

[97] Carvalho MR, Lima D, Reis RL, Correlo VM, Oliveira JM. Evaluating Biomaterial- and Microfluidic-Based 3D Tumor Models. Trends Biotechnol 2015;33. 667–78.

[98] Gupta N, Liu JR, Patel B, Solomon DE, Vaidya B, Gupta V. Microfluidics-based 3D cell culture models: Utility in novel drug discovery and delivery research. Bioeng Transl Med 2016;1. 63–81.

[99] Wong KHK, Chan JM, Kamm RD, Tien J. Microfluidic Models of Vascular Functions. Annu Rev Biomed Eng 2012;14. 205–30.

[100] van Duinen V, Trietsch SJ, Joore J, Vulto P, Hankemeier T. Microfluidic 3D cell culture: From tools to tissue models. Curr Opin Biotechnol 2015;35. 118–26.

[101] Skardal A, Devarasetty M, Forsythe S, Atala A, Soker S. A reductionist metastasis-on-a-chip platform for *in vitro* tumor progression modeling and drug screening. Biotechnol Bioeng 2016;113. 2020–32.

[102] Cho S, Yoon JY. Organ-on-a-chip for assessing environmental toxicants. Curr Opin Biotechnol 2017;45. 34–42.

[103] Zhang YSYN, Zhang YSYN, Zhang W. Cancer-on-a-chip systems at the frontier of nanomedicine. Drug Discov Today 2017;22. 1392–9.

[104] Tsai H-F, Trubelja A, Shen AQ, Bao G. Tumour-on-a-chip: microfluidic models of tumour morphology, growth and microenvironment. J R Soc Interface 2017;14. doi:10.1098/rsif.2017.0137.

[105] Polini A, Prodanov L, Bhise NS, Manoharan V, Dokmeci MR, Khademhosseini A. Organs-on-a-chip: a new tool

for drug discovery. Http://DxDoiOrg/101517/174604412014886562 2014. 335–52.

[106] Lovitt C, Shelper T, Avery V. Advanced Cell Culture Techniques for Cancer Drug Discovery. Biology (Basel) 2014;3. 345–67.

[107] Tung Y-C, Hsiao AY, Allen SG, Torisawa Y, Ho M, Takayama S. High-throughput 3D spheroid culture and drug testing using a 384 hanging drop array. Analyst 2011;136. 473–8.

[108] LaBarbera D V, Reid BG, Yoo BH. The multicellular tumor spheroid model for high-throughput cancer drug discovery. Expert Opin Drug Discov 2012;7. 819–30.

[109] Brancato V, Garziano A, Gioiella F, Urciuolo F, Imparato G, Panzetta V, et al. 3D is not enough: Building up a cell instructive microenvironment for tumoral stroma microtissues. vol. 47. Acta Materialia Inc.; 2017. doi:10.1016/j.actbio.2016.10.007.

[110] Brancato V, Gioiella F, Profeta M, Imparato G, Guarnieri D, Urciuolo F, et al. 3D tumor microtissues as an *in vitro* testing platform for microenvironmentally-triggered drug delivery systems. Acta Biomater 2017;57. 47–58.

[111] Horning JL, Sahoo SK, Vijayaraghavalu S, Dimitrijevic S, Vasir JK, Jain TK, et al. 3-D tumor model for *in vitro* evaluation of anticancer drugs. Mol Pharm 2008;5. 849–62.

[112] Godugu C, Patel AR, Desai U, Andey T, Sams A, Singh M. AlgiMatrix™ Based 3D Cell Culture System as an In-Vitro Tumor Model for Anticancer Studies. PLoS One 2013;8. e53708.

[113] Kang S-WW, Bae YH. Cryopreservable and tumorigenic three-dimensional tumor culture in porous poly(lactic-co-glycolic acid) microsphere. Biomaterials 2009;30. 4227–32.

[114] Xu X xi, Liu C, Liu Y, Li N, Guo X, Wang S jun, et al. Encapsulated human hepatocellular carcinoma cells by alginate gel beads as an *in vitro* metastasis model. Exp Cell Res 2013;319. 2135–44.

[115] Pradhan S, Chaudhury CS, Lipke EA. Dual-phase, surface tension-based fabrication method for generation of tumor millibeads. Langmuir 2014;30. 3817–25.

[116] Zhang P, Guan J. Fabrication of Multilayered Microparticles by Integrating Layer-by-Layer Assembly and MicroContact Printing. Small 2011;7. 2998–3004.

[117] Deveza L, Ashoken J, Castaneda G, Tong X, Keeney M, Han L-H, et al. Microfluidic Synthesis of Biodegradable Polyethylene-Glycol Microspheres for Controlled Delivery of Proteins and DNA Nanoparticles. ACS Biomater Sci Eng 2015;1. 157–65.

[118] Zhang Wang W, Yu W, Xie Y, Zhang, Zhang Y, et al. Development of an *in vitro* multicellular tumor spheroid model using microencapsulation and its application in anticancer drug screening and testing. Biotechnol Prog 2005;21. 1289–96.

[119] Yeung P, Sin HS, Chan S, Chan GCF, Chan BP. Microencapsulation of neuroblastoma cells and mesenchymal stromal cells in collagen microspheres: A 3D model for cancer cell niche study. PLoS One 2015;10. 1–22.

[120] Cui X, Liu Y, Hartanto Y, Bi J, Dai S, Zhang H. Multicellular Spheroids Formation and Recovery in Microfluidics-generated Thermoresponsive Microgel Droplets. Colloids Interface Sci Commun 2016;14. 4–7.

[121] Huang H, Ding Y, Sun XS, Nguyen TA. Peptide Hydrogelation and Cell Encapsulation for 3D Culture of MCF-7 Breast Cancer Cells. PLoS One 2013;8. doi:10.1371/journal.pone.0059482.

[122] Alessandri K, Sarangi BR, Gurchenkov V V., Sinha B, Kiessling TR, Fetler L, et al. Cellular capsules as a tool for multicellular spheroid production and for investigating the mechanics of tumor progression *in vitro*. Proc Natl Acad Sci 2013;110. 14843–8.

[123] Xu X, Prestwich GD. Inhibition of tumor growth and angiogenesis by a lysophosphatidic acid antagonist in an engineered three-dimensional lung cancer xenograft model. Cancer 2010;116. 1739–50.

[124] Markvicheva E, Zaytseva-Zotova D, Akasov R, Burov S, Chevalot I, Marc A. Multicellular tumor spheroids in microcapsules as a novel 3D *in vitro* model in tumor biology. BMC Proc 2013;7. P116.

[125] Estrada MF, Rebelo SP, Davies EJ, Pinto MT, Pereira H, Santo VE, et al. Modelling the tumour microenvironment in long-term microencapsulated 3D co-cultures recapitulates phenotypic features of disease progression. Biomaterials 2016;78. 50–61.

[126] Guzman A, Sánchez Alemany V, Nguyen Y, Zhang CR, Kaufman LJ. A novel 3D *in vitro* metastasis model elucidates differential invasive strategies during and after breaching basement membrane. Biomaterials 2017;115. 19–29.

[127] Son H, Moon A. Epithelial-mesenchymal Transition and Cell Invasion. Toxicol Res 2010;26. 245–52.

[128] Tse JM, Cheng G, Tyrrell JA, Wilcox-Adelman SA, Boucher Y, Jain RK, et al. Mechanical compression drives cancer cells toward invasive phenotype. Proc Natl Acad Sci 2012;109. 911–6.

[129] Yu L, Ni C, Grist SM, Bayly C, Cheung KC. Alginate core-shell beads for simplified three-dimensional tumor spheroid culture and drug screening. Biomed Microdevices 2015;17. doi:10.1007/s10544-014-9918-5.

[130] Lee KH, No DY, Kim S-H, Ryoo JH, Wong SF, Lee S-H. Diffusion-mediated in situ alginate encapsulation of cell spheroids using microscale concave well and nanoporous membrane. Lab Chip 2011;11. 1168.

[131] Leong W, Soon C, Wong S, Tee K, Cheong S, Gan S, et al. In Vitro Growth of Human Keratinocytes and Oral Cancer Cells into Microtissues: An Aerosol-Based Microencapsulation Technique. Bioengineering 2017;4. 43.

[132] Privalova AM, Uglanova S V, Kuznetsova NR, Klyachko NL, Golovin YI, Korenkov V V, et al. Microencapsulated Multicellular Tumor Spheroids as a Tool to Test Novel Anticancer Nanosized Drug Delivery Systems <I>In Vitro</I>. J Nanosci Nanotechnol 2015;15. 4806–14.

[133] Feng Xu, Jonathan Celli2, Imran Rizvi2, Sangjun Moon1, Tayyaba Hasan2, 3,* and U, Demirci. A three-dimensional *in vitro* ovarian cancer coculture model using a high-throughput cell patterning platform. Dev Biol 2004;276. 391–402.

2. Aims

The aim of this thesis was the development of an *in vitro* 3D heterogenic model of lung cancer capable of correctly reproducing complex populational interactions present *in vivo*. In the hope of engineering a model that would allow to further diminish the gap between results obtain in *in vitro* and those obtained in the clinical setting. Thus, speeding up therapeutic compounds screening and possible novel therapies discovery. Thus, the specific aims of this master thesis were the following:

- Synthesis and characterization of a PCL MP-based scaffold in a size range of 60-100 µm;
- Biofunctionalization of produced MPs surface by layer-by-layer adsorption of cationic Poly-L-Lysine and anionic Hyaluronic Acid polyelectrolytes;
- Characterization of coated layer-by-layer modified microparticles (LbL-MPs);
- Inclusion of functionalized LbL-MPs into 3D-MCTS spheroid models containing combinations of A549, HF and BM-MSC populations for production of *in vivo* similar MCTS;
- Analysis of LbL-MPs cytotoxic potential in diverse co-culture settings;
- Characterization of 3D-MCTS size, circularity, morphology and ability to recapitulate key tumor features formation over a culture period of 7 to 14th days;
- Analysis of 3D-MCTS internal organization and collagen deposition via histological staining and fluorescence microscopy;
- Evaluation of BM-MSC organization inside the 3D-MCTS, and of their capacity to remain in culture over 14 days;
- Analysis of co-culture and microparticle influence in overall chemotherapeutic resistance of 3D-MCTS to Doxorubicin.

3. Materials and Methods

3.1. Materials

Polycaprolactone (PCL; Mn: 80 000), Polyvinyl Alcohol (PVA; MW: 30 – 70 KDa) and Poly-L-lysine hydrobromide (PLL; MW: 30 000-70 000 Da) were acquired from Laborspirit (Loures, Portugal) produced by Sigma Aldrich. Chitosan chloride (MW: 50-150 KDa) was acquired from Novamatrix (Sandvika, Norway). Hyaluronic acid sodium salt polymer (MW: 80 – 100 KDa) was obtained from Carbosynth Limited (Berkshire, United Kingdom).

Cell culture materials including T-75 and T-175 cell culture treated T-flasks (CN 83.3911.002 and 83.3912.002); 96-wells flat-bottom sterile polystyrene suspension plates were obtained from (Starstedt, S.A., (Nümbrecht, Germany). D- Phosphate buffered saline (CN: 55-031-PCR) was obtained from Corning (Diagnostica Longwood; Spain); All the following reagents cell culture media and supplements, were purchased from Thermo Fisher Scientific Europe, namely: Ultra-Low-Adhesion (ULA) round-bottom 96-wells plates (CN: 10023683); Trypan Blue (CN: 15250061), Fetal Bovine Serum (FBS; E.U. approved, South America origin), Dulbecco's Modified Eagle Medium-High Glucose (DMEM-HG),(CN:11995065 Ham's F-12K Kaighn's Medium (HAMs-F12), Alpha Modified Eagle's Medium (α-MEM), (CN: 12561056); TrypLE™ Express (CN: 12605010); Antibiotic/antimitotic (ATB) solution (CN: 15140122). containing Penicillin-Streptomycin (10000 units/mL of penicillin and 10000 µg/mL of streptomycin.). For *in vitro* models characterization,Goat anti-Mouse IgG (H+L) Secondary Antibody, Alexa Fluor 488 (CN: A-11029); Collagen I Antibody (5D8-G9) (CN: MA1-141); E-cadherin antibody (67A4), Calcein-AM, (CN: C3099); Propidium Iodide (PI) (CN: P1304MP) were all purchased from Thermofisher Scientific Inc (Alfagene, Portugal). Anti-human CD44-FITC (CN: 338804) was purchased from Taper (Grupo Taper S.A., Lisboa Portugal). All other reagents and salts were of analytical grade and used without further purification.

3.2. Microparticles Production

Few works have so far reported the use of microparticles for the assembly of 3D-MCTS. In this thesis polycaprolactone microparticles with sizes ranging from 63 µm to 100 µm were explored, with the rationale that they provide a sufficiently large surface area to

promote cells adhesion. Moreover, it was hypothesized that hyaluronan (HyA) coated MPs would improve cell attachment via HyA interaction with key cell surface receptors such as CD44 and RHAMM that are generally overexpressed in cancer cells[81]. This size was also selected to prevent microparticles cellular internalization and allow reproducible and cohesive 3D spheroids assembly. Polycaprolactone (PCL) microparticles were selected due to their extensive use as microparticle-based scaffolds for precisely engineered cellular aggregates [82,83]. Moreover, PCL has been extensively used as a biomaterial for biomedical applications due to its biocompatibility, low cost, and slow biodegradation rate [84].

Electrospraying and microfluidic based techniques were initially used by adapting experimental conditions previously reported in literature [81–84], to attempt the production of polycaprolactone monodisperse particles in the desired size. Compared with emulsion-based methods, electrospraying allows the manufacture of highly monodisperse micro and nano particles[88]. Being somewhat a more complex technique, optimization of the diverse parameters associated with microparticle production through electrospraying methodologies was attempted. Variations in: (i) PCL (w/v) %, (ii) tip-to-collector distance (TTC), (iii) droplet forming needle gauge, (iv) flow-rate of PCL solution, (v) applied voltage, (vi) recovery method were performed (supplementary table 2). The variation of either electric field charge, TTC or dispersing needle gauge resulted in the production of smaller particles. On the contrary a higher flow rate, polymer concentration and consequently viscosity of solutions resulted in particles with higher sizes. However, independently of parameters applied for particles manufacture particles recovery was challenging. Herein, aluminum foil or PVA solutions of varying concentrations and volumes with or without stirring were used to collect PCL particles. However, the recovery from aluminum foil was difficult, with low yields being obtained. The use of PVA solved this limitation by the produced microparticles did not evidenced the desired size or spherical shapes. Particles size dispersion were in the order of nanometers to 10 µm, with the maximum diameter obtained having been of 81 µm (supplementary table 3). Overall the produced MPs exhibited surfaces with rough irregular patterns and varying shapes (Figure 4). Consequently, electrospraying was disregarded in favor of microfluidics and emulsion production methodologies, which allowed higher rates of productions and manufacture of particles closer to the desired specifications.

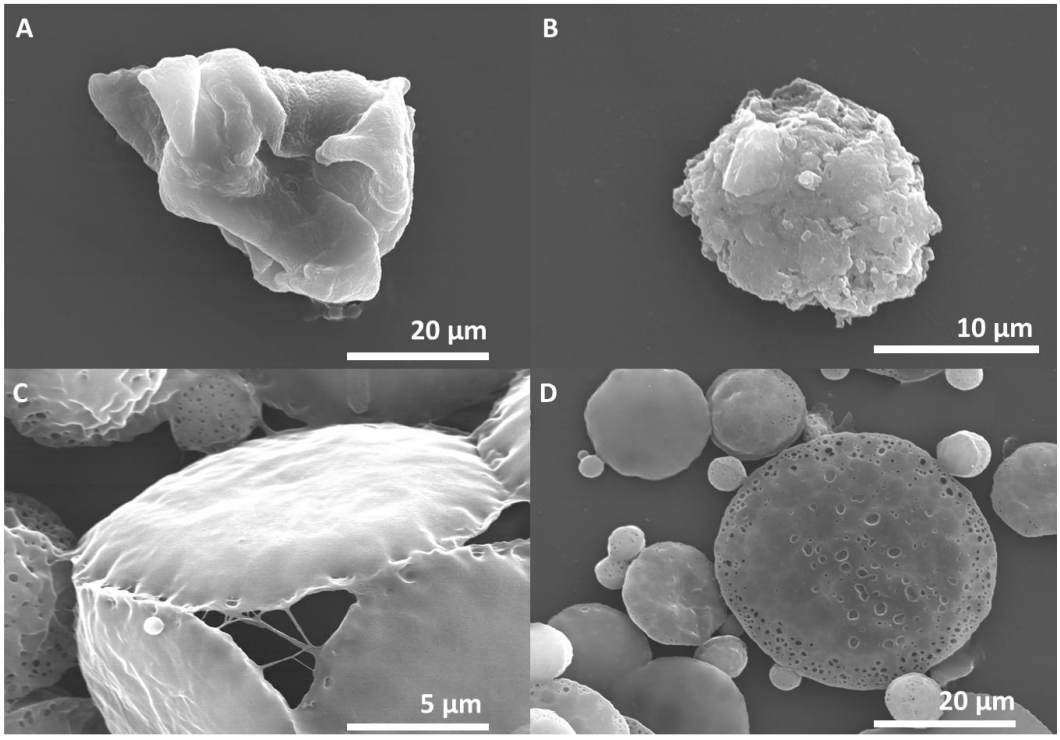

Figure 4. SEM analysis of MPs produced through electrospraying techniques during optimization steps of MPs productions, respectively formulation A13, A12, A9, A17 (A, B, C, D). Flattened morphology might result from collision with recovery aqueous phase while the droplet still contained high amounts of solvent.

Microfluidic based techniques allow the production of more monodisperse formulations through the use of extremely controlled flow-focusing chips. Microfluidics versatility has been explored in the context of cell encapsulation, establishment of dynamic 3D *in vitro* models[89], and also for the manufacture of nano- and microparticles for drug delivery and tissue engineering applications having been recently reviewed by several authors[90–92]. A variety of channel designs can be imprinted into microfluidic chips. Control over channel dimensions and chip materials (e.g., polydimethylsiloxane or quartz) can dictate particle production speed, reproducibility and yield[93,94]. Microparticles produced through microfluidics were assembled by channeling oil (Dichlomethane – DCM) and aqueous phase (PVA) into a flow-focusing quartz microfluidic chip (Figure 5 (B)), under a specific flow rate that resulted in a dripping regime of the oil phase into monodisperse droplets. Such pure PCL-DCM oil droplets were then dried under reduced pressure what resulted in the fabrication of MPs with relatively low size dispersity (figure 5) and also spherical shapes.

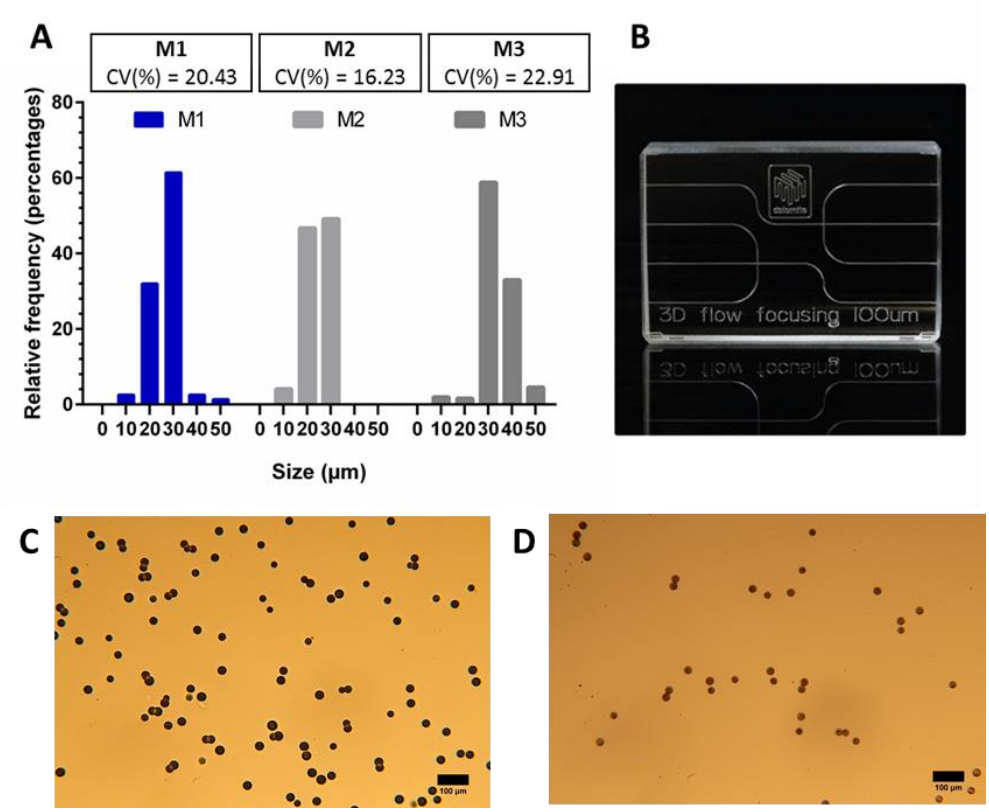

Figure 5. PCL MPs produced with hydrophobic microfluidic 3D flow focusing quartz chip (B) presented an average size of 20-40 µm, with formulation M3 presenting the closest approximation to the desired size. Formulations M1 (C) and M2 (D), serve as examples to demonstrate the elevated monodispersity obtained using microfluidic chips. Contrary to emulsion obtained MPs, microfluidic obtained MPs presented an elevated degree of similarity, with the maximum perceptual variation coefficient being of 22.91% for formulation M3 being relatively closer to monodispersity.

This promising preliminary data rendered microfluidics ideal to produce the desired microparticles. However, difficulty in stabilizing fluxes when testing new formulations resulted in channel clogging due to PVA-PCL interaction in the channels when, making the optimization of new formulations a laborious process. Although microfluidic based approaches proved efficient regarding size and shape of MPs the time-consuming optimization required to produce relatively small quantities of MPs and the fact that punctual destabilization of the microchip could either lead to blocking and consequently a stop in production, led to the choice of emulsion based techniques for microparticles production and for the manufacture of particle based 3D tumor models.

Ultimately PCL microparticles where produced by using the oil-in-water (O1/W1) emulsion-solvent evaporation technique. Diverse parameters of the(O1/W1) emulsion where varied, namely: (i) PCL concentration in the organic solvent-based oil phase (O1); (ii) PVA surfactant concentration in aqueous phase (W1); (iii) volume ratio of aqueous to organic

phase; (iv) magnetic stirring speed, (v) distance of oil phase dispersing needle to the surface of the aqueous phase in the beaker. A summary of the parameters modified for the formulation of different microparticles is provided in Supplementary Table 1.

For laboratorial scale production of different microparticles, the oil phase (O1) was comprised by a 5 % (w/v) PCL (MW: 80,000 $g.mol^{-1}$) solution, dissolved in DCM. The aqueous phase (w) consisted of a 0.5 % (w/v) PVA solution (MW: 30,000-70,000), that was prepared from a stock solution of PVA 5 % (w/v) previously prepared by dissolving 50 g of PVA in 1 L of distilled water under stirring (700 rpm) at 80 ºC, for at least 4-5 h until complete dissolution of the polymer.

To form the water-oil emulsion 8 mL of the PCL 5 % (w/v) solution (O1 phase) were dispersed into 150 mL of PVA 0.5 % (w/v) solution (aqueous phase) stirred (800 rpm) in a beaker with a maximum capacity of 300 mL. To decrease microparticles size polydispersity and batch-to-batch variability a compressed air, piezoelectric-based, pumping system (OB1 MK3 – Elveflow ® Microfluidic Flow Control System) was used to disperse the oil phase from a 22-gauge blunt tip needle, by using an air pressure of 5 bar. The PCL solution was ejected directly into the center of the stirring aqueous phase from a fixed height of 12 cm (measured from the needle tip to the base of the stirring plate), Figure 6. To facilitate solvent evaporation the excess volume of W1 phase was carefully removed to a volume of 50 mL. The microparticle-containing solution (reduced to 50 mL) was then placed under horizontal stirring at 170 rpm during at least 8 h at room temperature (RT) inside a fume-hood to promote solvent evaporation and PCL microparticles assembly. Following solvent evaporation, any residual PVA on the PCL microparticles solution was washed 3 times by using vortex-centrifugation steps (1000 rpm, 5 min, RT).

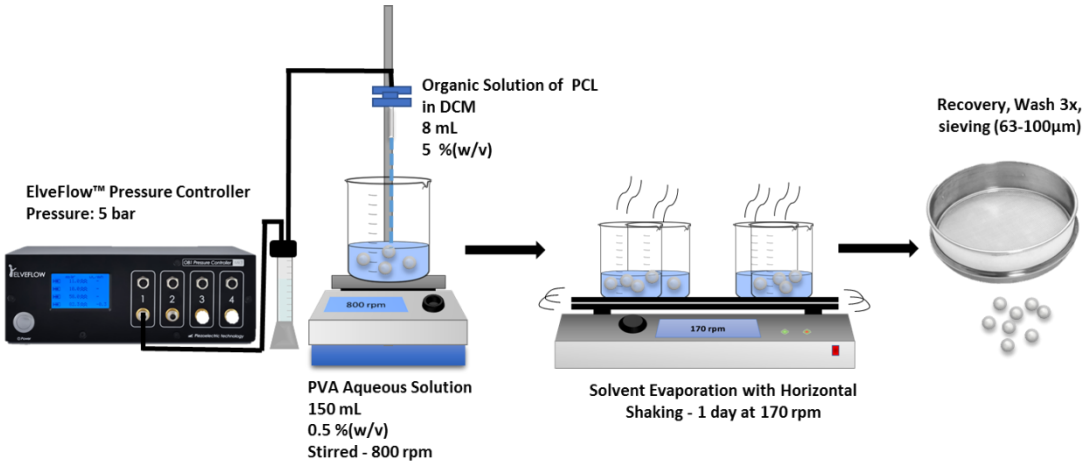

Figure 6. Schematic of microparticle production and sieving process. A needle with a 21 gauge was used.

The particles were then sieved through stainless steel sieves (VWR Portugal, CN: 510-0715 and 510-0710) with decreasing sizes: (i) 100 µm, and (ii) 63 µm mesh. After sieving, PCL microparticles were recovered by centrifugation (1500 rpm for 5 min, RT), and frozen at -80 ºC overnight. The samples where then freeze dried at (-86 ºC, 0.076 bar) for a minimum period of 48 h. All particles were stored in a moisture free environment until use.

3.3. Bioinstructive microparticles production via Layer-by-Layer

Sieved microparticles in the size range of 63-100 µm were then subjected to plasma treatment, with the objective of modifying particle surfaces making them more hydrophilic due to plasma species adsorption. Thus, facilitating electrostatic self-assembly of the initial Poly-L-Lysine layer during the initial layer-by-layer procedure. For this purpose, 200 mg of previously sieved microparticles where placed in a sterile beaker covered with aluminum foil. The samples were then inserted in the vacuum chamber of a plasma generating equipment (ATTO, Barcelona, Spain). Plasma treatment was performed by using atmospheric air as the operating gas. The compartment was then sealed with vacuum created by an air pump, being then subjected to plasma treatment in air, charged at 30 V at a pressure of 0.4-0.6 mbar for 5 min. To guarantee that the entire surface of the particles was subjected to plasma treatment the compartment was slowly re-pressurized and the container with the particles was stirred, repositioned inside the cylinder and subjected to plasma treatment. This procedure was performed 3 times.

A layer-by-layer (LbL) supramolecular electrostatically driven surface functionalization with positive and negatively charged polymers treatment was performed to functionalize microparticles surface through self-assembling of electrostatic bilayers of positively charged PLL (MW: 30 000-70 000 Da) and negatively charged hyaluronic acid (HyA) (MW: 80 000 – 100 000 Da) as reported in the literature with minor modifications [86]. This technique has been extensively used by our research group to functionalize surfaces and assemble free standing multi-layered films for tissue engineering and regenerative medicine applications [87]. In this thesis the technique was used to increase cellular adhesion to the microparticles as well as providing an ECM similar environment capable of stimulating possible the establishment of drug resistant phenotypes in cancer cells due to the interactions with low-medium molecular weight HyA which as previously shown stimulates CD44 and RHAMM receptors having leading to MDR appearance in several cancers [34,88]. For the LbL-based surface functionalization a maximum of 250 mg of

plasma treated PCL MPs (LbL-MPs) with a negative surface charge were immersed in 20 mL of an aqueous solution of PLL (1 mg/mL) for 10 min, then recovered and washed in distilled water for 5 min.

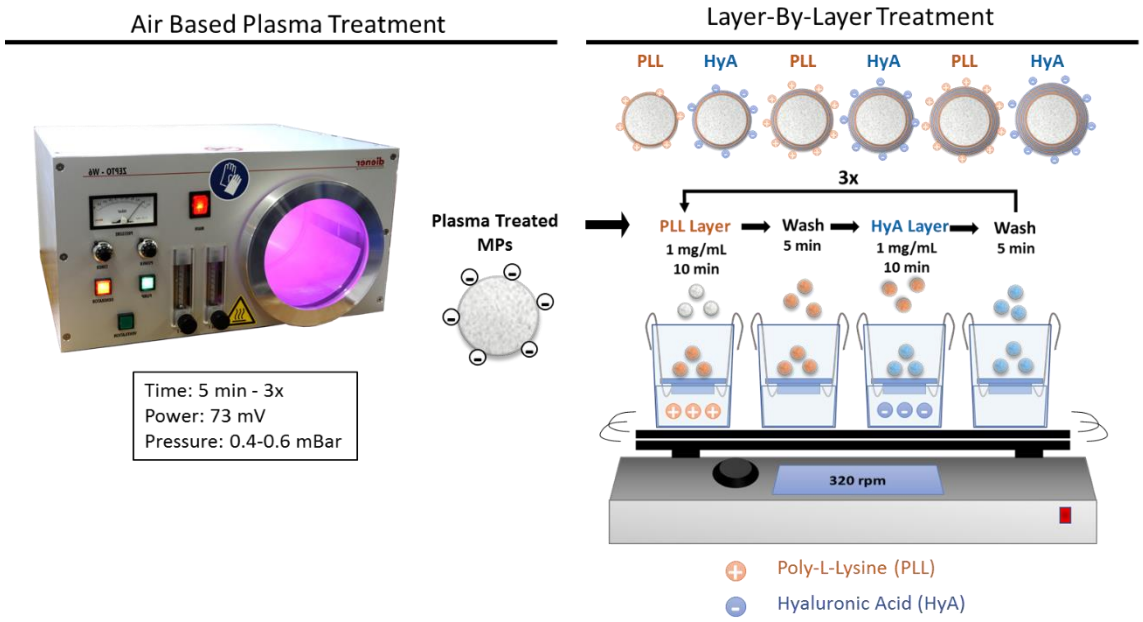

Figure 7. Plasma treatment and Layer-by-layer treatment scheme of PLL-HyA layer deposition onto Plasma treated microparticles.

Afterwards before being submersed in an aqueous solution of HyA (1 mg/mL) for 10 min, and re-washed for 5 min. This process was repeated 3 times to allow the formation of 3 PLL-HyA bilayers. Washing and layer deposition in polymer containing solutions were performed under stirring in a horizontal shaker (320 rpm, RT) to assure homogenous distribution of immersing solution. All solutions were sterilized by filtration prior to LbL (Sterile cellulose acetate syringe Filter 0.2 µm, Ø = 25 mm, VWR CN: 514-0061).

3.4. Zeta Potential Analysis of Polyelectrolyte Polymers Deposition

Zeta potential measurements were used to verify the efficacy of LbL polyelectrolyte layers deposition in MPs surface. This analysis was performed in pristine PCL MPs and at each consecutive LbL deposition step. All measurements where performed in a Zetasizer Nano ZS (Malvern, Worcestershire, UK), An extension of the Henry Equation applying the approximation of Smoluchowski was used for performing the measurement as described elsewhere (ISO 13099-1:2012 [89]). Duration of the equilibration of the sample in Nano ZS was set at 100s. Three measurements were achieved consecutively on the same sample with no delay between measurements. The number of runs performed per measurement was set

to a minimum of 10, maximum of 100, while selection of applied voltage and the selection of attenuation were set to automatic. Zeta potential analysis was performed before layer-by-layer in simple MPs, and at each consecutive layer-by-layer deposition step in LbL-MPs. Measurements were performed at 25 ºC. The ZetaSizer software was used to record and process the electrophoretic mobility data (v. 7.04).

3.5. Microparticles characterization

Microparticles morphology and particle size and was evaluated by optical contrast light microscopy (Primostar, Carl Zeiss, Germany). Particle size analysis was performed after PVA washing, after sieving and after layer-by-layer procedures. Acquired images where analyzed using open-source software ImageJ [90]. the size distribution of each microparticle formulation through area analysis by using a supervised algorithm that analyzed a minimum of 300 particles.

Scanning Electron microscopy (SEM) imaging was used to analyze microparticle morphology and surface topography. For SEM analysis particle samples were dispersed in deionized water and drop-wise added to an aluminum stub containing a glued tissue culture treated polystyrene insert. The samples were then dried at 37 ºC overnight, sputter coated with gold/palladium and observed in a Hitachi S-4100 scanning electron microscope (Hitachi, Japan) operated at a voltage in the range of 15-25 kV and at various magnifications.

3.6. Cell Culture

All cells were manipulated in aseptic conditions and cultured at 5 % CO_2, 95 % atmospheric oxygen, in humidified, temperature controlled incubators at 37 ºC. Cells where maintained in T-75 and T-175 cm^2 cell culture flasks (Sarstedt, S.A. 83.3911.002 and 83.3912.002), with cell culture media exchanges every 3-5 days. The non-small cell lung carcinoma cell line A549 (ATCC CRM-CCL-185™) was cultured in HAMs-F12 medium supplemented with 10 % (v/v) FBS and 1 % (v/v) ATB. The human primary dermal fibroblasts cell line (HF) (ATCC®-PCS-201-012™) were cultured in DMEM-HG supplemented with 10 % (v/v) FBS and 1 % (v/v) ATB. Adult Bone Marrow-Derived Mesenchymal Stem Cells (BM-MSCs) (ATCC®-PCS-500-012™) were maintained in α-MEM supplemented with 10 % (v/v) FBS and 1 % (v/v) ATB. All cells where detached from culture flasks upon attaining approximately 80-85 % confluency by using TrypLE™ Express

Enzyme (1X) detaching reagent. Throughout all studies performed in this thesis BM-MSCs were used from passages 3 to 7 to assure stemness properties maintenance.

3.7. 3D *In vitro* lung tumor models assembly via Liquid-Overlay Technique

Homotypic monoculture 3D MCTS with A549 cells, heterotypic co-culture spheroids: A549-HF and A549-MSCs cells, or tricultures: A549-HF-MSCs cells, were self-aggregated at different cell ratios (Table 1, section 4.1), by using the liquid-overlay technique, also known as forced-floating methodology. To form 3D MCTS cells were initially cultured in ULA round bottom 96-wells plates. Prior to each assay, LbL-MPs were sterilized under UV light for a minimum of 30 min, with particles being resuspended in HAMs-F12 cell culture medium supplemented with 10 % FBS and 1 % ATB. Cells were trypsinized using TrypLE™ Express after which cells were resuspended in the respective culture media, stained with trypan blue 0.4 % (w/v) (Thermo Fisher Scientific, CN: 15250061) and counted using an hematocytometer. Multiple or single-cell suspensions composed by the different cell populations to culture were then created. Each cell suspension was prepared to guarantee a maximum volume of 150 μL of culture medium per well. Afterwards cells were left in culture or incubated with LbL-MPs in the respective wells. Prior to each assay, LbL-MPs were sterilized under UV light (30 min) and resuspended in complete HAMs-F12 cell culture medium. To produce different 3D *in vitro* models that would better recapitulate the tumor microenvironment cellular heterogeneity different parameters were manipulated, namely: (i) the cellular concentrations per well, (ii) the cell-to-cell ratios between malignant and mesenchymal/endothelial cells and (iii) the cell-to-particle ratios. The specific ratios used for each condition are summarized in (Table 1, section 4.1).

3.8. - 3D tumor microtissues characterization

3D *in vitro* lung tumor models morphology, growth and circularity was analyzed overtime via optical contrast microscopy by using an inverted microscope (Primovert, Carl Zeiss, Germany). Images of 3D-MCTS were acquired on specific timepoints (days 1, 7 and 14). A minimum of 6 spheroids were analyzed per condition per time point. Image analysis was carried out by using the open-source software ImageJ (Fiji package) and a supervised algorithm based on the code developed by Ivanov and coworkers.

For SEM analysis spheroids were processed as reported in the literature [47,91,92]. In brief, 3D MCTS with and without LbL-MPs were removed from culture media and washed with D-PBS, fixed in formaldehyde 4% (v/v) solution in D-PBS, at 37 ºC for 2 h. The samples were then subjected to dehydration with graded ethanol concentrations (25 %, 50 %, 75 %, 90% (v/v)), for 20 min. All samples were then carefully mounted in aluminum stubs by using double sided adhesive carbon tape (Agar Scientific, Essex, United Kingdom) and sputter coated with gold/palladium. All spheroids were being imaged in a Hitachi S-4100 scanning electron microscope (Hitachi) operated at a voltage in the range of 15-25 kV and at various magnifications.

3.9. - Cell viability assays

The cell viability and necrotic core formation of different homotypic and heterotypic 3D *in vitro* lung tumor microtumors (3D MCTSs and 3D MCTs LbL-MPs), were analyzed at specific timepoints (7^{th} and 14^{th} days) through different methodologies, through different methodologies, namely: (i) Non-radioactive Alamar Blue® Cell Viability Assay, (ii) CellTiter 96® Aqueous One Solution Cell Proliferation Assay (MTS), and (iii) Live/Dead assay

Alamar blue was used to access 3D tumor models viability during the initial steps of homotypic and heterotypic mono-, bi- and triple co-cultures optimization. Both assays were performed in accordance with manufacturers guidelines. The only exception was Alamar Blue incubation time, which was performed overnight instead of the standard 2-4 h period. Alamar Blue resazurin reduction to resorufin was determined by fluorescence measurements (λ_{ex}: 540 nm, λ_{em}: 600 nm). All measurements where performed in a Synergy HTX microplate reader by using a 96-well black-clear bottom plate (VWR, CN: CORN3915).

To evaluate 3D MCTS necrotic core formation, spheroids were labelled with Calcein-AM (Cal-AM) (4 μg/mL) and Propidium Iodide (PI) (10 μg/mL) for 30 min at 37 ºC, according to literature reports for 3D models [47]. Following incubation, the different 3D tumor models (spheroids and 3D microparticle-assembled microtissues) were washed 3 times with D-PBS and either imaged immediately by fluorescence microscopy, or fixed in 4 % formaldehyde (v/v) for posterior observation.

3.10. 3D-MCTS Characterization by Widefield and Confocal Laser Scanning Fluorescence Microscopy

Collagen I and E-cadherin expression were analyzed at specific timepoints (7 and 14 days) through immunocytochemistry. This analysis was performed to better understand phenotypical and morphological changes observed over culture in the diverse 3D-MCTS, resulting from the inclusion of microparticles in the 3D *in vitro* tumor models and from diverse coculture conditions. For immunocytochemistry analysis spheroids were fixated in formaldehyde 4 % (v/v) in D-PBS at 37 ºC for 4 h or overnight, carefully passaged for a new plate using a sterile Pasteur pipette, washed and incubated for 1 h with blockage solution 1 % BSA in D-PBS at 4 ºC, washed and incubated with the primary antibody overnight at 4 ºC, washed and if necessary incubated with secondary antibody for 1 h at room temperature otherwise immediately visualized in a fluorescence or confocal microscope. All washes were performed in D-PBS and repeated 3 times before each step. Image acquisition was performed in. Analysis of acquired images was performed in Zeiss Zen Black software (2017) and in Zeiss Zen Blue software (2017).

3.11. Histological analysis

Histological analysis of dual co-culture (A549-HF) and triculture (A549-HF-MSCs) of 3D MCTS and 3D MCTS cultured in LbL-MPs was performed in order to analyze microtumors internal organization and collagen deposition. In brief, 3D-MCTS with and without LbL-MPs were removed from culture media and washed with D-PBS, fixed in formaldehyde 4 % (v/v) solution in D-PBS, at 37 ºC for 2 h. The samples were then subjected to dehydration with growing concentrations of ethanol (25 %, 50 %, 75 %, (v/v)), for 20 min, per condition. Afterwards, 3D microtumors were stored at 4 ºC in ULA plates. For histological analysis the different spheroid samples were imbedded into HistoGel™ (previously heated to 70 ºC in a water bath for 2 h), and then rapidly cooled into hardening, and then processed for standard paraffin fixation. Paraffin blocks containing 3D MCTS were sliced into 5 μm thick samples and stained with: (i) Hematoxylin and Eosin (H&E) for internal structures morphological analysis, and (ii) Masson's Trichrome for possible evaluation of collagen deposition. Histology slides were then analyzed by using an inverted optical contrast light microscope (Primovert, Carl Zeiss, Germany).

3.12. Flow cytometry analysis

The effect of hyaluronan bioinstructive LbL-MPs in 3D MCTS CD44 expression was analyzed by flow cytometry. For this analysis, 3D MCTS and 3D MCTS LbL-MPs with 7

days of culture were dissociated by incubation in a 1:1 mixture of Accumax® and TrypLE™ Express for 30 min, at 37 ºC. After this incubation, spheroids were disrupted by gentle pipetting and incubated in HAMs-F12/10 % FBS/1 % ATB for 30 min. The resulting single cells suspensions were then recovered by centrifugation (300 g, 5 min, 37 ºC). The different samples were incubated with anti-human CD44-FITC conjugate antibody (5 µl/ml in PBS) for 30 min, at 37 ºC. Single cells were then recovered by centrifugation and washed with D-PBS for 3 times. In addition, 2D monocultures of A549, HF and MSCs were also analyzed for their CD44 expression. Prior to FCM analysis all sampled were sieved through 40 µm cell strainers. Flow cytometry analysis was carried out in a BD Accuri C6 flow cytometer (BD Bioscience, San Diego, CA, USA) were a total of $5x10^3$ events per sample were acquired in cells assigned ROI and recorded in the FL-1 channel (FITC). Flow cytometry data was processed and analyzed in FCS Express software (v. 6, trial license).

3.13. Chemotherapeutic drug cytotoxicity screening in 3D MCTS platforms

3D-MCTS containing or not LbL-MPs or non-treated MPs (NT-MPs) were cultured for 7 to 14 days on HAMs-F12 medium. Upon achieving the desired culture time, 3D-MCTS were incubated with Doxorubicin, (also known as Adriamycin), a pharmacological compound commonly used in the clinical setting for combinatorial chemotherapy of solid tumors, used in the context of NSCLC in combination with other pharmacological compounds such as paclitaxel, docetaxel, irinotecan, topotecan, and gemcitabine [93,94]. Doxorubicin is a member of the family of anti- biotic anthracyclines, acting as an DNA intercalating agent that impedes topo isomerase II action. This therapeutic compound is beset by severe dose-limiting toxicity, poor target selectivity susceptibility to MDR mechanism development being a substrate for multidrug-resistant proteins [94]. Having been chosen by its susceptibility to the action of MDR P-glycoprotein efflux pumps, doxorubicin was incubated in spheroids at growing concentration 0; 0.7; 7; and 17 µM, over period of 72 h to 120 h. Cellular viability in 3D assays was measured using a luminescent based assay that quantifies present ATP (Cell Titer Glo™). CellTiter-Glo ® reagent was added, in accordance with stipulated protocol, to each well in a 1:1 reagent to medium ratio. The luminescence signal was read after a total of 30 min incubation, of which 5 min incubation were under vigorous agitation on a horizontal shaker at 400 rpm, and 25 min, at RT under no agitation. Luminescence was read in opaque white plates (Pierce 96-Well Polystyrene Plates, White

Opaque - Thermo Fisher Scientific). In addition, cell viability was also measured through MTS used for IC50 analysis in 2D *in vitro* monotypic and heterotypic co-culture. MTS data was acquired through absorbance readouts of the formed soluble tetrazolium salt (λ=490 and λ=650 nm).

3.14. Statistical Analysis

All statistical analysis was performed using Graphpad Prism 6 Software (Prism 6™). One-way analysis of variance (One-ANOVA) and Two-way analysis of variance (Two-ANOVA) with Holm-Sidak's post-hoc test. A minimum of 6 replicates was used for statistical analysis. Unless otherwise indicated, $p < 0.05$ was considered statistically significant

4. Results and Discussion

4.1. Bioinstructive Microparticles for Self-Assembly of Mesenchymal Stem Cell 3D Tumor Spheroid Hybrids

Subchapter 4.1.

This subchapter is based on the article entitled

"***Bioinstructive Microparticles for Self-Assembly of Mesenchymal Stem Cell 3D Tumor Spheroid Hybrids***"

Manuscript in preparation

Bioinstructive Microparticles for Self-Assembly of Mesenchymal Stem Cell 3D Tumor Spheroid Hybrids

Ferreira, L.P., Gaspar, V.M., Mano, J.F.

[1]Department of Chemistry, CICECO – Aveiro Institute of Materials, University of Aveiro, Campus Universitário de Santiago, 3810-193, Aveiro, Portugal

[#]Corresponding author:
Professor João F. Mano
Department of Chemistry, CICECO – Aveiro Institute of Materials
University of Aveiro, Campus Universitário de Santiago
3810-193, Aveiro, Portugal
E-mail: jmano@ua.pt
Telephone: +351 234370733

Abstract

3D multicellular tumor spheroids (3D-MCTS) that mimic the tumor microenvironment *in vitro* are gaining increased interest as platforms for screening innovative anti-cancer therapeutics. However, to date few models have explored the combination of cancer-ECM components with tumor-modulatory mesenchymal stem cells (MSCs). Herein we engineered 3D lung 3D-MCTS that mimic the existence of tumor stromal and ECM components by combining heterotypic Fibroblasts/MSCs/A549 cancer cells triple co-cultures with bioinstructive hyaluronan-functionalized microparticles (HyA-MPS) for the first time. Microparticles inclusion provided anchoring hotspots that driven cells self-assembly into 3D-MCTS when cultured in non-adherent substrates. This approach increased the expression of CD44 in 3D models and recapitulated the effect of native tumor-ECM. The obtained results demonstrated that the size and morphology of hybrid 3D spheroids was reproducible and that triculture microtumors have a characteristic necrotic core. Interestingly, cell tracking assays demonstrated that MSCs spontaneously migrate within different microtumor regions along time, suggesting a dynamic crosstalk with cancer cells and stromal fibroblasts. Furthermore, bi-culture A549-MSCs cell-particle hybrid 3D spheroids have shown a higher resistance to Doxorubicin (Dox) than their 3D control spheroids. On the other hand, triculture 3D hybrid and standard triculture spheroids demonstrated a similar resistance to the drug. Overall, such findings evidence the importance of fibroblasts and MSCs combination with cancer cells and should be considered in chemotherapeutics performance evaluation. In addition, the developed bioinstructive microparticle testing platforms showed potential to be used as an enabling technology to include different tumor ECM components in 3D *in vitro* models in the future.

Keywords: 3D Tumor Models, Drug screening, Lung Cancer, Mesenchymal Stem Cells, Bioinstructive Microparticles

1. Introduction

Presently, the *in vitro* pre-clinical validation models recommended by regulatory agencies to screen for candidate anti-cancer therapeutics are mainly based on the use of 2D cancer cell monolayers and *in vivo* animal models [1,2]. Both of these are increasingly seen as inadequate approximations of human tumors and or their complex microenvironment [3,4]. 2D monocultures lack the ability of correctly recapitulating spatial organization, cell-cell and cell-matrix interactions, biochemical cues and TME heterogeneity found in patients [5]. While animal models are recognizably expensive, laborious and ethically controversial alternatives, often lacking correct representation of the human tumor stroma [6,7]. Improved representation of the TME in PCVMs is thus necessary step for improving basic cancer biology research and drug-screening procedures.

Three-dimensional (3D) multicellular tumor spheroid (3D-MCTS) currently receive an increased attention in the field of anti-cancer drug discovery due to their ability to robustly recapitulate specific features of *in vivo* tumors [8]. Moreover, such models allow a straightforward combination of several malignant and non-malignant cell populations in a 3D environment that promotes cell-cell contacts and communication [9]. Cells cultured in 3D-MCTS are self-aggregated to form *in vitro* microtissues capable of mimicking oxygen/nutrient and pH gradients of human solid tumors [10]. Such provides an *in vivo* similar environment in which cancer cell phenotypical, genetical and metabolical heterogeneity can be easily recapitulated. However, despite better portraying the diverse cellular components of tumor microenvironment (TME) than 2D models, in general 3D-MCTS lack pre-existing ECM components, with matrix being deposited by cells during culture [11]. Inclusion of ECM-mimetics (e.g., Hyaluronic Acid [12], Collagen [13], Fibrinoge [14]), may therefore improve 3D-MCTS ability to correctly mimic the tissue specific-ECM that is present during tumorigenesis. This component is known to influence the process of metastasis, invasion, and acquisition of multi-drug resistance [15].

Regarding lung cancer ECM, one key component that has been associated with poor patient outcome when present in elevated concentrations is Hyaluronic acid (HyA) [16–18]. This natural polymer composed by disaccharides of D-glucuronic acid and D-N-acetylglucosamine [19] is found ubiquitously in human tissues, being commonly associated with several tumors ECM [19,20]. Several studies observed that cancer cells associated to a HyA-rich ECM environment demonstrated increased expression of two key HyA receptors:

(i) CD44, a marker associated with multidrug resistance (MDR) [21,22]; and (ii) RHAMM (receptor for hyaluronan-mediated motility, also known as cluster of differentiation 168 – CD168), is a receptor associated with invasion and metastasis through changes in motility, polarity and directed migration, as well as involved in matrix remodeling proteins production (e.g., MMP-9 or PAI-1)[20]. Yet, it is important to mention in the context that in the context of the development of bioinstruted 3D-MCTS, other TME components must also be taken into consideration. Such is particularly important concerning the cellular diversity and heterogeneity found in the TME. From the different cellular elements of the TME (e.g., cancer cells, cancer stem cells, cancer associated fibroblasts (CAFs), (please see introductory section 1.1, figures 1 and 2), some have yet to be included in 3D-MCTS *in vitro* models.

In this context, MSCs are becoming increasingly recognized as cellular constituents of the TME, playing paramount roles in multiple cancers [23–26]. MSCs have been involved in the regulation of the immune response in the TME [27,28], alteration of the surrounding tumor-ECM [29,30], conversion of fibroblasts to CAFs [31], initiation of epithelial-to-mesenchymal transition (EMT) by cancer cells [32], as well as metastasis [27]. Despite these contributions to cancer progression, reports of MSCs inhibiting and suppressing tumor proliferation, invasion and metastasis also exist [33]. The diverse roles of MSCs in lung cancer have been recently extensively revised elsewhere [30]. Given their polyvalent role, the representation of MSCs in 3D models is critical for the correct recapitulation of human tumors in an *in vitro* setting. However, few works have performed such inclusion in a 3D environment, and even fewer in a heterotypic system capable of representing the two main populations of the TME cancer cells and fibroblasts.

From this standpoint, herein we manufactured a novel 3D-MCTS lung tumor model capable of recapitulating cell-cell and cell-HyA specific interactions that mimic cell-ECM crosstalk. The latter was accomplished by incorporation of bioinstructive microparticles (MPs) produced with the layer-by-layer deposition technique. Moreover, MSCs were also co-cultured with cancer cells and fibroblasts for the first time in 3D *in vitro*3D-MCTSto evaluate their influence in the obtained results demonstrate that bioinstructive MPs promote the assembly of robust and reproducible 3D-MCTS and that the inclusion of HyA influences the expression of CD44 receptor, as well as response to therapy.

2. Materials and Methods

2.1. Materials

Polycaprolactone (PCL; Mn: 80 000), Polyvinyl Alcohol (PVA; MW: 30 000 – 70 000 Da) and Poly-L-lysine hydrobromide (PLL; MW: 30 000-70 000 Da) were acquired from Laborspirit (Loures, Portugal). Chitosan chloride (MW: 50-150 KDa) was acquired from Novamatrix (Sandvika, Norway). Hyaluronic acid sodium salt polymer (MW: 80 000 – 100 000) was obtained from Carbosynth Limited (Berkshire, United Kingdom). Ultra-Low-Adhesion (ULA) round-bottom 96-wells plates, Fetal Bovine Serum (FBS; E.U. approved, South America origin), Dulbecco's Modified Eagle Medium-High Glucose (DMEM-HG), Ham's F-12K Kaighn's Medium (HAMs-F12), Alpha Modified Eagle's Medium (α-MEM), TrypLE™ Express, Goat anti-Mouse IgG (H+L) Secondary Antibody, Alexa Fluor 488, Collagen I Antibody (5D8-G9); E-cadherin-PE antibody, Calcein-AM, Propidium Iodide (PI) were all purchased from Thermofisher Scientific Inc (Alfagene, Portugal). Anti-human CD44-FITC was purchased from Taper (Grupo Taper S.A., Lisboa Portugal). All other reagents and salts were of analytical grade and used without further purification.

2.2. Methods

2.2.1. PCL microparticles production

PCL microparticles where produced by using the oil-in-water (O1/W1) emulsion-solvent evaporation technique. The oil phase (O1) was comprised by a 5 % (w/v) PCL dichloromethane (DCM) solution . The aqueous phase (w) consisted of a 0.5 % (w/v) PVA aqueous solution that was prepared from a stock solution of PVA (5 % (w/v)). To form the water-oil emulsion 8 mL of PCL (O1 phase) were dispersed into 150 mL of PVA by using a high precision piezoelectric-based air pumping system (OB1 MK3 – Elveflow® Microfluidic Flow Control System) operated at an air pressure of 5 bar. The microparticle-containing solution (reduced to 50 mL) was then placed under horizontal stirring at 170 rpm during at least 8 h, at room temperature (RT), inside a fume-hood to promote solvent evaporation and PCL microparticles hardening. Following this, PCL microparticles were washed 3 times by using vortex-centrifugation cycles (1000 rpm, 5 min). The particles were then sieved through stainless steel sieves to obtain particle size ranges from 63 µm to 100

μm. All particles were freeze dried for 48 h and stored in a moisture free environment until further use.

2.2.3. Bioinstructive microparticles production via Layer-by-Layer

Prior to surface functionalization microparticles were subjected to plasma treatment. For this purpose, 200 mg of previously sieved microparticles where placed in a sterile beaker covered with aluminum foil. Plasma treatment was performed by using atmospheric air charged at 30 V, for 5 min. To guarantee that the entire surface of the particle was subjected to plasma treatment the compartment was slowly re-pressurized and the beaker containing the particles was stirred, repositioned inside the cylinder and subjected to plasma treatment for 3 times.

For Layer-by-layer (LbL) surface functionalization 250 mg of plasma treated PCL MPs (LbL-MPs) with a negative surface charge were immersed in 20 mL of PLL (1 mg/mL, filtered 0.22 μm) for 10 min and washed in distilled water for 5 min. For the buildup of the negative layer, PLL-MPs were transferred into an HyA solution (1 mg/mL, filtered 0.22 μm) for 10 min, and re-washed for 5 min. This process was repeated 3 times to allow the formation of 3 PLL-HyA bilayers.

2.2.4. Zeta Potential analysis of polyelectrolyte polymers deposition

Zeta potential measurements were used to verify the efficacy of LbL polyelectrolyte layers deposition in MPs surface. This analysis was performed in pristine PCL MPs and at each consecutive LbL deposition step. All measurements where performed in a Zetasizer Nano ZS (Malvern,Worcestershire, UK), at 25 ºC by using the automatic mode and disposable zeta potential cell. The ZetaSizer software was used to record and process the electrophoretic mobility data (v. 7.04).

2.2.5. Microparticles characterization

Microparticles morphology and particle size and was evaluated by optical contrast light microscopy (Primostar, Carl Zeiss, Germany). Acquired images where analyzed using open-source software ImageJ [34]. the size distribution of each microparticle formulation through area analysis by using a supervised algorithm that analyzed a minimum of 300 particles.

Scanning Electron microscopy (SEM) imaging was used to analyze microparticle morphology and surface topography. For SEM analysis particle samples were dispersed in deionized water and drop-wise added to an aluminum stub containing a glued tissue culture treated polystyrene insert. The samples were then dried at 37 ºC overnight, sputter coated with gold/palladium and observed in a Hitachi S-4100 scanning electron microscope (Hitachi, Japan) operated at a voltage in the range of 15-25 kV and at various magnifications.

2.2.6. Cell Culture

All cells were manipulated in aseptic conditions and cultured at 5 % CO_2, 95 % atmospheric oxygen, in humidified, temperature controlled incubators at 37 ºC. The non-small cell lung carcinoma cell line A549 (ATCC CRM-CCL-185™) was cultured in HAMs-F12 medium supplemented with 10 % (v/v) FBS and 1 % (v/v) ATB. The human primary dermal fibroblasts cell line (HF) (ATCC®-PCS-201-012™) were cultured in DMEM-HG supplemented with 10 % (v/v) FBS and 1 % (v/v) ATB. Adult Bone Marrow-Derived Mesenchymal Stem Cells (BM-MSCs) (ATCC®-PCS-500-012™) were maintained in α-MEM supplemented with 10 % (v/v) FBS and 1 % (v/v) ATB. All cells where detached from culture flasks upon attaining approximately 80-85 % confluency by using TrypLE™ Express Enzyme (1X) detaching reagent. Throughout all studies performed in this thesis BM-MSCs were used from passages 3 to 7 to assure stemness properties maintenance.

2.2.7. 3D *In vitro* lung tumor models assembly via Liquid-Overlay Technique

Homotypic monoculture 3D-MCTS with A549 cells, heterotypic co-culture spheroids: A549-HF and A549-MSCs cells, or tricultures: A549-HF-MSCs cells, were self-aggregated at different cell ratios (Section 4.1 table 1), by using the liquid-overlay technique, also known as forced-floating methodology. To form 3D-MCTS cells were initially cultured in ULA round bottom 96-wells plates. Multiple or single-cell suspensions composed by the different cell populations to were seeded in the wells. Afterwards cells were left in culture or incubated with LbL-MPs in the respective wells. Prior to each assay, LbL-MPs were sterilized under UV light (30 min) and resuspended in complete HAMs-F12 cell culture medium. To produce different 3D *in vitro* models that would better recapitulate the tumor microenvironment cellular heterogeneity different parameters were manipulated, namely: (i) the cell number per well, (ii) the cell-to-cell ratios between malignant and

mesenchymal/endothelial cells and (iii) the cell-to-particle ratios. The specific ratios used for each condition are summarized in (Section 4.1 table 1).

2.2.8. 3D tumor microtissues characterization

3D *in vitro* lung tumor models morphology, growth and circularity was analyzed overtime via optical contrast microscopy by using an inverted microscope (Primovert, Carl Zeiss, Germany). Images of 3D-MCTS were acquired on specific timepoints (days 1, 7 and 14). A minimum of 6 spheroids were analyzed per condition per time point. Image analysis was carried out by using the open-source software ImageJ (Fiji package) and a supervised algorithm based on the code developed by Ivanov and coworker [35].

For SEM analysis spheroids were processed as reported in the literature [36–38]. In brief, 3D-MCTS with and without LbL-MPs were removed from culture media and washed with D-PBS, fixed in formaldehyde 4% (v/v) solution in D-PBS, at 37 ºC for 2 h. The samples were then subjected to dehydration with graded ethanol concentrations (25 %, 50 %, 75 %, 90% (v/v)), for 20 min. All samples were then carefully mounted in aluminum stubs by using double sided adhesive carbon tape (Agar Scientific, Essex, United Kingdom) and sputter coated with gold/palladium. All spheroids were being imaged in a Hitachi S-4100 scanning electron microscope (Hitachi) operated at a voltage in the range of 15-25 kV and at various magnifications.

2.2.9. Cell viability assays

The cell viability and necrotic core formation of different homotypic and heterotypic 3D *in vitro* lung tumor microtumors (3D-MCTSs and 3D-MCTS LbL-MPs), were analyzed at specific timepoints (7 and 14 days) through different methodologies, namely: (i) Non-radioactive Alamar Blue® Cell Viability Assay, (ii) CellTiter 96® Aqueous One Solution Cell Proliferation Assay (MTS), and (iii) Live/Dead assay.

Alamar blue was used to access 3D tumor models viability during the initial steps of homotypic and heterotypic mono-, bi- and triple co-cultures optimization. Both assays were performed in accordance with manufacturers guidelines. The only exception was Alamar Blue incubation time, which was performed overnight instead of the standard 2-4 h period. Alamar Blue resazurin reduction to resorufin was determined by fluorescence measurements (λ_{ex}: 540 nm, λ_{em}: 600 nm). All measurements where performed in a Synergy HTX microplate reader by using a 96-well black-clear bottom plate.

2.2.10. 3D-MCTS characterization by Widefield and Confocal Laser Scanning Fluorescence Microscopy

Collagen I and E-cadherin expression were analyzed at specific timepoints (7 and 14 days) through immunocytochemistry. This analysis was performed to better understand phenotypical and morphological changes observed over culture in the different 3D-MCTS, For immunocytochemistry analysis 3D-MCTS were fixed in formaldehyde 4% (v/v) in D-PBS, at 37 ºC, for 4 h or overnight, at RT. The spheroids were then carefully transferred to a new 96 well ULA plate, washed and incubated for 1 h with blocking solution 1% BSA in D-PBS at 4 ºC followed by a washing step. Then 3D-MCTS were incubated with the primary antibody overnight at 4 ºC (E-cadherin 5 µL/mL; Collagen I: 2.5 µL/mL), washed (D-PBS, 3 times), and if necessary incubated with secondary antibody for 1 h, RT. Acquisition of fluorescence micrographs was performed in a widefield microscope (Axio Imager M2, Carl Zeiss, Germany), or in laser scanning confocal microscopes (LSM 510 Meta, and LSM 880 Aryscan, Carl Zeiss, Germany). Analysis of acquired images was performed in Zeiss Zen Black software (2017) and in Zeiss Zen Blue software (2017).

To evaluate 3D-MCTS necrotic core formation, the spheroids were labelled with Calcein-AM (Cal-AM) (4 µg/mL) and Propidium Iodide (PI) (10 µg/mL) for 30 min at 37 ºC, according to literature reports for 3D models [38]. Following incubation, the different 3D tumor models (3D-MCTS and 3D-MCTS LbL-MPs) were washed 3 times with D-PBS and were either imaged immediately by fluorescence microscopy, or fixed in 4% formaldehyde (v/v) for posterior observation.

2.2.11. Histological analysis

Histological analysis of dual co-culture (A549-HF) and triculture (A549-HF-MSCs) of 3D-MCTS and 3D-MCTS cultured in LbL MPs was performed in order to analyze microtumors internal organization and collagen deposition. In brief, 3D-MCTS with and without LbL-MPs were removed from culture media and washed with D-PBS, fixed in formaldehyde 4% (v/v) solution in D-PBS, at 37 ºC for 2 h. The samples were then subjected to dehydration with growing concentrations of ethanol (25 %, 50 %, 75 %, (v/v)), for 20 min, per condition. Afterwards, 3D microtumors were stored at 4 ºC in ULA plates. For histological analysis the different spheroid samples were imbedded into HistoGel™ (previously heated to 70ºC in a water bath for 2 h), and then rapidly cooled into hardening, and then processed for standard paraffin fixation. Paraffin blocks containing 3D-MCTS were

sliced into 5 μm thick samples and stained with: (i) Hematoxylin and Eosin (H&E) for internal structures morphological analysis, and (ii) Masson's Trichrome for possible evaluation of collagen deposition. Histology slides were then analyzed by using an inverted optical contrast light microscope (Primovert, Carl Zeiss, Germany).

2.2.12. Flow cytometry analysis

The effect of hyaluronan bioinstructive LbL-MPs in 3D-MCTS CD44 expression was analyzed by flow cytometry . For this analysis, 3D-MCTS and 3D-MCTS LbL MPs with 7 days of culture were dissociated by incubation in a 1:1 mixture of Accumax® and TrypLE™ Express for 30 min, at 37 ºC. After this incubation, spheroids were disrupted by gentle pipetting and incubated in HAMs-F12/10% FBS/1% ATB for 30 min. The resulting single cells suspensions were then recovered by centrifugation (300 g, 5 min, 37 ºC). The different samples were incubated with anti-human CD44-FITC conjugate antibody (5 μl/ml in PBS) for 30 min, at 37 ºC. Single cells were then recovered by centrifugation and washed with D-PBS for 3 times. In addition 2D monocultures of A549, HF and MSCs were also analyzed for their CD44 expression. Prior to FCM analysis all sampled were sieved through 40 μm cell strainers. Flow cytometry analysis was carried out in a BD Accuri C6 flow cytometer (BD Bioscience, San Diego, CA, USA) were a total of $5x10^3$ events per sample were acquired in cells assigned ROI and recorded in the FL-1 channel (FITC). Flow cytometry data was processed and analyzed in FCS Express software (v. 6, trial license).

2.2.13. Chemotherapeutic drug cytotoxicity screening in 3D-MCTS platforms

The produced 3D-MCTS were cultured for 7 to 14 days on HAMs-F12 medium to be used as testing platforms for Doxorubicin cytotoxicity evaluation in monotypic monocultures (A549 cells), heterotypic bi co-cultures (HF/A549), and triple co-cultures (HF/A549/MSCs). Upon achieving the desired culture time, 3D-MCTS were incubated with Doxorubicin (Dox) chemotherapeutic at different concentrations ranging from 0.7 to 17 μM, over a period of 72 h or 120 h. Cellular viability of 3D-MCTS was then evaluated by using a luminescence-based assay specifically designed to quantify cellular ATP in *in vitro* 3D cellular aggregates assembled either *via* scaffold-based or scaffold free methods (Cell Titer

Glo™ Luminescent cell viability assay, Promega, Madisson, WI, USA). CellTiter-Glo® assays were performed accordance with the manufacturer instructions. In brief, following incubation with Dox the medium was removed and 3D-MCTS were incubated with a mixture of HAMs-F12/10%FBS/1% ATB medium and CellTiter-Glo® reagent at a 1:1 ratio. The samples were stirred in a plate stirrer for 5 min at RT, and incubated for 25 min, at RT. Luminescence was then measured in 96-well opaque flat-bottom white plates by using a Synergy HTX microplate reader programmed with an integration time of 1 sec. Non-treated 3D-MCTS were used as controls. In addition, MTS cell viability assays were also used to investigate Dox IC50 in 2D *in vitro* monotypic and heterotypic co-cultures. MTS data was acquired through absorbance readouts of the formed soluble tetrazolium salt (λ=490 and λ=650 nm). MTS data was obtained by using a Synergy HTX microplate reader equipped with a monochromator and photodiode detector that allowed absorbance measurements.

2.15. Statistical Analysis

All statistical analysis was performed using Graphpad Prism 6 Software (Prism 6™). One-way analysis of variance (One-ANOVA) and Two-way analysis of variance (Two-ANOVA) with Holm-Sidak's post-hoc test. A minimum of 6 replicates was used for statistical analysis. Unless otherwise indicated, $p < 0.05$ was considered statistically significant.

3 – Results and Discussion

The establishment of *in vitro* 3D microtumor models that are relevant for drug screening in the pre-clinical discovery pipeline require should correctly represent tumor heterogeneity and unique microenvironment components so as to provide a better *in vitro/in vivo* correlation [39]. Currently, the great majority of 3D tumor models employed in drug-screening are based on the utilization of scaffold-free 3D-MCTS models. These models are easy to assemble, capable of representing in detail dimensional cell-cell interactions found *in vivo* and relatively easy to analyze being suitable for high-throughput drug screening approaches [39–41]. However, by definition spheroid models lack pre-existent matrix components, with ECM deposition occurring only through activity of cultured cells [8]. The representation of key aspects of TME in a reproducible and significant way, such as in co-cultures capable of simulating the phenotypes and genetic profiles of cultured cells found in *in vivo,* contribute for the establishment of important pre-clinical models bestowed with a

predictive power higher than that of conventionally used 2D or even 3D monoculture models [3,42,43]. One approach to overcome limitations regarding the presence of pre-existent ECM in 3D-MCTS is through the addition of ECM-like scaffolds in the format of bioinstructive microparticles. The incorporation of microparticle technology (extensively used in the field of tissue engineering for delivery of cellular aggregates), adapted into the process of co-culture tumor spheroids 3D aggregation is a valuable technology to combine hyaluronan, a key ECM component, with the study of how diverse cell lineage combinations, of A549, HF and BM-MSCs interact and respond to chemotherapeutics, namely doxorubicin.

This integrative approach aims to bridge the gap between *in vivo* and *in vitro models* through both representation of cellular heterogeneity, and correct representation of two TME associated key populations namely HF and BM-MSCs.

To assemble bioinstructive, MPs-based 3D-MCTS, PCL microparticles were initially produced through the emulsion/solvent evaporation technique. The manufactured particles demonstrated size polydispersity as expected. To narrow size dispersity to the desired range diverse formulations were tested. The obtained size distributions respective to each tested formulation are presented in figure (1 B). Respective distribution of particles within the desired size range for each formulation are shown in figure (1 A).

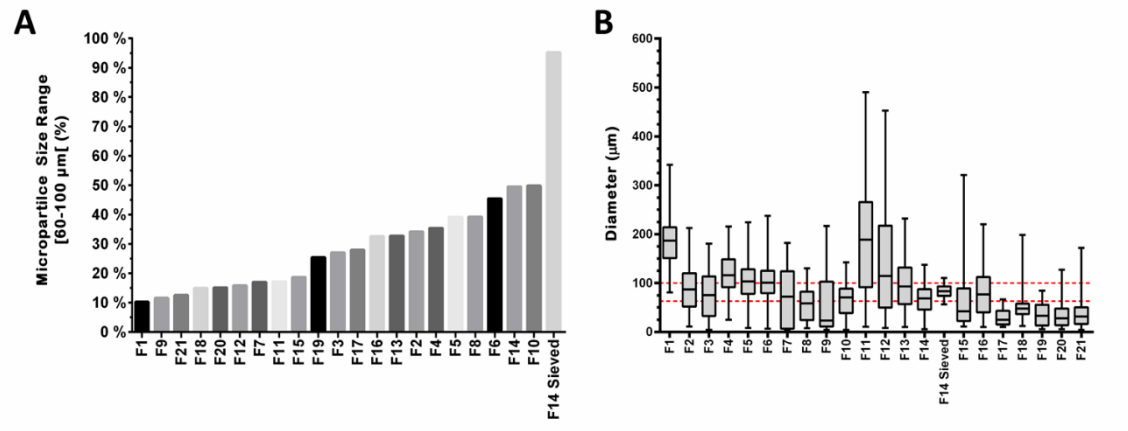

Figure 1. PCL microparticles size characterization. (A) – Percentage of PCL MPs within the desired size range of 60-100 µm for each tested emulsion formulation. Although formulation F10 presented the finest results regarding size, formulation F14 making use of double the PCL solution allowed to duplicate the time efficiency of the production process while allowing the recovery of an identical percentage of particles. (B) – Box Whiskers graphic demonstrating size dispersion, and minimum and maximum sizes obtained in tested formulations. Particle size was analyzed through optical microscopy, acquired images were processed using ImageJ software.

The parameters involved in the production of MPs, (, were optimized for the efficient manufacture of particles within the desired size range of 60-100 μm. During optimization stages it was clear that higher PCL concentration in the oil phase, while maintaining PVA concentration constant, lead to a markedly increase in the average diameter and polydispersity of MPs. Contrarily, lower PCL concentrations resulted in a size shift towards smaller-sized particles. Tested formulations using 7.5 % (w/v) PCL resulted in highly polydisperse microparticle populations, with diameters ranging from 10 to ~500 μm (Formulations F11, F12 - figure 1), while formulations of 2.25 % (w/v) PCL resulted in particles with diameters of 4 to ~24 μm. Increasing PVA concentration on the aqueous phase up to 2 % (w/v), while maintaining PCL concentration in 5 % (w/v), in the oil phase, reduced size polydispersity of produced MPs (as can be seen by comparing formulations F13 to F11 and F12). An increase in the stirring velocity of the aqueous solution most often resulted in the production of smaller particles and changes in morphology, such as the acquisition of elliptical morphology and rougher surfaces were observed (Figure 2).

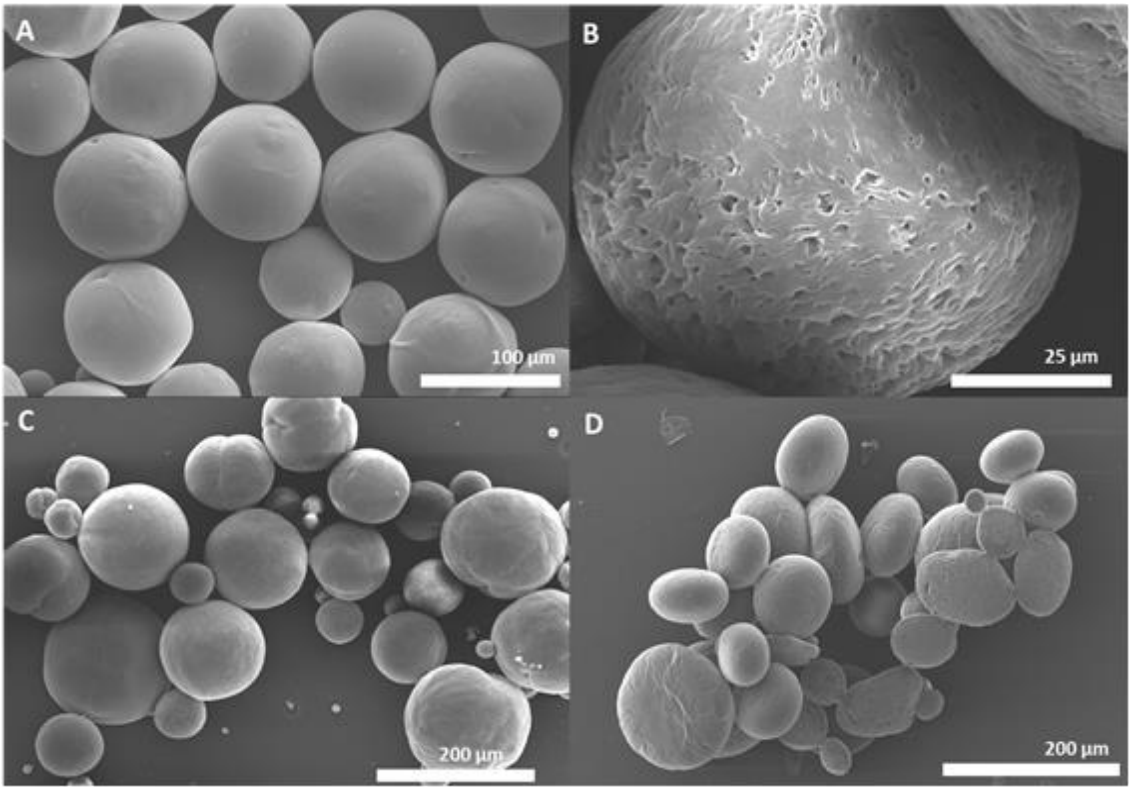

Figure 2. Scanning electron microscopy analysis of PCL microparticles produced by O/W emulsion. Owing to an increase in the stirring speed of the aqueous phase formulation F4 (S14) (B and C) and F7 (s19) (C) present rough/porous surfaces, with F4 presenting various shapes and F7 elliptical morphology when compared to F10 (A).

Formulations F14 was found to be optimal for the recovery of MPs in the desired size range. In comparison to F10, F14 allowed to efficiently double the production of MPs due to the increased volume of PCL solution used, while presenting similar morphology and size distribution to F10 (figure 3). Sieving of formulation F14 increased the percentage of particles in the desired size from 49.5 % to 95.2 %, with the final population of sieved particles presenting a coefficient of variation (CV) of 14.86%, thus being closer to that of a monodisperse formulation (Figure 3).

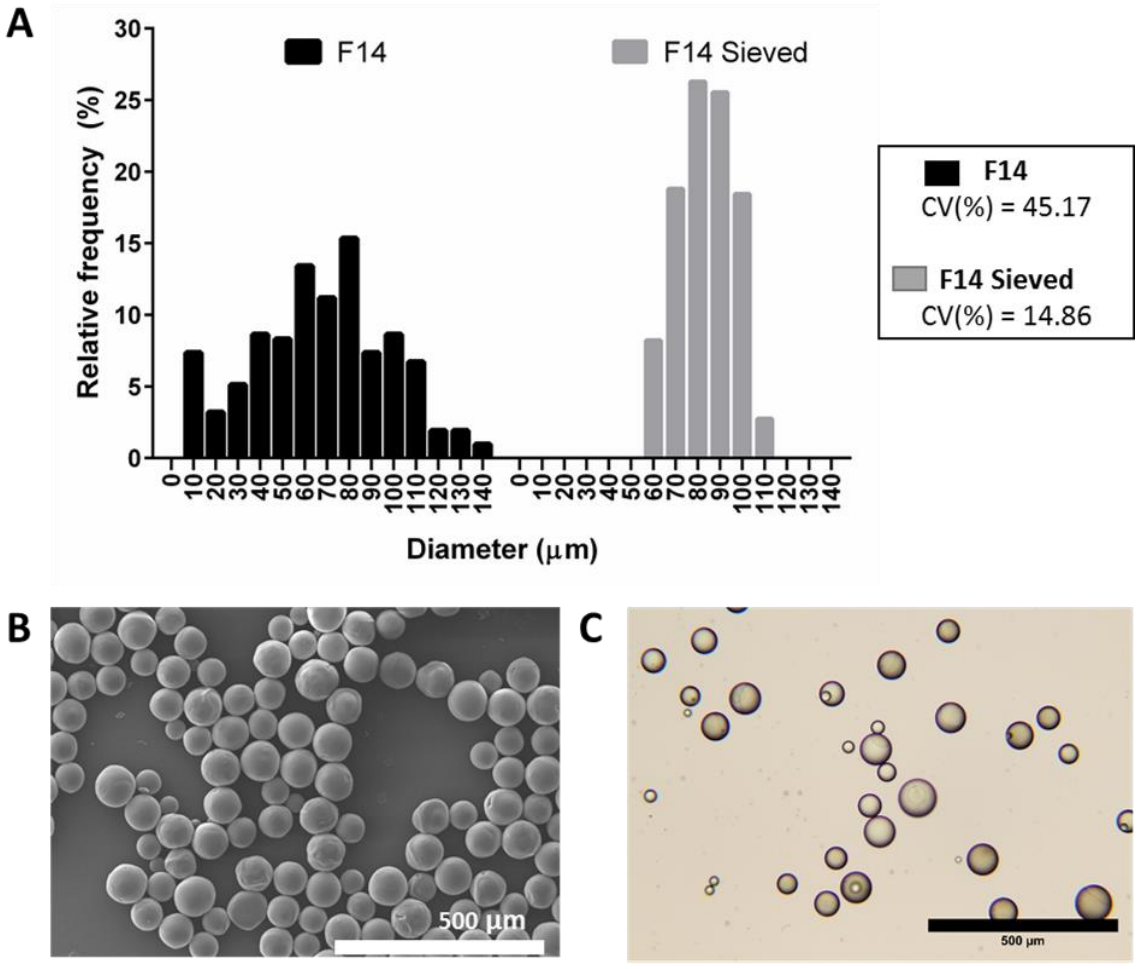

Figure 3. Characterization of PCL MPs formulation F14. (A) – Size distribution of formulations F14 and F14 post-sieving demonstrate the effectiveness of the sieving procedure. (B,C) – SEM and light microscopy characterization of Formulation F14 MPs morphology and surface features.

3.2. Layer-by-Layer functionalization of microspheres surface

Following the optimization of MPs synthesis and recovery, the particles were subjected to plasma treatment to allow an easier and more efficient Layer-by-layer deposition of either Chitosan or Poly-l-lysine (PLL) polyelectrolyte polymers onto particles

surface. HyA was chosen to manufacture bioinstructive MPs due to its role as a key component in tumor-ECM interactions, being also associated to poor disease prognosis in patients with lung cancer [17,44]. Furthermore, HyA excessive production and aberrant splicing, derived of the overexpression of hyaluronic acid synthase 1 and 2 [45], has been connected to the onset of MDR in different tumor [46,47]. Chitosan was also investigated for LbL MPs functionalization due to its cell adhesive properties, biocompatibility and positive charge that could be used to complex HyA via electrostatic interactions.

To study the surface deposition of polyelectrolyte polymer nanolayers and consequential surface charge reversal, zeta potential measurements where performed. The obtained values of zeta potential changed accordingly to the electrostatic charge of the specific layer deposited onto MPs (figure 4). The results obtained from CH-HA showed a higher variance than those obtained from PLL-HA modified MPs, with the final layer in the CH-HA MPs evidencing a smaller negative charge than in the PLL-HA 6th layer. As such, PLL/HyA layered polyelectrolyte MPs were selected for further studies. Different reports in the literature support the use of PLL-HyA LbL layers for supporting embryonic stem cells growth in 3D culture [47], and for breast tumor microenvironment modellin [48].

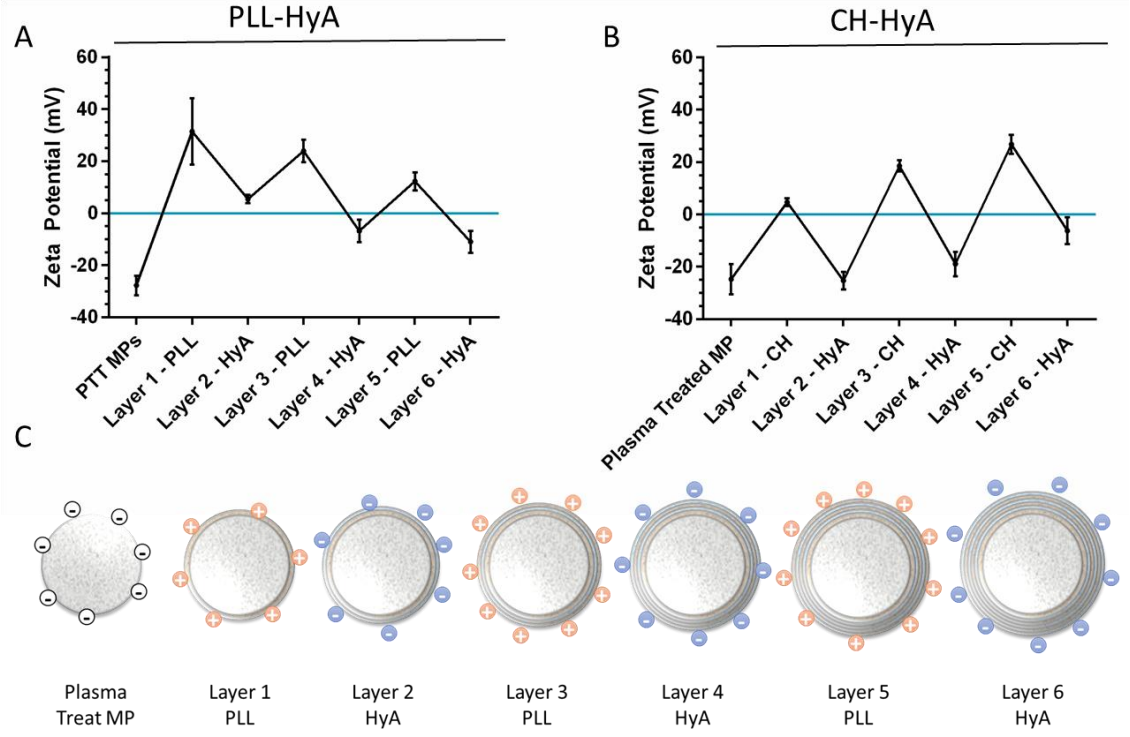

Figure 4. Zeta potential measurements on MPs after plasma treatment and sequential polyelectrolyte polymers deposition. PLL (A) or CH (B), and HyA. Layer 6 of PLL-HA has an average Zeta potential of -11 mV, concordant with Hyaluronic

Acid deposition. Schematic of the LbL process used to coat plasma treated PCL microparticles (C). Data is represented as mean ± s.d, (*n*=3).

Depending on parameters such as deposition time, concentration of polymers in dipping solution, temperature, and number of layers deposited LbL treatments can lead to alteration of both MPs surface texture and morpholog [49]. To analyze if any change occurred to either morphology, size or texture of the particles these were subjected to optical and SEM microscopy analysis. The obtained micrographs showed that no change occurred due to either of established parameters. LbL-PCL particles maintained both their size distribution, and morphology (figure 5 A,B,C), with only minor changes occurring to the surface, namely with a minor increase on roughness (Figure 5 D, E, F).

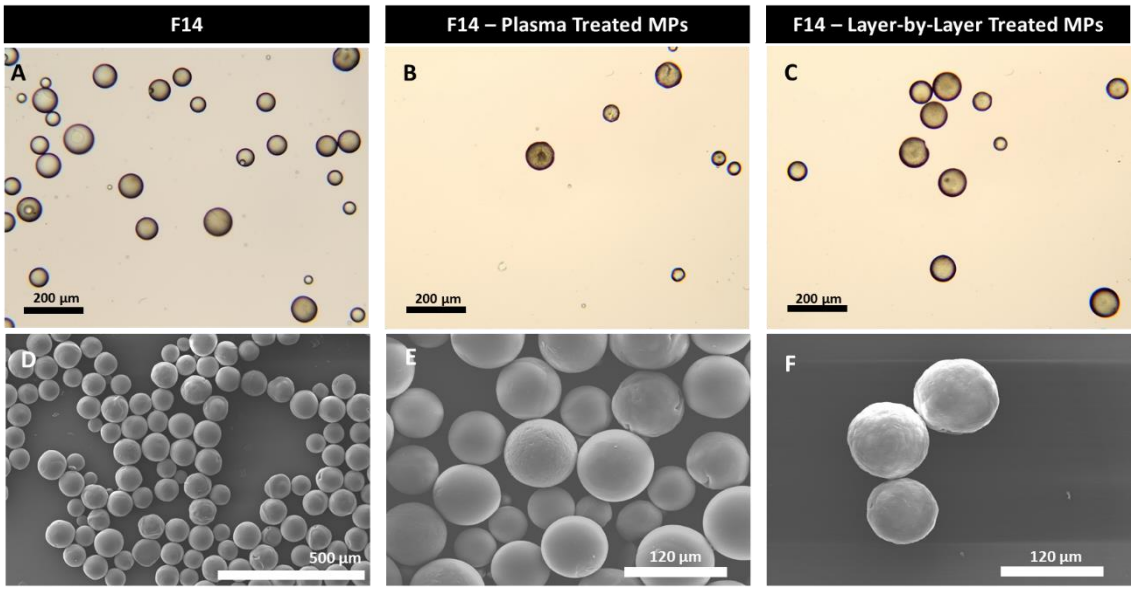

Figure 5. Optical contrast microscopy and SEM analysis of LbL PCL particles. Microparticles prior to plasma treatment (A,D), after plasma treatment (B,E) and post LbL treatment (C,F). Close-up image on LbL treated particles demonstrates a slight modification of surface texture red. Images acquired using optical microscopy (A,B,C). Images acquired through SEM microscopy (D,E,F).

After optimizing and producing LbL bioinstructive microparticles surface functionalized with HyA assays were undertaken to access the how the inclusion of the LbL treated MPs (LbL-MPs) could affect overall 3D-MCTS assembly and viability during culture along time.

3.3. 3D-MCTS assembly and morphological characterization

Culturing cells in a 3D setting allows the integration of a multitude of interactions absent in 2D models [5,50]. Such models provide an environment in which cells contact directly with involving neighboring cell in a three-dimensional space, expanding, contracting, and assembling into microtissues with morphological, phenotypical and genetic characteristics similar to solid human tumors [51]. The representation of key hallmarks such as necrotic core formation, correct recapitulation of cellular interactions between different populations, is crucial to manufacture predictive models that are suitable for drug-screening [39,52–54]. With the objective of recapitulating such characteristics composite microparticle encompassing 3D-MCTS triculture models containing non-small cell lung cancer cells (A549), human dermal fibroblasts (HF), and bone-marrow derived mesenchymal stem cells (BM-MSC), were established using relevant ratios based on previous literature reports [30,38,55–58]. The inclusion of this diverse cellular landscape allowed the development of an *in vitro* model that better represents the tumor TME and its heterogenic cellular components [59,60].

To access ideal cell and particle density, for cultured 3D-MCTS to develop *in vivo* tumor-like characteristics, preliminary tests were performed using A549 monoculture and A549-HF dual coculture 3D-MCTS. Several literature reports use different ratios of cancer-to-stroma cells, such as fibroblasts or mesenchymal stem cells, with no consensus having been established so far [38,57,61–63]. Previous works by Amann and coworkers reported prolific effects of coculture of A549 and Colo699 cancer cells lines with SV80 lung fibroblasts in a 1:2 ratio [62]. These testing platforms showed an increased proliferation and α-SMA expression, associated with CAF like phenotypes, when fibroblasts were cocultured with A549[62]. Such populations have been recognized to increase cancer cells survival and worsen prognostic in the clinical setting. For example tumors of the breast, colon [62,64], with higher stroma content have a higher chance of relapse and development of MDR during treatment.

Various cell seeding and microparticle combinations were attempted (Table 1), with the objective of creating 3D-MCTS with diameters >500 µm, thus being capable of exhibiting the nutrient, metabolite and hypoxic gradients associated with *in vivo* solid tumors [65]. Establishing a necrotic core in the interior of the spheroid, while maintaining solidity and shape uniformity over extended periods of culture is important to reduce assay-to-assay variability. The balance between the complexity/physiological relevance LbL-MPs 3D-

MCTS and their ability to be used in the future for high throughput analysis was also sought after.

Table 3. Culture conditions tested for optimal spheroid formation.

Culture Type	Cell Lines	Population Ratios*	Seeding Densities (Cell/well)	MPs Concentration (mg/well)	Ref**
Monoculture	A549	**1**	5000 10000 15000 30000 45000	0.0 0.025 0.050	[55]
Biculture	A549 HF	**1:2**			[38,57,58,62]
Biculture	A549 BM-MSCs	**10:1**	15000 30000 45000	0.0 0.025	[30,56]
Triculture	A549 HF BM-MSCs	**10:20:1**			[30,38,55–58]

* ratios are respective of the cell populations referred on column to the left. **references are referent to the implementation of populations ratios. After preforming initial assays with monoculture and dual coculture 3D-MCTS an optimized number of conditions was tested in dual and triculture models making usage of BM-MSCs.

Preliminary optimization of spheroid cultures was performed using mono and dual coculture spheroids of A549 and HF, formed by 5, 10, 15, 30 and 45 thousand cells and with varying quantities of LbL-MPs (0; 0.050 or 0.025 mg/spheroid). Image analysis over time allowed to access 3D-MCTS growth and contraction profiles in the diverse populations tested. Analysis of size variations in mono and dual coculture 3D-MCTS of A549 and HF revealed distinct patterns of growth and contraction resultant from the inclusion TME associated populations (Figure 6 and 7).

Monoculture spheroids of A549 presented the largest areas and slowest contraction ratios of the four tested coculture conditions, (monoculture of A549, dual coculture of HF or MSCs, Triculture of HF-A549-MSCs) resulting in relatively uncondensed spheroids. Over the period of 14 days these spheroids formed more compact microtissues, with the biggest spheroids composed of an initial cell density of 45 000 cells presenting diameters at day 1 that well exceeded 1 mm, and at day 14 of 600-800 µm (Figure 6). The size reduction observed in A549 monoculture spheroids, was not observed in spheroids containing other TME associated populations such as HF, for which at day one 3D-MCTS (initial cell seeding density =45 000 cells) presented diameters of only approximately 500 µm without LbL-MPs and of ~750 µm when containing 0.050 mg of LbL-MPs (Figure 7).

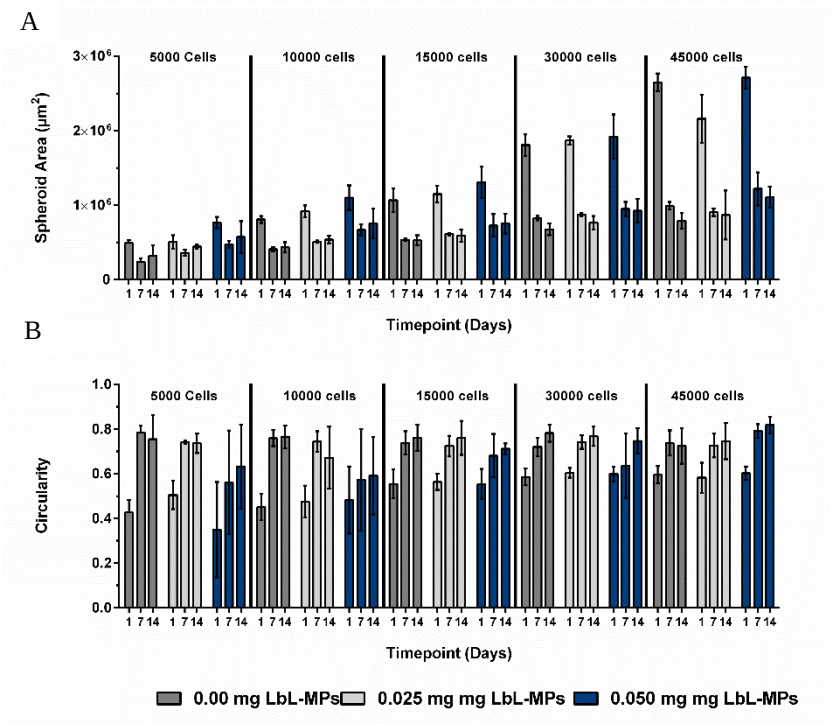
A
5000 Cells
10000 cells
15000 cells
30000 cells
45000 cells
Spheroid Area (µm²)
Timepoint (Days)
B
Circularity
Timepoint (Days)
0.00 mg LbL-MPs
0.025 mg mg LbL-MPs
0.050 mg mg LbL-MPs

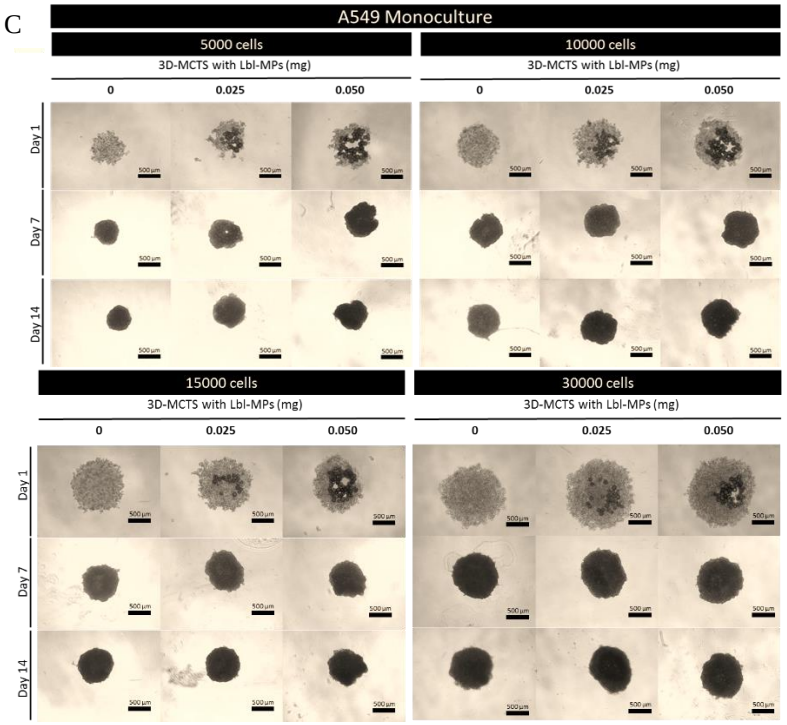
C
A549 Monoculture
5000 cells
10000 cells
15000 cells
30000 cells
3D-MCTS with Lbl-MPs (mg)
0
0.025
0.050
Day 1
Day 7
Day 14

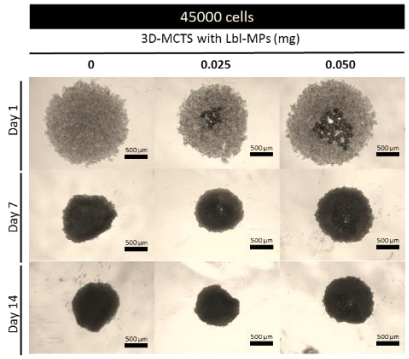

Figure 6. Size Variation of A549 monoculture spheroids over the course of preliminary assays. Spheroids area (A) and circularity (B) measurements were performed for each at 1, 7 and 14th days of culture (C) Optical contrast micrographs processed in ImageJ software. Scale bar represents 500 µm.

The addition of dermal fibroblasts to monoculture spheroids in a A549-HF 1:2 ratio lead to the formation of significantly different 3D spheroids in what concerns size and circularity (Figure 7). The addition of particles at either 0.025 and 0.050 mg per LbL-MPs 3D-MCTS resulted in slightly higher spheroid areas at initial time points (figure 6 and 7), in comparison to control 3D-MCTS. From day 1 to day 7 a significant reduction in spheroids area was obtained as a result of cells aggregation into compact spheroids, these results are in accordance with other literature examples for 3D-MCTS without microparticles [38] .

It is important to emphasize that spheroids containing 0.050 mg of microparticles were in some cases unable to form cohesive spherical microtissues, this observation was particularly prevalent in A549 monoculture spheroids (Figure 6). Smaller spheroids of 5000 or 10 000 cells and those containing 0.050 mg of LbL-MPs were also very difficult to handle and lacked necrotic core in monocultures of A549 at 14 days (supplementary Figure 4) These findings evidenced that 0.025 mg of LbL-MPs per spheroid provided the most promising results for the subsequent studies involving the additional inclusion of HFs and MSCs, to ultimately assemble triculture A549-HF-MSCS LbL-MPs 3D-MCTS.

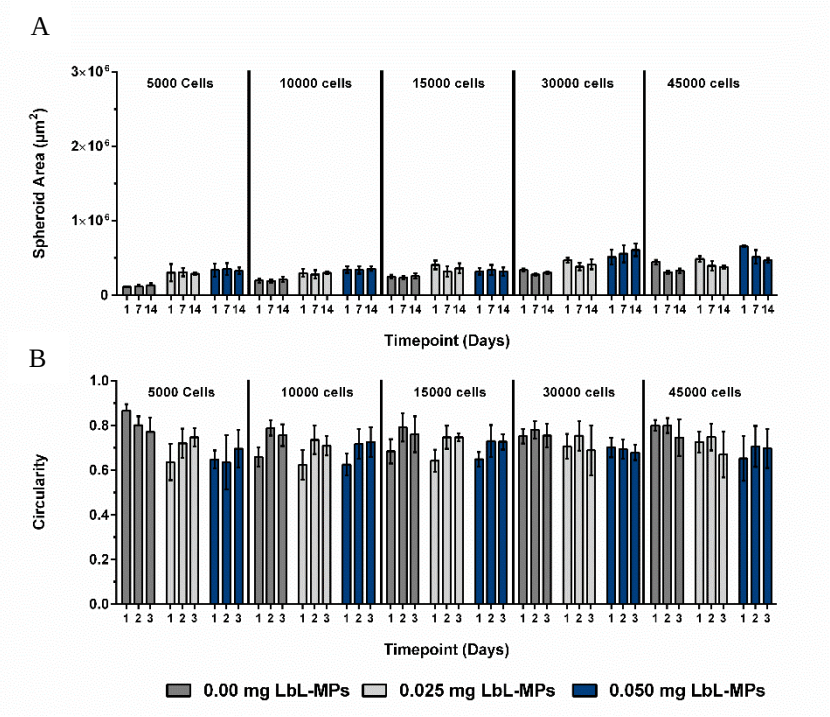
A
Spheroid Area (µm²)
3×10⁶
2×10⁶
1×10⁶
0
5000 Cells
10000 cells
15000 cells
30000 cells
45000 cells
1 7 14
Timepoint (Days)
B
Circularity
1.0
0.8
0.6
0.4
0.2
0.0
1 2 3
Timepoint (Days)
0.00 mg LbL-MPs
0.025 mg LbL-MPs
0.050 mg LbL-MPs

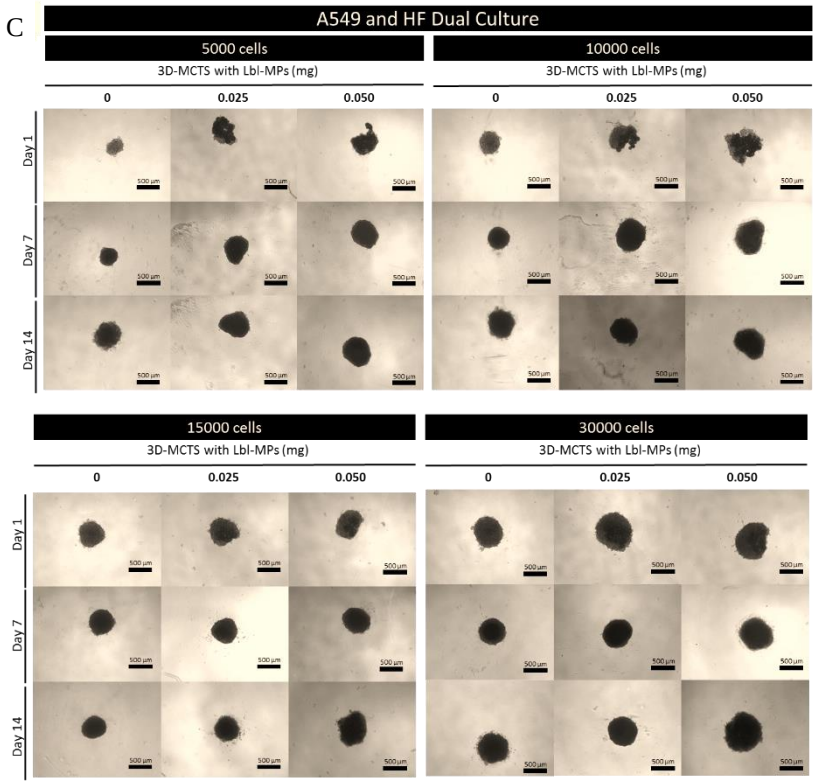
C
A549 and HF Dual Culture
5000 cells
10000 cells
15000 cells
30000 cells
3D-MCTS with Lbl-MPs (mg)
0
0.025
0.050
Day 1
Day 7
Day 14
500 µm

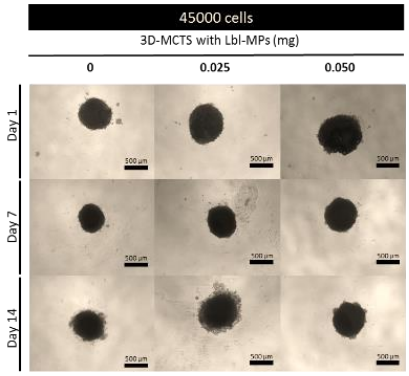

Figure 7. Size Variation of A549-HF spheroids over the course of preliminary assays. Spheroids area (A) and circularity (B) measurements were performed for each condition at 1, 7 and 14 days of culture (C) Optical contrast micrographs processed in ImageJ software. Scale bar represents 500 µm.

After performing the preliminary assays and establishing optimal culturing conditions for A549 and A549-HF spheroids, the area and circularity of coculture spheroids of A549-MSCs in a ratio 10:1 (A549-MSCs), and triculture spheroids in a ratio 10:20:1 (A549-HF-MSCs) was also analyzed. The ratio of cancer cells to MSCs was chosen in accordance to previously established observations, by Liu and coworkers, that smaller ratios of BM-MSCs to A549 cells seem to favor pro-tumorigenic interactions *in vitr [*30].

Spheroids contraction and area variations when A549 cells were combined with MSCs in dual coculture or tricultures revealed that dual A549-MSCs and Triculture 3D-MCTS presented similar size and contraction profiles to those of A549-HF. Interestingly triculture spheroids had the smallest sizes and formed the most densely packed microtissues of all conditions, regardless of LbL-MPs inclusion or not (Figure 8).

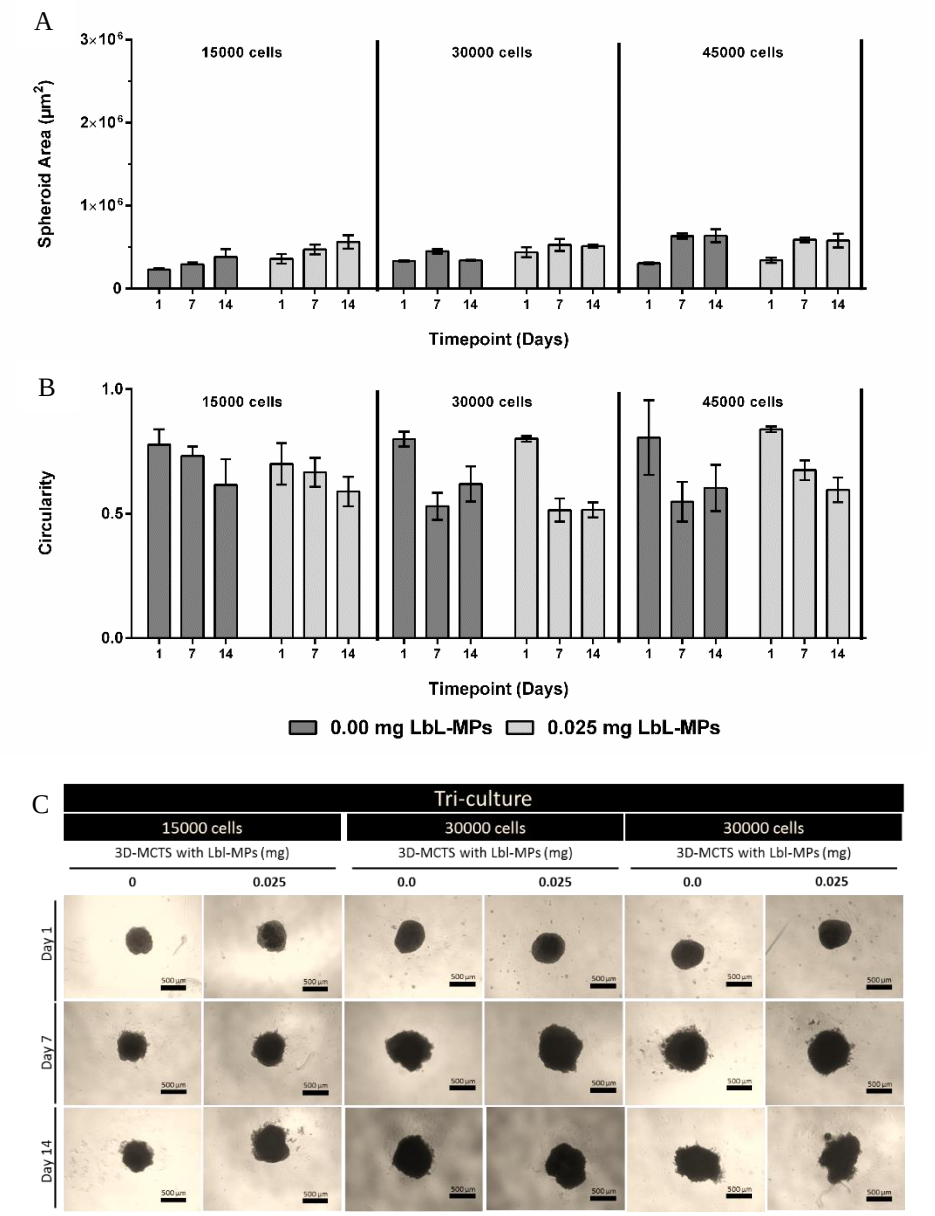

Figure 8. - Size Variation of Triculture spheroids over the course of preliminary assays. Spheroids area (A) and circularity (B) measurements were performed for each condition at 1, 7 and 14 days of culture (C) Optical contrast micrographs processed in ImageJ software. Scale bar represents 500 µm.

In comparison to monocultured models, dual cocultures and triculture 3D-MCTS with LbL-MPs and 3D-MCTS without MPs presented increased contraction (figure 8 and 14). This observation could be related to ECM components secretion mediated by HF and MSCs, since these two cell types are recognized to contribute immensely to ECM deposition in human TME [66].

3.4. 3D-MCTS cellular density and necrotic core formation

Analysis of mono, dual and triculture 3D tumor microtissues, with and without LbL-MPs, demonstrated that sizes bigger than 400 µm were easily obtained under the studied conditions. In this size range, cells are subjected to nutrient/oxygen/pH gradients and generally start to form a characteristic necrotic core similar to that obtained in human solid tumors [67]. To analyze if a dense mass of necrotic cells was formed Live/Dead assays based in fluorescent microscopy imaging of spheroids stained with Calcein-AM (Cal-AM)/PI. This assay is based on a cell-permeant dye which is converted to a green-fluorescent form after intracellular esterase hydrolysis, and propidium iodide (PI) a fluorochrome capable of staining nuclear material in necrotic cells. Live/Dead assays further corroborated previous observations made through optical microscopy analysis regarding size and density of cultured spheroids.

As evidenced by fluorescence microscopy, A549 LbL-MPs 3D-MCTS necrotic core was readily visible after 14 days of culture (figure 9 A). Interestingly, in A549-HF LbL-MPs 3D-MCTS the necrotic core was already visible at 7 days of culture, thus evidencing the that the inclusion of HF stromal cells leads to the formation of a denser/more compact spheroid. This increased core density has a significant influence in the penetration of nutrients/oxygen into deep microtumors regions which in turn promotes the establishment of necrotic regions [68,69].

A

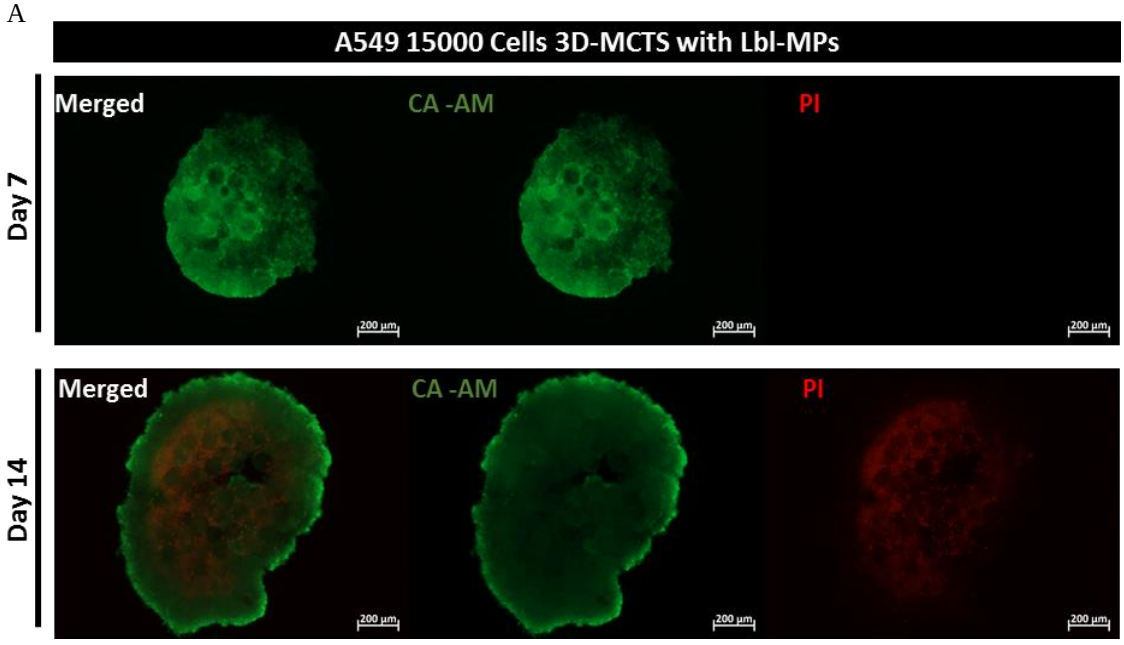

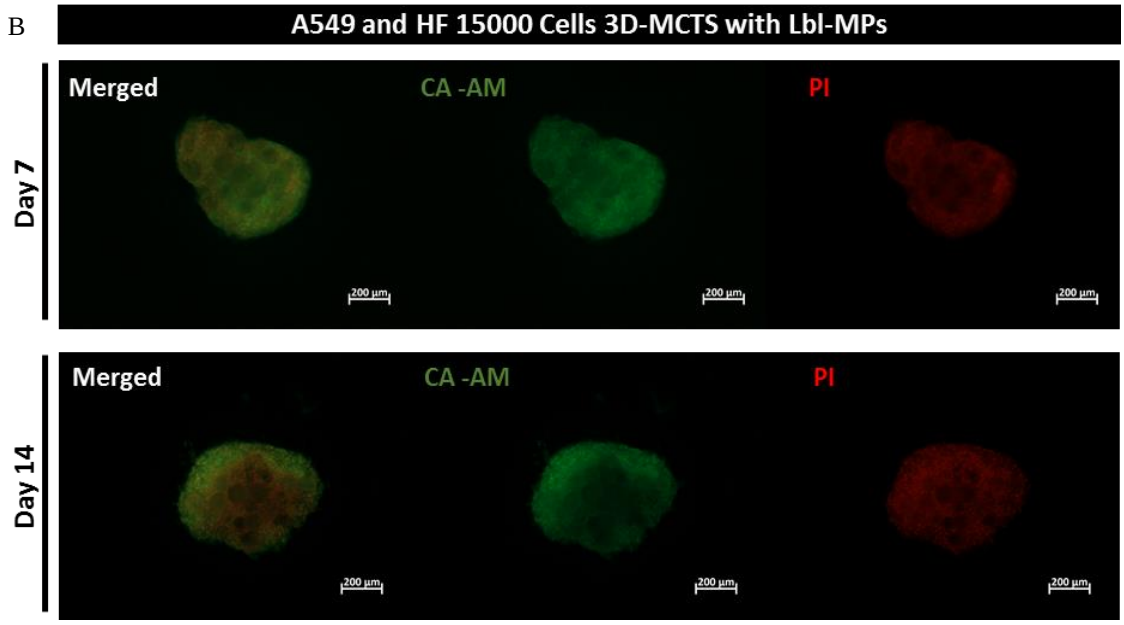

Figure 9. Fluorescence microscopy micrographs of 3D-MCTS Live/Dead staining. A549 3D-MCTS (A) and dual co-culture spheroids (A549-HF) (B) both with LbL-MPs (0.025 mg). Comparison of both conditions revealed that while in monoculture spheroids the necrotic core was only established at 14 days of culture, in the dual coculture conditions (and further conditions tested) it was visible from day 7 onward. Scale bars = 200 µm.

Live/Dead analysis of more complex A549-HF-MSCs triculture 3D-MCTS, with and without LbL-MPs, revealed the establishment of well-defined necrotic regions at 7 days of culture (Figure 10, A), for all cellular conditions (15 000 to 45 000 cells, Figure 10). These spheroids presented necrotic core formation around 7 days, in contrast to A549 3D-MCTS models (15 000 cells, Figure 9). Interestingly, contrary to literature reports regarding breast cancer 3D spheroids disruption and loss of stability upon MSCs addition [70], in the lung cancer 3D models produced with LbL MPs nothing was observed during culture for 14 days. Instead an increase in A549-HF-MSCs 3D spheroids density and compaction was observed (Figures 8 and 10).

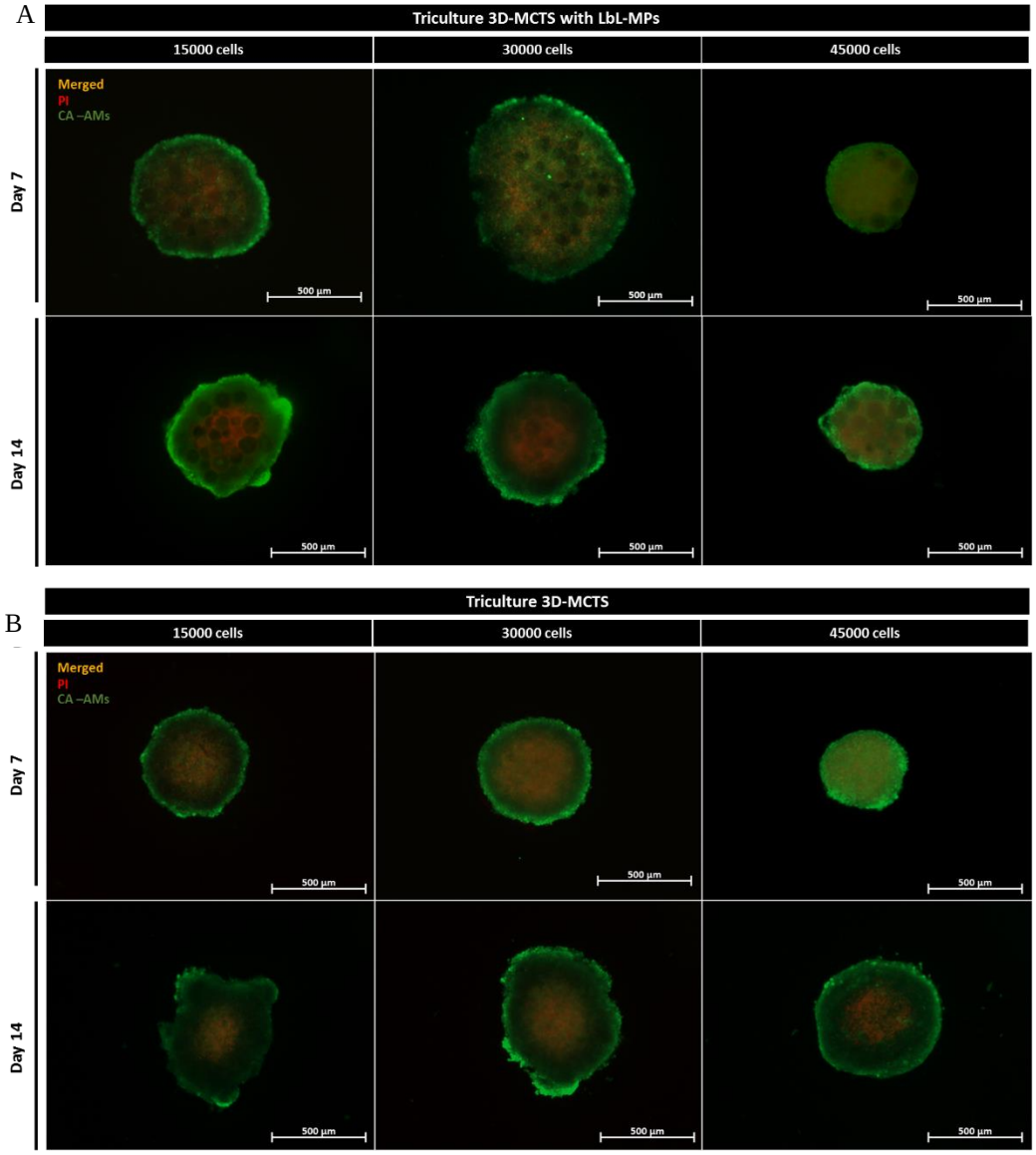

Figure 10. Live/Dead assays were carried out in cultured Spheroids being incubated with CA AM (green) and PI (red) and analyzed in fluorescence microscope, over the course of culture (B). Analysis was performed at 7 and 14 days post seeding. Scale bars =500 µm.

The obtained results regarding the establishment of the necrotic core, as well as the characteristic proliferative rim (Figure 10, Cal-AM green channel) indicated that the produced 3D-MCTS recapitulate two major aspects of *in vivo* solid tumors. Mimicking the growth kinetics with cultured cells in an environment with nutrient and oxygen restrictions, as well as pH gradients results in the establishment of diversified metabolical and phenotypical cell traits as seen in solid human tumors [54,71,72].

Adding to this, the accumulation of catabolites and growth factors such as VEGF or HIF-1α, decurrent from increased hypoxic conditions and associated cellular dead can lead

to phenotypic alteration in cancer cells and associated MSCs [73]. Such could give rise to pro-tumoral interactions between MSCs and cancer cells as shown by Chaturvedi and coworkers, for breast cancer and BM-MSCs co-cultures, in which hypoxia induced interactions promoted metastasis [74]. Interestingly, accumulation of hypoxic and pro-inflammatory factors can also lead to an increased propensity for metastasis and MDR, from a therapeutic perspective these are critical aspects that should be considered [10,54].

3.5. 3D-MCTS cellular viability

To complement Live/Dead assays and to study whether the insertion of MPs into cultures elicited a cytotoxic effect cultured cells viability assays were performed in microtumor models by using Alamar blue (Figures 11, 12, and 13). Viability assays performed in the tested culture conditions showed that inclusion of bioinstructive $(PLL/HyA)_3$ LbL microcarriers for assembly of A549 microtumors and A549-HF 3D-MCTS had no effect in cells metabolic activity. In particular, the obtained results demonstrated that independently of LbL-MPs concentration no statistically significant variation in viability was observable when comparing LbL-MPs spheroids to standard 3D-MCTS, both at 7 and 14 days of culture (Figure 11).

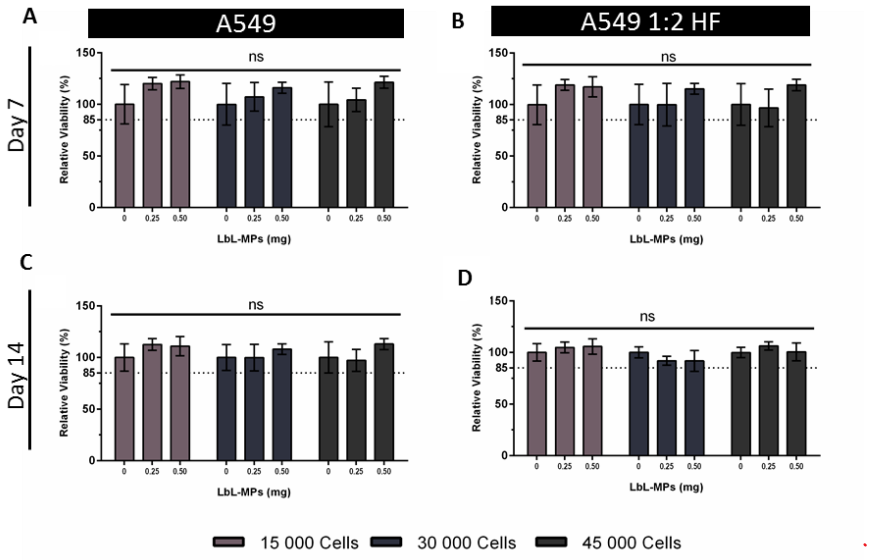

Figure 11. Cell viability assays performed in LbL-MPs 3D microtumors using different concentrations of bioinstructive microparticles. A549 LbL-MPs 3D-MCTS (A,C) and dual coculture A549-HF LbL-MPs 3D-MCTS at a ratio of 1:2 (B,D). Data is presented as mean ± s.d., (n=6). N.s. – represents non-significant differences. **p<0.05, ***p<0.01.

In addition, cell viability analysis of A549-MSCs cocultured microtumors in 0.025 mg LbL-MPS indicated that 15 000 and 30 000 cells have a significant decrease in metabolic activity. Inversely, for 45 000 cells 3D spheroids display a significant increase in cell viability was observed in both cultures using LbL-MPs and pristine PCL microparticles. At 14 days of culture no statistically significant differences where observed in 3D microtumors containing $(PLL/HyA)_3$ LbL bioinstructive (LbL-MPs) or pristine PCL MPs (non-treated MP represented as NT-MPS).

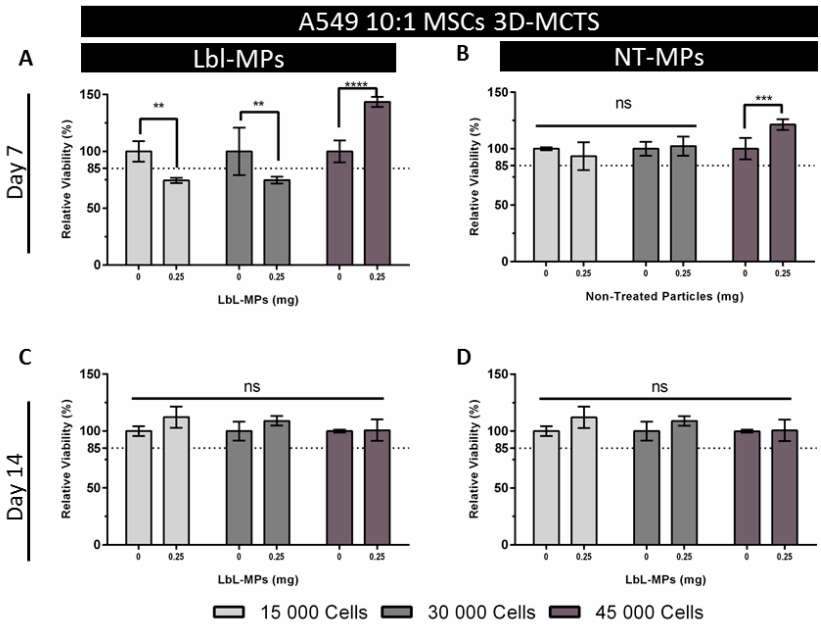

Figure 12. Cell viability assays performed in coculture spheroids of A549-MSCs in a 10:1 ratio, using spheroids with LbL-MPs (A,C), and pristine PCL particles (NT-MPs) (B,D). Data is presented as mean ± s.d., (*n*=6). N.s. – represents non-significant differences. **p<0.05, ***p<0.01.

For A549-HF-MCS 3D spheroids with LbL-MPs a significant increase of almost two-fold was observed (figure 13, A), indicating that this combination could possibly increase the metabolic profiles of cells 7 days of culture. The remaining culture conditions and time points exhibited neither increase nor decrease in metabolical activity due to the inclusion of microparticles (either LbL functionalized or pristine PCL MPs).

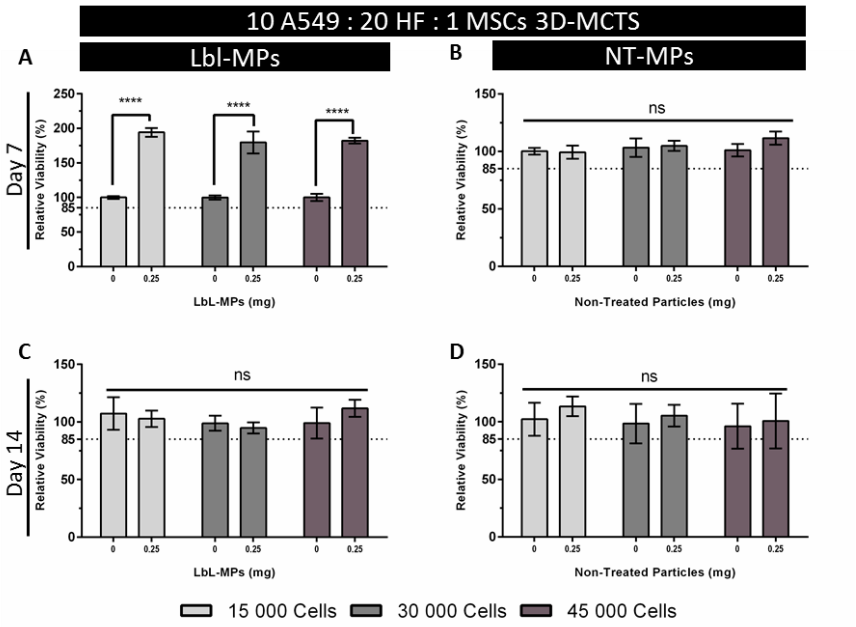

Figure 13. Viability Assays performed in Triculture spheroids of A549, HF and MSCs in a 10:20:1 ratio, respectively using spheroids with treated (A,C), and non-treated particles (B,D). Triculture spheroids of 7 days containing treat MPs showed a two-fold in metabolic activity when compared to non-containing MP controls.

As for LbL-MPs concentration 0.025 mg of MPs per spheroid demonstrated the best results regarding spherical shape and monodispersity\similarity of spheroids cultured with LbL-MPs.

Taking into consideration the former results regarding area, circularity, compactness, necrotic core formation and metabolic activity over time, spheroids with 30 000 cells, with or without LbL-MPs, in a concentration of 0.025 mg per spheroid, were used from herein onwards. Such selection was performed because this condition was highly reproducible in for all the tested cell combinations (A549, A549-HF and A549-HF-MSCs). The area and morphology of spheroids with 30 000 cells spheroids was extensively characterized for all culture conditions, as portrayed below, through the analysis of n=30 spheroids for each condition so as to assure a confidence level for further drug screening studies.

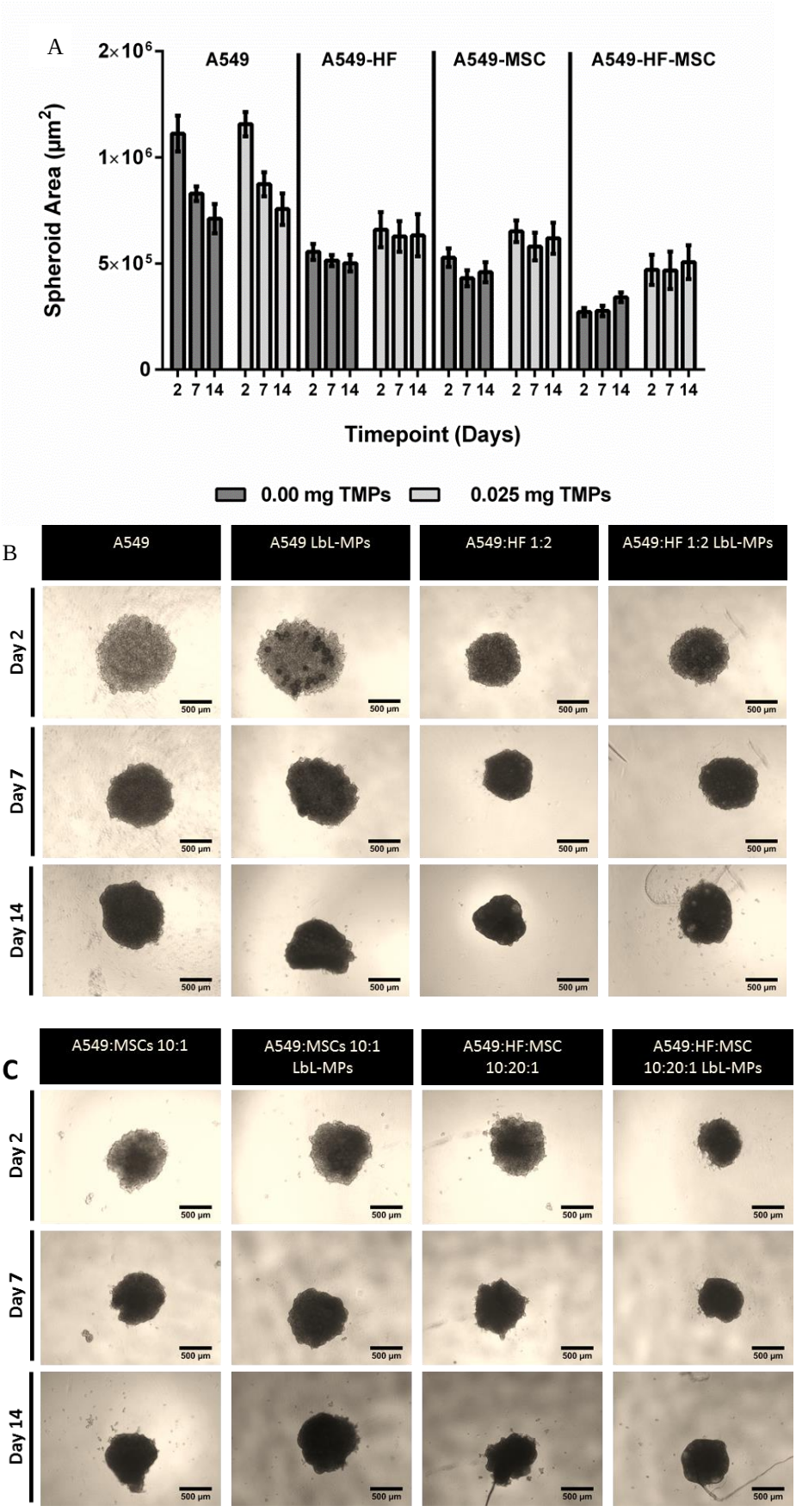
A
A549
A549-HF
A549-MSC
A549-HF-MSC
Spheroid Area (µm²)
2×10⁶
1×10⁶
5×10⁵
0
2 7 14
Timepoint (Days)
0.00 mg TMPs
0.025 mg TMPs
B
A549
A549 LbL-MPs
A549:HF 1:2
A549:HF 1:2 LbL-MPs
Day 2
Day 7
Day 14
500 µm
C
A549:MSCs 10:1
A549:MSCs 10:1 LbL-MPs
A549:HF:MSC 10:20:1
A549:HF:MSC 10:20:1 LbL-MPs

Figure 14. Size variation of spheroids of diverse co-culture conditions assemble with a initial cell density of 30,000 and with or without 0,025 mg of LbL treated MPs per spheroid (A). 3D-MCTS were analyzed through inverted microscopy over the course of culture, with pictures having been taken at days 2,7 and 14 post seeding (A).

3.6. 3D-MCTS histological analysis

H&E and Masson's Trichrome (MT) staining were performed on A549-HF cocultures and A549-HF-MSCs 3D spheroids with and without LbL-MPs so as to access internal cellular organization and if ECM components deposition was occurring. Analysis of obtained histological cuts revealed a compact internal cellular organization (figure X). Compared to other reports with A549 spheroids this result seems to be expected for the established culture times [75]. A closer analysis of spheroids with LbL-MPs revealed that cells adhering to MPs were spread and extended over their surface, thus establishing contact on one side with the included HyA matrix and on the other with involving cells while retaining a three-dimensional non-flat structure (figure 15 – A, B). Furthermore, regions with high amount of LbL-MPs seem to had no nuclear staining using H&E stains, concordant with microparticles presence.

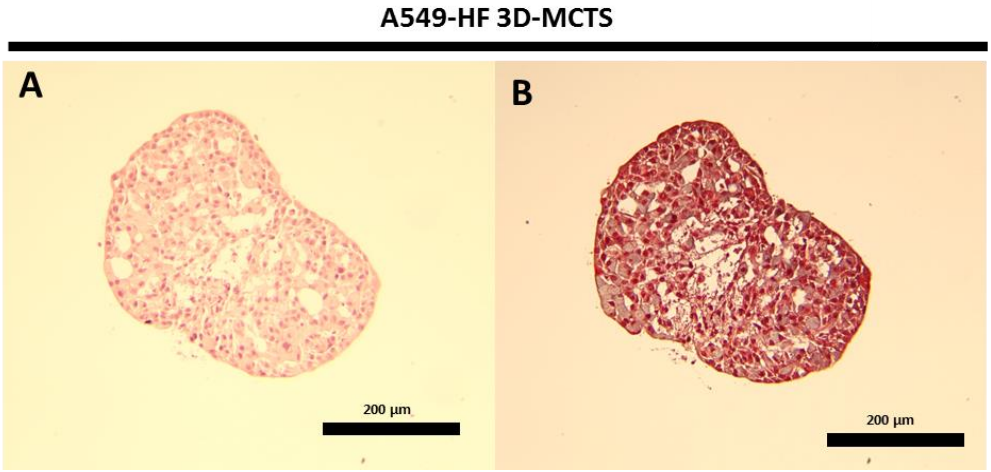

Figure 15. Optical constrast micrographs of histological staining of A549-HF spheroids at 7 days of culture. Samples were stained with H&E (A) and MT (B).

Regarding triculture spheroids Masson's Trichrome (MT) staining demonstrated that at day 7, collagen deposition occurred in both microtumors containing LbL-MPs or only cells (Figure 16. blue circles). evidencing more visibly blue stained regions (figure 16 C and D). This result is accordance with the observation of increased contraction rates observed in both triculture and dual coculture spheroids. Demonstrating the ability of the spheroids to build their own ECM.

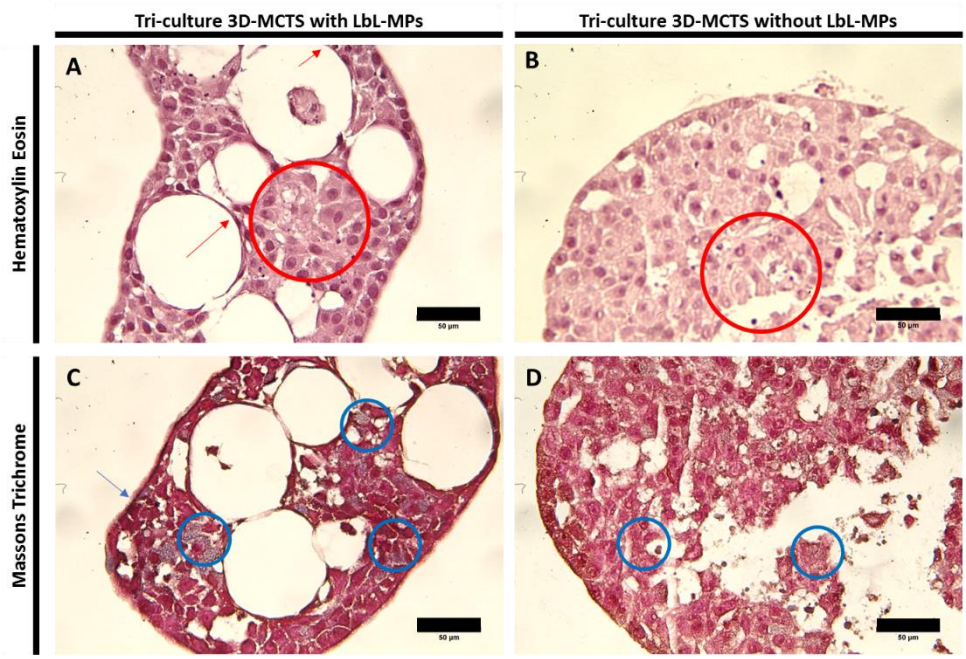

Figure 16. Histological analysis of A549-HF-MSCs triculture spheroids. Spheroids with (A,B,) and without LbL-MPs (C,D),. Internal organization of cells around MPs in image A, with cells clearly adhering to the surface of the LbL-MPs and acquiring an elongated shape (A – red arrows), furthermore a possible necrotic region is observed (red cicle) (A,B – red circle) in a spheroid section surrounded by MPs (A) and in the inner most section of the spheroids without LbL-MPs (B). At day 7 ECM deposition is already visible in both spheroids occurring however predominantly in triculture spheroids with MPs (C and D-blue arrows and circles). Scale bar = 50 µm.

3.5. Cell Tracking and migration over time

Previous reports demonstrated MSCs ability to migrate and penetrate deep into tumor masses [76,77]. As such cell tracking assays were performed with the aim of better understanding the internal organization of triculture spheroids and to observe if MCS populations either remained static over the course of culture or migrated. To do so, cells were stained with cell tracking lipophilic dyes [78], DiO (green) for A549, DiL (Yellow) for HF and DiD (red) for MSCs (Figures 17 and 18). These staining agents were passed down through cellular generations, being present in the spheroids with no considerable loss up to and beyond 14 days of culture, after which the intensity of the staining started to fade. Such approach allowed a qualitative assessment of the localization and migration of different cell populations in the spheroid structure over time. Results indicated that over the course of 7 days cultured MSCs are not entirely confined to the necrotic core region of the spheroid, and also demonstrated a tendency to migrate to and colocalize in deep internal regions of triculture spheroids. Furthermore, fluorescence microscopy data also confirmed that cultured

cells seem to adapt to the morphology of the microparticles extending themselves over the exposed surfaces as observed in histological analysis.

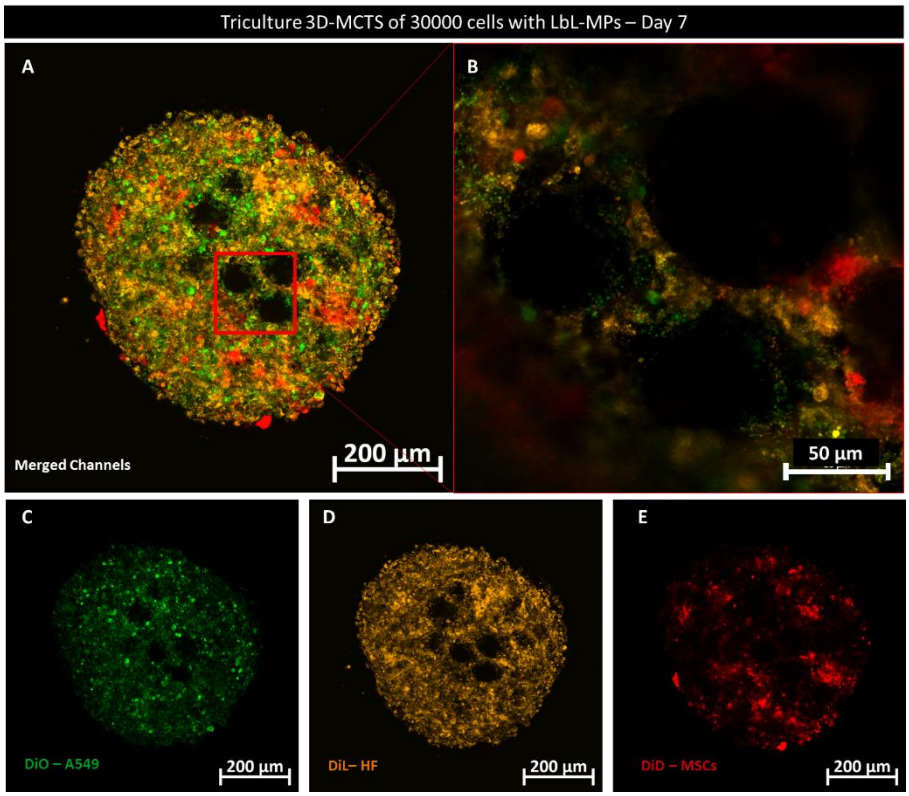

Figure 17. CLSM confocal imaging of cellular organization in triculture LbL-MPs spheroids at day 7. Composite micrograph with merged channels (A). Zoomed section containing cells attached to LbL-MPs (B). Stained A549 cells cancer cells (C) and fibroblasts (D) are arranged over the spheroid volume with no particular pattern contrasting with the cluster-like arrangement of BM-MSCs (E). Scale bar = 50 µm (B).

Furthermore, over the course of 14 days, the fluorescence signal emitted by DiD (the cell marker associated MSCs), remained inside cultured spheroids, denoting the presence of MSCs. Obtained images demonstrate an internal organization of pockets of mesenchymal stem cells inside triculture spheroids, surrounded by numerous A549 cancer cells and dermal fibroblasts with no apparent organization (Figure 18, 14 days). Interestingly, a tendency was seen for the loss of DiL signal, with an apparent superposition of the DiO signal, perhaps associated with a change in the populations ratios.

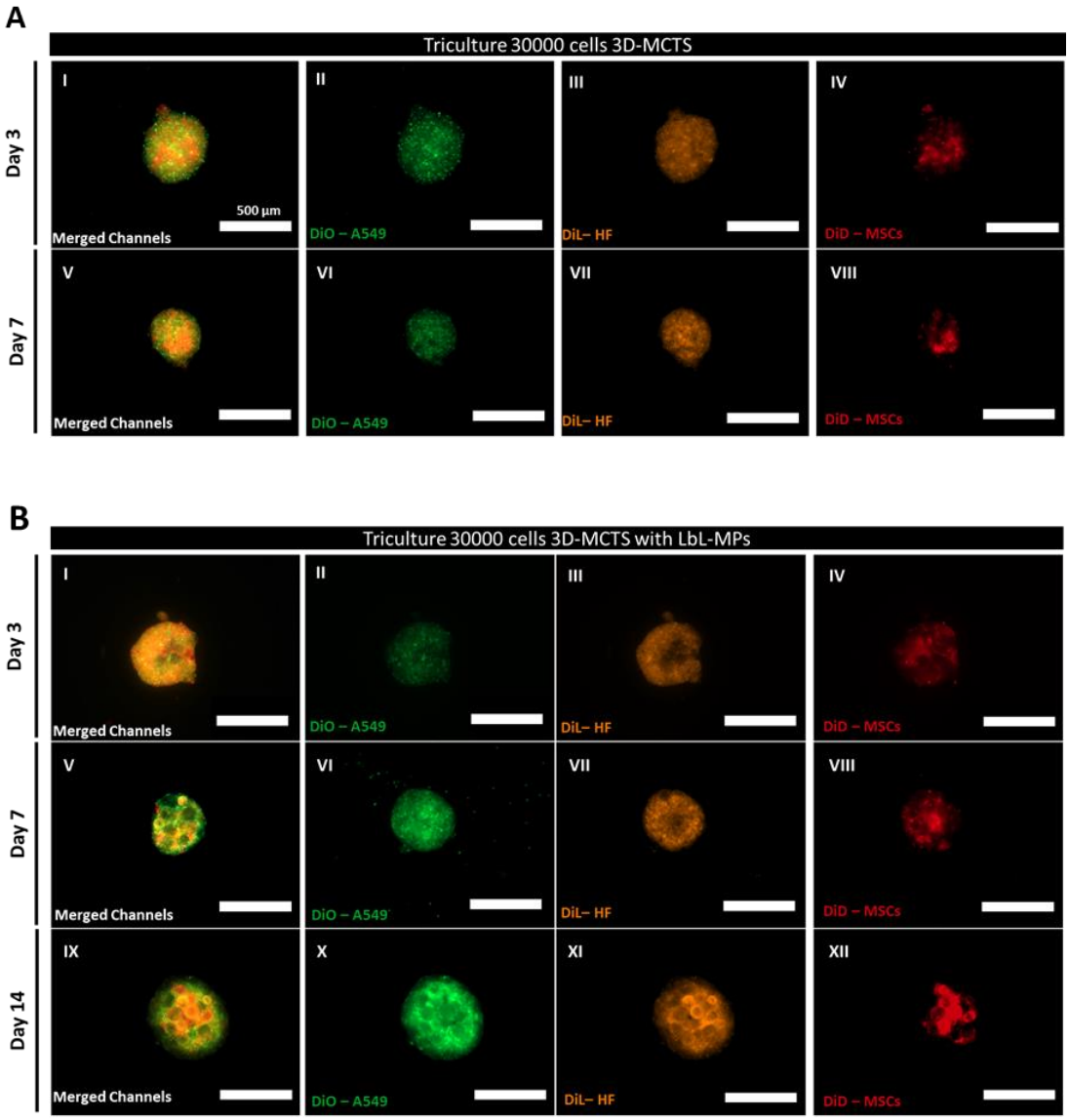

Figure 18. Widefield fluorescence micrographs of triculture 3D spheroids of 30 000 cells stained with cell tracking dyes demonstrated a tendency in spheroids without MPs (A), and with LbL-MPs (B) for MSCs to colocalize in the interior of the spheroid. MSCs formed visible cell clusters over time 7 and 14 days in both conditions. Scale bar = 500 µm.

3.6. Immunocytochemistry analysis of 3D-MCTS ECM and cell-cell Adhesion

Immunocytochemistry analysis was performed in A549-HF-MCSs 3D-MCTS spheroid models containing or not LbL-MPs to analyze if the increased cohesion observed over the extent of culture time in triple coculture spheroids could be derived from matrix deposition, and if the cell-cell adhesion molecule E-cadherin expression was in some way altered by the inclusion of MSCs. Collagen an abundant structural component of human

ECM, is constituted by several diverse types of which collage type I is the predominant form in most tissues [79]. During tumor progression established interactions between CAFs and cancer cells can lead for example to increased matrix deposition and collagen cross-linking, resulting in ECM architectural changes [79] characterized in part by increase collagen degradation, re-deposition and crosslinking, thus resulting in stiffening and contributing for the establishment of yet another barrier to therapeutic compounds penetration [80]. While collagen role in the TME has not yet been fully elucidated [79], increase collagen and ECM deposition in spheroids has been linked with increased interstitial pressure. More so, increased collagen deposition has also been connected in a paradoxical fashion to both increased metastasis in breast cancer due to referred matrix stiffening [81], and in fibroblast/A549 cell spheroids to increase integrin α11β1 expression due to collagen type I receptor stimulation, contributing to increase spheroid cohesion and decrease invasio [82]. The results obtained by immunocytochemistry analysis revealed that as soon as the 7th day of culture, as previously evidenced in histological data collagen deposition took place in triculture spheroids both containing or not LbL-MPs (figure 19). Revealing the ability of the produced spheroids to produce a collagenous matrix, similar to what is observed in *in vivo* tumors. Such leads to the formation of a network of collagen fibrils over the hole spheroid that can overtime contribute not only to cell adhesion and spheroid cohesion but also to necrotic core establishment.

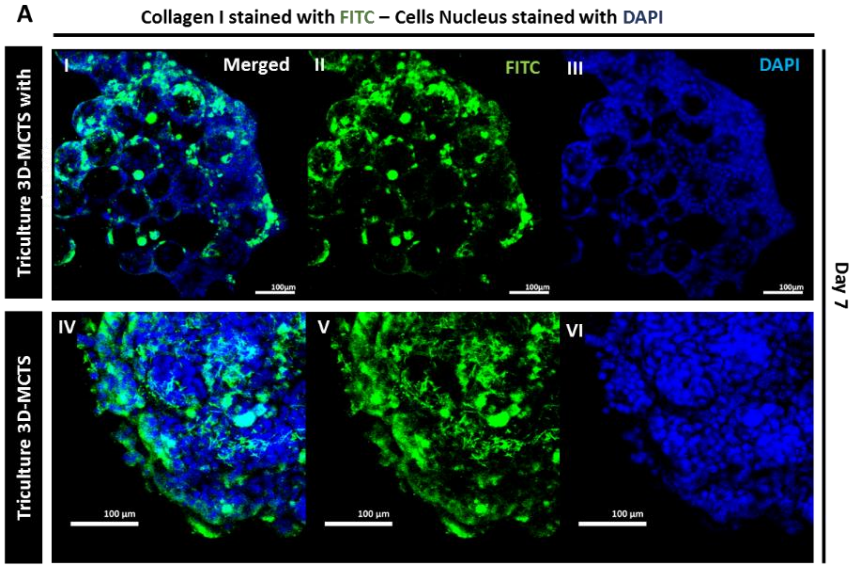

Figure 19. CLSM micrographs of triculture spheroids of 30 000 cells with (A – I,II,III) and without particles (A-IV,V,VI) at the 7th day of culture, stained with anti-collagen type I antibody conjugated with secondary fluorochrome FITC (green

channel), and with DAPI (blue channel). A green mesh of collagen can be seen deposited around and inside the 3D-MCTS, conferring it a higher degree of solidity and rigidity. This *de novo* produced collagenous matrix can act both as a structural component and as a store house of cellular signaling factors (e.g., growth factors)[83]. Scale bars represent 100 µm.

Regarding the expression of cell-cell adhesion domains it is important to understand a unique event that commonly occurs in tumors, the Epithelial to Mesenchymal Transition (EMT). Cancer cells EMT is one of the key hallmarks of cancer progression, being responsible for the majority of cancer related mortality. As previously discussed in the introductory section, EMT occurs through the modification and loss of specific cell-cell adhesion domains in the surface of cancer cells combined with changes in cell morphology and ability to translocate through the ECM until reaching vascular walls which they then transverse in a manner believed to be similar to that of diapedesis performed by immune cell [32,84]. Cadherins, transmembrane proteins that are responsible for cell-cell adhesion by homophilic interactions are abundantly expressed in epithelial tissues. In spheroids E-cadherins are also known to generate strong cell-cell cohesive forces during 3D spheroids formation process. Such has been observed for monoculture 3D spheroids of different cancer types such as breast, prostate and renal carcinoma [84,85]. Several reports have demonstrated MSCs ability to down-regulate E-cadherin expression in diverse cancers, in a manner dependent of their origin and even concentration [70,85,86]. In 3D spheroids both increased matrix deposition and consequent integrin [87] and cadherin [88] expression can lead to the formation of tightly compacted microtumors *in vitro* [89–91]. One of the key markers of EMT is the loss of E-cadherin expression, a type-1 transmembrane glycoprotein also known as epithelial cadherin, responsible the formation of cell-cell adhesion [70]. This protein has been found to be down regulated in several studies combining the cultures of cancer cells with either HF and MSCs in a population dependent manner [57,70,86]. As such immunocytochemistry was performed in triculture spheroids so as to analyze if any loss of E-cadherin was occurring over the culture period of 7 to 14 days. The obtained results presented in Figure 20 demonstrated no visible loss of E-cadherin in either dual coculture or triculture suggesting that EMT promotion was not occurring in cocultured populations. In contrary to previous observations by Dittmer and coworkers, 2009 for breast cancer, in the herein produced lung cancer 3D-MCTS models inclusion of BM-MSCs does not result in loss of E-cadherin expression.

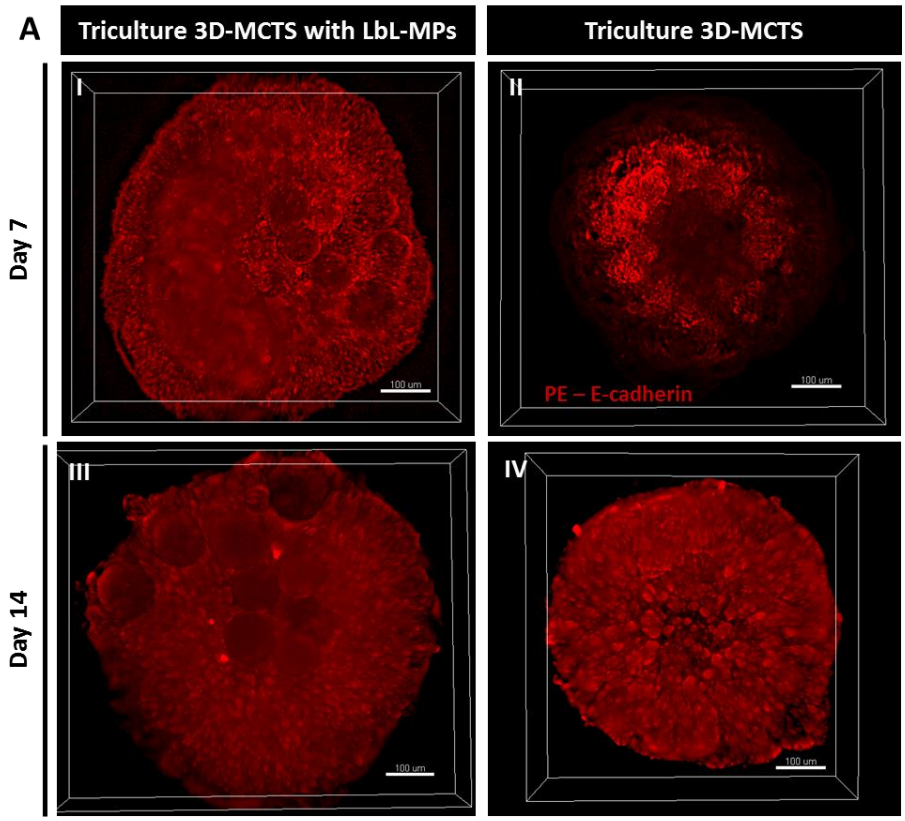

Figure 20. Widefield micrographs of E-cadherin stained A549-HF-MPs triculture spheroids of 30000 cells with LbL MPs (A,C) and without (B,D) at the 7th (A,B) and 14th (C,D) day of culture. Scale bars represent 100 µm.

Overall these findings first demonstrate 3D spheroids ability to closely mimic key aspects of an *in vivo* tumor through *de novo* collagenous matrix deposition. And also provide important insights into the effect of MCS addition in cell-cell contacts.

3.7. Flow cytometry analysis of CD44 expression

Previous studies demonstrated that the association of either CAFs, or MSCs with lung cancer cells *in vitro* resulted in higher expression of cell marker such as CD133, CD90 or CD44 by cancer cells [77,92], denoting a pro-tumoral influence of both populations in the tested conditions. Moreover, several studies also reported that in contact with hyaluronic acid-rich substrates, cancer cells increase their expression of CD44[93,94]. Increased CD44 expression has been connected with multi-drug resistance (MDR) and the development of cancer stem cell like phenotypes (ALDH/CD133+ cells) [95,96]. As such, the effect bioinstructive HyA functionalized LbL-MPs on cultured populations was investigated by

flow cytometry analysis of CD44 surface marker in different 3D-MCTS with 7 days of culture (figure 21).

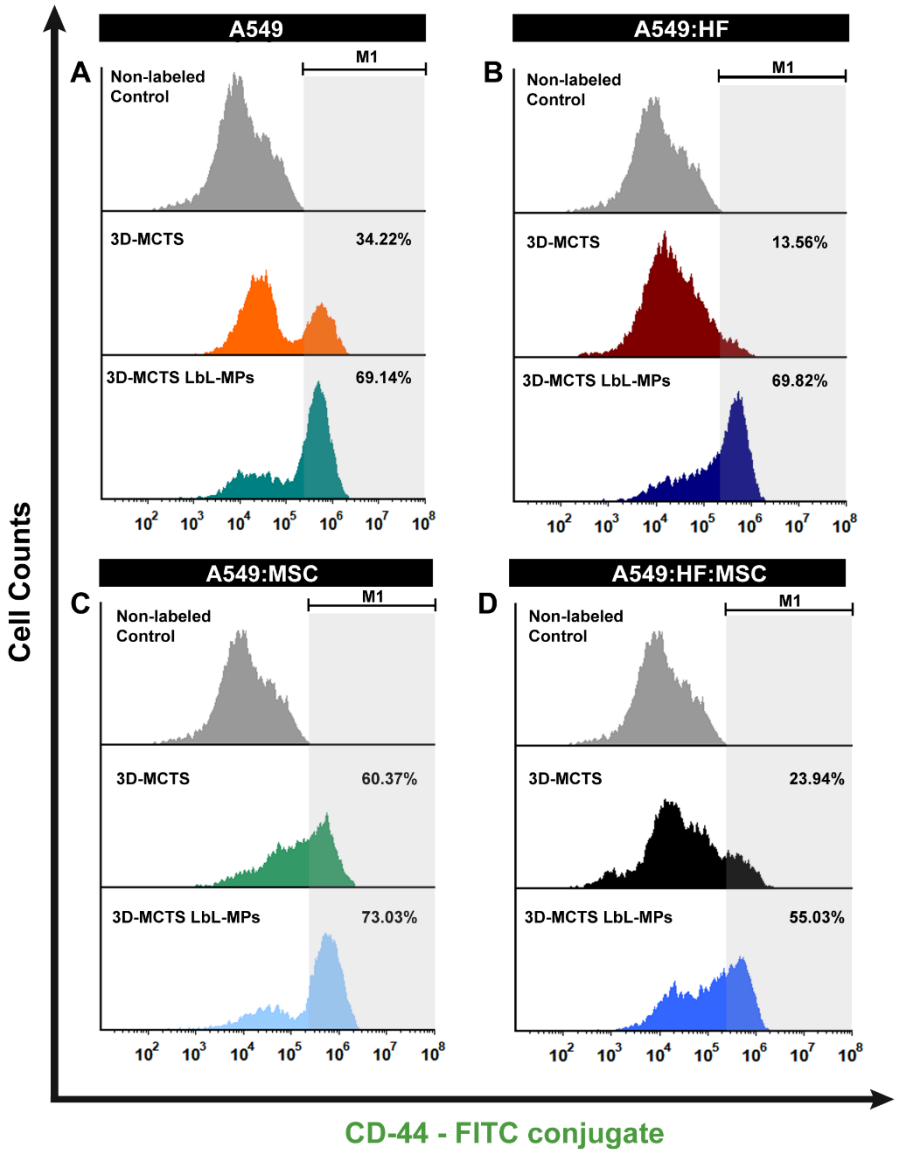

Figure 21. Flow cytometry analysis of CD44 surface marker analysis at the 7th day of culture in various 3D-MCTS with and without LbL-MPs. Data revealed that HyA LbL-MPs inclusion significantly increased the levels of CD44 in all culture settings.

The obtained results demonstrate a clear increase in CD44 expression seen in all coculture and monoculture conditions upon the inclusion of LbL-MPs. With diverse populations exhibiting CD44 expression, both monoculture, dual coculture using HF and triculture exhibited a ~2 fold increase in the percentage of CD44 positive cells when cultured with LbL-MPs. While dual cocultures of A549-MSCs displayed only a slight increase in the percentage of cells expressing CD44. 3D-MCTS of this culture condition express by

themselves high levels of $CD44^+$ cells. Having on account the ratio of 1 MSC per every 10 A549 cells, this high expression of CD44 cannot be simply justified by the inclusion of CD44 expressing BM-MSCs [31], and can thus also be attributed to the interactions established between cultured populations as seen in previous work [94,97,98]. A similar increase can also be seen by the inclusion of MSCs in dual coculture model of A549-HF compared to the triculture model, were a similar ratio of MSCs to cancer cells is used. Overall increased CD44+ in cancer cells has been connected with the development of cancer stem cell profiles in several diverse types of cancers namely NSCLC [96]. At the same time, other studies have found that CD44 expression by itself is of inconclusive value for the analysis of cancer stem cell populations. However, clear connections have been established between CD44 expression by cancer cells and increased MDR mechanisms correlated with P-Glycoprotein efflux pump expression [99]. As such the increased expression evidenced by the diverse coculture models when containing LbL-MPs can be indicative of the establishment of possible resistance mechanism also found in the clinical setting [17]. Such important results also corroborate the bioinstructive role of LbL-MPs in 3D-MCTS.

3.8. Chemotherapeutics drug screening assays in bioinstructed 3D-MCTS

Interactions between diverse populations present in the TME are known to be of paramount importance for the performance of chemotherapeutics. In fact the close interactions established between stromal and cancer cells through direct contact or indirect biomolecular cues such as cytokines, chemokines and growth factors that allow bidirectional communication ultimately lead to altered metabolic profiles, signaling pathways, and invasive behavio [100]. Moreover, this communication incites drug resistance through several cancer cells defense mechanisms that include: (i) decreased uptake of water soluble chemotherapeutic compounds such as Cisplatin, (ii) the modification of cancer cells metabolic regulation either through ‘self-genetic’ mutation or interaction with cellular components of the TME (e.g., fibroblasts, immune system cells and MSCs). Such unique crosstalk between cancer cells and their TME originates (iii) a decreased cell cycle arrest, increased repair of DNA damage, reduced apoptosis and alteration of the metabolism of drugs; (iv) lastly an increased in energy-dependent efflux of hydrophobic chemotherapeutics such as Doxorubicin is also often obtained [101,102]. The latter can occur through the

acquisition of MDR mechanisms such as the widely studied overexpression of ATP-binding cassettes (ABC) transporter proteins, to which multidrug resistance-associated protein 1 (MRP1), breast cancer resistance protein (BCRP), and P-glycoprotein efflux pumps are internally associated. Collectively all of these are responsible for higher excretion of internalized chemotherapeutic compounds [103,104]. Not only is coculture of cancer cells with HF and MSCs associated with increase expression of MDR mechanism, but also the presentation of cells in a three-dimensional environment by itself provides another barrier lacking in 2D cultures [50]. Existence of a necrotic core signalizes the lack of proper nutrient and medium penetration into the spheroid, leading to the accumulation of metabolites and byproducts of cells activity, such as reactive oxygen species (ROS) known to promote the upregulation of ABC-B1[105]. The end result is an area were therapeutic agents will have a greater difficulty penetrating both due to physical and biological barriers. From a bioengineering point of view modeling all of these hallmarks of *in vivo* tumors with 3D *in vitro* tumor models is highly desirable

Conventional *in vitro* preclinical validation models are mainly based in monocultures, lacking TME stromal cells representation [39,50]. Key populations such as HF and BM-MSCs are well known to affect, either positively or negatively, several cancers [66] leading to acquisition of resistance to therapeutic agents by metabolical alteration of cancer cell [106], apoptosis reductio [107], MDR associated protein overexpressio [108] or mitochondrial exchang [109]. By establishing a 3D coculture model capable of representing *in vitro* A549 cancer cells *in vivo* like interactions with HF and BM-MSCs, we aimed to represent the reality of tumor cellular heterogeneity [58,62,76,110]. Furthermore, the inclusion of hyaluronic acid aimed not only to increase cellular adhesion to the microparticles, but also to possibly increase the overall resistance of cancer cells towards doxorubicin through stimulation of CD44 and RAHMM receptors as it occurs *in vivo*. Being a huge component of lung cancer TME, HyA is associated with poor tumor cell differentiation and higher recurrence rate when present in elevated quantities [17]. More so, interactions of HyA stromal cells such as HF or MSCs, have also been connected as possible roots towards establishment a higher resistant profile by all cells of the TME [20].

To access if this theorized increase in resistance was present, resultant either from the inclusion of microparticles coated with PLL-HyA bilayers or coculture with key representative populations of lung cancer TME, drug screening assays were performed in

previously optimized mono, dual and triculture spheroids containing or not LbL-MPs. Doxorubicin (Dox) a commonly used chemotherapeutical agent in the clinics for cancer treatment was selected for these studies.

The lack of data directly comparing 2D and 3D culture conditions is a common pitfall in the development of novel 3D models [11]. Preliminary drug screening assays of mono and dual co-cultures were performed in 2D, using the same population ratios of those used for 3D spheroids assembly. Cell viability was accessed through MTS assay after a period of 72 h of Dox incubation. 2D monolayer cultures of A549 cells alone exhibited sensitivity profiles similar to those observed in previous studies [111,112]. 2D cultures of HF demonstrated a slightly similar sensitivity to Dox as that observed by A549 cultures, in acordance to other reports [113]. However, cocultures of A549 and HF in a 1:2 ratio demonstrated increased sensitivity for the cytotoxic compound, an unexpected finding when compared with previous literature reports regarding the interactions of A549 and lung fibroblasts [58,63,114]. Such could be explained from the dermal origin of the fibroblasts used herein.

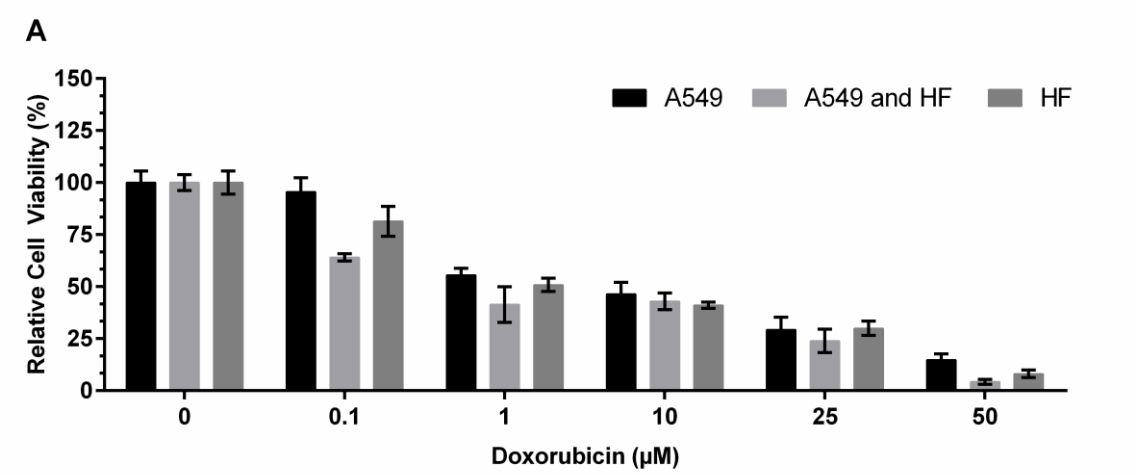

Figure 22. Doxorybicin cytotoxicity screening in performed in 2D monolayer cultures of A549, HF and cocultured A549-HF cells. Data is presented as mean ± s.d., (*n*=5).

Drug screening assays were performed in 3D spheroids cultivated over a period of 7 days to allow the establishment of cell-matrix and cell-cell contacts. The Inclusion of LbL-MPs into 3D-MCTS lead to the observation of significant differences regarding resistance profiles when compared to control 3D-MCTS. These were observable in all coculture conditions except triculture 3D-MCTS (figure 22). The lack of a significant increase in resistance due to the inclusion of LbL-MPs in triculture 3D-MCTS could result from the

complex set of interactions taking place due to the inclusion of so many diverse cellular populations. When compared to triculture 3D-MCTS with pristine PCL-MPs the latter evidenced a higher susceptibility to Dox, indicating that the LbL treatment to which MPs were subjected does in fact increase or at least equalize the spheroids ability to resist Dox cytotoxic effects (Figure 23).

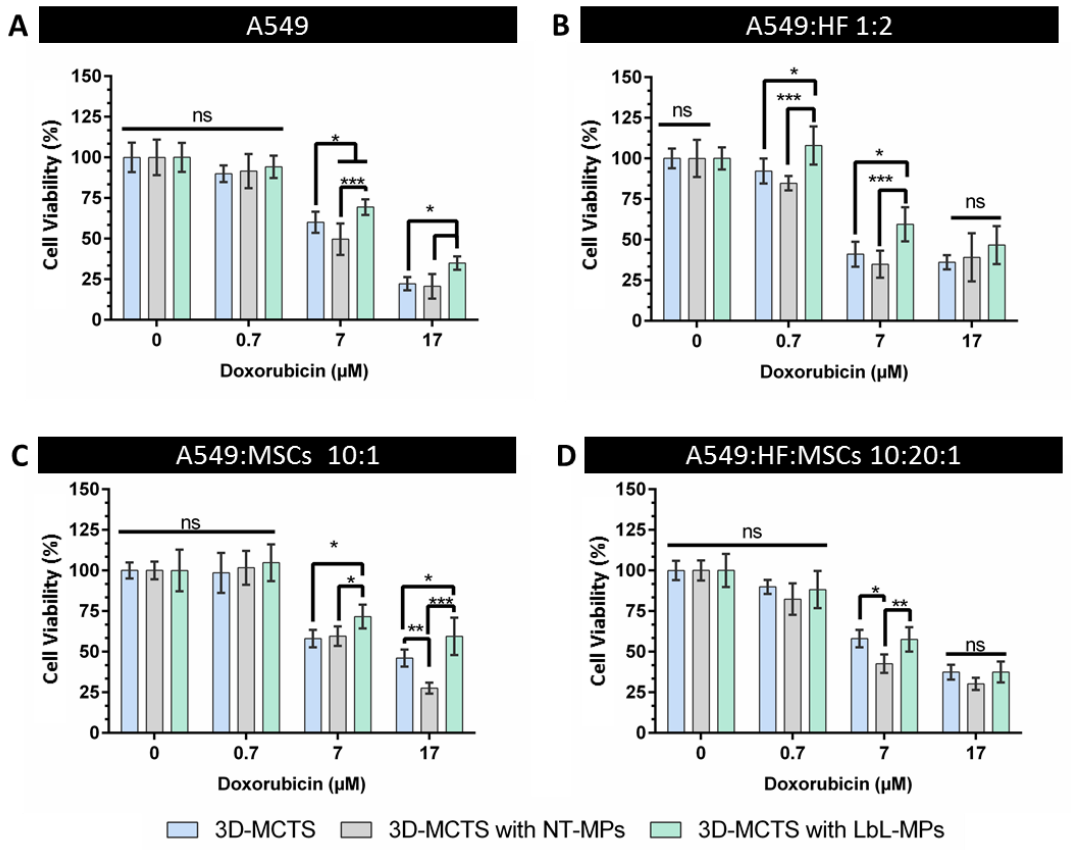

Figure 23. Drug cytotoxicity screening assay performed in spheroids with 7 days of culture with different culture conditions that included 3D-MCTS (control. blue bars), 3D-MCTS with pristine PCL-MPs (grey bars) and 3D-MCTS with LbL-MPS (green bars). A549 monoculture spheroids (A), dual coculture spheroids A549-HF (B), Biculture spheroids of A549-MSCs (C) and triculture spheroids of A549-HF-MSCs (D). Data is presented as mean ± s.d. (*n*= 5). * p<0.05, **p<0.01 and ***p<0.001. ns – represents non-significant differences.

The differences observed in cytotoxicity assays of control spheroids without MPs and in spheroids with LbL-MPs were clear in dual co-culture 3D-MCTS formed by HF-A549 and in monoculture A549 spheroids. In both conditions 3D-MCTS with LbL-MPs exhibited statistically significant (CI=95%, *p<0.05) increases in relative cellular viability, presenting ~0.20 to ~0.60-fold increase in cellular viability at the highest Dox concentrations (17 μM), when compared to controls of the same conditions (figure 23). The obtained results clearly

indicate that the inclusion of LbL-MPs containing HyA increased cultured cells ability to resist to high Dox chemotherapeutic concentrations.

The acquisition of higher resistance to Dox could be related to several factors, including the formation of more compact spheroids possibly through means of increased matrix deposition or via increased expression of CD44 markers as demonstrated by FCM analysis. Previous works by Han and coworkers, 2016, demonstrated that A549 spheroids cells assembly was mediated through a CD44-dependent mechanism [77]. With culture of A549 cells in HyA-rich substrates leading to an increased resistance of lung cells [115]. Consequently an increase in cell-cell interactions between HF and A549 cells could be directly correlated with the acquisition of resistance, thus increasing the ability of A549 to resist Dox, closely mimicking events in *in vivo* tumors [92].

Moreover, inclusion of pristine PCL-MPs resulted in a decrease of cell viability upon Dox administration, which could be associated to a lack of tighter cellular adhesion to NT-MPs since these only present a plasma treated PCL surface. These findings emphasize the positive role being played by the inclusion of the PLL-HyA bilayers. In fact, statistically significant decreases in cell viability were obtained in both triculture, and dual coculture spheroids of A549-MSCs and A549-HF, when compared to LbL-MPs and control 3D-MCTS. The difference between NT-MPS and LbL-MPs 3D-MCTS, indicates that the inclusion of $(PLL\text{-}HyA)_3$ bilayers improves 3D models resistance to Dox-mediated cytotoxicity, thus approaching these testing platforms to the reality of *in vivo* tumors containing HyA. In an overall analysis 3D-MCTS and LbL-MPs 3D-MCTS cultured in dual an triculture presented higher resistance (17 μM Dox), than their monoculture counterparts.

Interestingly, MSCs dual coculture LbL 3D-MCTS and control 3D-MCTS exhibited higher resistance when compared to all other conditions tested. This increased resistance could be correlated with the formation of tighter spheroids with MSCs having been observed to increase spheroids cohesion (figure 14), possibly through means of increased matrix deposition [86,108]. It is important to emphasize that these results are obtained with bone marrow derived MSCs and that MSCs of different origins may respond differently to therapy. Furthermore, such findings could also be correlated with the establishment of pro-tumoral interactions with cancer cells, or from the natural resistance exhibited by MSCs to Dox.

To test this hypothesis an unrealistic ratio of 1:1 MSCs A549 cells was subjected to the same culture conditions and Dox concentrations. The obtained results evidence a positive role of MSCs in A549 lung cancer cells resistance when cultured in low ratios, favoring A549 cells and a possible anti-tumoral effect when cultured in 1:1 ratio (Figure 24). Such findings demonstrate, the highly remarkable dual role of MSC [30,56] of which the study and correct representation is of paramount importance for the development of more robust and *in vivo*-like preclinical validation models.

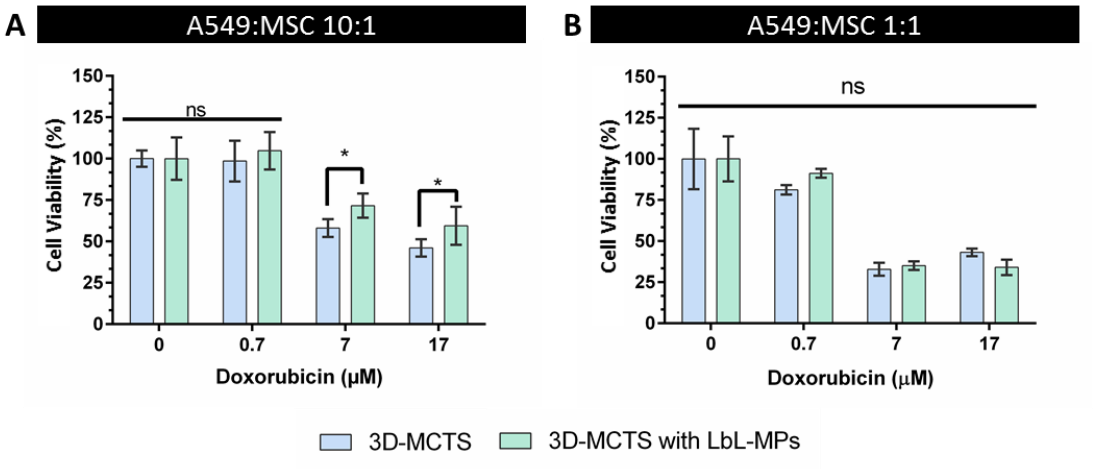

Figure 24. Drug cytotoxicity assays of dual cocultured A549-MSCs 3D-MCTS in a 1:10 (A) and 1:1 ratio (B), respectively. Data is presented as mean ± s.d. (*n*= 5).

Interestingly, the behavior of diverse populations was not constant with the increase of test concentrations for all conditions. While at intermediate concentrations of doxorubicin (7 µM) dual coculture spheroids of HF without LbL-MPs, present decreased resistance compared to other conditions, at the highest concentration (17 µM) both HF-A549 3D-MCTS and Triculture spheroids exhibited increased resistance when compared to A549 monoculture spheroids. Has previously mentioned addition of HyA LbL-MPs resulted in increased 3D-MCTS resistance.

Finally, triculture models exhibited an unexpected pattern of resistance, showing a similar behavior as dual coculture spheroids of A549 and HF and a trend of increased resistance (statistically significant) when compared to monoculture spheroids of A549 at the highest concentration (17 µM). The different data obtained just through the combination of A549, with HF and BM-MSCs elucidate the necessity of further analyzing the cooperation

of TME stromal cells with cancer cells. It is important to mention that this was the first time a 3D model comprising lung cancer cells, stromal fibroblasts, MSCs and HyA matrix was developed and used as a testing platform for evaluation of chemotherapeutics anti-cancer performance in TME relevant conditions.

4 - Conclusions

Through the utilization of a combination of coculture conditions, based on previous literature reports, an easy to assemble composite 3D-MCTS triculture model containing key TME populations such as HF and BM-MSCs was established by using microparticles as bioinstructive anchoring substrates. Inclusion of HF and MSCs stromal cells facilitated the formation of a characteristic necrotic core, the appearance of which is known to promote resistance to therapy *in vivo*. Moreover, the inclusion of bioinstructive microparticles allowed the addition of HyA, a main component of several tumor ECMs.

Overall the inclusion of a small percentage of bone marrow derived MSCs seemed to had a positive outcome for tumor resistance, improving the ability of A549 to form compact spheroids resist to doxorubicin in specific cell-cell ratios. Considering the diverse origins and niches of MSCs inside the human body it will be interesting in the future to analyze other types of MSCs and their influence in anti-cancer drugs resistance/susceptibility of these testing platforms.

In conclusion, the *in vitro* generated bioinstructed 3D-MCTS exhibit characteristics associated with *in vivo* tumors such as development of highly dense cell masses decurrent of both cell-cell and cell-ECM adhesion, matrix deposition. With composite 3D-MCTS with LbL-MPs serving effectively as tool for tackling one of the main flaws of spheroids-based models, i.e, the implementation of pre-existing ECM derived components, The produced *in vitro* models can be used to screen novel therapeutic compounds for lung cancer in more *in vivo*-like conditions. Due to its versatility, this enabling technology can also be used to study different combinations of cell populations and more complex ECM domains can be easily included, thus allowing the study of their specific functions and effects in cancer cells survival during treatment.

The current model can also be improved in the future in what regards the inclusion of dynamic testing conditions such as those provided by organ-on-a-chip testing platforms.

Such could provide an added layer of information and allow the opportunity to study other complex processes such as metastization and innovative compounds for its ablation.

5. References

[1] Ruggeri BA, Camp F, Miknyoczki S. Animal models of disease: Pre-clinical animal models of cancer and their applications and utility in drug discovery. Biochem Pharmacol 2014;87. 150–61.

[2] Shoemaker RH. The NCI60 human tumour cell line anticancer drug screen. Nat Rev Cancer 2006;6. 813–23.

[3] Nyga A, Cheema U, Loizidou M. 3D tumour models: Novel *in vitro* approaches to cancer studies. J Cell Commun Signal 2011;5. 239–48.

[4] Breslin S, O'Driscoll L. Three-dimensional cell culture: The missing link in drug discovery. Drug Discov Today 2013;18. 240–9.

[5] Pampaloni F, Reynaud EG, Stelzer EHK. The third dimension bridges the gap between cell culture and live tissue. Nat Rev Mol Cell Biol 2007;8. 839–45.

[6] Aparicio S, Hidalgo M, Kung AL. Examining the utility of patient-derived xenograft mouse models. Nat Rev Cancer 2015;15. 311–6.

[7] Cassidy JW, Caldas C, Bruna A. Europe PMC Funders Group Maintaining Tumour Heterogeneity in Patient-Derived Tumour Xenografts 2016;75. 2963–8.

[8] Thoma CR, Zimmermann M, Agarkova I, Kelm JM, Krek W. 3D cell culture systems modeling tumor growth determinants in cancer target discovery. Adv Drug Deliv Rev 2014;69–70. 29–41.

[9] Lazzari G, Couvreur P, Mura S. Multicellular tumor spheroids: a relevant 3D model for the *in vitro* preclinical investigation of polymer nanomedicines. Polym Chem 2017. doi:10.1039/C7PY00559H.

[10] Weiswald LB, Bellet D, Dangles-Marie V. Spherical cancer models in tumor biology. Neoplasia 2015;17. 1–15.

[11] Astashkina A, Grainger DW. Critical analysis of 3-D organoid *in vitro* cell culture models for high-throughput drug candidate toxicity assessments. Adv Drug Deliv Rev 2014;69–70. 1–18.

[12] Kievit FM, Florczyk SJ, Leung MC, Wang K, Wu JD, Silber JR, et al. Proliferation and enrichment of CD133+ glioblastoma cancer stem cells on 3D chitosan-alginate scaffolds. Biomaterials 2014;35. 9137–43.

[13] Ferrarelli LK. Cancer reactivated by collagen. Sci Signal 2016;9. ec165-ec165.

[14] Del Bufalo F, Manzo T, Hoyos V, Yagyu S, Caruana I, Jacot J, et al. 3D modeling of human cancer: A PEG-fibrin hydrogel system to study the role of tumor microenvironment and recapitulate the *in vivo* effect of oncolytic adenovirus. Biomaterials 2016;84. 76–85.

[15] Holle AW, Young JL, Spatz JP. In vitro cancer cell-ECM interactions inform *in vivo* cancer treatment. Adv Drug Deliv Rev 2016;97. 270–9.

[16] Jiang P, Li X, Thompson CB, Huang Z, Araiza F, Osgood R, et al. Effective targeting of the tumor microenvironment for cancer therapy. Anticancer Res 2012;32. 1203–12.

[17] Pirinen R, Tammi R, Tammi M, Hirvikoski P, Parkkinen JJ, Johansson R, et al. Prognostic value of hyaluronan expression in non-small-cell lung cancer: Increased stromal expression indicates unfavorable outcome in patients with adenocarcinoma. Int J Cancer 2001;95. 12–7.

[18] Stern R. Hyaluronan metabolism: A major paradox in cancer biology. Pathol Biol 2005;53. 372–82.

[19] Carvalho MP, Costa EC, Miguel SP, Correia IJ. Tumor spheroid assembly on hyaluronic acid-based structures: A review. Carbohydr Polym 2016;150. 139–48.

[20] Tolg C, McCarthy JB, Yazdani A, Turley EA. Hyaluronan and RHAMM in Wound Repair and the "Cancerization" of Stromal Tissues. Biomed Res Int 2014;2014. 1–18.

[21] Morel A-P, Lièvre M, Thomas C, Hinkal G, Ansieau S, Puisieux A. Generation of Breast Cancer Stem Cells through Epithelial-Mesenchymal Transition. PLoS One 2008;3. e2888.

[22] Cheng W, Liu T, Wan X, Gao Y, Wang H. MicroRNA-199a targets CD44 to suppress the tumorigenicity and multidrug resistance of ovarian cancer-initiating cells. FEBS J 2012;279. 2047–59.

[23] Cammarota F, Laukkanen MO. Mesenchymal stem/stromal cells in stromal evolution and cancer progression. Stem Cells Int 2016;2016. doi:10.1155/2016/4824573.

[24] Lopatina T, Gai C, Deregibus MC, Kholia S, Camussi G. Cross Talk between Cancer and Mesenchymal Stem Cells through Extracellular Vesicles Carrying Nucleic Acids. Front Oncol 2016;6. 125.

[25] Ridge SM, Sullivan FJ, Glynn SA. Mesenchymal stem cells: key players in cancer progression. Mol Cancer 2017;16. 31.
[26] Lazennec G, Lam PY. Recent discoveries concerning the tumor - mesenchymal stem cell interactions. Biochim Biophys Acta - Rev Cancer 2016;1866. 290–9.
[27] Gazdic M, Simovic Markovic B, Jovicic N, Misirkic-Marjanovic M, Djonov V, Jakovljevic V, et al. Mesenchymal Stem Cells Promote Metastasis of Lung Cancer Cells by Downregulating Systemic Antitumor Immune Response. Stem Cells Int 2017;2017. doi:10.1155/2017/6294717.
[28] Lu Y, Liu J, Liu Y, Qin Y, Luo Q, Wang Q, et al. TLR4 plays a crucial role in MSC-induced inhibition of NK cell function. Biochem Biophys Res Commun 2015;464. 541–7.
[29] Choe C, Shin YS, Kim SH, Jeon MJ, Choi SJ, Lee J, et al. Tumor-stromal interactions with direct cell contacts enhance motility of non-small cell lung cancer cells through the hedgehog signaling pathway. Anticancer Res 2013;33. 3715–24.
[30] Liu R, Wei S, Chen J, Xu S. Mesenchymal stem cells in lung cancer tumor microenvironment: Their biological properties, influence on tumor growth and therapeutic implications. Cancer Lett 2014;353. 145–52.
[31] Gottschling S, Granzow M, Kuner R, Jauch A, Herpel E, Xu EC, et al. Mesenchymal stem cells in non-small cell lung cancer-Different from others? Insights from comparative molecular and functional analyses. Lung Cancer 2013;80. 19–29.
[32] Xu MH, Gao X, Luo D, Zhou XD, Xiong W, Liu GX. EMT and acquisition of stem cell-like properties are involved in spontaneous formation of tumorigenic hybrids between lung cancer and bone marrow-derived mesenchymal stem cells. PLoS One 2014;9. doi:10.1371/journal.pone.0087893.
[33] Norozi F, Ahmadzadeh A, Shahrabi S, Vosoughi T, Saki N. Mesenchymal stem cells as a double-edged sword in suppression or progression of solid tumor cells. Tumor Biol 2016;37. 11679–89.
[34] Schneider CA, Rasband WS, Eliceiri KW. NIH Image to ImageJ: 25 years of image analysis. Nat Methods 2012;9. 671–5.
[35] Ivanov DP, Parker TL, Walker DA, Alexander C, Ashford MB, Gellert PR, et al. Multiplexing spheroid volume, resazurin and acid phosphatase viability assays for high-throughput screening of tumour spheroids and stem cell neurospheres. PLoS One 2014;9. 1–14.
[36] Lou Y-R, Kanninen L, Kaehr B, Townson JL, Niklander J, Harjumäki R, et al. Silica bioreplication preserves three-dimensional spheroid structures of human pluripotent stem cells and HepG2 cells. Sci Rep 2015;5. 13635.
[37] Ma M, Xu J, Purcell WM. Biochemical and Functional Changes of Rat Liver Spheroids during Spheroid Formation and Maintenance in Culture: I. Morphological Maturation and Kinetic Changes of Energy Metabolism, Albumin Synthesis, and Activities of Some Enzymes. J Cell Biochem 2003;90. 1166–75.
[38] Costa EC, Gaspar VM, Coutinho P, Correia IJ. Optimization of liquid overlay technique to formulate heterogenic 3D co-cultures models. Biotechnol Bioeng 2014;111. 1672–85.
[39] Cox MC, Reese LM, Bickford LR, Verbridge SS. Toward the Broad Adoption of 3D Tumor Models in the Cancer Drug Pipeline. ACS Biomater Sci Eng 2015;1. 877–94.
[40] Rodday B, Hirschhaeuser F, Walenta S, Mueller-Klieser W. Semiautomatic Growth Analysis of Multicellular Tumor Spheroids. J Biomol Screen 2011;16. 1119–24.
[41] Lin RZ, Chang HY. Recent advances in three-dimensional multicellular spheroid culture for biomedical research. Biotechnol J 2008;3. 1172–84.
[42] Benien P, Swami A. 3D tumor models: history, advances and future perspectives. Futur Oncol 2014;10. 1311–27.
[43] Tanner K, Gottesman MM. Beyond 3D culture models of cancer. Sci Transl Med 2015;7. 7–10.
[44] Augustin F, Fiegl M, Schmid T, Pomme G, Sterlacci W, Tzankov A. Receptor for hyaluronic acid-mediated motility (RHAMM, CD168) expression is prognostically important in both nodal negative and nodal positive large cell lung cancer. J Clin Pathol 2015;68. 368–73.
[45] Adamia S, Pilarski PM, Belch AR, Pilarski LM. Aberrant Splicing, Hyaluronan Synthases and Intracellular Hyaluronan as Drivers of Oncogenesis and Potential Drug Targets. Curr Cancer Drug Targets 2013;13. 347–61.
[46] Chanmee T, Ontong P, Kimata K, Itano N. Key Roles of Hyaluronan and Its CD44 Receptor in the Stemness and Survival of Cancer Stem Cells. Front Oncol 2015;5. 180.
[47] Khademhosseini A, Suh KY, Yang JM, Eng G, Yeh J, Levenberg S, et al. Layer-by-layer deposition of hyaluronic acid and poly-L-lysine for patterned cell co-cultures. Biomaterials 2004;25. 3583–92.
[48] Xu W, Qian J, Zhang Y, Suo A, Cui N, Wang J, et al. A double-network poly(Nε-acryloyl l-lysine)/hyaluronic acid hydrogel as a mimic of the breast tumor microenvironment. Acta Biomater

2016;33. 131–41.
[49] Richardson JJ, Cui J, Björnmalm M, Braunger JA, Ejima H, Caruso F. Innovation in Layer-by-Layer Assembly. Chem Rev 2016;116. 14828–67.
[50] Stock K, Estrada MF, Vidic S, Gjerde K, Rudisch A, Santo VE, et al. Capturing tumor complexity *in vitro*: Comparative analysis of 2D and 3D tumor models for drug discovery. Sci Rep 2016;6. 28951.
[51] Akasov R, Gileva A, Zaytseva-Zotova D, Burov S, Chevalot I, Guedon E, et al. 3D *in vitro* co-culture models based on normal cells and tumor spheroids formed by cyclic RGD-peptide induced cell self-assembly. Biotechnol Lett 2017;39. 45–53.
[52] Kumar S. Cellular mechanotransduction: Stiffness does matter. Nat Mater 2014;13. 918–20.
[53] Fennema E, Rivron N, Rouwkema J, van Blitterswijk C, De Boer J. Spheroid culture as a tool for creating 3D complex tissues. Trends Biotechnol 2013;31. 108–15.
[54] Semenza GL. The hypoxic tumor microenvironment: A driving force for breast cancer progression. Biochim Biophys Acta - Mol Cell Res 2016;1863. 382–91.
[55] Baek N, Seo OW, Kim M, Hulme J, An SSA. Monitoring the effects of doxorubicin on 3D-spheroid tumor cells in real-time. Onco Targets Ther 2016;Volume 9. 7207–18.
[56] Block GJ, Ohkouchi S, Fung F, Frenkel J, Gregory C, Pochampally R, et al. Multipotent stromal cells are activated to reduce apoptosis in part by upregulation and secretion of stanniocalcin-1. Stem Cells 2009;27. 670–81.
[57] Delinasios JG, Angeli F, Koumakis G, Kumar S, Kang WH, Sica G, et al. Proliferating fibroblasts and HeLa cells co-cultured *in vitro* reciprocally influence growth patterns, protein expression, chromatin features and cell survival. Anticancer Res 2015;35. 1881–916.
[58] Ji X, Ji J, Shan F, Zhang Y, Chen Y, Lu X. Cancer-associated fibroblasts from NSCLC promote the radioresistance in lung cancer cell lines. Int J Clin Exp Med 2015;8. 7002–8.
[59] Tu B, Zhu J, Liu S, Wang L, Fan Q, Hao Y, et al. Mesenchymal stem cells promote osteosarcoma cell survival and drug resistance through activation of STAT3. Oncotarget 2016;7. doi:10.18632/oncotarget.10219.
[60] Shen F, Chu S, Bence AK, Bailey B, Xue X, Erickson P a, et al. Quantitation of doxorubicin uptake, efflux, and modulation of multidrug resistance (MDR) in MDR human cancer cells. J Pharmacol Exp Ther 2008;324. 95–102.
[61] Xu K, Tian X, Oh SY, Movassaghi M, Naber SP, Kuperwasser C, et al. The fibroblast Tiam1-osteopontin pathway modulates breast cancer invasion and metastasis. Breast Cancer Res 2016;18. 14.
[62] Amann A, Zwierzina M, Gamerith G, Bitsche M, Huber JM, Vogel GF, et al. Development of an innovative 3D cell culture system to study tumour - Stroma interactions in non-small cell lung cancer cells. PLoS One 2014;9. doi:10.1371/journal.pone.0092511.
[63] Brancato V, Garziano A, Gioiella F, Urciuolo F, Imparato G, Panzetta V, et al. 3D is not enough: Building up a cell instructive microenvironment for tumoral stroma microtissues. vol. 47. Acta Materialia Inc.; 2017. doi:10.1016/j.actbio.2016.10.007.
[64] Santo VE, Rebelo SP, Estrada MF, Alves PM, Boghaert E, Brito C. Drug screening in 3D *in vitro* tumor models: overcoming current pitfalls of efficacy read-outs. Biotechnol J 2017;12. 1–18.
[65] Zanoni M, Piccinini F, Arienti C, Zamagni A, Santi S, Polico R, et al. 3D tumor spheroid models for *in vitro* therapeutic screening: a systematic approach to enhance the biological relevance of data obtained. Sci Rep 2016;6. 19103.
[66] Fong ELS, Harrington DA, Farach-Carson MC, Yu H. Heralding a new paradigm in 3D tumor modeling. Biomaterials 2016;108. 197–213.
[67] Eltzschig HK, Carmeliet P. Hypoxia and inflammation. N Engl J Med 2011;364. 1976–7.
[68] Grainger SJ, Putnam AJ. Assessing the permeability of engineered capillary networks in a 3D culture. PLoS One 2011;6. doi:10.1371/journal.pone.0022086.
[69] Keskin D, Kim J, Cooke VG, Wu CC, Sugimoto H, Gu C, et al. Targeting Vascular Pericytes in Hypoxic Tumors Increases Lung Metastasis via Angiopoietin-2. Cell Rep 2015;10. 1066–81.
[70] Dittmer A, Hohlfeld K, Lützkendorf J, Müller LP, Dittmer J. Human mesenchymal stem cells induce E-cadherin degradation in breast carcinoma spheroids by activating ADAM10. Cell Mol Life Sci 2009;66. 3053–65.
[71] Koppenol WH, Bounds PL, Dang C V. Otto Warburg's contributions to current concepts of cancer metabolism. Nat Rev Cancer 2011;11. 325–37.
[72] Derda R, Laromaine A, Mammoto A, Tang SKY, Mammoto T, Ingber DE, et al. Paper-supported 3D cell culture for tissue-based bioassays. Proc Natl Acad Sci 2009;106. 18457–62.
[73] Hughes I, Blasiole B, Huss D, Warchol ME, Rath NP, Hurle B, et al. The Tumor Microenvironment in Non-Small Cell Lung Cancer. Dev Biol 2004;276. 391–402.

[74] Chaturvedi P, Gilkes DM, Chak C, Wong L, Luo W, Zhang H, et al. Hypoxia-inducible factor – dependent breast cancer – mesenchymal stem cell bidirectional signaling promotes metastasis. J Clin Invest 2013;123. 189–205.
[75] Olsen TR, Mattix B, Casco M, Herbst A, Williams C, Tarasidis A, et al. Processing cellular spheroids for histological examination. J Histotechnol 2014;37. 138–42.
[76] Shi Y, Du L, Lin L, Wang Y. Tumour-associated mesenchymal stem/stromal cells: emerging therapeutic targets. Nat Rev Drug Discov 2016;16. 35–52.
[77] Han HW, Hsu S hui. Chitosan-hyaluronan based 3D co-culture platform for studying the crosstalk of lung cancer cells and mesenchymal stem cells. Acta Biomater 2016;42. 157–67.
[78] Probes M. Vybrant Cell-Labeling Solutions. Solutions 2001. 1–3.
[79] Fang M, Yuan J, Peng C, Li Y. Collagen as a double-edged sword in tumor progression. Tumor Biol 2014;35. 2871–82.
[80] Chen Z, Fillmore CM, Hammerman PS, Kim CF, Wong K-K. Non-small-cell lung cancers: a heterogeneous set of diseases. Nat Rev Cancer 2015;15. 247–247.
[81] Barcus CE, O'Leary KA, Brockman JL, Rugowski DE, Liu Y, Garcia N, et al. Elevated collagen-I augments tumor progressive signals, intravasation and metastasis of prolactin-induced estrogen receptor alpha positive mammary tumor cells. Breast Cancer Res 2017;19. 9.
[82] Lu N, Karlsen T V., Reed RK, Kusche-Gullberg M, Gullberg D. Fibroblast α11β1 integrin regulates tensional homeostasis in fibroblast/A549 carcinoma heterospheroids. PLoS One 2014;9. doi:10.1371/journal.pone.0103173.
[83] Kim SH, Turnbull J, Guimond S. Extracellular matrix and cell signalling: The dynamic cooperation of integrin, proteoglycan and growth factor receptor. J Endocrinol 2011;209. 139–51.
[84] Yilmaz M, Christofori G. EMT, the cytoskeleton, and cancer cell invasion. Cancer Metastasis Rev 2009;28. 15–33.
[85] Khakoo AY, Pati S, Anderson SA, Reid W, Elshal MF, Rovira II, et al. Human mesenchymal stem cells exert potent antitumorigenic effects in a model of Kaposi's sarcoma. J Exp Med 2006;203. 1235–47.
[86] Klopp AH, Lacerda L, Gupta A, Debeb BG, Solley T, Li L, et al. Mesenchymal stem cells promote mammosphere formation and decrease E-Cadherin in normal and malignant breast cells. PLoS One 2010;5. 1–9.
[87] Matrix Crosslinking Forces Tumor Progression by Enhancing Integrin Signaling. Cell 2009;139. 891–906.
[88] Ahmad T, Lee J, Shin YM, Shin HJH, Octavios N, Madhurakat Perikamana SK, Park SH, et al. Hybrid-spheroids incorporating ECM like engineered fragmented fibers potentiate stem cell function by improved cell/cell and cell/ECM interactions. Acta Biomater 2017. 1–15.
[89] Van Roy F, Berx G. The cell-cell adhesion molecule E-cadherin. Cell Mol Life Sci 2008;65. 3756–88.
[90] Lin RZ, Chou LF, Chien CCM, Chang HY. Dynamic analysis of hepatoma spheroid formation: Roles of E-cadherin and β1-integrin. Cell Tissue Res 2006;324. 411–22.
[91] Sodek KL, Ringuette MJ, Brown TJ. Compact spheroid formation by ovarian cancer cells is associated with contractile behavior and an invasive phenotype. Int J Cancer 2009;124. 2060–70.
[92] Shintani Y, Abulaiti A, Kimura T, Funaki S, Nakagiri T, Inoue M, et al. Pulmonary fibroblasts induce epithelial mesenchymal transition and some characteristics of stem cells in non-small cell lung cancer. Ann Thorac Surg 2013;96. 425–33.
[93] Misra S, Hascall VC, Markwald RR, Ghatak S. Interactions between hyaluronan and its receptors (CD44, RHAMM) regulate the activities of inflammation and cancer. Front Immunol 2015;6. doi:10.3389/fimmu.2015.00201.
[94] Wang K, Kievit FM, Erickson AE, Silber JR, Ellenbogen RG, Zhang M. Culture on 3D Chitosan-Hyaluronic Acid Scaffolds Enhances Stem Cell Marker Expression and Drug Resistance in Human Glioblastoma Cancer Stem Cells. Adv Healthc Mater 2016;5. 3173–81.
[95] Tsai CW, Young TH. CD44 expression trends of mesenchymal stem-derived cell, cancer cell and fibroblast spheroids on chitosan-coated surfaces. Pure Appl Chem 2016;88. 843–52.
[96] Leung EL-H, Fiscus RR, Tung JW, Tin VP-C, Cheng LC, Sihoe AD-L, et al. Non-Small Cell Lung Cancer Cells Expressing CD44 Are Enriched for Stem Cell-Like Properties. PLoS One 2010;5. e14062.
[97] Zhang Y, Zhang Z, Guan Q, Liu Y, Wu Z, Li J, et al. Co-culture with lung cancer A549 cells promotes the proliferation and migration of mesenchymal stem cells derived from bone marrow. Exp Ther Med 2017. 2983–91.
[98] Tao J, Ybarra N, El Naqa I. A549 Lung Cancer Cells Up-Regulate Proto-Oncogene Expression in

Mesenchymal Stem Cells. Int J Radiat Oncol 2014;90. S770.
[99] Miletti-González KE, Chen S, Muthukumaran N, Saglimbeni GN, Wu X, Yang J, et al. The CD44 receptor interacts with P-glycoprotein to promote cell migration and invasion in cancer. Cancer Res 2005;65. 6660–7.
[100] Wood SL, Pernemalm M, Crosbie PA, Whetton AD. The role of the tumor-microenvironment in lung cancer-metastasis and its relationship to potential therapeutic targets. Cancer Treat Rev 2014;40. 558–66.
[101] Szakács G, Paterson JK, Ludwig JA, Booth-Genthe C, Gottesman MM. Targeting multidrug resistance in cancer. Nat Rev Drug Discov 2006;5. 219–34.
[102] Hopper-Borge W-T and. Drug Resistance Mechanisms in Non-Small Cell Lung Carcinoma. J Can Res Updat 2014;2. 265–82.
[103] Lu JF, Pokharel D, Bebawy M. MRP1 and its role in anticancer drug resistance. Drug Metab Rev 2015;2532. 1–14.
[104] Silva R, Vilas-Boas V, Carmo H, Dinis-Oliveira RJ, Carvalho F, De Lourdes Bastos M, et al. Modulation of P-glycoprotein efflux pump: Induction and activation as a therapeutic strategy. Pharmacol Ther 2015;149. 1–123.
[105] Liou G-Y, Storz P. Reactive oxygen species in cancer. Free Radic Res 2010;44. 479–96.
[106] Lyssiotis CA, Kimmelman AC. Metabolic Interactions in the Tumor Microenvironment. Trends Cell Biol 2017;xx. 1–13.
[107] Hu Y-D, Zhang M-H, Hu Y-D, Xu Y, Xiao Y, Luo Y, et al. Human mesenchymal stem cells enhance autophagy of lung carcinoma cells against apoptosis during serum deprivation. Int J Oncol 2013;42. 1390–8.
[108] Talukdar S, Kundu SC. Engineered 3D silk-based metastasis models: Interactions between human breast adenocarcinoma, mesenchymal stem cells and osteoblast-like cells. Adv Funct Mater 2013;23. 5249–60.
[109] Spees JL, Olson SD, Whitney MJ, Prockop DJ. Mitochondrial transfer between cells can rescue aerobic respiration. Proc Natl Acad Sci U S A 2006;103. 1283–8.
[110] Östman A, Augsten M. Cancer-associated fibroblasts and tumor growth - bystanders turning into key players. Curr Opin Genet Dev 2009;19. 67–73.
[111] Punia R, Raina K, Agarwal R, Singh RP. Acacetin enhances the therapeutic efficacy of doxorubicin in non-small-cell lung carcinoma cells 2017. 1–19.
[112] Xu L, Li H, Wang Y, Dong F, Wang H, Zhang S. Enhanced activity of doxorubicin in drug resistant A549 tumor cells by encapsulation of P-glycoprotein inhibitor in PLGA-based nanovectors. Oncol Lett 2014;7. 387–92.
[113] El-Awady RA, Semreen MH, Saber MM, Cyprian F, Menon V, Al-Tel TH. Modulation of DNA damage response and induction of apoptosis mediates synergism between doxorubicin and a new imidazopyridine derivative in breast and lung cancer cells. DNA Repair (Amst) 2016;37. 1–11.
[114] Fang W Bin, Yao M, Cheng N. Priming cancer cells for drug resistance: role of the fibroblast niche 2014;9. 114–26.
[115] Leon G, MacDonagh L, Finn SP, Cuffe S, Barr MP. Cancer stem cells in drug resistant lung cancer: Targeting cell surface markers and signaling pathways. Pharmacol Ther 2016;158. 71–90.

5. Conclusions and Future Perspectives

No doubt remains about the capacity of the TME for modulating cancer progression. Stromal cellular and tumor-ECM components act as key factors on most aspects of tumor evolution, either promoting or not a pro-tumoral microenvironment. Nevertheless, the exact nature of these complex interactions remains to be fully understood. Development of novel innovative models that allow the study of such interactions is thus of chief importance.

Based on literature reports, an easy to assemble composite 3D-MCTS triculture model containing both key stromal cell populations of the TME (HF and BM-MSCs) and ECM mimetic microparticles was established. The inclusion of each one of the diverse components, cellular (HF and MSC) and ECM components (HyA), led to further approximation of these 3D-MCTS models to the reality of *in vivo* tumors. The addition of HF and MSCs population to A549 3D-MCTS resulted in different variations in spheroid morphology, size, circularity, internal organization, matrix deposition and behavior to treatment. Globally, such approach resulted in denser spheroids that evidenced necrotic core formation at an earlier time than monoculture 3D-MCTS of A549. More so, inclusion of a small percentage of BM-MSCs acted as one of the most significant factors in increasing overall resistance to Doxorubicin. Once present in the spheroid, MSCs migrated into its interior region over a period of 14 days, perhaps mimicking their role *in vivo* when present in the lung TME. Moreover, the inclusion of bioinstructive microparticles allowed the addition of HyA, a main component of several tumor ECMs. In accordance with previous studies, HyA inclusion resulted by itself in an overall increased resistance of LbL-MPs containing spheroids to Doxorubicin, denoting a positive influence of HyA in the activation of MDR mechanisms in 3D-MCTS models.

In conclusion, the *in vitro* generated bioinstructed 3D-MCTS exhibited characteristics associated with *in vivo* tumors such as development of highly dense cell masses decurrent of both cell-cell and cell-ECM adhesion and matrix deposition. Composite 3D-MCTS with LbL-MPs served effectively as a tool for tackling one of the main flaws of spheroids based models, by allowing the implementation of pre-existing ECM derived components, while still providing the same ease of analysis found in these models. Offering as such a malleable platform capable of recapitulating TME interactions and communication,

that not only could act as platforms for expediting compound-screening processes, but in which further studies with the intuit of characterizing the TME could be performed.

In the future, the design of the system could be improved to not only recapitulate the interactions derived of current populations, but as well include novel populations such as immune cells or endothelial cells. Such developments to the model complexity are not out of reach, with combinations of already implemented technologies such as combination of composite spheroid culture and microfluidic devices, or bioreactor technology. If coupled with microencapsulation methodologies, these models would allow the study of paracrine factors associated with immune suppression or angiogenesis. In fact, a large number of designs could be used for the study of specific interactions and communications that drive tumor progression. That would undoubtedly improve research of novel therapies and as such enhance the ability to improve cancer therapy a foreseeable future

.

6 - References:

[1] Wang L, Zhu B, Zhang M, Wang X. Roles of immune microenvironment heterogeneity in therapy-associated biomarkers in lung cancer. Semin Cell Dev Biol 2017;64. 90–7.

[2] Guo C, Morris SA. Engineering cell identity: establishing new gene regulatory and chromatin landscapes. vol. 46. WHO Library Cataloguing-in-Publication Data; 2017. doi:10.1016/j.gde.2017.06.011.

[3] Siegel R, Desantis C, Virgo K, Stein K, Mariotto A, Smith T, et al. Cancer Treatment and Survivorship Statistics , 2012. CA Cancer J Clin 2012;62. 220–41.

[4] American Cancer Society. Cancer Facts & Figures 2016. Cancer Facts Fig 2016 2016. 1–9.

[5] International Association for the Study of Lung Cancer. Lung Cancer Fact Sheet - 2016 - Europe 2017. 2016–7.

[6] Suresh R, Ali S, Ahmad A, Philip PA, Sarkar FH. Lung Cancer and Personalized Medicine. vol. 893. Aamir Ahma. 2016. doi:10.1007/978-3-319-24223-1.

[7] David S. Ettinger, MD; Douglas E. Wood, MD, FRCSEd; Dara L. Aisner, MD, PhD; Wallace Akerley, MD; Jessica Bauman, MD; Lucian R. Chirieac, MD; Thomas A. D'Amico, MD; Malcolm M. DeCamp, MD; Thomas J. Dilling, MD, MS; Michael Dobelbower, MD, PhD; Robert C. D P. Non–Small Cell Lung Cancer, Version 5.2017 - Clinical Practice Guidelines in Oncology. JNCCN J Natl Compr Cancer Netw 2017;15. doi:J Natl Compr Canc Netw 2017;15(4):504–535.

[8] Neal RD, Hamilton W, Rogers TK. Lung cancer. Bmj 2014;349. g6560–g6560.

[9] Chen Z, Fillmore CM, Hammerman PS, Kim CF, Wong K-K. Non-small-cell lung cancers: a heterogeneous set of diseases. Nat Rev Cancer 2015;15. 247–247.

[10] Pirinen R, Tammi R, Tammi M, Hirvikoski P, Parkkinen JJ, Johansson R, et al. Prognostic value of hyaluronan expression in non-small-cell lung cancer: Increased stromal expression indicates unfavorable outcome in patients with adenocarcinoma. Int J Cancer 2001;95. 12–7.

[11] Mestre-ferrandiz J, Sussex J, Towse A. The R & D Cost of a New Medicine. 2012.

[12] Cressman S, Browman GP, Hoch JS, Kovacic L, Peacock SJ. A Time-Trend Economic Analysis of Cancer Drug Trials. Oncologist 2015;20. 729–36.

[13] Paul SM, Mytelka DS, Dunwiddie CT, Persinger CC, Munos BH, Lindborg SR, et al. How to improve R&D productivity: the pharmaceutical industry's grand challenge. Nat Rev Drug Discov 2010;9. 203–14.

[14] Toniatti C, Jones P, Graham H, Pagliara B, Draetta G. Oncology drug discovery: Planning a turnaround. Cancer Discov 2014;4. 397–404.

[15] Hirsch FR, Scagliotti G V., Mulshine JL, Kwon R, Curran WJ, Wu YL, et al. Lung cancer: current therapies and new targeted treatments. Lancet 2017;389. 299–311.

[16] Housman G, Byler S, Heerboth S, Lapinska K, Longacre M, Snyder N, et al. Drug resistance in cancer: An overview. Cancers (Basel) 2014;6. 1769–92.

[17] Webster RM. Combination therapies in oncology. Nat Rev Drug Discov 2016;15. 81–2.

[18] Correia AL, Bissell MJ. The tumor microenvironment is a dominant force in multidrug resistance. Drug Resist Updat 2012;15. 39–49.

[19] Hanahan D, Weinberg RA. Hallmarks of cancer: The next generation. Cell 2011;144. 646–74.

[20] Wade M, Li Y-C, Wahl GM. MDM2, MDMX and p53 in oncogenesis and cancer therapy. Nat Rev Cancer 2013;13. 83–96.

[21] Rivlin N, Brosh R, Oren M, Rotter V. Mutations in the p53 Tumor Suppressor Gene: Important Milestones at the Various Steps of Tumorigenesis. Genes Cancer 2011;2. 466–74.

[22] Tabassum DP, Polyak K. Tumorigenesis: it takes a village. Nat Rev Cancer 2015;15. 473–83.

[23] Kenny PA, Bissell MJ. Tumor reversion: Correction of malignant behavior by microenvironmental cues. Int J Cancer 2003;107. 688–95.

[24] Quail D, Joyce J. Multifaceted effects of the microenvironment on tumor progression. Nat Rev Cancer 2017;in http://.

[25] Medrano-E'Vers A, Morales-Hernández AE, Valencia-López R, Hernández-Salcedo DR. Enfermedad granulomatosa crónica. Med. Interna Mex., vol. 33, 2017, p. 407–14. 407–14.

[26] Blanpain C. Tracing the cellular origin of cancer. Nat Cell Biol 2013;15. 126–34.

[27] Vicente-Dueñas C, Hauer J, Ruiz-Roca L, Ingenhag D, Rodríguez-Meira A, Auer F, et al. Tumoral stem cell reprogramming as a driver of cancer: Theory, biological models, implications in cancer therapy. Semin Cancer Biol 2015;32. 3–9.

[28] Klemm F, Joyce JA. Microenvironmental regulation of therapeutic response in cancer. Trends Cell Biol 2015;25. 198–213.
[29] Rozario T, DeSimone DW. The extracellular matrix in development and morphogenesis: A dynamic view. Dev Biol 2010;341. 126–40.
[30] Kim SH, Turnbull J, Guimond S. Extracellular matrix and cell signalling: The dynamic cooperation of integrin, proteoglycan and growth factor receptor. J Endocrinol 2011;209. 139–51.
[31] Badylak SF, Freytes DO, Gilbert TW. Reprint of: Extracellular matrix as a biological scaffold material: Structure and function. Acta Biomater 2015;23. S17–26.
[32] Egeblad M, Werb Z. New functions for the matrix metalloproteinases in cancer progression. Nat Rev Cancer 2002;2. 161–74.
[33] Cox TR, Gartland A, Erler JT. Lysyl oxidase, a targetable secreted molecule involved in cancer metastasis. Cancer Res 2016;76. 188–92.
[34] Stern R. Hyaluronidases in Cancer Biology. Hyaluronan Cancer Biol 2009;18. 207–20.
[35] Desgrosellier J, David C. Integrins in cancer: biological implications in therapeutic opportunities. Cancer, Nat Rev 2015;10. 9–22.
[36] Hood JD, Cheresh DA. Role of Integrins in Cell Invasion and Migration. Nat Rev Cancer 2002;2. 91–100.
[37] Wan L, Pantel K, Kang Y. Tumor metastasis: moving new biological insights into the clinic. Nat Med 2013;19. 1450–64.
[38] Eltzschig HK, Carmeliet P. Hypoxia and inflammation. N Engl J Med 2011;364. 1976–7.
[39] Fong ELS, Harrington DA, Farach-Carson MC, Yu H. Heralding a new paradigm in 3D tumor modeling. Biomaterials 2016;108. 197–213.
[40] Adamia S, Pilarski PM, Belch AR, Pilarski LM. Aberrant Splicing, Hyaluronan Synthases and Intracellular Hyaluronan as Drivers of Oncogenesis and Potential Drug Targets. Curr Cancer Drug Targets 2013;13. 347–61.
[41] Tanner K, Gottesman MM. Beyond 3D culture models of cancer. Sci Transl Med 2015;7. 7–10.
[42] Amann A, Zwierzina M, Gamerith G, Bitsche M, Huber JM, Vogel GF, et al. Development of an innovative 3D cell culture system to study tumour - Stroma interactions in non-small cell lung cancer cells. PLoS One 2014;9. doi:10.1371/journal.pone.0092511.
[43] McMillin DW, Negri JM, Mitsiades CS. The role of tumour–stromal interactions in modifying drug response: challenges and opportunities. Nat Rev Drug Discov 2013;12. 217–28.
[44] Roma-Rodrigues C, Fernandes AR, Baptista PV. Exosome in tumour microenvironment: Overview of the crosstalk between normal and cancer cells. Biomed Res Int 2014;2014. doi:10.1155/2014/179486.
[45] Bremnes RM, Donnem T, Busund L-T. Importance of tumor infiltrating lymphocytes in non-small cell lung cancer? Ann Transl Med 2016;4. 142–142.
[46] Carbone DP, Gandara DR, Antonia SJ, Zielinski C, Paz-Ares L. Non–Small-Cell Lung Cancer: Role of the Immune System and Potential for Immunotherapy. J Thorac Oncol 2015;10. 974–84.
[47] Costa EC, Gaspar VM, Coutinho P, Correia IJ. Optimization of liquid overlay technique to formulate heterogenic 3D co-cultures models. Biotechnol Bioeng 2014;111. 1672–85.
[48] Gaggioli C, Hooper S, Hidalgo-Carcedo C, Grosse R, Marshall JF, Harrington K, et al. Fibroblast-led collective invasion of carcinoma cells with differing roles for RhoGTPases in leading and following cells. Nat Cell Biol 2007;9. 1392–400.
[49] Östman A, Augsten M. Cancer-associated fibroblasts and tumor growth - bystanders turning into key players. Curr Opin Genet Dev 2009;19. 67–73.
[50] Liu R, Wei S, Chen J, Xu S. Mesenchymal stem cells in lung cancer tumor microenvironment: Their biological properties, influence on tumor growth and therapeutic implications. Cancer Lett 2014;353. 145–52.
[51] Park YM, Yoo SH, Kim S-H. Adipose-derived stem cells induced EMT-like changes in H358 lung cancer cells. Anticancer Res 2013;33. 4421–30.
[52] Heymach J V., Cascone T. Tumor Microenvironment, Angiogenesis Biology, and Targeted Therapy. Lung Cancer Fourth Ed 2014. 505–26.
[53] Patel SA, Meyer JR, Greco SJ, Corcoran KE, Bryan M, Rameshwar P. Mesenchymal Stem Cells Protect Breast Cancer Cells through Regulatory T Cells: Role of Mesenchymal Stem Cell-Derived TGF- . J Immunol 2010;184. 5885–94.
[54] Bersini S, Jeon JS, Dubini G, Arrigoni C, Chung S, Charest JL, et al. A microfluidic 3D invitro model for specificity of breast cancer metastasis to bone. Biomaterials 2014;35. 2454–61.
[55] Orimo A, Gupta PB, Sgroi DC, Arenzana-Seisdedos F, Delaunay T, Naeem R, et al. Stromal fibroblasts present in invasive human breast carcinomas promote tumor growth and angiogenesis through elevated

SDF-1/CXCL12 secretion. Cell 2005;121. 335–48.
[56] Casey SC, Amedei A, Aquilano K, Azmi AS, Benencia F, Bhakta D, et al. Cancer prevention and therapy through the modulation of the tumor microenvironment. Semin Cancer Biol 2015;35. S199–223.
[57] Graves EE, Maity A, Le Q-T. The Tumor Microenvironment in Non–Small-Cell Lung Cancer. Semin Radiat Oncol 2010;20. 156–63.
[58] Balkwill FR, Capasso M, Hagemann T. The tumor microenvironment at a glance. J Cell Sci 2012;125. 5591–6.
[59] Davies H, Bignell GR, Cox C, Stephens P, Edkins S, Clegg S, et al. Mutations of the BRAF gene in human cancer. Nature 2002;417. 949–54.
[60] Harris TJR, McCormick F. The molecular pathology of cancer. Nat Rev Clin Oncol 2010;7. 251–65.
[61] Ou SHI. Second-generation irreversible epidermal growth factor receptor (EGFR) tyrosine kinase inhibitors (TKIs): A better mousetrap? A review of the clinical evidence. Crit Rev Oncol Hematol 2012;83. 407–21.
[62] Califano R, Abidin A, Tariq N ul A, Economopoulou P, Metro G, Mountzios G. Beyond EGFR and ALK inhibition: Unravelling and exploiting novel genetic alterations in advanced non small-cell lung cancer. Cancer Treat Rev 2015;41. 401–11.
[63] Sandler A. Bevacizumab in Non Small Cell Lung Cancer. Clin Cancer Res 2007;13. 4613s–4616s.
[64] Zhang X, Zhang L, Xu W, Qian H, Ye S, Zhu W, et al. Experimental Therapy for Lung Cancer: Umbilical Cord-Derived Mesenchymal Stem Cell-Mediated Interleukin-24 Delivery. Curr Cancer Drug Targets 2012;13. 92–102.
[65] Hakkarainen T, Särkioja M, Lehenkari P, Miettinen S, Ylikomi T, Suuronen R, et al. Human Mesenchymal Stem Cells Lack Tumor Tropism but Enhance the Antitumor Activity of Oncolytic Adenoviruses in Orthotopic Lung and Breast Tumors. Hum Gene Ther 2007;18. 627–41.
[66] WHO. Global status report on noncommunicable diseases 2014. World Health 2014. 176.
[67] Ledford H. US cancer institute to overhaul tumour cell lines. Nature 2016;530. 391.
[68] Almatroodi SA, McDonald CF, Darby IA, Pouniotis DS. Characterization of M1/M2 Tumour-Associated Macrophages (TAMs) and Th1/Th2 Cytokine Profiles in Patients with NSCLC. Cancer Microenviron 2016;9. 1–11.
[69] Dittmer A, Fuchs A, Oerlecke I, Leyh B, Kaiser S, Martens JWM, et al. Mesenchymal stem cells and carcinoma-associated fibroblasts sensitize breast cancer cells in 3D cultures to kinase inhibitors. Int J Oncol 2011;39. 689–96.
[70] Wood SL, Pernemalm M, Crosbie PA, Whetton AD. The role of the tumor-microenvironment in lung cancer-metastasis and its relationship to potential therapeutic targets. Cancer Treat Rev 2014;40. 558–66.
[71] Barcellos-de-Souza P, Comito G, Pons-Segura C, Taddei ML, Gori V, Becherucci V, et al. Mesenchymal Stem Cells are Recruited and Activated into Carcinoma-Associated Fibroblasts by Prostate Cancer Microenvironment-Derived TGF-??1. Stem Cells 2016;34. 2536–47.
[72] An J, Enomoto A, Weng L, Kato T, Iwakoshi A, Ushida K, et al. Significance of cancer-associated fibroblasts in the regulation of gene expression in the leading cells of invasive lung cancer. J Cancer Res Clin Oncol 2013;139. 379–88.
[73] Ji X, Ji J, Shan F, Zhang Y, Chen Y, Lu X. Cancer-associated fibroblasts from NSCLC promote the radioresistance in lung cancer cell lines. Int J Clin Exp Med 2015;8. 7002–8.
[74] Gottschling S, Granzow M, Kuner R, Jauch A, Herpel E, Xu EC, et al. Mesenchymal stem cells in non-small cell lung cancer-Different from others? Insights from comparative molecular and functional analyses. Lung Cancer 2013;80. 19–29.
[75] Ahmad A, Gadgeel SM. Lung Cancer and Personalized Medicine: Novel Therapies and Clinical Management. Preface. vol. 890. 2016. doi:10.1007/978-3-319-24932-2.
[76] Liao D, Johnson RS. Hypoxia: A key regulator of angiogenesis in cancer. Cancer Metastasis Rev 2007;26. 281–90.
[77] Osmangazi E, Emre Y, Hospital C. The Significance and Relationship between Mast Cells and Tumour Angiogenesis in Non-small Cell Lung Carcinoma 2008. 88–95.
[78] Keskin D, Kim J, Cooke VG, Wu CC, Sugimoto H, Gu C, et al. Targeting Vascular Pericytes in Hypoxic Tumors Increases Lung Metastasis via Angiopoietin-2. Cell Rep 2015;10. 1066–81.
[79] Xian X, Håkansson J, Ståhlberg A, Lindblom P, Betsholtz C, Gerhardt H, et al. Pericytes limit tumor cell metastasis. J Clin Invest 2006;116. 642–51.
[80] Villaruz LC, Socinski MA. The Role of Anti-angiogenesis in Non-small-cell Lung Cancer: an Update. Curr Oncol Rep 2015;17. doi:10.1007/s11912-015-0448-y.

[81] Misra S, Hascall VC, Markwald RR, Ghatak S. Interactions between hyaluronan and its receptors (CD44, RHAMM) regulate the activities of inflammation and cancer. Front Immunol 2015;6. doi:10.3389/fimmu.2015.00201.
[82] Kim SY, Hwang JY, Shin US. Preparation of nano/macroporous polycaprolactone microspheres for an injectable cell delivery system using room temperature ionic liquid and camphene. J Colloid Interface Sci 2016;465. 18–25.
[83] Abedalwafa M, Wang F, Wang L, Li C. Biodegradable poly-epsilon-caprolactone (PCL) for tissue engineering applications: A review. Rev Adv Mater Sci 2013;34. 123–40.
[84] Chen DR, Bei JZ, Wang SG. Polycaprolactone microparticles and their biodegradation. Polym Degrad Stab 2000;67. 455–9.
[85] Wu YQ, Clark RL. Controllable porous polymer particles generated by electrospraying. J Colloid Interface Sci 2007;310. 529–35.
[86] Zhou F-L, Hubbard Cristinacce PL, Eichhorn SJ, Parker GJM. Preparation and characterization of polycaprolactone microspheres by electrospraying. Aerosol Sci Technol 2016;50. 1201–15.
[87] Jaworek A. Micro- and nanoparticle production by electrospraying. Powder Technol 2007;176. 18–35.
[88] Bock N, Woodruff MA, Hutmacher DW, Dargaville TR. Electrospraying, a reproducible method for production of polymeric microspheres for biomedical applications. Polymers (Basel) 2011;3. 131–49.
[89] Lopes CD, Gomes CP, Neto E, Sampaio P, Aguiar P, Pêgo AP. Microfluidic-based platform to mimic the *in vivo* peripheral administration of neurotropic nanoparticles. Nanomedicine 2016;11. 3205–21.
[90] Tsai H-F, Trubelja A, Shen AQ, Bao G. Tumour-on-a-chip: microfluidic models of tumour morphology, growth and microenvironment. J R Soc Interface 2017;14. doi:10.1098/rsif.2017.0137.
[91] Valencia PM, Farokhzad OC, Karnik R, Langer R. Microfluidic technologies for accelerating the clinical translation of nanoparticles. Nat Nanotechnol 2012;7. 623–9.
[92] Liu D, Zhang H, Fontana F, Hirvonen JT, Santos HA. Microfluidic-assisted fabrication of carriers for controlled drug delivery. Lab Chip 2017;17. 1856–83.
[93] Nabavi SA, Vladisavljević GT, Bandulasena M V., Arjmandi-Tash O, Manović V. Prediction and control of drop formation modes in microfluidic generation of double emulsions by single-step emulsification. J Colloid Interface Sci 2017;505. 315–24.
[94] Kwon HJ, Kim S, Kim S, Kim JH, Lim G. Controlled production of monodisperse polycaprolactone microspheres using flow-focusing microfluidic device. BioChip J 2017;11. 1–5.
[95] Khademhosseini A, Suh KY, Yang JM, Eng G, Yeh J, Levenberg S, et al. Layer-by-layer deposition of hyaluronic acid and poly-L-lysine for patterned cell co-cultures. Biomaterials 2004;25. 3583–92.
[96] Borges J, Mano JF. Molecular interactions driving the layer-by-layer assembly of multilayers. Chem Rev 2014;114. 8883–942.
[97] Stern R. Hyaluronan metabolism: A major paradox in cancer biology. Pathol Biol 2005;53. 372–82.
[98] ISO 13099-1:2012 - Colloidal systems -- Methods for zeta-potential determination -- Part 1: Electroacoustic and electrokinetic phenomena n.d. https://www.iso.org/standard/52807.html (accessed November 25, 2017).
[99] Schneider CA, Rasband WS, Eliceiri KW. NIH Image to ImageJ: 25 years of image analysis. Nat Methods 2012;9. 671–5.
[100] Lou Y-R, Kanninen L, Kaehr B, Townson JL, Niklander J, Harjumäki R, et al. Silica bioreplication preserves three-dimensional spheroid structures of human pluripotent stem cells and HepG2 cells. Sci Rep 2015;5. 13635.
[101] Ma M, Xu J, Purcell WM. Biochemical and Functional Changes of Rat Liver Spheroids during Spheroid Formation and Maintenance in Culture: I. Morphological Maturation and Kinetic Changes of Energy Metabolism, Albumin Synthesis, and Activities of Some Enzymes. J Cell Biochem 2003;90. 1166–75.
[102] Grossi F, Gridelli C, Aita M, De Marinis F. Identifying an optimum treatment strategy for patients with advanced non-small cell lung cancer. Crit Rev Oncol Hematol 2008;67. 16–26.
[103] Melguizo C, Cabeza L, Prados J, Caba O. Enhanced antitumoral activity of doxorubicin against lung cancer cells using biodegradable poly (butylcyanoacrylate) nanoparticles 2015. 6433–44.

7. Annexes

7.1 Annex I

Supplementary Table 1. - Here are presented the diverse tested emulsion parameters

Formulation	PCL w/v %	Oil Phase Volume (ml)	PVA w/v	Aqueous Phase Volume (ml)	Agitation (x1000 rpm)	TTC (cm)
F1	5.00	4	0.5	150	0.5	12
F2	5.00	2	0.5	150	0.8	12
F3	5.00	4	0.5	150	0.8	7
F4	5.00	4	0.5	150	1.2	12
F5	5.00	4	0.5	150	0.8	16
F6	5.00	4	0.5	150	1.2	16
F7	5.00	8	0.5	150	1.2	12
F8	4.00	8	0.5	150	0.8	12
F9	4.00	4	0.5	150	0.8	12
F10	5.00	4	0.5	150	0.8	12
F11	7.50	4	0.5	150	0.8	12
F12	7.50	8	0.5	150	0.8	12
F13	7.50	8	2	150	0.8	12
F14	5.00	8	0.5	150	0.8	12
F14 Sieved	5.00	8	0.5	150	0.8	12
F15	4.75	10	0.5	150	0.8	12
F16	5.00	10	0.5	150	0.8	12
F17	4.00	10	0.5	150	0.8	12
F18	5.00	10	0.5	150	1.2	12
F19	4.00	10	0.5	150	1.2	12
F20	2.25	10	0.5	150	0.8	12
F21	2.25	10	0.5	150	1.2	12

Supplementary Table 2. Formulations tested using electrospraying technique. Average sizes and morphologies of all produced formulations didn't match the specifications. TTC refers to tip to collector distance.

Formulation	PCL (w/v) %	TTC (cm)	Gauge (G)	Flow Rate (ml/H)	Volt (Kv)	Collection Method	Monodis-persity	Average Size
A1	5	(170_0)	22	4	10	Collected in - 20 ml PVA 2% not stirred	no	<20 µm
A2	5	(170_0)	22	4	10	Collected in - 60 ml PVA 2% not stirred (400 rpm)	no	<20 µm
A7	5	(07_0)	22	4	10	Collected in - 40 ml PVA 2% stirred (400 rpm)	no	<20 µm
A8	5	(08_0)	22	4	10	Collected in - 40 ml PVA 2% stirred (400 rpm)	no	<20 µm
A9	5	(08_0)	22	3	10	Collected in - 40 ml PVA 2% stirred (400 rpm)	no	<20 µm
A10	5	(08_0)	22	0.8	10	Collected in - 40 ml PVA 2% stirred (400 rpm)	no	<20 µm
A12	9	(08_0)	22	0.8	10	Collected in - 40 ml PVA 2% stirred (400 rpm)	no	<20 µm
A13	9	(08_0)	22	1	10	Collected in goble - 40 ml PVA 2% stirred (400 rpm)	no	<20 µm
A14	9	(08_0)	22	2	10	Collected in - 40 ml PVA 2% stirred (400 rpm)	no	<20 µm
A16	5	(08_0)	22	3	10	Collected in goble - 40 ml Water stirred (400 rpm)	no	<20 µm

A17	5	(08_0)	22	3	10	Collected in - 40 ml Water stirred (750 rpm)	no	<40 µm
A18	5	(08_0)	22	3	5	Collected in - 40 ml Water stirred (400 rpm)	no	<20 µm
A19	5	(08_0)	22	3	5	Collected in - 40 ml PVA 2% stirred (400 rpm)	no	<20 µm
A20	5	(08_0)	22	3	15	Collected in - 40 ml Water stirred (400 rpm)	no	<20 µm
A21	5	(08_0)	22	3	15	Collected in - 40 ml PVA 2% stirred (400 rpm)	no	<10 µm
A22	5	(08_0)	22	3	10	Collected in - 60 ml PVA 0.5% stirred (400 rpm)	no	<10 µm
A23	5	(08_0)	22	3	15	Collected in - 40 ml PVA 0.5% stirred 400 rpm)	no	<10 µm
A25	5	(100_0)	22	3)	8.8	Collected in - 40 ml PVA 0.5% stirred 400 rpm)	no	<10 µm
A26	5	(03.7_0)	22	36	10	Collected in - 60 ml PVA 0.5% stirred 600 rpm)	no	<10 µm
A27	5	(08_0)	22	3	10	Collected in - 60 ml PVA 0.5% stirred 600 rpm)	no	<10 µm
A28	5	(08_0)	22	3	10	Collected in - 40 ml PVA 0.5% stirred (400 rpm)	no	<10 µm
A29	5	(08_0)	22	3	7.5	Collected in - 40 ml PVA 2% stirred (400 rpm)	no	<10 µm
A30	5	(00_0)	22	3	10	Collected in - 40 ml PVA 0.5% stirred (400 rpm)	no	<10 µm

Supplementary Table 4. Tested microfluidic formulations.

Formulation	PCL (w/v) %	Pressure Central Channel (mbar)	PVA (w/v) %	Pressure Side Channels (mbar)
M1	0.05	270	0.02	300
M2	0.05	270	0.005	300
M3	0.075	540	0.02	300

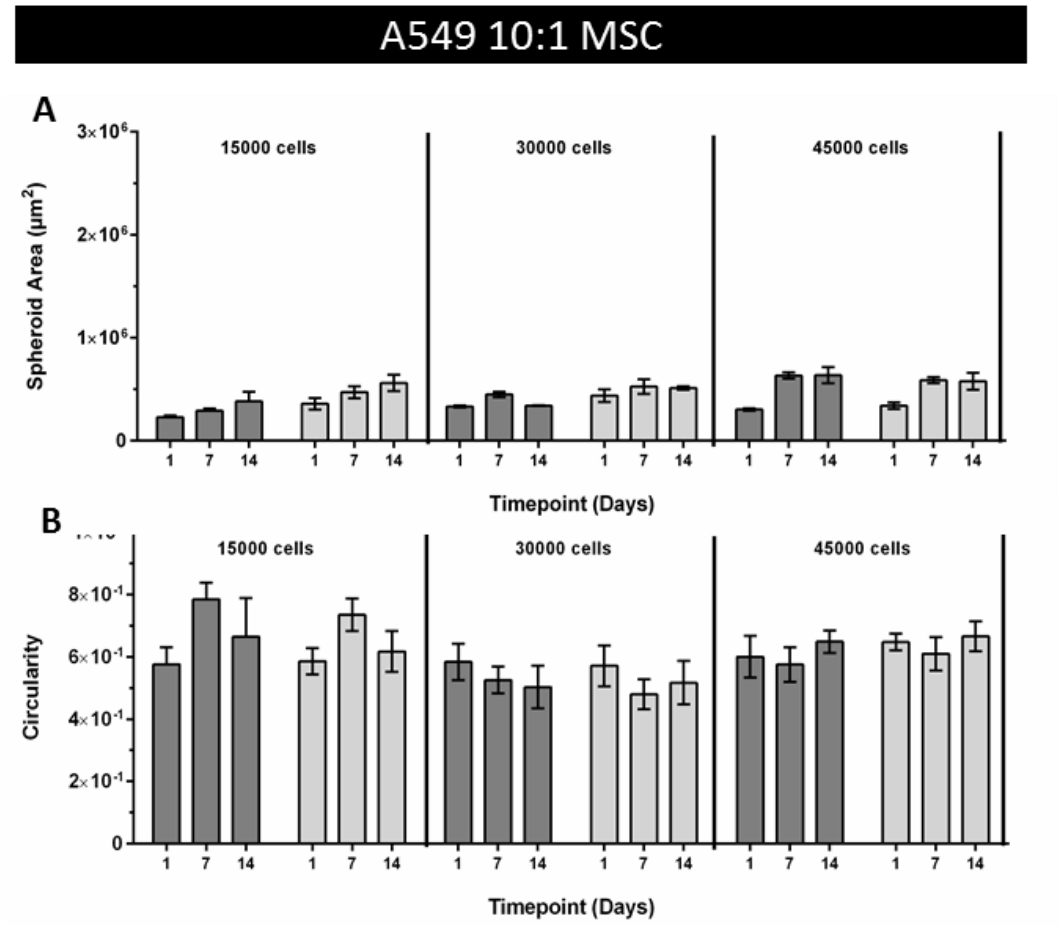

Supplementary Figure 1. Variation of Size (A) and circularity (B) of dual-coculture spheroids of A549 and MSCs

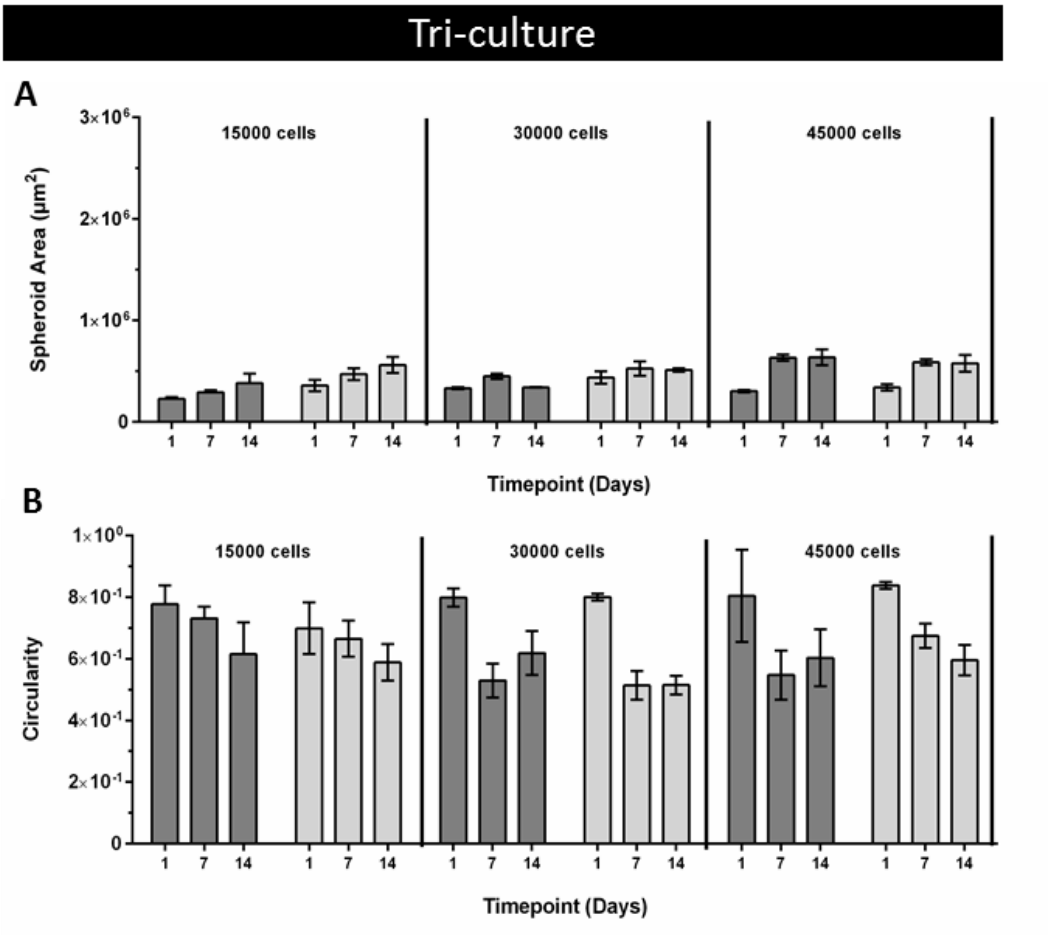

Supplementary Figure 2. Variation of Size (A) and circularity (B) of Triculture spheroids of A549 , HF and MSCs

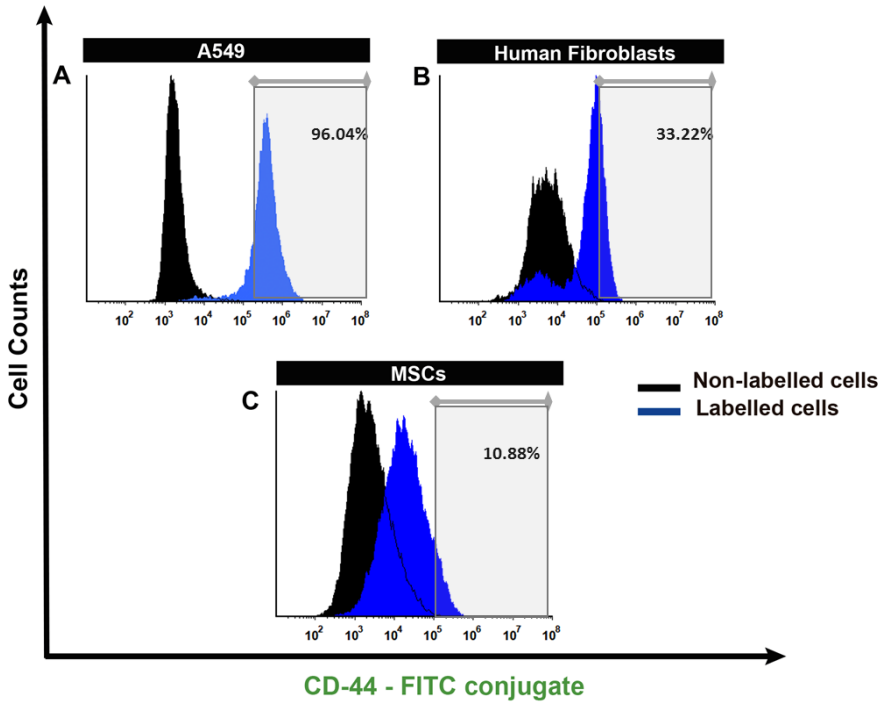

Supplementary Figure 3.8 CD44 surface markers expression in 2D monocultures of A549 (A), HF (B), MSCs (C).

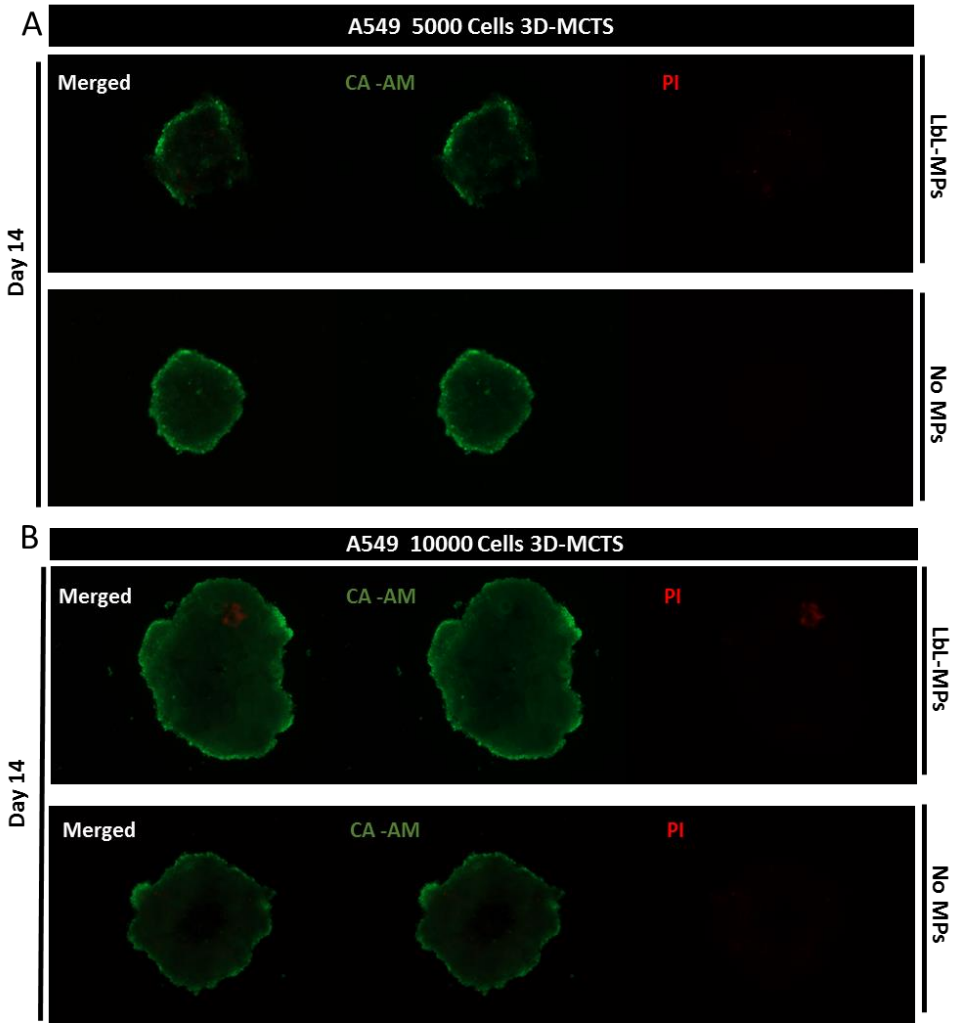

Supplementary Figure 4. Live dead imaging of A549 monoculture spheroids at day 14. No necrotic core was visible in both LbL-MPs containing and non-LbL-MPs containing spheroids.

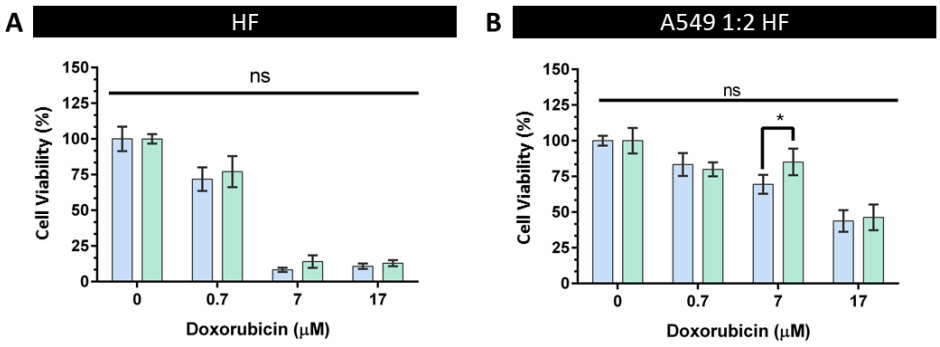

Supplementary Figure 5. Drug screening assay of HF monoculture compared to previously doxorubicin cytotoxicity assay of A549-HF dual coculture. As can be seen HF alone present a higher susceptibility to doxorubicin action than dual coculture spheroids.